Proceedings of the Workshop TRePro II

F. Huber, J. Lützenkirchen, W. Pfingsten, C. Tiffreau

Institut für Nukleare Entsorgung

Forschungszentrum Karlsruhe

in der Helmholtz-Gemeinschaft

Wissenschaftliche Berichte

FZKA 7482

Proceedings of the Workshop TRePro II

Florian Huber[1], Johannes Lützenkirchen[1], Wilfried Pfingsten[2], Christophe Tiffreau[3]

[1]Forschungszentrum Karlsruhe, Institut für Nukleare Entsorgung (INE), Germany

[2]Paul Scherrer Institut (PSI), Waste Management Laboratory (LES), Schwitzerland

[3]Centre d'Etudes de Cadarache, Laboratoire de Modélisation des Transferts dans l'Environnement, France

Forschungszentrum Karlsruhe GmbH, Karlsruhe

2009

Forschungszentrum Karlsruhe GmbH
Postfach 3640, 76021 Karlsruhe

Proceedings of the Workshop TRePro II

Karlsruhe, 2009

Summary

TRePro II 2009 took place at Forschungszentrum Karlsruhe, Institut für Nukleare Entsorgung (INE) in March 18 - 19, 2009. TRePro II was the fifth meeting in the series of "Karlsruher Geochemical Workshops". The intention of the series of workshops is to serve as a platform to discuss the state of the art and the understanding of geochemical reaction processes at mineral water interfaces.

- The first workshop, held in 1997 at the Forschungszentrum Karlsruhe, was entitled "Geochemical modelling - radio toxic and chemical toxic substances in natural aquatic systems".
- The second meeting was held in 1999 in Speyer focusing on "Mineral/water interactions close to equilibrium".
- The third workshop **TRePro**, held in 2002 in Karlsruhe, dealt with "Modelling of coupled transport reaction processes".
- The fourth workshop, held in 2004 in Karlsruhe **SOPRO 2004** dealt with sorption processes on oxide and carbonate minerals relevant for retention of radionuclides migrating from nuclear waste repositories. General focus was on fundamental studies from an experimental and theoretical point of view.

TRePro II 2009 was jointly organized by Forschungszentrum Karlsruhe, Institut für Nukleare Entsorgung (INE), Germany, Paul Scherrer Institut, Waste Management Laboratory (LES), Switzerland, CEA, Centre d'Etudes de Cadarache, Laboratoire de Modélisation des Transferts dans l'Environnement, France. Overall 50 participants from Germany, France, Switzerland, Spain, UK, The Netherlands, Czech Republic and USA attended a total of four oral sessions and one poster session. TRePro II 2009 took up the idea of TRePro 2002: "Modelling of coupled transport reaction processes". The intention of TRePro II 2009 was to serve as a forum for discussing the latest developments in modelling of coupled reaction and transport processes. The main idea of the workshop was to enhance the discussion between experimentalists and modellers from different domains. The main topics address were

- Codes: with respect to benchmarking – trends – challenges.

- Problems associated with scales such as up-scaling – model parameters – model complexity.

- Chemical Processes including sorption – redox – colloids generation and interactions – phase transformations – dissolution/precipitation.

- Reactive Transport and Safety: applications to nuclear waste storage – CO_2 sequestration and geothermal issues have been discussed.

Each session was started with a keynote lecture followed by oral contributions. Distinguished lectures were given by Philippe Ackerer, F, Sergey Churakov, CH, David Wesolowski, USA and Irina Gaus, CH.
Philippe Ackerer from Strasbourg University presented the French MoMaS benchmark exercise for reactive transport models, the definition of increasingly complex test cases and the results obtained by several groups. The French Waste

Management Organisation ANDRA provided for an award for the best results and thus attracted interest in the benchmark from all over the world. An important outcome from MoMaS was that for such kind of benchmarking, people having different backgrounds and fields of experiences have to find a common language to communicate. Sergey Churakov from Paul Scherrer Institute in Switzerland demonstrated the connection from modelling clays on atomistic scales by molecular dynamic methods to scales relevant in performance assessment of radioactive waste disposal. David Wesolowski from Oak Ridge National Laboratory (USA) demonstrated the powerful combined application of a wide range of macroscopic and spectroscopic methodologies in order to obtain information of the dynamics and reactivity at mineral-water interfaces. Methods involved in this multi-instrument study on one system were X-ray and neutron scattering, molecular simulation and macroscopic titration and adsorption measurements. The presentation of Irina Gaus from NAGRA covered the need for coupled reactive modelling in the field of CO_2 sequestration. She presented the state of the art of modelling in this field (encompassing the kind of mineral reactions, the reactions with engineered structures and those in the aquifers) and pointed to gaps in the thermodynamic data base that would be required for more comprehensive modelling.

The other presentations covered the development of models and corresponding test cases or benchmarks and for up-scaling procedures e.g. for acid uranium mining. In the chemical processes section the modelling of Eu interaction with mica surfaces and Cl or CO_2 was presented. Further talks addressed the evolution and dissolution of gas bubbles and the behaviour of organic toxic materials in contact with groundwater. In the "reactive transport and safety" session also issues like modelling crack systems in HLW glass blocks, Ni behaviour in the bentonite of a disposal in granite host rock as well as the impact of extreme climate states on the radionuclide transport in the Gorleben aquifer system were presented.

The session "presentation of codes" was intended to show the audience available codes developed by different research groups in terms not only of their capabilities and possible fields of applications but also concerning the respective style of programming. Here a promising trend is looming towards the use of object-oriented programming philosophy. In particular, the development of geochemical modelling software, which enables users to modify easily codes to their specific needs or to couple a code to an arbitrary conservative fluid and mass transport solver to simulate reactive transport, appears promising.

The TRePro II workshop covered a broad range of models, applications of models and modelling results. In the previous TRePro workshop (2002), a lot of experimental approaches and results of column experiments had been presented and main topics were colloids and redox processes. During the present workshop these issues had minor importance. Now, the combination of nanoscopic experimental techniques and molecular dynamics modelling highlighted the frontier of science in assessing retardation mechanisms on the molecular scale. This detailed knowledge is expected to be decisive to in backing up the use of the necessarily less sophisticated and detailed retardation approaches required for modelling coupled reactive processes or for a comprehensive numerical safety analysis.

The resonance of the participants support the idea of the "*Karlsruher Geochemical Workshops*" and another one will be organized in 2 or 3 years. A topic to be discussed could be related to dealing with various levels of uncertainty in models used in safety analyses.

Without several persons at INE the workshop would not have been possible:

Special thanks go to Bernhard Kienzler for initiating and to Horst Geckeis for constantly supporting the organisation of the workshop.

We are furthermore grateful to Stefanie Krieger and Elke Lukas who helped with various administrative aspects during the preparation.

The helpful input from various departments at FZK who were involved in the organisation is gratefully acknowledged.

Finally we thank all contributors to this FZKA Report.

Florian Huber, Johannes Lützenkirchen, Wilfried Pfingsten, Christophe Tiffreau

Table of contents

On the benchmarking of reactive transport codes: the MoMaS test cases

Phillippe Ackerer and Jérôme Carrayrou
Laboratoire d'Hydrologie et de Géochimie de Strasbourg,
Université de Strasbourg/EOST - CNRS1, rue de Blessig, 67000 Strasbourg, France.

MoMaS (Modeling, Mathematics and numerical Simulations related to nuclear waste management problems http://www.gdrmomas.org./) is a federation of French research groups which proposes numerical benchmarks to help evaluate computer codes. According to the interests of MoMaS, the benchmarks dedicated to reactive transport problems should be representative of the problems encountered in nuclear waste disposal simulations. One objective of these benchmarks is to interest a community as large as possible coming from geochemistry, hydrogeology and applied mathematics. Nevertheless, the high complexity of both transport and chemical phenomena occurring in such a system may be an obstacle for some researcher who may not be familiar with hydrogeological and geochemical concepts. Therefore, the problems proposed are built on the same mathematical concepts as real hydro-geochemical problems, but their description is simplified.

These benchmarks consist in three independent subjects, ranked by complexity: Easy, Medium and Hard. Each subject consists of a 1D and a 2D (Fig. 1) reactive transport problem. The flow and transport phenomena are the same for the three subjects. From one subject to the other, some chemical phenomena are added increasing the difficulties. Some input data for the 'easy' case are given in Table 1.
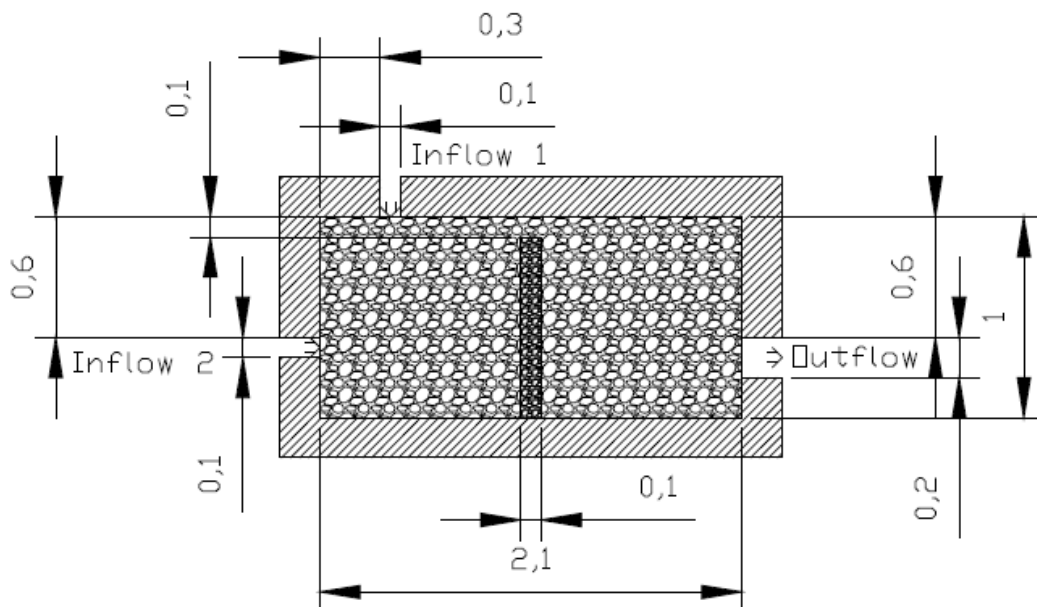
Fig. 1: The 2D configuration.

Table 1: Input data for the 'easy' test case.

	X_1	X_2	X_3	X_4	S	K
C_1	0	-1	0	0	0	1.00E-12
C_2	0	1	1	0	0	1
C_3	0	-1	0	1	0	1
C_4	0	-4	1	3	0	0.1
C_5	0	4	3	1	0	1.00E+35
CS_1	0	3	1	0	1	1.00E+6
CS_2	0	-3	0	1	2	1.00E-01
Total $(m.L^{-3})$	T_1	T_2	T_3	T_4	TS	
Initial for medium A	0	-2	0	2	1	
Initial for medium B	0	-2	0	2	10	
Injection $t \in [0,5000]$	Imposed total concentration at inflow boundary					
Inflow for 1D	0.3	0.3	0.3	0		
Zone 1 for 2D	0.3	0.3	0.3	0		
Zone 2 for 2D	0.3	0.3	0.3	0		
Leaching $t \in [5000,...]$	Imposed total concentration at inflow boundary					
Inflow for 1D	0	-2	0	2		
Zone 1 for 2D	0	-2	0	2		
Zone 2 for 2D	0	-2	0	2		

The results obtained by different groups coming from different countries will be presented and discussed. The main conclusions issued from these benchmarks are:
- Only few codes were able to solve the 'Hard' test cases,
- CPU times were quite high, although the size and the geometry of the domains are small,
- The spatial and temporal discretization significantly influenced the results, even for the 'Easy' test cases,
- The spatial discretization needs to be very fine,
- Higher order numerical methods seem to be more robust.

Intercomparison Exercise on Redox determination methods: A key activity within the EURATOM FP7 "ReCosy" Project

Marcus Altmaier
Institut für Nukleare Entsorgung, Forschungszentrum Karlsruhe, Postfach 3640, D-76021 Karlsruhe, Germany

The objective of the EURATOM FP7 Collaborative Project "Redox phenomena controlling systems" (CP ReCosy) is to provide an improved interpretation of redox processes for all relevant host-rock systems to be used within European Safety Cases. In this context reliable experimental methods to measure redox are required. The redox state of aqueous systems can either be determined by electrochemical or by the analytical determination of redox determining species followed by thermodynamic evaluation. Within ReCosy a considerable part of the work focuses on a deeper understanding of existing methods, and the development of new and improved redox determination methods.

The Intercomparison Exercise (ICE) is a key element in ReCosy, tackling the central question of how the redox state can be determined, what different redox determination methods register and if differences in the protocols between different groups/organizations is the reason for considerable differences in results reported by different groups. Confidence in the capability to determine the redox state is provided by the joint ReCosy Intercomparison Exercise on samples of varying complexity and a following careful discussion and assessment of the outcome.
About ten samples covering different types of redox systems and reflecting typical geochemical boundary conditions will be used for ICE:

- Four well defined reference systems expected to have very stable redox conditions. They are of major importance for evaluating the different techniques and handling protocols and assessing the trueness of the redox reading. They also cover different pH conditions and include:
  - *Fe-system at low ionic strength.*
  - *Fe-system at high salinity/brine conditions.*
  - *System with "simple" organics (e.g. hydrochinone).*
  - *System under hyperalkaline conditions.*
- A set of samples more relevant to the key question, i.e. near-natural groundwater samples with varying redox stability. Samples include:
  - *Groundwater with humic substances (Gorleben, Germany).*
  - *Clay-rock system (COX, France).*
  - *Granitic groundwater (Äspö, Sweden; Grimsel, Switzerland).*
  - *High salinity brines (Asse, Germany).*
- Homogenous *systems with microbiological activity* are also provided.

Additional activities at ICE will include presentations of advanced experimental techniques, a critical evaluation of different redox electrodes, expert information and practical advice on how to avoid artefacts from the measurement setup and a test of different pre-treatment protocols for conventional Pt-combination electrodes.

Significant time is reserved for a detailed presentation and discussion of results thus providing a unique platform for scientific exchange and an improved understanding of redox determination methods beyond the present state-of-the-art.

Several groups including one Associated Group will contribute to the ICE. Participation from outside the ReCosy project and the European Union is encouraged.

The Intercomparison exercise will be held from 16-20 November 2009 at the Institut für Nukleare Entsorgung, Karlsruhe, Germany. For further information, please see the project web page www.ReCosy.eu, or contact Marcus.Altmaier@ine.fzk.de .

Numerical simulation of multi-component non-aqueous phase liquid dissolution for the assessment of source zone screening models

Christof Beyer[1], Dirk Schäfer[1], Olaf Kolditz[2] and Sebastian Bauer[1]
[1] *Institute of Geosciences; Christian Albrechts University of Kiel; Ludewig-Meyn-Str. 10; 24118 Kiel, Germany*
[2] *Department of Environmental Informatics, Helmholtz Centre for Environmental Research UFZ, Permoserstr. 15, 04318 Leipzig, Germany*

Contamination of groundwater resources from spills of organic contaminants has become a serious environmental problem. At industrial sites non-aqueous phase liquids (NAPL) are frequently detected in the subsurface. NAPL bodies may be present as large spread out pools or as trapped and immobilized residual blobs contained in the pores of the matrix. NAPL phases often are complex mixtures of several organic components with individual physichochemical properties (e.g. molar weight, aqueous solubility). Dissolution of NAPL constituents from pools or residual saturation of a NAPL mixture and transport of these compounds with the groundwater flow poses a threat for downgradient receptors like e.g. drinking water supplies or aquatic ecosystems. Therefore, special attention has traditionally been given to the investigation, assessment and remediation of the contaminant plume rather than the contaminant source (i.e. the NAPL body). In recent years, however, focus shifted more towards strategies for the investigation and remediation of the source zone, as attacking the source of a contamination problem rather than its symptoms promises significant reductions of overall remediation times and costs in comparison to more conventional plume focused techniques.

A basic requirement for the planning and operation of NAPL source zone remediation is the ability to quantitatively predict source zone behaviour and longevity under natural gradient dissolution as well as remediation conditions. Accordingly, a lot of effort is spent on the development of models which are able to predict the coupled processes relevant at sites with subsurface NAPL contamination. As complex numerical models of multi-component NAPL dissolution usually require a large number of parameters, which are difficult to determine in the field, their applicability at contaminated sites is often limited and there is a strong demand for simplified screening models. These are often based on analytical expressions, require less parameters, but still are very useful for predictions of NAPL source zone behaviour and their emissions to the aqueous phase. Due to the limited accessibility of the subsurface, however, any site investigation is subject to uncertainty, reflecting the limited knowledge on the aquifer properties and the extent of the contamination. Consequently, as any site investigation method also source zone screening models can hardly be verified in the field. To cope with this situation, the Virtual Aquifer concept has been developed, where field investigation methods are evaluated by application in synthetic, i.e. virtual, contaminated aquifers. In this way a screening model's results may be compared to the "true" contamination situation, as this (in contrast to a real site) is known from the synthetic aquifer.

In order to be able to generate virtual contaminated aquifers, which are sufficiently close-to-reality to allow the assessment of NAPL screening models, highly detailed process based numerical models of coupled flow, transport and NAPL dissolution are

required. Therefore, the GeoSys finite element code (Kolditz and Bauer 2004; Kolditz and Shao 2008) was recently extended by a highly detailed and flexible kinetic multi-component NAPL dissolution model. The model is able to consider theoretically any number of NAPL bodies in different geometries (i.e. pools, spherical or cylindrical blobs). Each NAPL body may have its own component composition. Generally, any number of NAPL constituents may be considered. Mass exchange between a NAPL geometry and the water phase is calculated according to Fick's 1st law. For NAPLs consisting of mixtures of individual substances, each substances equilibrium concentration in water is computed according to Raoult's law. A flexible formulation of the dependency of the mass transfer rate coefficient on substance (e.g. aqueous diffusion coefficient) and porous medium properties (e.g. mean grain size, water viscosity, flow velocity) allows the consideration of a wide number of functional relationships for the description of the dissolution kinetics.

Currently, the kinetic dissolution model is validated against an analytical solution by Hansen and Kueper (2007). The Hansen and Kueper model was developed to quantify the temporally changing composition of a multi-component NAPL body in moving groundwater and the consequent changes of the NAPL constituents concentrations in the surrounding groundwater. It is suited for both, pooled configurations and residual NAPL in blob geometries. As any analytical model, the Hansen and Kueper model is based on a number of simplifying assumptions:

- The model predicts the NAPL composition as well as aqueous phase concentrations at the downstream end of the NAPL source zone

- The component composition of the NAPL is spatially invariant at a particular instant in time.

- Intra-NAPL diffusion is fast in relation to phase partitioning.

- For pools the local equilibrium assumption is employed, i.e. inter-phase mass transfer is faster than solute transport away from the NAPL.

- Within a zone of residual NAPL, NAPL saturation and mixing are sufficient to allow the assumption of a single concentration composition at the downstream end of the source zone, which follows Raoult's law (global equilibrium assumption).

Fig. 1 shows an example of the temporal development of the component composition at the down-stream end of a mixed residual NAPL source, which initially consists of the chlorinated hydrocarbons PCE, TCE and TCM. The Hansen and Kueper model predicts almost complete depletion of TCM in relatively short time, while TCE and PCE depletion requires significantly more time due to their higher initial concentrations and lower aqueous solubilities.

The Hansen and Kueper model may be used as a site screening model, e.g. for the prediction of the lifespan of a source zone. Also, aqueous phase concentrations at the end of the source zone calculated with this model may serve as time variant boundary conditions for numerical transport simulations. Clearly, the simplifications of the analytical model listed above may limit its applicability in some practical cases. Using our numerical model and the Virtual Aquifer approach we will explore the effects of these limitations on the prediction of the behaviour of mixed source zones. By gradually increasing the complexity of a synthetic contamination scenario, the assumptions of the analytical model will be progressively violated and its predictions can be evaluated against the Virtual Aquifer data obtained from the numerical model.
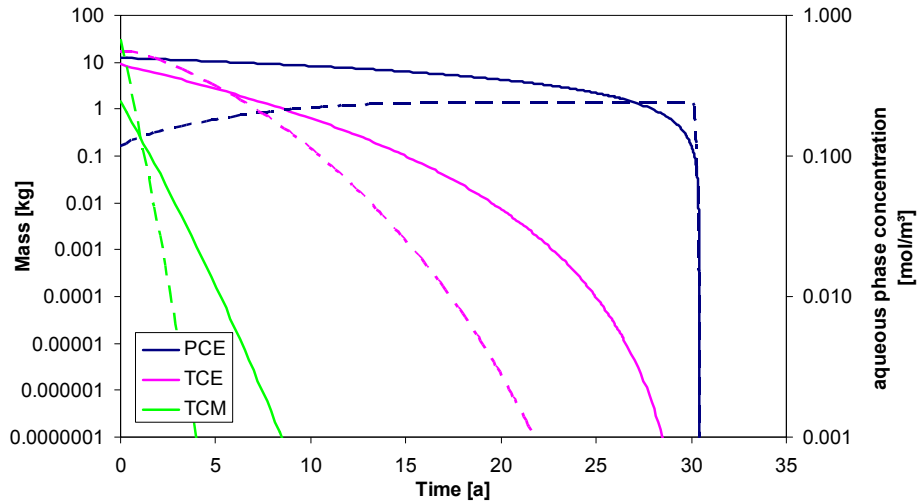
Fig. 1. Mass of PCE, TCE and TCM at the end of a residual NAPL source zone (full lines) and consequent aqueous phase concentrations (dashed lines) as functions of time.

References

Hansen, S.K., Kueper, B.H. (2007). An analytical solution to multi-component NAPL dissolution equations. Advances in WaterResources 30, 382–388.

Kolditz, O., Bauer, S. (2004). A process-oriented approach to computing multi-field problems in porous media. Journal of Hydroinformatics 6, 225-244.

Kolditz, O., Shao, H. (2008). Developer Benchmark Book on THMC Components of Numerical Codes GeoSys / Rockflow V. 4.7; Helmholtz Centre for Environmental Research (UFZ): Leipzig.

Modeling the long term behaviour of glass in deep geological repositories: interactions between glass, steel and argilite

Olivier Bildstein, Jean-Eric Lartigue, Laurent Trotignon and Emmanuel Piault
Laboratory for Modeling of Transfers in the Environment, CEA, Saint Paul-lez-Durance 13108, France

The concept developed in France for the disposal of vitrified high level waste in deep geological repositories includes the containment in steel canisters, for mechanical stability, and confinement at *ca.* 500 m into an argillaceous host rock. Concrete is also used in combination with steel as reinforcement material for structure of the galleries and shafts. After emplacement of the canisters and closure of the repository, the site will progressively re-saturate and the alteration of the different materials will start: corrosion of the canisters, degradation of concrete, and ultimately, the alteration of glass.

This contribution is concerned with the perturbations that will affect the lifetime of the glass matrix especially due to the interactions with the different materials present in the near field of the repositories. The evolution of the near field system is complex also due to geochemical and transport processes are highly coupled. Steel corrosion and glass alteration produce an increase of pH which in turn affects the rate of glass alteration. The concentration of dissolved silica is also key to the rate of glass alteration and, along with the concentration of other elements such as iron and aluminum; it determines the nature of steel corrosion product and clay alteration products. These interactions also lead to transformations of the initial clay minerals affecting confining properties such as swelling and capacity to exchange cations. Modeling results also show that significant changes in porosity may occur at the interface between materials, due to the precipitation of secondary minerals thus impacting the overall performance of the system.

Coupled reaction-transport is used to calculate the corrosion of the steel canister and the glass alteration phase in presence of corrosion products (CP), looking at mass transfer for chemical elements, especially iron and silica, pH, porosity change. According to the operational model currently used at the CEA and the calculations performed on the glass-iron-clay system, the alteration rate of glass and the evolution of the system strongly depend on the pH at the interface with glass and whether or not the CP sorption sites are saturated with silica. The time at which this sorption capacity will be saturated is crucial to the system. Therefore, there is a need for more understanding of the mechanisms of "immobilisation" of silica on CP and on metallic iron (including sorption, nucleation and precipitation of silica), and for more reliable data on this process. In this regard, the nature of PCs plays an important role and depends on how the partial pressure of gases such as CO_2 and H_2 are regulated in the NF.

Porosity changes are another important process that might influence the glass alteration. Indeed, porosity decreases due to the precipitation of CP and silica rich phases. Clogging is scarcely observed in experiments, either because it does not occur at all or because the timescale of this process is not accessible to experiments. If confirmed, it may directly impact the source term for RN, especially if we consider a dependence of the glass alteration rate with respect to aqueous silica concentration

close to the glass surface: silica transport will be reduced at this location and will tend to accumulate resulting in the decrease of the alteration rate of glass and of the release of RN. Even though, because this process might be of great importance for the evolution of the system, especially at high temperature (~90°C), there is a need for more understanding of the mechanism at play when the porosity is vanishing due to geochemical interactions in a porous media.

EURATOM FP7 Collaborative Project "Redox phenomena controlling systems" (CP ReCosy)

Gunnar Buckau[1], Lara Duro[2] and Bernhard Kienzler[1]

[1]*Institut für Nukleare Entsorgung, Forschungszentrum Karlsruhe, Herrmann-von-Helmholtz-Platz 1, 76344 Eggenstein-Leopoldshafen, Germany*
[2]*Amphos XXI Consulting S.L., Passeig de Rubi 29-31 E08197 Valldoreix – Barcelona, Spain*

Potential radionuclide migration from radioactive waste repositories is strongly affected by redox phenomena. This refers to all the different parts of such a potential migration path, starting with the waste itself. The dissolution of spent fuel is associated with oxidation of U(IV) to the soluble U(VI). The conversion, stability and potential dissolution of waste container material are also related to redox processes. The same is true for conversion of material in the engineered barrier. In the crystalline and salt host rock systems, the far-field conditions, stability, formation and dissolution of minerals, will depend on changes in the groundwater composition, associated with changes in climatic conditions and land-use. In all these cases the redox conditions will play a key role for dissolution and mineral formation rates, the sorption of radionuclides on these minerals and the timely change of their inventory. Redox conditions also determine the chemical state of several radionuclides and thus govern their retention/mobility. For the disposal safety assessment, thus, relevant conditions and processes need to be identified, and the capability to make long-term prediction under varying conditions is required. The pre-requisite for this is the capability to determine the redox conditions, including the understanding of the type of information different redox determination methods provide.

In order to provide the necessary knowledge corresponding to above discussed topics, the Euratom FP7 CP ReCosy was established. It started 1 April 2008 with 32 Partners from the European Union, Russia and a European Joint Research Centre. The project will run for four years. The consortium has an open structure with the possibility for additional organizations to join the project on an association basis. There are presently two Associated Groups and two more organizations are negotiating its participation. Key project events are annual workshops, open to participation also from outside the project. The outcome of the annual workshops is published in the form of proceedings, where also the scientific-technical progress of the project is documented and yearly updated. The 1st Annual Project Workshop was held in Barcelona, 10-12 February 2009 with the proceedings (FZKA report 7466) in preparation. Next Annual Project Workshop will be held 16-19 March, in Larnaca, Cyprus. General information about the project, key publications and forthcoming events can be found at the project WEB site www.recosy.eu.

Up-scaling of molecular diffusion coefficients in clays: A two scale approach

Sergey Churakov[1] and Thomas Gimmi[1,2]
[1]*Laboratory for Waste Management, PSI, 5232 Villigen, Switzerland*
[2]*RWI, Institute of Geological Sciences, University of Bern, CH-3012 Bern, Switzerland*

Mass transport in clays is restricted to diffusion in the pore space saturated with the electrolyte solution. Interlayer, externally bound diffuse double-layer and "mobile" pore solutions are distinguished depending on the local environment (Fig. 1). The interlayer porosity is specific to the smectite group of clay minerals showing swelling behaviour. Smectite minerals are composed of stacks of quasi two dimensional layers with a particle size on the order of micrometers. Due to isomorphic substitutions, smectite particles carry a permanent electrical charge which is compensated by mono and divalent cations occupying the inter-particle space. When clays are brought in contact with an aqueous solution, water molecules enter the inter-particle space and hydrate the inter-layer cations. Typical thicknesses of the interlayer space in smectite minerals vary from one to three water layers, depending on the water pressure and the particle charges. Diffuse double-layer is formed at the external interface of permanently charged mineral surfaces and the aqueous electrolyte. Such interfaces are characterised by an inhomogeneous distribution of electrolyte ions whose coulomb potential compensates the corresponding electrostatic potential produced by the charged mineral. High ionic concentration near the surface and strong interaction with the surface influence the diffusion of water and ions in the diffuse double-layer. Typical size of a diffuse double layer is of the order of nanometres depending on the ion strength of the solution. Finally, "mobile" solution is found in macro-pores in which the effects of the surface interactions are negligible (Fig 1).
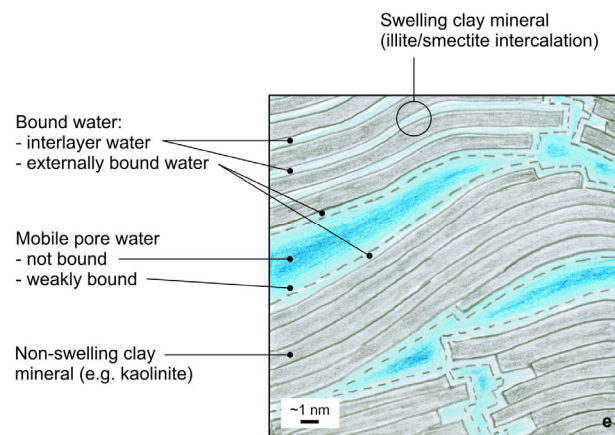
Fig. 1. A schematic representation of pore solution in compacted clays.

In highly compacted natural clay rocks, 50 to 80% of the pore water is influenced by clay surfaces, and for compacted smectites, as used in engineered barriers even up to 95% of the accessible porosity is attributed to the interlayer space. The water diffusion in such highly compacted clays is reduced by the interaction of water molecules with the surfaces of the clay particles and by the complexity of the diffusion path. Assuming a sub stratified arrangement of clay particle, where transport

occurs mostly in the two dimensional inter-layer space and along lateral interfaces of clay stacks (edge sites), the effective diffusion path in a given direction is considerably longer than the corresponding physical dimensions of the sample. For example, lower effective diffusion coefficients are measured in the direction perpendicular to the stratification than along the stratification.

Several attempts have been made to assess the reduction of diffusion coefficients in compacted clays by molecular modelling techniques. Diffusion coefficients of water and ions in the interlayer of montmorillonite were estimated by classical molecular dynamics simulations as a function of compaction (Kosakowski et al. 2008). Recently, the structure of water confined between edges of clay minerals was deduced from ab initio molecular dynamics simulations (Churakov 2007). Neutron scattering experiments, which probe a short range (~50 ps) dynamics of water molecules, confirm the results of molecular modelling (Gonzàlez Sanchez et al. 2007) Atomistic molecular dynamics simulations consider the interactions between atoms and molecules explicitly in terms of atom-atom pair-wise interaction potentials. Such a detailed system description sets limits on the size of the systems being considered. At present, atomistic simulations can treat systems up to about ten nanometres in size. Therefore, such simulations cannot directly probe the effects of geometrical arrangements of the clay particles on aqueous diffusion. The typical size of clay particles is of the order of a micrometre, so simulation domains of a comparable size are necessary to consider the complex arrangement of clay particles.

In order to assess the influence of the particle arrangements on the diffusion coefficients of water we developed a random walk model that operates on a pore-scale description of heterogeneous clays. In this model the water transport is described by structureless point particles moving randomly according to position-dependent diffusion coefficients. The diffusion coefficients depend on the local environment, which can be either interlayer pores or pore space at the lateral edges of clay particles. These local diffusion coefficients are derived from small scale (nanometre size) molecular dynamics simulations. The distribution of the clay particles is derived indirectly from experimental data on the pore size distribution and estimates of preferential particle orientation. To test the agreement between the results obtained at different modelling scales and the consistency of different numerical concepts, the outcome of the random walk simulations was checked against the result of the molecular dynamics simulations on a small scale with a simplified particle arrangement that could be treated by both modelling approaches (Fig. 2).
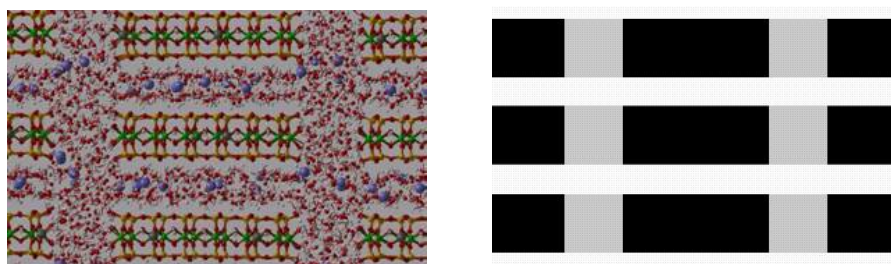
Fig. 2. A snapshot from molecular dynamics simulations of water diffusion in Na-montmorillonite (left) and an equivalent representation of the system in the random walk simulations (right). Black areas represent clay particles, which are not accessible for the molecules in the solution. White and gray

shaded areas are the regions with interlayer and diffuse double layer diffusion coefficients, respectively.

We then applied the random-walk model on a macroscopic scale, taking into account local diffusion coefficients determined by molecular modelling, using a representative pore-scale description of heterogeneous clay (Fig. 3). The, random walk simulations allowed us to extract macroscopic transport parameters such as the tortuosity of the diffusion pathway (often referred to as the geometry factor). Depending on the heterogeneities of the clay structure, however, many simulations on domains with a size on the order of 0.1 μm are required to obtain representative results, or simulations on larger domains of about 1-10 μm. To speed up the simulations, some averaging of pore-scale properties is required.

Fig. 3. An example of clay (elongated particles) and quartz grains (gray area) distribution in the full scale simulations. The solution accessible pore space is shown as white area.

We show that with our hierarchical simulation technique we are able to upscale results from molecular modelling to continuum scales. We also demonstrated that geometry factors similar to those measured could be obtained from a pore-scale description of the samples. Finally, some generally unknown details of the pore-scale structure such as closeness of the contact between different particles are important for the overall results. Thus, further work improving the pore-scale description will be required to strengthen this up-scaling approach.

References

Kosakowski G., Churakov S.V., Thoenen T. (2008) Diffusion of Na and Cs in montmorillonite. *Clays and Clay Minerals* 56 177-193.

Churakov, S.V. (2007). Structure and dynamics of the water films confined between edges of pyrophyllite: A first principle study. *Geochimica et Cosmochimica Acta* 71 1130-1144.

González Sánchez F., Juranyi F., Gimmi T., van Loon L.R., Unruh T., Diamond L.W. (2008). Translational diffusion of water and its dependence on temperature in charged and uncharged clays: A neutron scattering study. *Journal of Chemical Physics* 129 174706.

Generation of a semi-stochastic cracks network for modelling mass transfers and chemical reactions - Application to a vitrified nuclear wastes block -

David Crevoisier and Frédéric Bouyer
CEA, DEN, Laboratoire du Comportement à Long Terme, F-30207 Bagnols-sur-Cèze, France

Introduction

Vitrification is the process chosen in France as well as in several others countries to immobilize high-level radwaste after the treatment of spent nuclear fuel. Calcined waste mixed with additives is molten at around 1100°C and then poured into stainless steel containers. During the cooling of the glass block, a cracks network appears to release mechanic constrains due to the change of density with the temperature decrease. To store glass containers in a deep geological disposal, the actual French concept considers that the overpack and the container will be corroded after 4000 years and the glass alteration by the groundwater will occur on the whole apparent surface named reactive surface (external surface and as well as cracks surface), leading to a fraction of radionuclides to be released in the closed surrounding environment. Long term behaviour of the glass block in the geological disposal concept mainly depends on the glass alteration rate and the reactive surface of the glass. Indeed, exposed to water, the altered glass releases a total amount of elements (including radionuclides) proportional to the reactive surface. The reactive surface of a nuclear glass block has been assessed by test performed on full scale glass block but the cracks network has not been yet modelled.

Due to the high complexity of the cracks network, its characterisation is the first essential step to achieve. It will allow to link between the different observations performed in laboratory and the further numerical modelling of long-term flow and chemical behaviour within the cracked glass block.

For mostly numerical modelling tools used in this work, the domain is generally represented by a mesh, which characteristics influence the quality of the numerical behaviour of the simulations. In the context of this study, the mesh should be:
- representative of a real network,
- coherent (conform to the specificities of the modelling tools) and
- with identifiable and controllable characteristics (in order to study the effects of different types of networks on the physical behaviour of simulated processes)

The aim of this work is thus (i) to define the nature of the characteristics of a known cracks network, to then (ii) be able to generate a set of stochastic meshes with common characteristics. Due to the complexity of the represented domains, a straight simulation using these generated meshes could lead to serious numerical problems (excessive computing time and numerical divergence). The search for an equivalent porous media could be an interesting solution and an alternative to reduce these problems. Modelling mass transfers and chemical reactions within these different meshes will allow linking up typical physical behaviours to networks characteristics.

Characterisation of an observable cracks network

The first step of this work is to define the global and local characteristics of a sample analysed by tomography and representative of an inactive glass canister. A numerical post-treatment gives a set of facets for visualising the cracks network. The process consists then first in rebuilding the neighbourhood of the facets list. This step is performed using an octree structure to store geometrical data. The octree is a space-dividing, hierarchical tree data structure for the discretized representation of 3D volumetric geometry (Meagher et al. 1982). Each final node (octree leaf) contains only one point. This representation allows significant optimisations of geometrical operations with high numerical and time performances. As an example, the figure 1 illustrates the search of a point which coordinates are known in a set of points.

A pre-treatment of these data is then performed. It allows the verification of the topological coherence of the network (each element - facets, segments and points - are properly linked to the adequate number of neighbours, no superposition of facets occurs) and a cleaning of facets to discard non-pertinent information (particularly, facets which area is lower than a user defined criterion). Geometrical processes (O´Rourke 1998), derived from the decomposition of a volume into convex parts, define the median lines of the network. Their analysis allows a quantitative and qualitative definition of the sample characteristics. It gives statistical distributions of directions, lengths and apertures of the cracks as well as their connectivity.
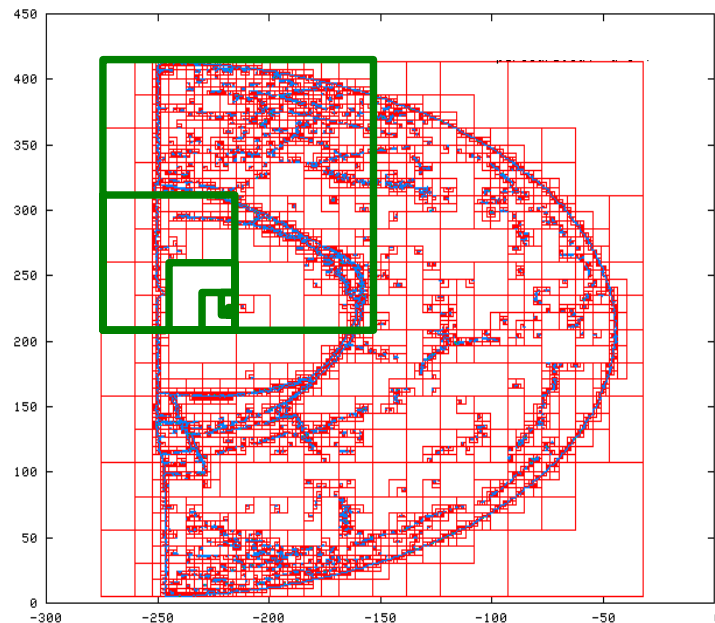
Fig. 1. Division and subdivision of a spatial domain containing a set of points (in blue) according to the octree method. The octree structure (degraded here in 2D) allows the search of a point in 6 steps (green boxes) whereas a standard direct method scans the whole set of points. The red boxes are the spatial domain corresponding to each node of the tree.

Generation of a semi-stochastic cracks network

Thanks to the previously set up algorithmic processes, the semi-stochastic network generator is developed following the inverse progression. First, statistical distribution

of directions, lengths and connectivity is provided by the user and allows the network stochastic generation of median lines on which an aperture distribution is associated. Thus, all generated meshes have some controllable characteristics and some stochastic characteristics. This tool would also be able to capitalise different sources of data (tomography, microscopy) with different resolutions. Moreover, studies currently led in French laboratories (CEA, IMFS, ENS Ulm, Ecole Polytechnique) on the genesis of the cracks network could be later used to improve the representative aspect of the semi-stochastic network.

Search of equivalent porous media

Considered domains can be complex. It deals with glass blocks which dimensions are around the meter, whereas the dimensions of some cracks can be close to the micrometer. Modelling mass transfers and chemical reactions on such domains can lead to prohibitive computing time and numerical divergence of the simulations even if calculation capacities involved are significant. Simulations on equivalent porous media could reduce drastically these problems. Experiments led by Laure Chomat (Chomat 2008) on the alteration of a structured homogeneous glass network (figure 2) will allow a first calibration and validation of this search for homogenised coefficients. Modelling tools available and used in our laboratory are Trio_U (Bieder et al. 2003) for simulating mass transfer and Hytec (van der Lee 1997) for simulating chemical reactions.
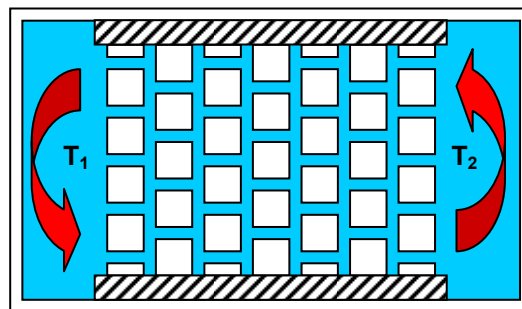
Fig. 2. Alteration experiments on a structured homogeneous glass network (2). A heat gradient provides a flow through the network. The apertures of the cracks are constant. The total amount of leached glass elements is monitored for more than one year now, as well as the water velocity in some points of the network.

The second step consists in extending the first one to a structured network with non constant cracks apertures (figure 3) modelized by an anisotropic matrix permeability for the media. Finally, these conclusions will be brought into a general use for the definition of an equivalent porous media to model an unstructured stochastically generated network (figure 4).
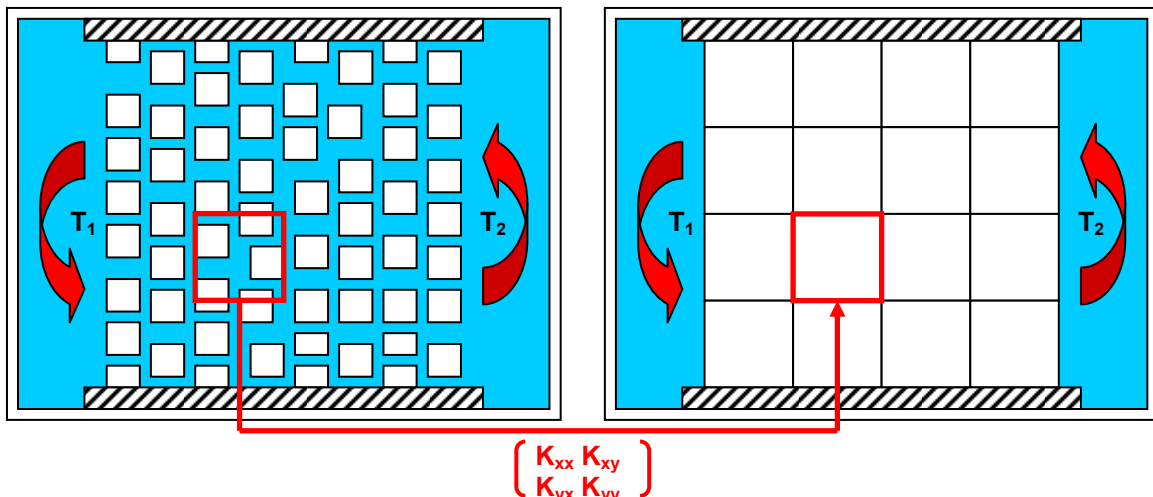
Fig. 3. Definition of an equivalent porous media for a structured network with non-constant cracks apertures. The equivalent porous media is defined by blocks. Each block is characterized by its porosity and its anisotropic permeability.
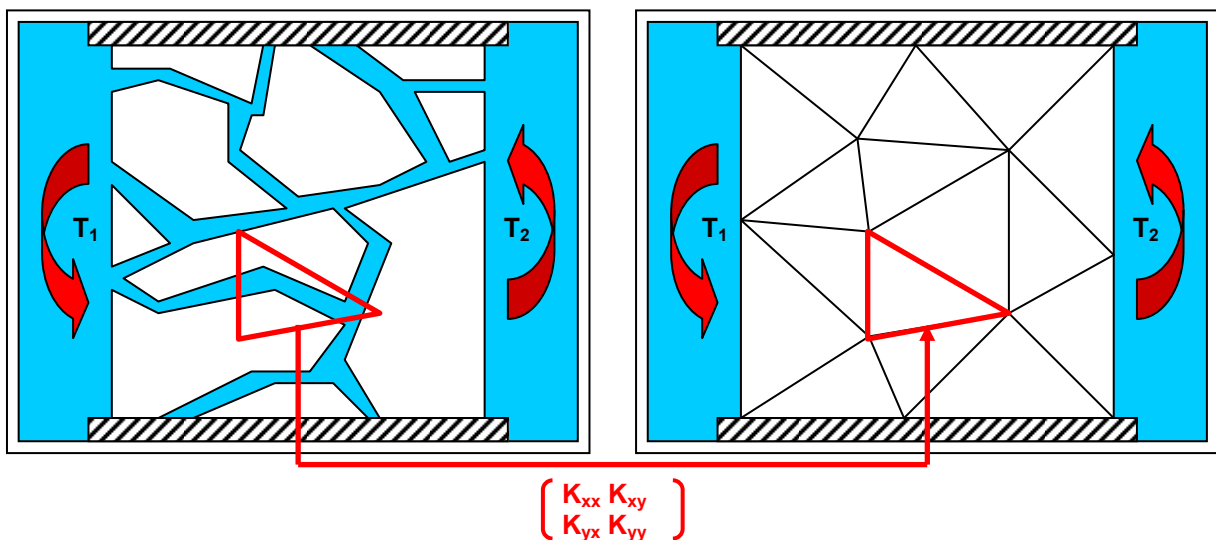
Fig. 4. Same method as described in figure 3, applied on an unstructured semi-stochastic generated network.

For each network system, the main challenge is, the definition of the geometrical characteristics of the representative elementary volumes which minimise the errors on the simulations results between a mesh described explicitly by each cracks and the homogenised mesh.

References

Meagher D. (1982). Geometric modeling using octree encoding, IEEE Computer Graphics and Image Processing 19 (2) pp. 129–147

O'Rourke, J. (1998). Computational Geometry in C (second edition). Cambridge University Press. New York.

Chomat L. (2008). Compréhension de l'altération à long terme des colis de verre R7T7 : étude du couplage chimie transport dans un milieu fissuré. Thèse de doctorat. Université Paris VI – Pierre et Marie Curie.

Bieder, U.; C.Calvin et al. (2003). Detailed Thermal Hydraulic Analysis of Induced Break Severe Accidents using the massively parallel CFD code Trio_U. 5th International Conference on Supercomputing for Nuclear Applications (SNA - 2003) 22/09/2003 - 24/09/2003 Paris France.

van der Lee, J. (1997). Modélisation du comportement géochimique et du transport des radionucléides. PhD Ecole nationale supérieure des Mines de Paris.

DIAMOND: Academic Innovation in Support of UK Radioactive Waste Management

Neil Hyatt[1], Simon Biggs[2], Francis Livens[3], James Young[2] and Nick Evans[4]

[1]*Dept. of Engineering Materials, The University of Sheffield, Mappin St, Sheffield, S1 3JD, UK.*

[2] *School of Process, Environmental and Materials Engineering, University of Leeds, LS2 9J2. UK.*

[3] *Dept. of Chemistry, The University of Manchester, Oxford Road, Manchester, M13 9PL. UK.*

[4] *Dept. of Chemistry, Loughborough University, Ashby Road, Loughborough, LE11 3TU, UK*

INTRODUCTION

Policy for the management of the UK's radioactive waste legacy resulting from 60 years of civil nuclear power has been defined in several recent reports [1-5]. The overall cost of waste treatment, packaging and storage, together with decommissioning and remediation activities, for which the Nuclear Decommissioning Authority (NDA) are currently responsible, is estimated to be £70 Bn [6,7]. Geological disposal of radioactive wastes, in a mined repository, is now accepted by Government as the "best available approach" for long-term management of the waste. It is to be supported by a "robust programme of interim storage" - recommended by the Committee for Radioactive Waste Management (CoRWM) [3-5].

It is recognised that academic research and development will play a pivotal role in reducing the cost and timescale of the clean-up and decommissioning programme [8]. Furthermore, public confidence in radioactive waste management and disposal depends on rigorous peer review of the academic understanding, data and models that underpin the long-term predictions of wasteform behaviour and evolution of the disposal environment [3,9]. The research challenge is compounded, however, by a critical nuclear skills shortage: it is estimated that the UK nuclear defence, power, and clean-up industries require more than 15,000 new degree level professionals in the next 15 years, and this number excludes potential demand from new nuclear build, repository construction and renewal of the nuclear deterrent [10].

Recognising that "integration of [academic expertise in] biological, environmental, and physical sciences together with engineering" was essential to "stimulate novel ideas/approaches in nuclear waste management", the UK Engineering and Physical Research Council (EPSRC) launched a "Call for Research Proposals in the area of Nuclear Waste Management and Decommissioning" in 2007. The DIAMOND consortium, was awarded £4.3 M, to deliver a 4 year national research and training programme in radioactive waste management across the Universities of Leeds, Loughborough, Manchester and Sheffield, and University and Imperial Colleges, London. This consortium is the first integrated trans-disciplinary and multi-institution academic research network in the UK, focused on radioactive waste management. Broadly, the strategic aims of the consortium are to:

- Carry out internationally leading science and engineering in the broad area of decommissioning and radioactive waste management.

- Support research that will underpin the development of innovative technologies for nuclear decommissioning, waste management and disposition.
- Broaden the UK research base in science and engineering that focuses on radioactive waste technologies and thereby help address a developing skills gap.
- Develop and support new links between investigators in universities that have established nuclear science programmes and those universities that are developing such programmes.
- Develop new inter- and intra-university links to facilitate multi-disciplinary collaboration   and stimulate new applications of knowledge at the interface between disciplines.
- Train the next generation of scientists and engineers in nuclear waste management and decommissioning.

STRUCTURE AND ORGANISATION

Activities are arranged in 3 Work Packages (WPs) and Cross-Cutting Themes (CCTs). The matrix structure has been designed to maximise opportunities for sharing and exchange of knowledge across the consortium. The identifiers in each box refer to individual research projects described in detail on our website (www.diamondconsortium.org). The aim is to link activities that can take a particular waste type (for example corroded Magnox sludge) from its current state through characterisation and handling to treatment and packing, interim storage to secure disposal. The CCT champions are recognised experts who will take responsibility for maximising knowledge and technology transfer between the WPs.

Table 1: Matrix detailing work packages and cross cutting themes.

			Cross Cutting Themes		
			CCT1 Characterisation	CCT2 Treatment & Packaging	CCT3 Disposal
			Francis Livens (Manchester)	Neil Hyatt (Sheffield)	Howard Wheater (Imperial)
Work Package	WP1 Environment, Migration & Risk	Nick Evans (Loughborough)	1.3.1.1, 1.3.1.2, 1.3.1.4, 1.3.2.1	1.3.1.1, 1.3.1.3, 1.3.1.4, 1.3.2.2, 1.3.3.1, 1.3.3.2	1.3.1.1, 1.3.1.2, 1.3.1.3, 1.3.1.4, 1.3.2.1, 1.3.2.2, 1.3.3.1, 1.3.3.2, 1.3.3.3, 1.3.3.4
	WP2 Decommissioning, Legacy & Site Termination	Mike Fairweather (Leeds)	2.3.1.1, 2.3.2.1, 2.3.2.2, 2.3.3.2, 2.3.3.3	2.3.1.2, 2.3.1.3, 2.3.1.4, 2.3.2.2, 2.3.2.3, 2.3.2.4, 2.3.3.1, 2.3.3.2, 2.3.3.3	2.3.1.4, 2.3.2.4
	WP3 Materials Design, Development & Performance	Bill Lee (Imperial)	3.3.1.3, 3.3.3.2	3.3.1.1, 3.3.1.2, 3.3.1.3, 3.3.2.1, 3.3.2.2, 3.3.2.3, 3.3.2.4, 3.3.3.2, 3.3.3.4, 3.3.4.1, 3.3.4.2, 3.3.4.3	3.3.1.1, 3.3.1.2, 3.3.1.3, 3.3.2.1, 3.3.2.2, 3.3.2.3, 3.3.2.4, 3.3.3.1, 3.3.3.2, 3.3.3.3, 3.3.3.4, 3.3.4.1, 3.3.4.2, 3.3.4.3

The consortium staff are from a wide range of disciplines, such as radiochemists, radiation chemists, physicists, materials, earth and environmental scientists and process, civil and structural engineers. Each project includes a minimum of 2

researchers from different disciplines and/or universities. We believe this will provide an invaluable opportunity to stimulate new ideas across disciplines where contact rarely occurs. We are also deliberately interfacing with researchers who may not conventionally see a role in the nuclear waste research area. The diversity of issues to be addressed is immense and requires a wide range of innovative solutions drawn from an equally wide range of disciplines, as summarised schematically in Fig. 1. The consortium's main purpose is to be adventurous and deliver real innovation, and the majority of our scientific program falls within this description. However, we also believe that there is a role for the consortium to play in the delivery of research that will have a more immediate value to the industry and we will explore how the consortium can have maximum short-term impact.
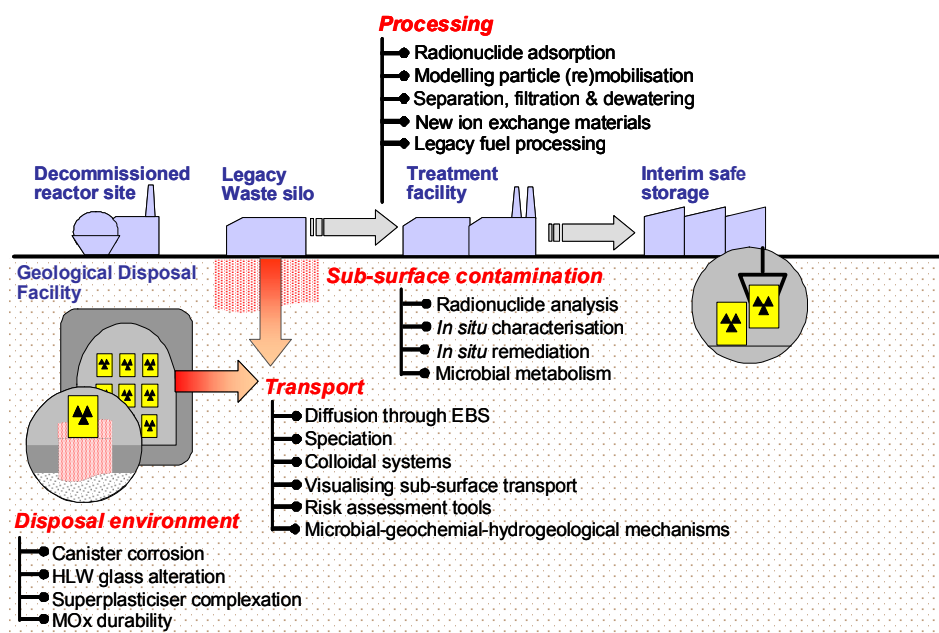
Fig. 1. Schematic representation of research questions to be addressed by the DIAMOND consortium.

WP 1: Environment, Migration and Risk - to define the processes which control transport of key radioactive contaminants in natural and engineered environments.

Cleaning up contaminated land is a substantial component of site restoration and forms the major focus. Large volumes of contaminated land are present at many nuclear sites, notably Sellafield. The range of contaminants present, and the potential for mixed contamination, represents a major challenge. In particular, the potential for migration of soluble and colloidal species in the subsurface is a key uncertainty in defining site end points, developing decommissioning and clean-up strategies, and quantifying the associated costs. Currently, most clean-up is through invasive technologies, so there is an opportunity to innovate through exploitation of more cost-effective *in situ* technologies such as barrier treatment systems. Many of the uncertainties and technical challenges associated with geological disposal of immobilised radioactive wastes are critically dependent on the rate of release from the engineered facility, and on the subsequent behaviour of the radionuclides in the

disturbed zone and the far field. These processes have close parallels in site remediation, so these two themes are linked in this work package.

WP 2: Decommissioning, the Historic Legacy and Site Termination - To provide new techniques and technologies in support of legacy waste management, decommissioning and monitoring of site end points.

Heterogeneous wastes in fuel storage and handling facilities are a key target of WP2; they comprise of irradiated fuel, contaminated materials and corrosion products. Volumes and compositions (chemical and radioactive) are poorly known, so improved and accurate characterisation is a priority, and technologies for retrieval and treatment are also required. Furthermore, past activities have created small volumes of "orphan wastes" for which no clear management route exists, whose diversity requires versatile methods for treatment and immobilisation. Links between proposed treatment strategies for these waste materials will obviously be beneficial, so information exchange is expected to be a key benefit of this consortium. Progress towards safe site end-points is a complex process, requiring the dismantling and removal of plant and buildings, identification, characterisation and removal of contaminated material, passive safe storage of packaged wastes and long-term monitoring of the cleared site. However, in contrast to substantial industrial activity in these areas, academic activity is relatively sparse. One approach is to seek out opportunities for technology transfer into the nuclear industry, particularly from the aerospace and medical sectors. We will also focus on quantification of inventories, contaminant transport through engineered pathways and waste retrieval. For site end points, long-term restriction of contaminant mobility is important, so cost effective *in situ* monitoring is a valuable technology, and the durability of waste containers in interim safe storage are important research questions.

WP 3: Materials - Design, Development and Performance - To provide innovations in the processing and immobilisation of problematic wastes, the synthesis of novel wasteform materials and improved understanding of wasteform and container performance in interim storage and disposal environments.

The focus is on immobilisation and safe interim storage of nuclear wastes and fuels. Decisions regarding the re-use, long term storage and disposal of some strategic nuclear materials, including Pu and spent fuels, require specific knowledge gaps to be addressed. A key task is to understand, quantify and predict the evolution during interim storage of spent AGR fuel, separated Pu and MOX fuel, in order to inform decisions on re-packaging and storage requirements. This is supported by research aimed at improving understanding of radiation damage mechanisms in model ceramic materials at a fundamental level. We will also undertake research, integrated with WP2, to address the immobilisation of high activity sludges, fuel element debris, and defence and pyrochemical wastes, in glass-ceramic wasteforms. We aim to capture the advantage of high temperature processing technologies to deliver high volume reduction, throughput and product durability, while simultaneously achieving acceptable emission thresholds. This will be complemented by aiming at developing novel encapsulants and improved cementing systems for the encapsulation of reactive metals, graphite and loosely packed wastes. We will also develop novel routes to inert matrix fuels and ceramic wasteforms. A further element is addressing

a key knowledge deficit in the corrosion behaviour of UK HLW glasses, particularly actinide and fission product retention.

INDUSTRIAL ENGAGEMENT AND INTERNATIONAL LINKS

Industrial stakeholders and regulators will be key beneficiaries of the knowledge and understanding generated. Engagement with these organisations is an integral part of our activities, with aim of guiding research activity, to ensure delivery to end user requirements, providing access to corporate knowledge, technical expertise and laboratories in support of research and training to students and post docs. The consortium received strong support from over 20 companies for the successful proposal. Industrial stakeholders will also contribute to the activities of the consortium as members of the International Advisory Group, advising on strategic direction and providing ideas for development of the group. Members of the consortium have a range of important international partnerships in nuclear research, e.g. ANSTO, FZK, CEA, Los Alamos, INL and PNNL. We will seek routes to allow these links to be developed for mutual benefit and are especially interested in developing collaborative opportunities for training.

REFERENCES

Managing Radioactive Waste Safely: Proposals for Developing a Policy for Managing Solid   Radioactive Waste in the UK, DEFRA, (2000).

The Nuclear Legacy: A Strategy for Action. Cm 5552 DTI London (2002)

Managing our Radioactive Waste Safely: CoRWM's recommendations to Government, (2006).

Moving Forward CoRWM's Proposals for Implementation: CoRWM 1703, (2006).

Managing Radioactive Waste Safely: A Framework for Implementing Geological Disposal. Cm 7386. DEFRA, London (2008).

Taking Forward Decommissioning. National Audit Office Report (2008).

Nuclear Decommissioning Authority Business Plan 2008-2011 (2008).

NDA Strategy Document, (2006).

Radioactive Waste: Special Eurobarometer 227 / Wave 63.2 - TNS Opinion and Social,   EC, (2005).

Nuclear and Radiological Skills Study- Report of the Nuclear Skills Group, (2002).

Modelling the Influence of Humic Acid on the Sorption of U(IV) to Kaolin

Nick Evans[1] and Nick Bryan[2]
[1]*Department of Chemistry, Loughborough University, Ashby Road, Loughborough, LE11 3TU, UK*
[2]*Centre for Radiochemistry Research, School of Chemistry, The University of Manchester, Oxford Road, Manchester, M13 9PL, UK*

Safety assessments for radioactive waste disposal require estimations of the migration of radionuclides in heterogeneous terrestrial environments. Immobilisation of radionuclides on minerals in aquatic systems exerts an important influence on migration through the geosphere. Natural organic matter, especially humic substances, can significantly affect the transport of radionuclides. Mobile and immobile humic acid (HA) will be present in the geosphere, capable of exerting opposing effects on radionuclide transport, due to the formation of mobile and immobile metal-humate complexes.

Many potential radioactive waste repository far-field conditions are reducing, so any uranium present is likely to be in the +4 oxidation state. Normally U(IV) is sparingly soluble and, therefore, essentially immobile, either due to precipitated solid phases such as $UO_2(am)$, or immobilisation on mineral surfaces. However, in environmental systems it could complex with humic acid and become mobile, whilst on the other hand, HA-U(IV) complexes could sorb to surfaces and become immobile.

This study examines the relationship between the distribution of humic acid between aqueous and immobilised phases and the distribution of U(IV) between the same phases. Given that the binding of U(IV) to HA is strong (Warwick et al.) it might be assumed that U(IV) will 'follow' the distribution of humic acid, and not be directly affected by the kaolin surface. Were this to be the case, it would make the prediction of U(IV) migration in humic acid containing groundwaters much simpler. This is the hypothesis tested in this work, using kaolin as a representative solid phase, and varying pH from 4 to 8. Although the binding between U(IV) and humic acid is strong, it also varies significantly with pH (Reiller et al. 2008), hence rather than measure the value of log β for every different pH used in the study, the relationship derived from Reiller et al. was used, i.e. log βHA = 3.26 pH + 0.14. Data from Warwick et al. (experimental measurements of log β for U(IV)-AHA) were used, amongst others, for deriving the relationship. The hypothesis can be indirectly tested experimentally by investigating the following relationship:

$$\frac{[U]_{kaolin}}{[U]_{solution}} \, \alpha \, \frac{[HA]_{kaolin}}{[HA]_{solution}} \, or \, \frac{[U]_{kaolin}}{[U]_{solution}} = c \frac{[HA]_{kaolin}}{[HA]_{solution}}$$

Hence, a graph of [U]sorbed/[U]solution as a function of [HA]sorbed/[HA]solution can be plotted, and if the gradient (c) is equal to 1, then the surface is not contributing directly to the binding, since [U]sorbed and [U]solution are determined only by [HA]sorbed and [HA]solution. However, if c is not equal to 1, then the surface is contributing directly to [U]sorbed.

Experimental

All solutions were prepared in an N_2 atmosphere, using water that had been sparged, boiled and contacted with Fe(s) to remove traces of O_2. Kaolin (Aldrich) (mean particle diameter 570 nm, BET surface area 10.88 m^2 g^{-1}, CEC 5.2 meq/100 g) was used as supplied. ^{233}U was purchased from Amersham. Previously characterised (Fairhurst 1996) Aldrich HA (mean molecular mass = 5700 amu, mean diameter = 2.663 nm, PEC = 5.3 x 10^{-3} mol g^{-1}) was used. 4-morpholineethanesulfonic acid (MES, Fisher) was used to stabilise pH and provide a minimum ionic strength.

A U(IV) stock solution was prepared by precipitating amorphous $UO_2 \cdot 2H_2O$ in NALGENE bottles by mixing CO_3^{2-} free NaOH, $Na_2S_2O_4$(aq) and $UO_2(NO_3)_2$(aq). After 2 weeks the precipitates were centrifuged, washed with $Na_2S_2O_4$ solution and re-centrifuged. The majority of the supernatants were then removed by filtering and the uranium solubility measured. This was found to be between 1.2 and 4.6 x 10^{-9} mol dm^{-3}, indicating complete reduction. This solution was used to prepare U(IV) solutions at the required pH values at 1.0 x 10^{-9} mol dm-3. 20 cm^3 aliquots were contacted with 0.1 g of kaolin in NALGENE vials in the presence of 15 to 200 ppm HA. Samples were prepared in duplicate, mixed, and equilibrated for 14 days. The pH was then measured before filtering and measuring the activity remaining in solution. To determine the distribution of HA between solution and solid phases, solutions of HA the absorbance of these solutions was measured at 254 nm.

Results and Discussion

In a comparable U(IV)–kaolin binary system around 20-40% of the U(IV) was in solution, with the greater immobilisation occurring at higher pH (Evans et al. 2009). In this study, the presence of humic acid solubilised up to 90% of the U(IV), with higher solubilities at higher HA concentrations and pH values. However, examining the results in more detail shows the following. At pH 4, low HA concentrations (15 to 50 ppm) resulted in more immobilisation of U(IV), leaving between 10 and 35% in solution, as opposed to 40% in its absence. At 75 ppm HA, 42% was solubilised and at higher concentrations (100-200 ppm) up to 94% of the U(IV) was in solution at steady state. At pH 6, in the absence of HA 27% of the U(IV) was in the aqueous phase. At HA concentrations above 15 ppm, more than 27% of the uranium were solubilised, up to 85% at 200 ppm. At pH 8, in the absence of HA, 20% of the U(IV) was in the aqueous phase, however, even small concentrations of HA such as 15 ppm, caused a large increase in the aqueous concentration of U(IV), from 40% at 15 ppm to 90% at 200 ppm. The final Eh of the systems indicated that good redox control had been maintained.

The main reason for performing these studies is to enable predictive modelling to be used on the huge variety of systems of a related nature. If the kaolin surface is not saturated then there is the possibility of U(IV) binding to the surface directly, or via an humic acid ternary complex. The degree of coverage of the kaolin surface by humic acid can be roughly estimated by assuming monolayer coverage and that the humic acid molecules are flat tessellated circles. Calculations give a value of between 2 and 29% surface coverage, depending on pH and [HA]. This leaves a large proportion of kaolin surface available for humic acid fractionation or direct binding to U(IV).
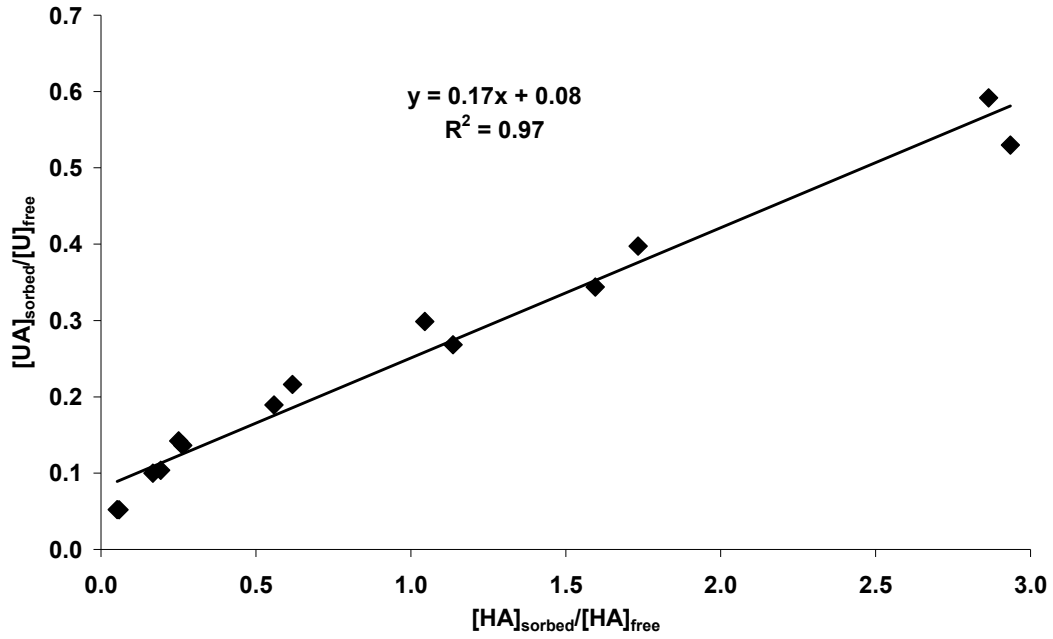
Fig. 1. U(IV) distribution as a function of HA distribution at pH 4, [HA] = 15-200 ppm, solid-solution ratio = 200 g ml^{-1}, [U(IV)]total = 1 x 10^{-9} mol dm^{-3}, Eh = -588 ± 48 mV.
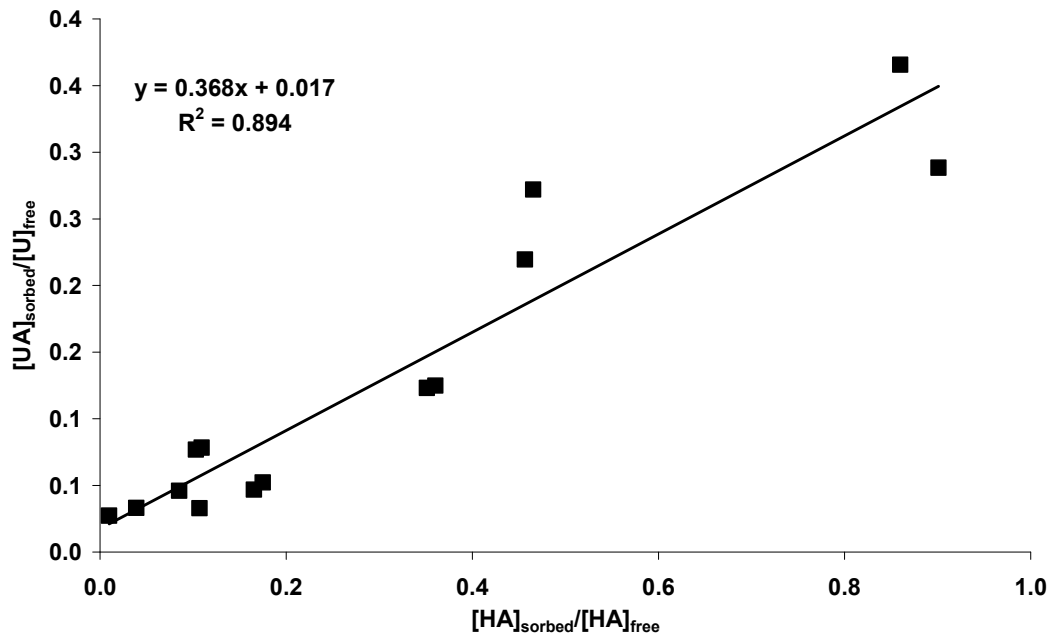
Fig. 2. U(IV) distribution as a function of HA distribution at pH 6, [HA] = 15-200 ppm, solid-solution ratio = 200 g ml^{-1}, [U(IV)]total = 1 x 10^{-9} mol dm^{-3}, Eh = -646 ± 29 mV.
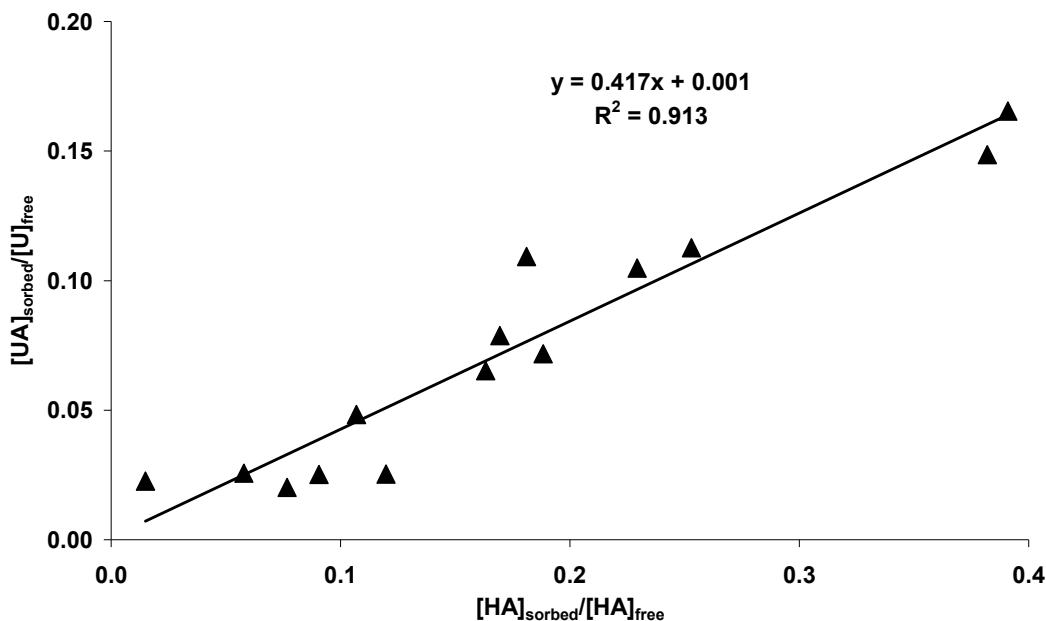
Fig. 3. U(IV) distribution as a function of HA distribution at pH 8, [HA] = 15-200 ppm, solid-solution ratio = 200 g ml^{-1}, [U(IV)]total = 1 x 10^{-9} mol dm^{-3}, Eh = -595 ± 40 mV.

Figures 1-3 show the ratio of kaolin-sorbed to solution U(IV) as a function of the ratio of kaolin-sorbed to solution humic acid. If the U(IV) distribution followed the humic acid distribution, the plots would have a gradient of 1. However, for these systems the plots have gradients of 0.17, 0.368 and 0.417 for pH 4, 6 and 8 respectively. These indicate that there is a lower level of uranium(IV) immobilisation than can be accounted for by just direct humic acid ternary immobilised complexes. This suggests that any fractionation of the humic acid on the surface is leading to the formation of a weaker U(IV)-HA complexes than the equivalent aqueous complex at that pH. However, this effect gets much less marked as the pH rises, and the U(IV)-HA binding becomes correspondingly stronger. An alternative explanation is the direct binding of U(IV) to kaolin is occurring. This should make the data susceptible to modelling by the linear additive model (LAM). However, attempts to fit this data to the LAM completely fail, suggesting that the former explanation is more likely, i.e. that the U(IV) does indeed bind to the surface via ternary complexes, but that the binding in these surface complexes is weaker than the equivalent aqueous U(IV)-HA species.

Conclusions

In the equivalent U(IV)–surface binary system ca. 20-40% of the U(IV) was in solution, with more immobilisation occurring at higher pH values. humic acid solubilised up to 90% of the U(IV), with higher solubilities at higher humic acid concentrations and higher pH values. However, there was a lower level of U(IV) immobilisation than can be accounted for by just measuring humic acid immobilisation. This suggests that any fractionation of the humic acid on the surface is leading to the formation of a weaker U(IV)-HA complex than the equivalent aqueous complex at that pH. However, this effect gets less marked as the pH rises.

Acknowledgements

References

Fairhurst AJ, (1996). The Role of Inorganic Colloids in the Transport of Toxic Metals Through the Environment, Doctoral Thesis, Loughborough University

Reiller P, Evans NDM, Szabó G (2008). Conditional stability parameters for the actinides(IV)-humic acid system: a search for consistency. Radiochim Acta, 96(6):345-358

Warwick P, Evans N, Hall A, Walker G, Steigleder E (2005). Stability Constants of U(VI) and U(IV)-Humic acid Complexes. J Radioanal Nucl Chem, 266(2):179

Evans N, Warwick P, Lewis T, Bryan N (2009). The Influence of Humic Acid on the Sorption of Uranium(IV) to Kaolin, Submitted to Environmental Chemistry Letters, January 2009

The Impact of Extreme Climate States on the Radionuclide Transport in the Overburden of a Salt Dome

Judith Flügge[1], Eckhard Fein[1], Ulrich Noseck[1], Anke Schneider[1]and Walter Pohl[2]

[1] Gesellschaft für Anlagen- und Reaktorsicherheit, Abteilung Langzeitsicherheitsanalysen, Theodor-Heuss-Str. 4, 38122 Braunschweig, Germany
[2] Technische Universität Braunschweig, Institut für Umweltgeologie, Pockelsstr. 3, 38106 Braunschweig, Germany

In long-term safety assessments for radioactive waste repositories, geological timescales have to be considered. A time frame for the assessment of one million years is proposed in the course of the revision of the German safety criteria. Drastic climatic changes are expected to occur during that time. The aim of this study was to identify the main effects of extreme climatic changes on the groundwater flow and the transport of radionuclides through the sedimentary overburden of a hypothetical nuclear waste repository in a salt dome in Northern Germany by means of numerical modelling. Although for a normal evolution of a repository in rock salt, the radionuclide mobilisation and release from the host rock can be excluded, it has to be considered in a safety case. The Gorleben-Rambow salt structure was selected as a reference site (Klinge et al. 2007; Köthe et al. 2007).

The regarded future climate states were selected taking paleo-climatological information and model calculations into account. In recent years, the anthropogenic influence on the climate evolution raised increasing interest. Comprehensive model calculations show that very high anthropogenic emissions of persistent greenhouse gases might lead to long-term changes in climate evolution on a time scale of up to several tens of thousand up to hundred thousand years. Therefore, a future glacial might be protracted for another 500,000 years (Archer and Ganoploski 2005). Based on this, a climatic evolution with constant climate conditions was selected as a reference (Constant Climate). An important feature of the interglacials was the change in sea level due to the melting of the ice sheets. Model calculations predict a possible global sea level rise up to approx. 80 m as a result of the melting of the world-wide ice volume (Williams and Hall 1993). At the Gorleben site, this would result in a sea level of approx. 50 m above ground. A second climate state, the Sea Water Inundation state, was derived from these model calculations. During the Pleistocene, several glacials and interglacials occurred with different impacts on the examined site. The Elsterian and Saalian Glacial featured a large glaciation with an inland ice-sheet that covered the Gorleben area. The Weichselian ice-sheet did not extend as far (Ehlers at al. 1984). Thus, the Gorleben area was not covered by an ice-sheet during the Weichselian but instead was subject to periglacial permafrost conditions with depth up to 140 m (Klinge at al. 2007). A future glaciation is assumed to have an ice-sheet extension similar to the Weichselian. These conditions were chosen as a third possible future climate state, referred to as the Permafrost state.

To identify the impacts of the selected climate states on the groundwater flow and the radionuclide transport, a generalised two-dimensional model was set up according to the geology of the Gorleben-Rambow salt structure (Fig. 1). The north-south striking abstracted model has a length of 16.4 km and a thickness of 400 m. It comprises three hydrogeological layers representing a lower and an upper aquifer with an intercalated aquitard. The model comprehends the most important structural

characteristics of the Gorleben hydrogeological system: The contact between the salt dome and the lower aquifer in the Elsterian Gorleben channel, the northwestern rim syncline, which was constituted during the uplift of the salt dome, and the local absence of the aquitard creating a direct contact between the upper and the lower aquifer. One hydraulic window is located in the southern area of the model. Due to the fact, that the existence and the location of further hydraulic windows are still beeing discussed, two model variations were realised. Model 1 features only one hydraulic window, while model 2 comprises a second hydraulic window at the northern boundary of the northwestern rim syncline. The current hydrogeological situation at the site was modelled in a first step (Present Climate). Based on this, the Constant Climate state was simulated. The flow simulations for the climate states Sea Water Inundation and Permafrost were started with the flow fields and salt concentrations resulting from the simulations for the Present Climate and Constant Climate. All flow simulations for future climate states were run over several 100,000 years until reaching the steady-state, hypothesising that the climate states will prevail for such long periods in time. The results could be compared and analysed, pointing out the main processes and the principle differences in flow and transport caused by each climate state. The transport simulations were run over one million years model time using constant flow fields. Selected radionculides with different sorption characteristics and half-lifes are: C-14, Zr-93, I-129, Cs-135 and the radionuclides of the uranium-238 decay series, U-234, Th-230 and Ra-226. They are assumed to enter the model area at the centre of the salt dome contact in the lower aquifer (Fig. 1). In addition to that, the influence of the mineralisation of the groundwater on sorption was taken into account by choosing respective sorption coefficients for each hydrogeological unit.
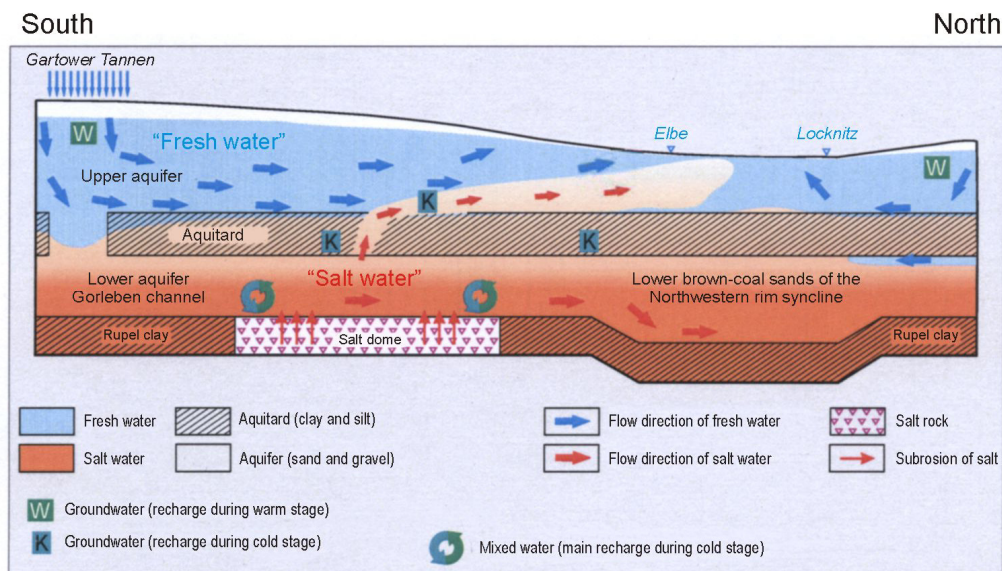
Fig. 1. Simplified, schematic cross section through the model area.

Groundwater flow and radionuclide transport differ strongly for the various climate states (Fig. 2, Fig. 3). Most important differences are constituted in the dominant transport process, i. e. advection or diffusion, the flow direction and the retardation of the radionuclides. This results in different arrival times at the model surface as well as different locations of maximum radionuclide concentrations at the surface. Apart from the dependence on the hydrogeological unit, the retarding role of the sorption

particularly depends on the salinity of the groundwater. The sorption coefficient is one of the most important parameters. For example, the strongly sorbing Zr-93 does not reach the model surface in any climate state, while the weakly sorbing I-129 is found at the model surface in each climate state.

With the presented hydrogeological model, the most important characteristics of the present hydrogeological system at the Gorleben site could be reproduced in sufficient detail (Present Climate). Assuming prevailing climatic conditions like in the Present Climate state, steady-state conditions will be reached after 150,000 years to 200,000 years at the most (Constant Climate). In both climate states, advection is dominating the groundwater flow. The second hydraulic window in combination with an enlarged inflow into the lower aquifer in model 2 causes different flow directions of the groundwater within the lower aquifer compared to model 1. The flow is directed southward in model 1 and northward in model 2. In model 2, the upper aquifer shows fresh water conditions, while the aquitard and the lower aquifer show saline conditions. Saline conditions are found in all units of models 1. Kd values were set accordingly. Maximum radionuclide concentrations are therefore found in the southern part of the model surface in model 1 and in the northern part above the second hydraulic window in model 2 (Fig. 3 a). All radionuclides except Zr-93 reach the model surface within the time span of one million years.

For the Sea Water Inundation state, the North Sea is assumed to transgress into the area during a warm stage. Therefore, a water column of 50 m thickness and a salt concentration equal to the North Sea salt concentration was supposed to cover the model area. In this climate state, it takes more than 700,000 years to reach steady-state salt concentrations, while a steady-state flow field is reached after less than 50,000 years already. Groundwater flow ceases and diffusion processes are affecting the distribution of contaminants. Saline conditions were found in all hydrogeological units. The fact, that the dominant transport process for the radionuclides is the diffusion yields to the following consequences: Firstly, hydrogeological properties have a low impact on the transport and therefore the results for the radionuclide transport in the two models are nearly identical. Secondly, radionuclide transport takes place radially from the source, so that the radionuclides reach the model surface approx. vertical above the salt dome (Fig. 3 b).

The periglacial Permafrost state is caused by a near-by inland ice sheet during a cold stage. Formation of permafrost is restricted to the upper aquifer. In the model, permafrost is imple-mented in form of a distinct reduction of permeability. Unfrozen zones with the original perme-ability of the aquifer occur under the thermal influence of rivers and lakes, here the rivers Elbe (above the northwestern rim syncline) and Seege (at the southern border of the model). A high fresh water inflow into the lower aquifer from the north is implemented on the account of a near-by inland ice sheet and its melt water, which infiltrates into the lower aquifer further north. Thus, the highest flow velocities are observed for this climate state in the lower aquifer, where advection is the dominant transport process. Most of the radionuclides are flushed out of the model domain in the lower aquifer. Diffusion dominates in the frozen upper aquifer. Freshwater presence in parts of the model domain induces a higher sorption of the radionuclides (model 2). Therefore, the sorption coefficients are elevated here and the radionuclides are retarded more. Most of the radionuclides are transported out of the model domain in the southern direction. For example, Cs-135 does not reach the model surface within one million years (Fig. 3 c). Maximum radionuclide concentrations at the surface are observed in the unfrozen zones.

a: *Constant Climate*

b: *Sea Water Inundation*

c: *Permafrost*
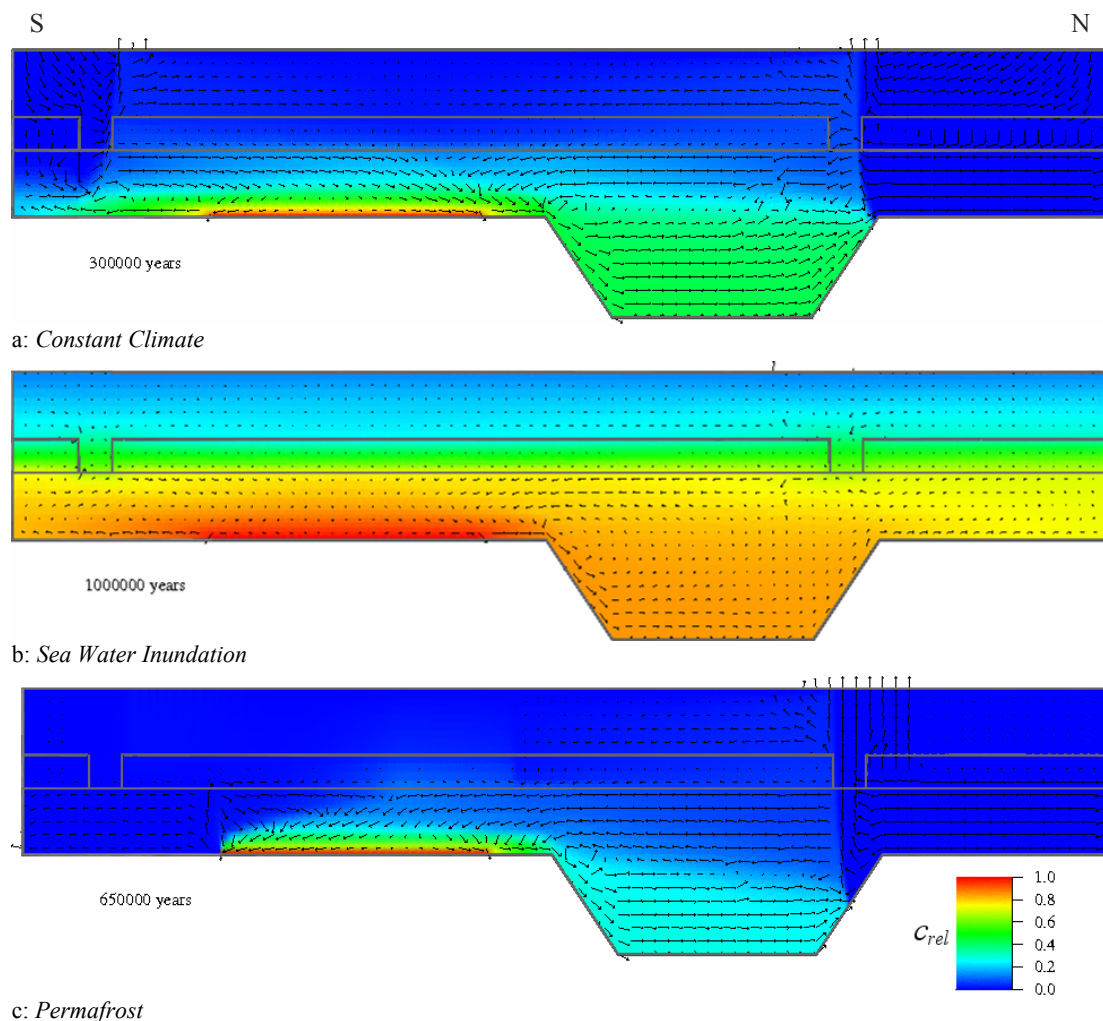
Fig. 2. Relative salt concentrations (colours) and groundwater velocity fields (length of velocity vectors proportional to velocity) for the different climate states.

This work is the basis for more detailed investigations regarding the impact of extreme climatic changes on the safety of radioactive waste repositories. Two follow-up projects will furthermore improve the knowledge about possible impacts of extreme climate changes. The aims of the projects are to use more complex models regarding the hydrogeology and to combine the different climate states in more realistic time spans and sequences. It is intended to use temporally and spacially variant sorption coefficients that depend on the actual geochemical conditions.

a: *Constant Climate*

b: *Sea Water Inundation*
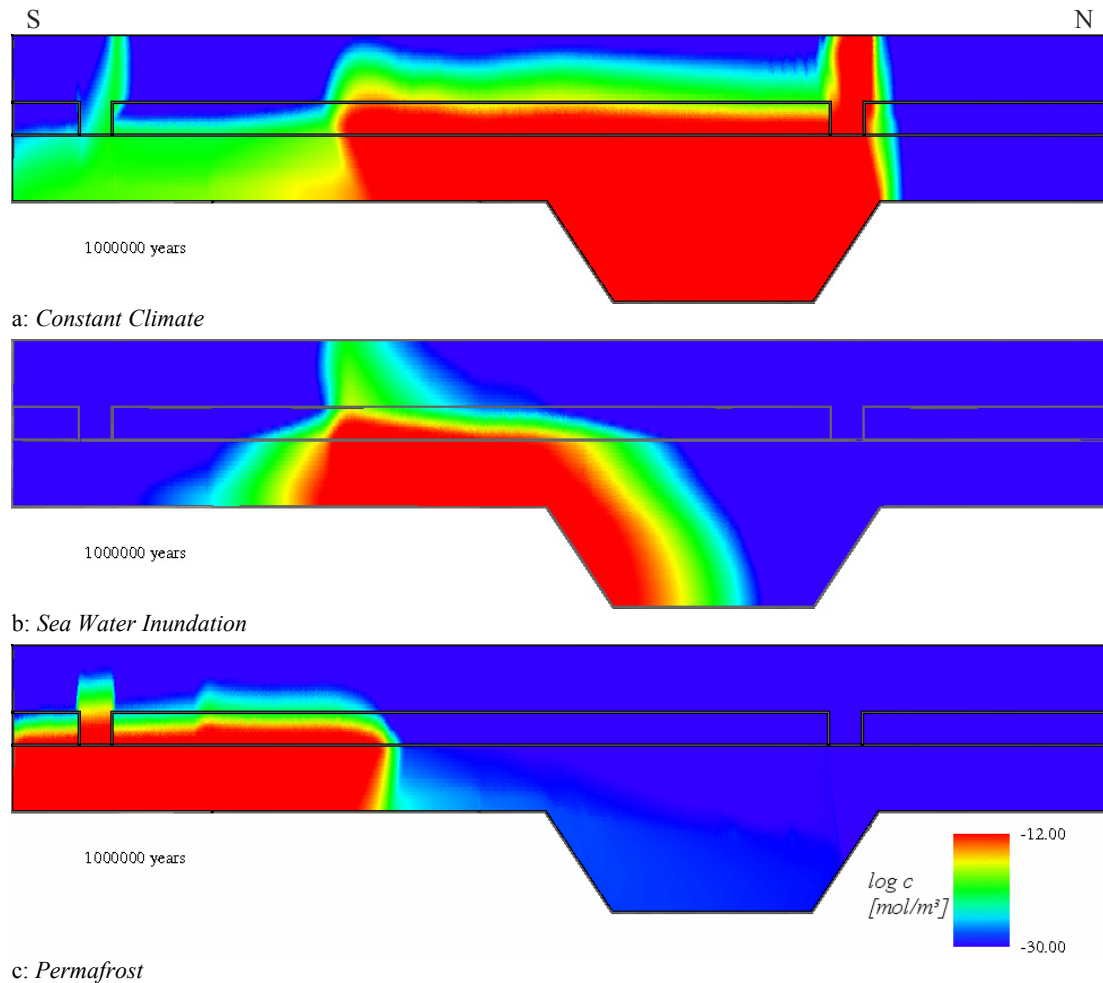
c: *Permafrost*

Fig. 3. Cs-135 concentrations for the different climate states after 106 years model time.

References

Archer D., Ganopolski A. (2005). A movable trigger: Fossil fuel CO2 and the onset of the next glaciation. Geochem. Geophys. Geosyst. 6, Q05003, doi:10.1029/2004GC000891

Ehlers J., Meyer K.-D., Stephan H.-J. (1984). The pre-Weichselian Glaciations of North-Western Europe. Quat. Sci. Rev. 3: 1-40

Klinge H., Boehme J., Grissemann C., Houben G., Ludwig R.-R., Rübel A., Schelkes K., Schildknecht F., Suckow A. (2007). Standortbeschreibung Gorleben, Teil 1: Die Hydrogeologie des Deckgebirges des Salzstocks Gorleben. Geol. Jb., C 71: 199

Köthe A., Hoffmann N., Krull P., Zirngast M., Zwirner R. (2007). Standortbeschreibung Gorleben, Teil 2: Die Geologie des Deck- und Nebengebirges des Salzstocks Gorleben. Geol. Jb. C 72: 147

Williams R.S., Hall D.K. (1993). Glaciers. In: Gurney, R.J., Foster, J.L., and Parkinson, C.L. [Eds]: Atlas of Satellite observations related to global change. Cambridge (Cambridge Univ. Press), 401-422.

A Fortran 90 object-oriented tool for geochemical processes

Pablo Gamazo[2], Sergio A. Bea[1], JesusCarrera[1], Carlos Ayora[1], Francesc Batlle[2] and Maarten W.Saaltink[2]

[1]*Institute of Earth Sciences, 'JaumeAlmera' (CSIC), c/ LluisSole` i Sabaris s/n, 08028 Barcelona, Spain*
[2]*Technical University of Catalonia (UPC), c/ Jordi Girona 1-3, 08034 Barcelona, Spain*

Introduction

Reactive transport modeling is extensively used to understand migration of solutes and their interaction with geological materials. This discipline has exerted an important influence on numerous Earth Science fields including hydrogeology, geochemistry (Ayora et al. 1998), biogeochemistry (Mayer et al. 2001), soil physics (Simunek and Suarez 1994), and fluid dynamics (Bachler and Kohl 2005).

Reactive transport codes have been traditionally developed in languages such as Fortran77, Pascal, etc. These languages are based on procedural-oriented programming (POP).The fundamental unit of decomposition is the procedure that is coded as a subroutine or function. Codes beyond many 10^4 lines based on POP are rigid and monolithic, not easy to modify or extend (even by the code author). Meysman et al. (2003a) go as far as stating that a gap has developed between software engineering and reactive transport modeling. This gap cannot be reduced by means of POP. Object-Oriented Programming (OOP) may be a suitable alternative.

The main feature of OOP is its reliance on objects, which are data structures characterized by shared data types and functions applied to these data. Chemical processes entail a well defined identity (e.g. stoichiometric coefficients, equilibrium constants, concentrations, thermodynamic activity coefficients) that are used to perform well defined functions (speciation, mixing, equilibrium with mineral phases, etc). Thus, chemical processes seem ideally suited to OOP, which facilitates modularity and transportability in the implementation of chemical processes in other Earth Science applications. Modularity means that the tool could offer functions involving complex chemical calculations. External users (e.g. other codes) could carry out chemical calculations using this tool. Transportability means that the same tool can be implemented in different codes (e.g. in a conservative transport simulator, in a chemical speciation code).

The objective of this work is to present a specialized chemical process tool programmed in F90 and based on OOP termed CHEPROO (CHEmical PRocesses Object-Oriented). It provides the basic functionalities required for coupling to any transport simulator. By adopting the OOP methodology, this tool exhibits features such as extensibility and flexibility for users and programmers. A more detailed description of CHEPROO is given by Bea et al. (2009).

CHEPROO object-oriented inspired principles

OOP consists of grouping entities that share both the type of data that describe them and the type of functions they can perform. The resulting data structure (set of attributes) and functions (method) is termed a 'class'. Specific entities from a class

are called 'objects' resulting from assigning values to the attributes. For example, all chemical reactions have a name, a number of species, stoichiometric coefficients, an equilibrium constant, and if the reaction is kinetic, a rate law. Chemical reactions can perform maintenance operations (i.e. create, read, destroy) and be used for computing the concentration of secondary species (equilibrium reactions) or reaction rates (kinetic reactions). Therefore, 'reaction' defines the class and specific reactions (e.g. 'calcite dissolution/precipitation') would be objects of this class.

OOP is based on three features that facilitate the design, maintenance and growth of programs: 1) encapsulation, 2) inheritance and 3) polymorphism. Encapsulation of objects makes it possible to hide the details of internal implementation, while providing an explicit interface for them. This feature facilitates code extension because changes in internal details of the service can be made without affecting the use of the object. Inheritance is formally defined as the ability to reuse and share the data and methods of existing classes to construct hierarchical classes. For example, an object of the class 'phase' can be of type mineral, aqueous, gas (Fig. 2). This feature greatly facilitates extensibility. In the above example, simply adding the specialization 'solid mixture' would allow the code to work with this new type of phase without any other modification. Inheritance allows us to reuse previously created classes while reducing the size of the program. Polymorphism allows us to use the same name on methods implemented in different classes.

F90 supports object-oriented features like encapsulation and polymorphism, but unlike truly object-oriented languages such as C++ or Java, inheritance is not directly supported. However, it can be emulated according to Decyk et al. (1998). Details on OOP are given in Decyk et al. (1998), Akin (1999), Carr (1999), Meysmanetal. (2003a) and Gorelik (2004).

CHEPROO: Class organization

All the chemical processes are represented by a class termed CHEPROO. This class encapsulates two different classes termed Nodal Chemistry and Chemical System (Fig.1). The Nodal Chemistry class contains state data (e.g. concentrations, temperature, mass of water, cation exchange capacity) of a portion of the physical system and is designed to define many objects (e.g. nodes of a finite element mesh). The Chemical System class contains the entire description of a geochemical system (species, phases, reactions and kinetic laws. It is designed to describe few objects (e.g. zones of an aquifer with different active minerals). Both classes are associated with each other. The methods implemented in the Chemical System class are mainly used by the Nodal Chemistry class.
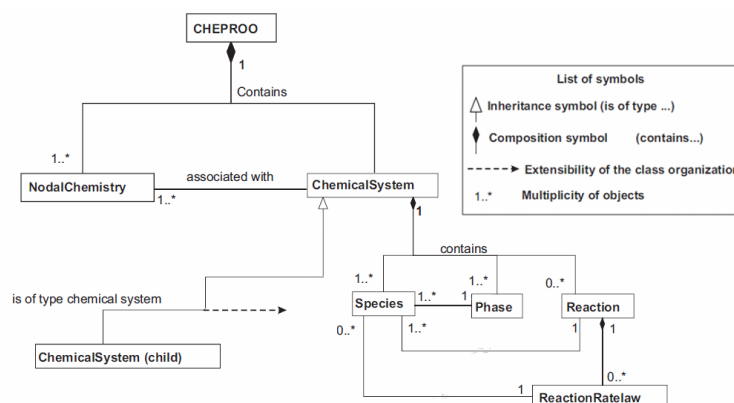
Fig. 1. Class organization of CHEPROO and Chemical System class.

3.1 Chemical system class, the geochemical system

The entire description of the geochemical system (except composition data that are stored in the Nodal Chemistry class) is contained in the Chemical System class (e.g. species, stoichiometric matrix, thermodynamic models, kinetic rate laws, etc.). Within the Chemical System class, the information is encapsulated in child classes: species, phase, reaction and reaction rate law. Chemical System specializations can be created to accommodate different definitions of the components (using inheritance). Two of them are currently implemented, the component definition of Steefel and MacQuarrie (1996) (here called 'Classic Chemical System class'), and the component definition of Saaltink et al. (1998) (here called 'Retraso Chemical System class').

The Chemical System class offers many functions such as providing information on the set of primary species, and computing total concentrations or chemical speciation. The input for these computations is the compositional information (e.g. concentrations, activity coefficients, temperature) stored in Nodal Chemistry.

3.2 Species class, the basic entity

The Species class constitutes the basic entity and is shared by the remaining classes, i.e., the same species object can be shared by a phase object, reaction object and reaction rate law object. The species class describes the properties of a geochemical species. Aqueous species are described by their electrical charge, ion size or molecular weight. Mineral species are described by the molar volume. The only operations on the Species class are related to the access of these attributes.

3.3 Phase class, the thermodynamic behaviour

The phase class describes a phase and its thermodynamic behavior. It is used to represent the 'non-ideality' of the chemical system. Phases are traditionally defined as homogeneous parts of the chemical system with boundaries with adjacent phases that are mechanically separable. This holds for all types of CHEPROO phases, except for surface phases, which are used for sorption and exchange processes. The phase class contains the species class and its attributes that depend on the nature of the phase (e.g. the dielectric constant for the aqueous phase). The main function of the Phase class is to compute the thermodynamic activity coefficients of the species involved. Thermodynamic models also depend on the nature of the phase. For example, both diluted water (Davis class) and brine (Pitzer class) are specializations of 'Aqueous Phase' but their thermodynamic behavior is different (Fig. 2).

Thus, the thermodynamic behavior of dilute water can be defined as ideal or calculated according to Debye-Hückel-based formulas. Brines behave according to the ionic interaction model (Pitzer Class). Note that compositional data are not stored in this class. In fact, the molality vector is provided by nodal chemistry objects to chemical system objects through the methods implemented in it.

A similar analysis is followed for mineral and gas phases. The thermodynamic behavior of solid and gas phases can be defined as a pure phase or as an ideal or non-ideal solution (Fig. 2). Different approaches to treat non-ideal solid solutions (i.e. regular, subregular) and different equations of state for non-ideal pure gases and gas mixtures are incorporated as specialized classes.

A specific phase class is the surface class that can be used to hold surface and cation exchange species. Cation exchange and electrostatic complexation models

(e.g. triple layer, constant capacitance and double layer) are supported in CHEPROO.
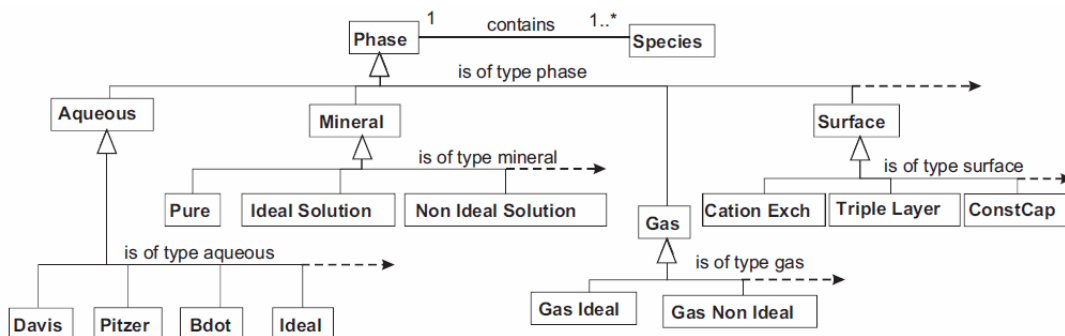
Fig.2. Class organization of Phase class

3.4 Reaction class

The Reaction class establishes the relationship between species in the same phase (homogeneous reaction), or species in different phases (heterogeneous reaction). The Reaction class is associated with 'Species' and 'Reaction Rate Law' classes (Fig. 1). In addition, it encapsulates other data like the stoichiometric coefficients, the equilibrium constant and the power function coefficients for the temperature dependence of the equilibrium constant. The main method implemented in the Reaction class solves the mass action equation associated and its derivatives with respect to the participating species. It can solve the concentration of an aqueous or a surface complex, a ratio between the ionic activity product and the equilibrium constant, or a partial pressure of a gas species. If a reaction object is defined as kinetic, the class can additionally calculate the reaction rate (and its derivatives with respect to all species). Internally the reaction rate calculation is carried out by the associated reaction rate law object.

3.5 Reaction rate law class, the kinetic behavior of the reaction

This class contains mathematical expressions of kinetic laws for chemical reactions. Two specializations of this class are implemented; one that calculates the reaction rates using an extended Lasaga expression (Steefel and Yabusaki, 1996), and another one that use Monod expression.

3.6 Nodal Chemistry class, compositional information and geochemical state variables

The Nodal Chemistry class forms the basic operational entity of the geochemical problem and contains the compositional information. Nodal Chemistry objects are used to simulate the chemistry of parcels of water. These parcels may represent samples, batch experiments, portions of a contaminated soil or aquifer, etc. Therefore, this class contains all direct and derived state variables generally used in standard geochemical calculations (e.g. concentrations, activity coefficients, ionic strength, temperature, mass of water, kinetic reaction rates, surface area of minerals, derivatives of state variables, sorption sites). In addition, each Nodal Chemistry object is associated with one Chemical System object, and can perform any chemical operation (Fig. **1.**).

Methods offered by Nodal Chemistry class can be classified into four groups of methods: internal maintenance (e.g. create, destroy, set, read/write), access to compositional information encapsulated it (e.g. access to concentrations or total

concentrations), reaction path (mixing, evaporation, addition of minerals, etc.), setting compositional information.

3.7 CHEPROO class, handling compositional information and chemical processes
The attributes of the CHEPROO class were described at the beginning of this section. The most significant methods are organized into six groups: A) internal maintenance, B) reading/writing, C) management of the reaction path operations, D) reactive transport calculations, E) access to general chemical information (e.g. concentrations or its derivatives with respect to primary species), F) access to chemical information for coupling with other processes (e.g. changes in porosity, fraction of water or salt in liquid).
A CHEPROO object can manage reaction path operations (group of methods C) on and between nodal chemistry objects. For example, on a group of nodal chemistry objects, we may evaporate the ith Nodal Chemistry object, add calcite in the jth, mix the ith and jth, and store the result in the kth Nodal Chemistry object. On the other hand, many methods in this class are oriented to reactive transport calculations (group of methods D).

Linking CHEPROO to other codes

We outline here the use of CHEPROO for solving reactive transport problems based on either SIA or DSA. We assume that a user has a conservative transport simulator and wishes to modify it to include reactive transport. There are two different alternatives to couple CHEPROO. One is to use it as a "solver" and the other is to use it as a "variable manager".
The first alternative can be used when conservative transport problem is solved using a matrix based method (typical 2nd order finite element or finite differences discretizations). CHEPROO will receive transport information from the conservative transport code (basically the original matricial system) and will set and solve the reactive transport matricial system.
If CHEPROO is used as a "variable manager" then the reactive transport matricial system must be built by the hosting program. CHERPOO will only provide information about chemical variables values and its derivatives (component concentration, sink terms due to kinetics, etc.). The last alternative has more impact on the original code, but has less restrictions on the method for calculating conservative transport.

The code is available at: http://www.h2ogeo.upc.es/software/CHEPROO/index.htm.

References

Akin J.E. (1999). Object oriented programming via Fortran90. Engineering Computations 16(1), 26–48.
Ayora C.,Taberner C.,Saaltink M.W.,Carrera J. (1998). The genesis of dedolomites: a discussion based on reactive transport modeling. Journal of Hydrology 209(1–4), 346–365.
Bachler D.,Kohl T. (2005). Coupled thermal–hydraulic–chemical modeling of enhanced geothermal systems. Geophysical Journal International 161(2), 533–548.
Bea S.A., Carrera J., Batlle F., Ayora C., Saaltink M.W. (2009) (in press). CHEPROO: A Fortran 90 object-oriented module to solve chemical processes in Earth Science models. Computers & Geosciences (2009),doi:10.1016/j.cageo.2008.08.010
Carr M. (1999). Using Fortran 90 and object-oriented programming to accelerate code development. IEEE Antennas and Propagation Magazine 41(6),85–90.
Curtis G.P. (2003). Comparison of approaches for simulating reactive solute transport involving organic degradation reactions by multiple terminal electron acceptors. Computers &Geosciences 29(3), 319–329.
Decyk V.K., Norton C.D. , Szymanski B.K. (1998). How to support inheritance and run-time polymorphism in Fortran 90. Computer Physics Communications 115(1),9–17.

Gorelik A.M. (2004). Object-oriented programming in modern Fortran. Programming and Computer Software 30(3), 173–179.

Mayer K.U., Benner S.G.,Frind E.O.,Thornton S.F.,Lerner D.N. (2001). Reactive transport modeling of processes controlling the distribution and natural attenuation of phenolic compounds in a deep sandstone aquifer. Journal of Contaminant Hydrology 53(3–4), 341–368.

Meysman F.J.R., Middelburg J.J., Herman P.M.J., Heip C.H.R. (2003a). Reactive transport in surface sediments. I. Model complexity and software quality. Computers & Geosciences 29 (3), 291–300.

Saaltink M.W., Ayora C., Carrera J. (1998). A mathematical formulation for reactive transport that eliminates mineral concentrations. Water Resources Research 34 (7), 1649–1656.

Simunek J., Suarez D.L. (1994). 2-dimensional transport model for variably saturated porous-media with major ion chemistry. Water Resources Research 30 (4), 1115–1133.

Steefel C. (2001). GIMRT, version 1.2: software for modeling multi- component, multidimensional reactive transport. User's guide. Technical Report UCRL-MA-143182, Lawrence Livermore National Laboratory, Livermore, CA.

Steefel C., Yabusaki S. (1996). OS3D/GIMRT, Software for multicompo- nent multidimensional reactive transport. User manual and pro- grammers guide. PNL-11166, Pacific Northwest National Laboratory, Richland, WA.

Steefel C.I., MacQuarrie K.T.B. (1996). Approaches to modeling of reactive transport in porous media. Reactive Transport in Porous Media 34, 83–129.

Watson I.A., Oswald S.E., Banwart S.A., Crouch R.S., Thornton S.F. (2005). Modeling the dynamics of fermentation and respiratory processes in a groundwater plume of phenolic contaminants interpreted from laboratory-to field-scale. Environmental Science & Technology 39 (22), 8829–8839.

Coupled modelling challenges in CO$_2$ storage

Irina Gaus
Nagra, Hardstrasse 73, 5430 Wettingen, Switzerland

Before implementing CO$_2$ storage on a large scale its viability regarding injectivity, containment and long-term safety for both humans and environment is crucial. Assessing CO$_2$-rock interactions is an important part of that as these potentially affect physical properties through highly coupled processes. Increased understanding of the physical impact of injected CO$_2$ during recent years elucidated the potential CO$_2$ pathways and indicated where and when CO$_2$-rock interactions are potentially occurring. These can be summarised as: (1) injection phase and near well environment interactions, (2) long-term reservoir and cap rock interactions, (3) CO$_2$-rock interactions along leakage pathways (well, cap rock, fault), (4) CO$_2$-rock interactions causing potable aquifer contamination as a consequence of leakage, (5) water-rock interactions caused by aquifer contamination through the CO$_2$ induced displacement of brines and finally (6) enhanced CO$_2$-rock interactions by engineering practices. Recent progress in coupled modelling for CO$_2$ purposes is discussed and future modelling opportunities are highlighted. One of the major gaps remaining is the lack of basic thermodynamic and kinetic data at relevant temperature and pressure conditions. Significant challenges are the coupled solute transport and geomechanical modelling, the modelling of impurities in the CO$_2$ stream and assessing the temporal impact of CO$_2$-rock interactions on porosity and permeability.

Occurrence of CO$_2$-rock interactions during CO$_2$ storage.

During the lifetime of a CO$_2$ storage scheme various groups of CO$_2$-rock interactions can be distinguished (Fig. 1). Once injection has started, supercritical CO$_2$ (SC-CO$_2$) will dissolve and interactions will occur between injected CO$_2$ and well materials. If CO$_2$ is injected as a liquid, either in the well or in the well environment (Fig.1-(1)) it will become supercritical. In the direct well environment dry supercritical CO$_2$ will prevail, which might still be at a different temperature than the target host rock. Gradually CO$_2$ temperature will adjust to the reservoir temperature and temperature driven CO$_2$-rock interactions will disappear. Longer-term interactions (Fig.1-(2)) between host rock and cap rock are the subsequent group of interactions, assuming that CO$_2$ remains contained in the target host rock. Leakage scenarios need to be investigated for each site and depending on the specific scenario, CO$_2$ rock interactions will occur whereby the coupling between the type of interaction with the flow regime is of crucial importance (Fig.1-(3)). If CO$_2$ has escaped along these leakage pathways it might enter potable aquifers and cause unwanted impacts on the quality of the water (Fig.1-(4)) used for human consumption. Also, because of the induced pressured built up during many years of injection, displacement of brine in adjacent layers might occur, again with deleterious effects on the quality of potable aquifers (Fig.1-(5)). A last type of interactions are these that are enhanced or induced through engineering practices with the objective to immobilise CO$_2$ faster or prohibit CO$_2$ induced reactions. Examples for the latter are co-injecting substances that interact with CO$_2$ or modifying the flow regime to increase the impact of certain interactions.

Recent progress in coupled modelling for CO$_2$ purposes

During the last years, considerable effort went into both the inclusion of additional processes in the models and the improvement of the calculation efficiency; these have allowed for calculations on larger grids taking into account more complex chemistries relevant to CO$_2$ storage. Examples are the development of additional CO$_2$ specific modules (such as CO$_2$-EOS for TOUGHREACT) and the development of new codes such as COORES (Le Gallo et al., 2006, 2008) and GEM-GHG (Nghiem et al. 2004) that are capable of modelling the geochemical interactions caused by the CO$_2$ injection on a large scale, thereby fully taking into account multiple phase flow and density effects as well as detailed geochemistry. Other significant efforts are currently ongoing in the domain of incorporating geomechanics (Rudqvist et al. 2006, Le Gallo et al. 2006) and assessing chemical interactions in highly concentrated brines with large ionic strengths (based on the Pitzer based approach), going beyond the currently often applied ion activity models (Zhang et al. 2006).
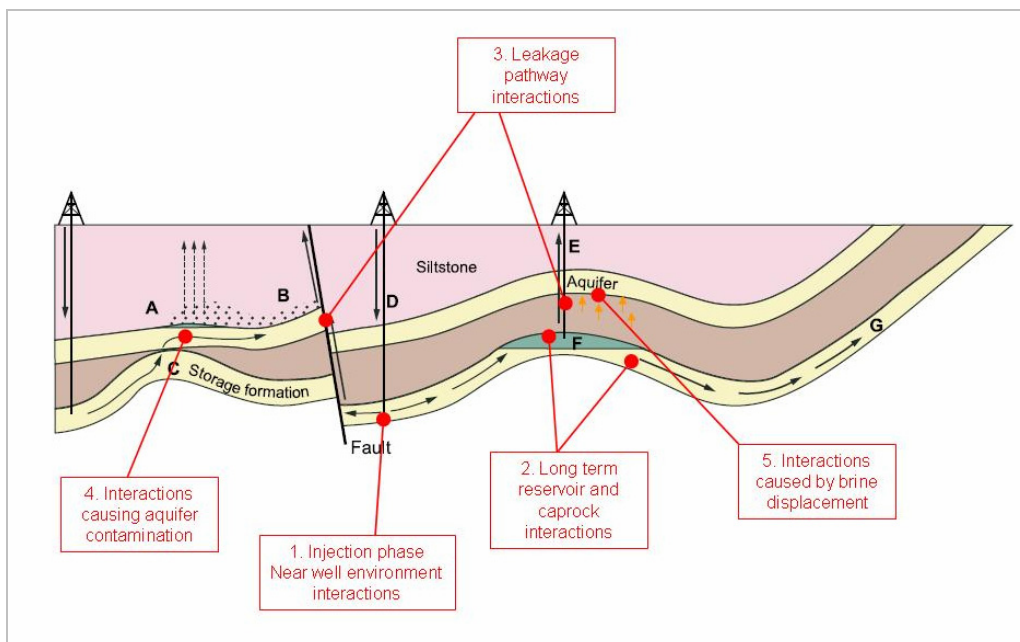
Fig. 1. Conceptual diagram of a CO2 injection scheme and identified clusters of CO2 rock interactions (modified from IPCC, 2005).

A distinction can be made between pure geochemical modelling, not taking into account of transport processes, and coupled modelling. The latter can be coupled flow and chemistry modelling (also including the effect of temperature), and it can also include geomechanical interactions (THMC modelling: thermal hydraulic mechanical chemistry coupled modelling). A review on coupled flow and transport modelling is given in Gaus et al. (2008). In this paper four main types of modelling applications are distinguished: long-term integrity applications (1), near well applications and impacts on injectivity (2), well integrity (3) and calibration and validation of experiments (4) each having its own spatial and temporal scale of interest. For each application an overview of the existing literature and the state of the art is given. The following key issues for improvement can be identified:

For long-term integrity applications, one of the major uncertainties is the impact of the alumino-silicate reactivities especially with respect to their kinetic rates and the extent to which they are impacting the host rock (as influenced by the reactive surface areas, mineral availabilities and precipitation mechanisms). The difficulties of capturing the uncertainties in the long-term modelling and assessing the trapping capacity is illustrated based on the Sleipner example, where several research groups modelled the long-term trapping in the Utsira formation (Johnson et al. 2004; Frangeul et al. 2004; Thibeau et al. 2007; Audigane et al. 2007). Even in this low reactive formation, where mineral trapping is not assumed to play a major role, model outcomes differ significantly due to the uncertainties in the underlying data and the different choices that are made by the modellers as a consequence of that. However, as the impact of mineral trapping is minor in the case of the Utsira Sands, the models do not lead to contradictory results. Nevertheless, the predictive value of these models could be improved significantly if more effort would be made to determine kinetics rates that are applicable to the timescale of the models, either by upscaling measured laboratory rates, or, by deriving semi quantitative kinetic rates from the analysis of natural analogues or other systems.

Regarding injectivity modelling, the complex phenomena occurring around the injection well in terms of brine concentration leading to very high ionic strengths and inducing precipitation reactions, interactions with violent flow regimes around the injection well with large pressures differentials, potential flushing of preferential flow paths and potential geomechanical impacts form the main challenge. Currently it is not possible to prioritise the dominant processes that affect the well environment in the short and the long term. Coupled model applications are still in the early stage and are only partly capturing the phenomena described above. The relative importance of the dominant processes that should be included in the models could further be explored.

For geochemical well integrity modelling, the difficulties for defining the correct conceptual models are twofold. Firstly, the characterisation of reactions between low pH brine and cement requires further investigation, especially with respect to altered cements. Many papers focus on high pH-water cement interactions because of its relevance in a nuclear waste context. There it became clear that the inclusion of CSH gels and solid solutions as well as the selection of the secondary minerals play a crucial role in correctly representing the interactions (Lothenbach and Winnefield 2006; Savage et al. 2007). Secondly, it remains unclear in this stage which combined CO_2 transport mechanism is capable of causing a significant impact in terms of geochemical interactions as many paths along various interfaces are suggested (eg casing/cement interflow, matrix flow, cement/caprock interface flow). Current detailed geochemical modelling efforts are restricted to simple 1-dimensional interface models (eg Jacquemet et al. 2006).

Recurring uncertainties in all modelling applications aiming at assessing the impact of geochemical interactions on porosity and the permeability, are due to the fact that the relationship between precipitation and porosity and permeability remains extremely difficult to quantify. The implementation of this relationship in the numerical codes has not been revised in the context of CO_2 storage. Upscaling results from pore scale modelling could address (part of) this issue.

The coupling of geomechanical codes with coupled flow-geochemical codes remains a further challenge, although much needed to assess the interplay between the two phenomena. This does not only require code development, but also the development of the datasets to feed into these codes and the correct treatment of uncertainties

since both geomechanical and geochemical processes are defined by highly uncertain parameters.

In the context of risk assessment modelling, certain modelling approaches simplify geochemical interactions by including only the anticipated result of the geochemical impact in the models, namely the corresponding porosity and permeability changes. Although for certain scenarios it has been shown that geochemical reactions are not influencing risk in a significant way (e.g. geochemical cap rock interactions in diffusion dominated systems), many of the issues listed above illustrate the need for more detailed research to verify that the geochemical reactions and their coupled impact on flow and geomechanics are not capable of dominating the system at a certain point in time and space and thus determining the risk.

Outlook for future modelling opportunities

Based on the interaction environments as described above, the following future (coupled) modelling opportunities can be identified.

Injection phase – near well environment: water-cement interactions, their kinetics and their impact on cement degradation; the impact of brine evaporation and precipitation as a consequence of H_2O dissolution in SC-CO_2; the adaptation of coupled flow-geochemistry models to be able to model highly saline brine interactions; the characterisation of the complex flow regime in the near well including temperature differences between the injected CO_2 and the reservoir and its impact on geochemical reactions (including density effects as well as preferential flow paths).

Long-term host rock and cap rock interaction: reducing the uncertainty of the kinetics of long-term reactions to allow for a more accurate assessment of the trapping capacity versus time; further investigation of the long-term reaction paths, especially with respect to the existence of intermediate mineral phases; revisit the relationship between precipitation and impact on porosity and permeability in a CO_2 storage specific context, both for diffusion dominated systems in low permeability cap rocks as in advection dominated systems in the host rock.

Leakage pathways: in case leakage exists, leakage pathways that are characterised by a large flux of SC-CO_2 or acidified brine are most prone to induce geochemical reactions, as large mass transfers can generate a significant impact. Regarding leakage along a wellbore, especially interactions along interfaces (steel/cement, cement/host rock, cement/cap rock), need to be investigated under CO_2 relevant conditions for both pure SC-CO_2 and acidified brine. To make progress beyond current modelling, the geometry of the well and the pressure regime needs to be taken into account in modelling applications. Reaction sequences should be further refined (inclusion of solid solutions, CSH gels, etc).

Aquifer contamination: with respect to interactions regarding aquifer contamination through acidification by dissolved CO_2, changes in the composition of the water are of main interest. These can be triggered by geochemical reactions whereby the overall mass transfer is orders of magnitude smaller than in reservoir interactions at great depth. More refined geochemical processes are needed (ion exchange, surface complexation, redox reactions) to explain relatively small changes in water chemistry (e.g. release of heavy metals under low pH conditions) that will affect the quality. This puts different constraints on coupled models.

Finally, the possibility of co-injecting other gaseous compounds - present in the gas stream as a result of the capture process - together with CO_2 is currently considered for economic reasons. The chemical reactivity of each of these compounds (eg O_2,

N_2, NO, SO_2, H_2S) has to be evaluated and their mutual impact modelled, especially since some of them are far more reactive than CO_2.

References

Audigane P., Gaus I., Czernichowski-Lauriol I., Pruess K., Xu T. (2007). Two dimensional reactive transport modelling of CO_2 injection in a saline aquifer at the Sleipner site, North Sea. American Journal of Science 307, 974-1008.

Frangeul J., Nghiem L., Emmanuel C., Thibeau S. (2004). Sleipner/Utsira CO_2 geological storage: full field flow and geochemical coupling to assess the long-term fate of the CO_2: Proceedings AAPG Annual Conference, Dallas, Texas, 18-21 April, 2004, Paper AAPG 86278.

Gaus I., Audigane P., André L., Lions, J., Jacquemet N., Durst P., Czernichowski-Lauriol I., Azaroual M. (2008). Geochemical modelling and solute transport modelling for CO_2 storage, what to expect from it? International Journal of Greenhouse Gas Control 2, 605-625.

IPCC (2005). IPCC Special report on carbon dioxide capture and storage. Prepared by Working Group III of the Intergovernmental Panel on Climate Change [Metz, B., O. Davidson, H. C. de Coninck, M. Loos, L. A. Meyer (eds.)]. Cambridge University Press, Cambridge, United Kingdom and New York, NY, USA, 442 pp.

Jacquemet N., Pironon J., Saint-Marc J. (2007). Mineralogical changes of a well cement in various H_2S-CO_2(-brine) fluids at high pressure and temperature. Environ. Sci. Technol. 42, 282-288.

Johnson J.W., Nitao J.J., Knauss K.G. (2004). Reactive transport modeling of CO_2 storage in saline aquifers to elucidate fundamental processes, trapping mechanisms, and sequestration partitioning: in Geol. Soc. London Spec. Pub. 233 Geologic Storage of Carbon Dioxide, Baines, S.J., Worden, R.H., eds., p. 107-128.

Le Gallo Y. (2008). Post-closure Migration for CO_2 Geological Storage and Regional Pressure Inferences. Proceedings of the 9th International Conference on Greenhouse Gas Control Technologies, 16 - 20 November 2008, Washington. In press..

Le Gallo Y., Trenty L., Michel A., Vidal-Gilbert S., Parra T., Jeannin, L. (2006). Long-term flow simulations of CO_2 storage in saline aquifer. Proceedings of the GHGT8 conference - Trondheim (Norway), 18-22/06/2006.

Lothenbach B., Winnefield F. (2006). Thermodynamic modelling of the hydration of Portland cement. Cement and Concrete Research 36, 209 – 226.

Nghiem L., Sammon P., Grabenstetter J., Ohkuma H. (2004). Modelling CO_2 storage in aquifers with a fully-coupled geochemical EOS compositional simulator: Paper SPE 89474 for the SPE/DOE 14th Symposium on Improved Oil recovery, Tulsa, Oklahoma, 17-21 April, 2004.

Rudqvist J., Birkholzer J., Tsang C.-F. (2006). Modelling hydrological and geochemical processes related to CO_2 injection in a faulted multilayer system. Proceedings of the GHGT8 conference - Trondheim (Norway), 18-22/06/2006.

Savage D, Walker C, Arthur R, Rochelle C, Oda C, Takase H. (2007). Alteration of bentonite by hyperalkaline fluids: a review of secondary minerals. Physics and Chemistry of the Earth 32, 287-297.

Thibeau S., Nghiem L.X., Okhuma H. (2007). A modelling study of the role of selected minerals in enhancing CO_2 mineralisation during CO_2 aquifer storage. 2007 Annual Technical Conference and Exhibition, Anaheim, Calfornia, USA, 11-14 November 2007, Paper SPE109739.

Zhang G., Spycher N., Sonnenthal E., Steefel C. (2006). Implementation of a Pitzer activity model into TOUGHREACT for modelling concentrated solutions. Proceedings, TOUGH Symposium 2006, Lawrence Berkeley National Laboratory, Berkeley, California, May 15–17 (Report LBNL-60016).

Modeling retardation effects by barium and strontium solid solutions on radium cations in the near field of radioactive waste repository

Haibing Shao[1,3], Georg Kosakowski[2], Dmitrii A. Kulik[2] and Olaf Kolditz[1,3]
1 Department Environmental Informatics, Helmholtz Centre for Environmental Research - UFZ, Permoserstrasse 15, 04318 Leipzig, Germany
[2] Laboratory for Waste Management, Paul Scherrer Institute, 5232 Villigen PSI, Switzerland
[3] Applied Environmental System Analysis, Dresden University of Technology, Helmholtzstraße 10, 01069 Dresden, Germany

A typical application for reactive transport modeling is to simulate the migration of radionuclides out of a nuclear waste repository. Radium, one of the products in the uranium decay chain, is expected to be present in high and in intermediate level waste packages. Normally, for the transport of radium in the near-field of a waste repository, it is assumed that it behaves chemically similar to other rare earth metals like barium or strontium. Their transport in clay materials that are used as e.g. as tunnel backfills is retarded mainly by cation-exchange and to a lesser degree by surface complexation. Consideration of such sorption mechanisms in reactive transport calculations requires the use of non-linear sorption isotherms. For performance assessment calculations they are translated into linear isotherms (NAGRA, 2002). A process not considered so far in this approach is the incorporation of radium into solid solutions with barium and strontium sulfates and carbonates.

To simulate this aqueous - solid solution system, we used a new combination of the multi-component mass transport code GeoSys and the Gibbs Energy Minimization (GEM) solver GEMIPM2K. The two codes are coupled in a Sequential Non-Iterative Approach (SNIA). For each time step, the mass transport equation is first solved by GeoSys using the finite element method (Wang and Kolditz 2007), and the chemical equilibrium is thereafter calculated on each node of the domain by GEMIPM2K – the kernel of GEMS-PSI code package (Kulik et al. 2008). The coupled code was verified by a widely used benchmark of dissolution-precipitation in a calcite-dolomite system.

In order to demonstrate the influence of solid solution formation on the transport of mobile Ra^{2+} cations, we present a strongly simplified one-dimensional scenario of a tunnel connecting to an intermediate level radioactive waste repository. According to the engineering design, the bentonite will be mixed with sand and used as a backfill material in the tunnel. Due to the low permeability of this material (up to 5.0×10^{-11} m/s) and low hydraulic gradient, the transport of radionuclides in the tunnel will be dominated by diffusion. Uniform diffusion coefficients for all chemical components were selected equal to 5.0×10^{-10} m^2/s according to a technical report by Nagra (2002). The temperature was assumed to be 25 °C and pressure 1 bar. We used a boundary condition of constant radium concentration representing the source leakage of the radionuclides out of the repository at the right end of the tunnel backfill. The source term, i.e. the aqueous concentration of Ra^{2+}, was fixed at 1.0×10^{-6} mol/l. Such a concentration is possible in the cementitious backfill material of caverns for intermediate level waste (Nagra, 2002). At the left end, we set a constant concentration for dissolved sulfate, which could emerge e.g. as a product of pyrite (FeS_2) oxidation during the tunnel excavation period. As the time span of analysis (around 100 year) is much shorter than the half-life of ^{226}Ra (1700 years), radioactive decay is not considered in this model. However, it is assumed that re-crystallization

or co-precipitation rates of carbonate and sulfate solid solutions are fast enough to approach chemical equilibrium within the mass transport time step.

Bentonite usually contains some sorbed strontium and barium together with significant amounts of calcium carbonate, re-crystallization of which may lead to the formation of carbonate solid solutions between $RaCO_3$, $BaCO_3$, $SrCO_3$, and $CaCO_3$ end members. Because we are interested in a first step in the incorporation of Ra in Ba and Sr solid solutions we only consider aqueous speciation of these metals, as well as their carbonate and sulfate mineral forms, but no sorption on clay component. Ingression of sulfate, e.g. from wall rock, may result in re-partitioning of Ba, Ra and Sr into sulfate solid solutions. Consequently, in the geochemical model setup we consider both carbonate and sulfate non-ideal solid solutions of Ba, Sr and Ra together with calcite. Ternary carbonate and sulfate solid solution phases are each included twice because of the possible miscibility gaps which would result e.g. in Sr and Ba dominated sulfate phases co-existing in the particular equilibrium state.

The simulation was set up in a way that at the beginning, Ra^{2+} cations and SO_4^{2-} anions diffuse into the tunnel from the opposite ends. Due to the presence of excess carbonate in the pore water of the bentonite-sand mixture, Ra^{2+} is first captured in Ba-Sr carbonate solid solutions. However, when sulfate anions enter the system, the carbonates are expected to be replaced with much less soluble Ba-Sr sulfates (barite and celestite). In turn, as the dissolved aqueous sulfates arrive at these areas, the aqueous Ra^{2+} radium in carbonates will be re-partitioned into sulfates, and the Ra^{2+} aqueous concentration will strongly decrease. In this way, most of the mobile radium will be immobilized in sulfate solid solutions. Upon further supply of sulfate ions, the dissolved concentrations of Ba, Sr and Ra are expected to continue to decrease, because of the so-called "common-anion" effect.

The numerical reactive transport simulation results confirm this scenario. Fig 1 shows the evolution of sulfate (SO_4^{2-}) and radium (Ra^{2+}) aqueous concentrations. At the beginning of simulation, both sulfate and Ra^{2+} diffuse into the model domain, and small fraction of radium is fixed in radium-containing Ba-Sr carbonates. At around 40
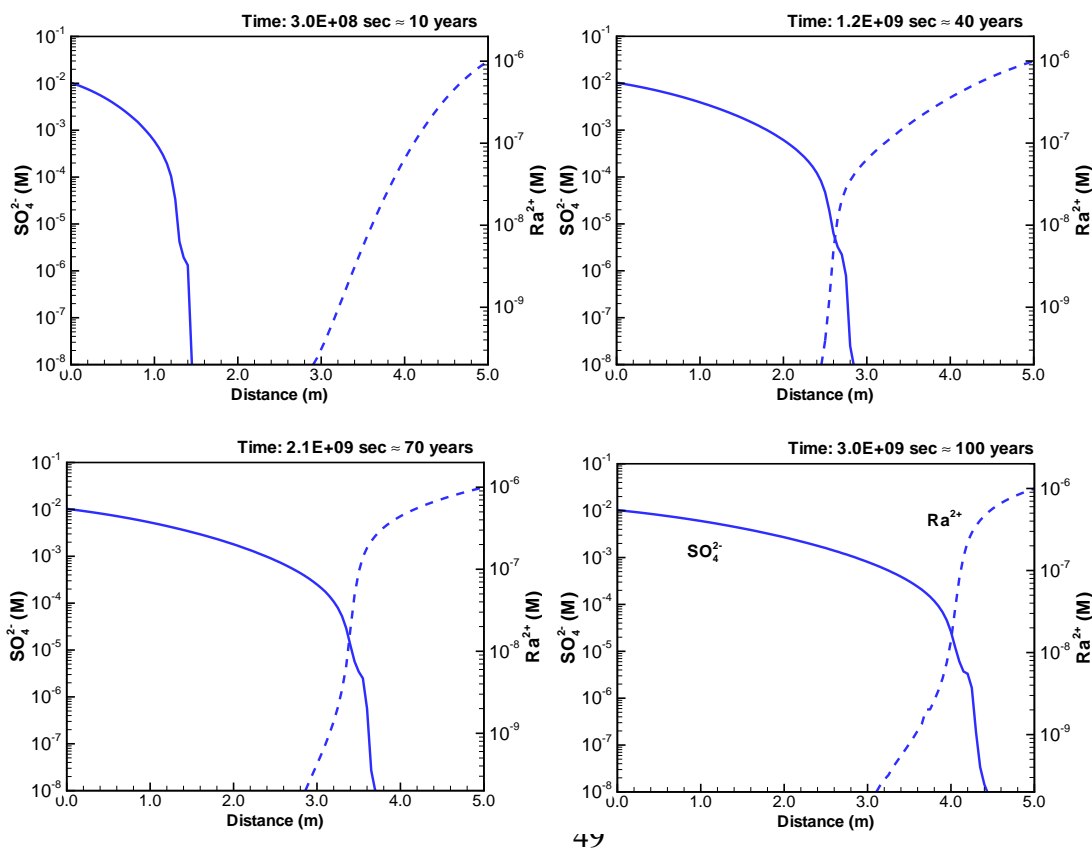
Fig 1. Sulfate and radium aqueous concentration profiles at about 100 years; solid lines are SO_4^{2-} and dashed lines are Ra^{2+} results.

years, when the sulfate front encounters the Ra^{2+} front, the carbonate solid solutions are transformed into the radium-containing sulfate solid solutions. This causes a sharp decline of the aqueous Ra^{2+} concentration. At the same time, Ba and Sr are also re-partitioned into sulfate phase. As the sulfate ingression proceeds, the mobile Ra^{2+} can no longer diffuse further into the tunnel. Instead, the dissolved aqueous Ra^{2+} is gradually fixed into stable sulfate solid solutions.

As a result of the numerical study, it can be shown that the formation of sulfate solid solutions must strongly retard the transport of radium. In Fig 2 we compare the reactive transport results with analytical solutions for linear sorption effects. The following set of Ra distribution coefficients K_D = 0.0, 3.0×10^{-4}, 2×10^{-3} and 0.1 m^3/kg from the Nagra Technical Report (2002) was used for comparison. These values stand for no retardation, pessimistic, reference and optimistic estimation of the Ra sorption in compacted bentonite, respectively. We would like to note that the K_D values given in Nagra (2002) are based solely on a cation exchange mechanism. According to Bradbury and Bayens (2003) only very few experimental data sets for the sorption of Ra on clay minerals are available.

Therefore, they assumed that Ra is present as bivalent cation in solution and that it is sorbed by cation exchange analogous to other alkali-earth metals e.g. Ca, Mg, Sr and Ba. If appropriate data for Ra are
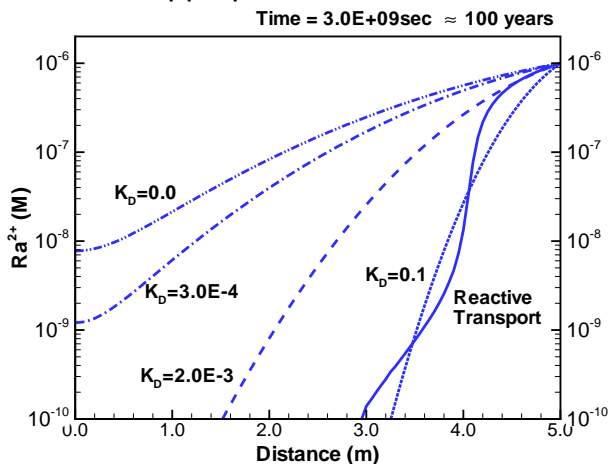
Fig 2. Comparison of the retardation behavior using solid solution and the traditional KD concept. Solid lines are concentration profiles of Ra^{2+} using the solid solution approach; dashed-double-dotted lines, dashed-dotted lines, dashed lines and dotted lines are profiles calculated for KD values of 0.0, 3×10^{-4}, 2×10^{-3} and 0.1 m^3/kg, respectively.
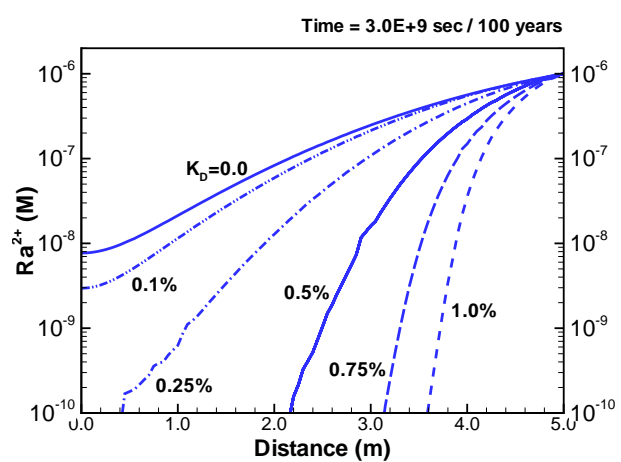
Fig 3. Sensitivity of retardation effects regarding the available amount of sulfate. From right to left, the curves are Ra^{2+} concentration profiles calculated for 1%, 0.75%, 0.5%, 0.25% and 0.1% of gypsum initially existing in the solid phase of the buffer material, compared to the amount of calcite respectively. The leftmost solid line is the reference profile calculated for a KD value of zero.

not available, Sr and Ba are often used as chemical analogues. Compared with the solid-solution incorporation, cation exchange is a different sorption mechanism in which Ra^{2+} competes with major cations (Ca^{2+}, Na^+, K^+) for permanent-charge sites in clay present in the (large) amount limited by the cation exchange capacity. In general, both mechanisms are expected to compete for metal cations. In the present study, cation exchange was omitted from the chemical model in order to simplify the analysis of the effects of solid solutions on the transport of Ra.

To test the model sensitivity, the amounts of barium, strontium and sulfate were varied and the simulation results compared. First, the amounts of barium and strontium were scaled down with a factor of 10^2 and 10^4. Simulations show that Ra^{2+} is still heavily retarded even with 0.01% of the original barium and strontium inventories. This means that the Ba-Ra or Sr-Ra solid solutions can be formed even with very limited amount of barium and strontium, presuming there is enough sulfate available. In addition, we tested the influence of the sulfate content on the incorporation of radium in the solid-solutions. In the system of interest, the limiting dissolved concentration of sulfate is expected to be set by the solubility of gypsum ($CaSO_4 \cdot 2H_2O$). Hence, we prepared five chemical setups of the backfill material containing 0.1%, 0.25%, 0.5%, 0.75% and 1% mass of gypsum, respectively. They were used as initial conditions in the reactive transport model. The sulfate-rich left boundary was removed, to let only Ra^{2+} diffusing from right to left. It was found that the amount of sulfate heavily influences the formation of solid solutions (Fig 3). With 0.1 wt% of gypsum added, the calculated Ra^{2+} profile is close to the reference curve that has no retardation effect. The more sulfate is available the more strongly Ra^{2+} is retarded. Therefore, the availability of sulfate seems to be the most important factor for the retardation of radium.

In summary, with the model presented in this work, it can be shown that the aqueous Ra concentration could be lower by 3~4 orders of magnitudes in the presence of sulfate solid solutions. However, this fixation capacity is highly influenced by the sulfate inventory available in the medium. Currently, this chemical model is being further extended to include ion exchange effects, with the clay mineral montmorillonite acting as an ion-exchanger. With this model involving solid solutions, we are able to predict the transport of radionuclides in a more realistic way and reduce the conservatism of the oversimplified models (linear isotherms) used for performance assessment.

References

Bradbury M.H., Baeyens B. (2003). Near field sorption data bases for compacted MX-80 bentonite for performance assessment of a high-level radioactive waste repository in Opalinus clay host rock, PSI Bericht Nr. 03-07, Nagra NTB 02-18, Paul Scherrer Institut, Villigen, Switzerland, ISSN 1019-0643.

Kulik D.A., Dmytrieva S.V., Chudnenko K.V., Thoenen T., Wagner Th. (2008). GEM-Selektor (GEMS-PSI) - Research package for thermodynamic modeling of aquatic (geo)chemical systems by Gibbs Energy Minimization. Paul Scherrer Institut, http://gems.web.psi.ch/.

Nagra (National Cooperative for the Disposal of Radioactive Waste). (2002). Nagra Technical Report 02-06: Models, Codes and Data for Safety Assessment. Wettingen, Switzerland, ISSN 1015-2636.

Wang W., Kolditz O. (2007). Object-oriented finite element analysis of thermo-hydro-mechanical (THM) problems in porous media, Int. J. Numerical Methods in Engineering 69, 162-201.

Interaction of uranyl with quartz – Experiments and modelling

Florian Huber and Johannes Lützenkirchen
Forschungszentrum Karlsruhe, Institut für Nukleare Entsorgung, P.O. Box 3640, 76021 Karlsruhe, Germany

The linear uranyl (UO_2^{2+}) is the thermodynamically stable form of uranium under oxidizing conditions. It is known to form strong aqueous complexes with various ligands, including carbonate and aqueous silica. Several studies about the adsorption of uranium(VI) from aqueous solutions onto a wide range of solid materials (e.g. Fe- and Al-oxides/hydroxides, clay and quartz) under different chemical conditions (pH, ionic strength, presence of different complexing ligands, total quantity of uranium, etc.) are available. All the studies involving silica or quartz revealed a more or less strong impact of the solution composition on the adsorption of uranyl (e.g. Kohler et al. 1996; Lützenkirchen and Huber 2007, Huber and Lützenkirchen 2009). Because of the relatively easy procedure, batch experiments are the common way to study the adsorption behaviour of potential contaminants. Upscaling of batch results to contaminant transport in the environment should be done carefully due to the static nature of the batch technique and the dynamic nature of the migration process. This concerns for example the particle size: in laboratory experiments most frequently colloidal materials are used, whereas matrix material such as quartz in the environment usually has much larger grain sizes. In this respect, more realistic approaches to study the behaviour of contaminants in contact with potential sorbents are (dynamic) column experiments. These, however, require more effort than batch experiments and are more prone to experimental as well as interpretational problems. Results of batch experiments might be considered as first information about a given system which in a second step should be transferred to more realistic conditions by carrying out the respective column experiments.

The aims of this study were:
(1) experimental determination of adsorption data from batch experiments for a range of quartz samples for the system uranyl–quartz in CO2 free systems
(2) comparison of the experimental results with blind predictions using a surface complexation model calibrated on batch and column data
(3) experimental determination of adsorption data from column experiments with uranyl using 2 different quartz samples
(4) modeling of the column experiments using reactive transport code HBGC123D (Gwo, et al. 2000)

The reported batch adsorption results are reasonably predicted by the applied surface complexation model. The model also successfully described batch and column data on a quartz sample with grains smaller than the quartz particles used in the present study by a factor of ca. 25 under otherwise similar conditions. But the model was incapable of describing the breakthrough behavior of uranyl species for the columns with the coarser quartz samples. This failure was attributed to the heterogeneity of the quartz particles used, which may be more important for column breakthrough than for batch adsorption data.

References

Gwo J. P. et al. (2000). HBGC123D: A high performance computer model of coupled hydrogeological and biogeochemical processes. Computers and Geosciences, 27(2001): 1231-1242.

Huber F., Lützenkirchen, J. (2009). Uranyl retention on quartz—New experimental data and blind prediction using an existing surface complexation model. Aquatic Geochemistry, DOI 10.1007/s10498-009-9060-9.

Kohler M., Curtis G.P., Kent D.B., Davis J.A. (1996). Experimental investigations and modelling of uranium(VI) transport under variable chemical conditions. Water Resources Research 32.

Lützenkirchen J., Huber F. (2007). Heterogeneities in Adsorption from Aqueous Solution — An Example of the Effect of Surface Coverage. Adsorption Science and Technology, 25(7): 503-516..

Modelling Heterogeneity Effects on Radionuclide Transport in the Far Field of a Radioactive Waste Repository

Sneh Jain and Nick Evans
Department of Chemistry, Loughborough University, Loughborough, Leics, LE11 3TU, UK

Introduction

In the UK, extensive consideration is being given to nuclear waste containment and disposal. Deep geological repositories are at the forefront of the solution and it is likely that nuclear waste material will be stored in crystalline volcanic rock wherever it is eventually stored. A large proportion of the overburden rock in the UK is sandstone, so an understanding of the transport behaviour of radionuclides in this type of material is essential, to establish the long-term effects of deep burial of nuclear wastes.

This project examines simple chemically homogeneous materials such as quartz to establish the components of the sorption process, working towards more complex (both in physical and chemical terms) simulated rock systems. The physical and chemical heterogeneities of a rock system at different scales need to be modelled to account for parameters such as porosity. Our ultimate aim is to model the sorption and transport behaviour of various radionuclides

Transport modelling allows an understanding of scaling, taking into consideration physical and chemical components such as spatial variation and chemical retardation. Modelling, through the use of values derived from column experiments, will allow the effect of upscaling to be seen. The scaling of the retardation factor of a chemical species is related to the variability of the sorption coefficients in the rock and mineral. Column experiments are used to establish these values to allow for challenges of upscaling to be overcome.

The K1D model, a flexible research code which allows the inclusion of kinetic data alongside transport and chemical equilibria, will be used to demonstrate the movement in aqueous media of radionuclides in silicate-based materials with increasing heterogeneity.

Column experiments

Initial experimental studies will examine the movement of radionuclides in short columns of no longer than 6 cm packed with SiO_2. This silicate has a homogeneous extended structure, which facilitates entry into this work. Following this, more complex silicate systems will be investigated. It is intended that our study will use the following systems, listed in increasing order of their chemical and structural complexity: SiO_2, Quartz, metal-doped Quartzes, Quartz/iron oxide, Sand, synthetic sandstone and finally an intact sandstone core.

The column dimensions and design will be based on our recent work (Warwick 2005; Warwick 2007). Very slow electrolyte flow rates (5-15 ml per day) will be used, with delivery by syringe pump, to mimic ground water flow conditions. Higher flow rates might cause the radionuclides to move through the column by advection, which would less accurately simulate typical ground water flow conditions. Columns will be wet packed. In order to pretreat (adjust pH etc.) the silicate surface, $NaClO_4$ (aq) will be run through the column.

It is proposed that for Eu^{3+}, Th^{4+}, Ni^{2+} and Cs^+ (the radionuclides under initial investigation) the following variables will be examined:
- Effect of column packing – heterogeneity of the silicate system
- Flow rate of the radionuclide solution
- Column length
- Presence of humic acid, to simulate the natural organic material present in soil which could complex the metal ions and mediate their transport
- Anthropogenic organics such as EDTA or CDP (cellulosic decomposition products), to chelate the metal ions

If this phase of our study is successful then our approach will be extended to include: TcO^{4-}, I^- and U(VI).

Throughout our study the following parameters will remain constant:
- Ground water composition (0.1 mol dm^{-3} $NaClO_4$), pH 5-6
- Particle size of silicate material under investigation,
- Humic acid concentration (10 ppm).

Humic acid is a naturally occurring colloid with a high affinity for cations. Water-soluble metal-humate complexes are important transport agents through the geosphere. For radionuclides in geological nuclear waste repositories, speciation with humic acid and mobility of these complexes are important phenomena to understand. Transport of the metal-humate species on silicate materials forms a significant part of our project.
Where humic acid is used, the column will be pre-equilibrated with humic acid, to achieve a uniform concentration of 10 ppm along the column. This will allow the effect of the radionuclide under investigation with silicate in the presence of humic acid to be monitored.
Columns will be run by upflood/ downflood techniques (Warwick 2005; Warwick 2007). Upflood will involve loading the column with metal ions, which are dissolved in aqueous NaClO4. Downflood will involve pumping ground water through the column. In some experiments, humic acid will be dissolved in the aqueous phase and used in both the upflood and downflood steps. By determining how much metal ion is removed from the column in the downflooding, we can calculate how much metal is retained by the silicate.

Additional parameters for measurement

We will establish through calibration experiments whether metal ion or humic acid retention on the apparatus occurs. Porosity and dispersivity of the silicate material in each column will be measured using tritiated water to enable comparison of results from different experiments.
Previous work suggests that Th^{4+} and Eu^{3+} (Raju et al. 2007 and Hasany et al. 1997) are likely to attach more tightly to the sand, and that Ni^{2+} should be mostly recoverable (Hasany et al. 1997) in the absence of humic acid. Cs^+ (Jan et al. 2007) is not particularly sorbing to quartz. It is hoped that these behaviours will be simulated by our columns.
Humic acid will separately be passed through the column without the presence of metal ions to examine its sorption onto the silicate material.

We will analyse metal ion and humic acid concentrations remaining on the silicates following the downflooding by cross-sectional analysis of packed materials.

Our initial studies with humic acid will use unlabelled material. In later work we will radiolabel the humic acid with ^{125}I to see how it distributes through the column.

Modelling radionuclide transport

The modelling code, K1D, should allow us to address factors with respect to the radionuclide and the mineral system:

Solution phase species of the radionuclide

The interaction of humic acid, surface and radionuclide in a ternary system
The interaction of humic acid with the mineral
The interaction of radionuclide with the mineral

The importance of our experiments lies in the upscaling of heterogeneous systems, in this case sandstone, to assess the transport of radionuclides within. We will be able to model the kinetic parameters of the transport process determined through our experiments, and also the stability constants of the speciated metals. Beginning with structurally simple silicate materials, we will be able to model more complex geological systems.

References

Bryan N. D., Jones D. L. M., Keepax R. E., Farrelly D. H., Abrahamsen L. G., Pitois A., Ivanov P., Warwick P. and Evans N. (2007). J. Environ. Monit., 9, 329-347.

Bryan N. D., Barlow J., Warwick P., Stephens S., Higgo J. J. W. and Griffin D. (2005). J. Environ. Monit., 7, 196-202.

Raju C. S. K. and Subramanian M. S. (2007). J. Haz. Mat., 145, 315-322.

Hassany S. M and Khurshid S.J. (1997). Applied Radiation and Isotopes, 48, 143-146.

Jan Y. L., Tsai S. C., Jan J. C. and Hsu C. N. (2006). J.l Radioanal. Nuc.r Chem., 267, 225-231.

Interaction of trivalent ions with various aluminium minerals

Tomas Kupcik[1], Nina Huittinen[2], Thomas Rabung[1], Johannes Lützenkirchen[1];
Horst Geckeis[1,3] and Thomas Fanghänel[4,5]

[1] *Forschungszentrum Karlsruhe, Institut für Nukleare Entsorgung, P.O. Box 3640, 76021 Karlsruhe, Germany*
[2] *University of Helsinki, Laboratory of Radiochemistry, P.O. Box 55, 00014 Helsinki, Finland*
[3] *Universität Karlsruhe, Institut für Anorganische Chemie, Engesser Strasse 15, 76131 Karlsruhe, Gemany*
[4] *Universität Heidelberg, Physikalisch-Chemisches Institut, Im Neunheimer Feld 253, 69120 Heidelberg, Germany*
[5] *European Comission, Joint Research Centre, Institute for Transuranium Elements, P.O. Box 2340, 76125 Karlsruhe, Germany*

Recent studies on Cm(III) sorption onto mineral surfaces performed with time resolved laser fluorescence spectroscopy (TRLFS) and X-Ray absorption spectroscopy (EXAFS) revealed striking similarities for Cm(III) species bound to γ-Al_2O_3, (001) sapphire and clay minerals (Rabung et al. 2006). This finding was taken as indication for >Al-OH functional groups acting as primarily complexing ligands in all cases and the existence of similar surface structures. The exact type of Cm(III) arrangement at the Al_2O_3 surfaces is, however, difficult to derive as those oxides are thermodynamically unstable in contact with aqueous solution and undergo (surface) phase transformation [Lee et al. 1995; Lefèvre et al. 2002). Thus, the experiments are extended to the respective Al-hydroxides gibbsite and bayerite known to form as secondary solid phases at Al_2O_3 surfaces.

Cm/Gd/Eu(III) sorption onto the laboratory-synthesized Al-hydroxide samples is investigated by batch experiments and TRLFS at constant ionic strength (0.1 M $NaClO_4$) under argon atmosphere in a pH range between 4 and 11. As a comparison, experiments are performed with α-Al_2O_3 –powder. In general, the extent of metal ion sorption increases with decreasing isoelectric point (pH_{iep}), which is intelligible as charge repulsion of sorbing metal cations and solid surface decreases. This finding indicates that >Al-OH groups at the different solid surfaces have clearly different acid/base properties. By comparing pH_{iep} data, it becomes obvious that hydrated Al_2O_3 surfaces (pH_{iep}=9-10) cannot be considered as consisting of pure bayerite ($pH_{iep} \sim 9$) or gibbsite ($pH_{iep} \sim 11$). TRLFS emission spectra for Cm(III) sorbed onto the different solids are consequently different and even suggest the presence of different types of Cm(III) surface species. pH dependent dissolution and precipitation reactions significantly affect the speciation of sorbed Cm(III) leading to the appearance of "incorporated" species in case of the well crystalline hydroxides gibbsite (platelets) and bayerite (rods). Such phenomena are not observed in experiments with spherical α– and γ-Al_2O_3 particles. Equilibration of a gibbsite suspension at its solubility minimum and increasing or decreasing the pH in presence of sorbed Cm(III) prevents formation of "incorporated" Cm(III) species. However, even there very slow desorption reaction rates become apparent, which are not noticed with Al_2O_3 particles. The experiments point to the important impact of surface dynamics on actinide sorption reactions.

References

Rabung Th., Geckeis H., Wang X.K., Rothe J., Denecke M.A., Klenze R., Fanghänel Th.(2006). Cm(III) sorption onto γ-Al$_2$O$_3$. New insight into sorption mechanisms by time-resolved laser fluorescence spectroscopy and extended X-ray absorption fine structure, Radiochim. Acta, 94, 2006, 609.

Lee D. H. Sr., Condiate R. A. (1995). An FTIR spectral investigation of the structural species found on alumina surfaces., Mater. Lett., 23, 241.

Lefèvre G.; Duc M.; Lepeut P.; Caplain R.; Fedoroff M. (2002). Hydration of γ-Alumina in Water and Its Effects on Surface Reactivity., Langmuir, 18, 7530.

Development of a coupled transport and geochemical reaction code and a first application to CO_2 sequestration

Dedong Li and Sebastian Bauer
Institute for Geosciences, Christian-Albrechts-University Kiel, Ludewig-Meyn-Str. 10, 24118 Kiel, Germany

Carbon capture and storage (CCS) is considered today as a key option for mitigating the climate effects of greenhouse gas emission, especially of CO_2. In CCS process, the carbon dioxide is captured at large industrial sources, transported to storage sites and then injected into deep geological formations. There CO_2 is retained by structural trapping as residual phase due to an impervious overburden, dissolved in the formation water and involved into geochemical reactions with the host rock, which may result in the mineralization of CO_2. In order to assess and predict the effectiveness of all the individual storage mechanisms at one site and to make a valid prognosis of future behaviour of CO_2 and the formation, numerical modelling is required. This is especially true if the possibility of leaks is considered. Only coupled transport and geochemical reaction models can give quantitative estimates of mineral reactions and trapping mechanisms as a function of space and time. Therefore, a numerical simulation code is required which is able to handle the governing processes and account for the prevailing conditions. The typical conditions for CO_2 geologic storage are pressures of up to 500 bar or higher, wide temperature ranges (30-95 °C) and high salinities of up to 300 g/l. This requires the usage of suitable geochemical methods.

In this paper, the implementation of an interface between the research code GeoSys/RockFlow and the thermo-kinetic simulation software ChemApp is presented. GeoSys/RockFlow (KOLDITZ and SHAO, 2008) has been developed over the last years into a multi-phase multi-component reactive transport simulator, which has been applied amongst others in simulations of geothermal reservoirs, simulations of the disposal of nuclear waste disposal and simulations of biodegradation processes in the shallow ground water. GeoSys/RockFlow can account for the corresponding mechanical, hydraulic and thermal processes.

GeoSys/RockFlow is designed in a process-oriented and object-oriented way (KOLDITZ and BAUER, 2004), i.e. the individual processes are each resembled by an independent object. The individual processes are coupled in different ways, the standard way being the sequential iterative approach. Due to this code structure the implementation of a new interface to ChemApp is feasible within a short time.

ChemApp (ERIKSSON and PETERSEN, 2008), developed by GTT-Technologies, is a thermo-chemical software library based on the Gibbs free energy minimization, which is especially powerful in complex equilibrium calculations for multi-component, multi-phase systems. It consists of a rich set of subroutines, which provides almost all the necessary tools for the equilibrium calculation. ChemApp has been successfully applied in a multitude of projects, in particular to model the thermo-chemical aspects of processes involving inorganic, complex solution phase chemistry (PETERSEN and HACK, 2007). PHREEQC (PARKHURST and APPELO, 1999) ,as a classical geochemical reaction program, has been widely applied in ground water geochemistry. The following table shows advantages and disadvantages of ChemApp and PHREEQC in their main features. ChemApp seems to be more capable of accounting for the high temperature, high pressure and high salinity conditions prevailing during CO_2

storage. This finding may be evaluated using test examples and a data set from the Weyburn CO_2 storage field site.

Table 1: Main features of ChemApp and PHREEQC.

Features	ChemApp	PHREEQC
history	since 1996	~30 years
aqueous solution complex species	Yes	Yes
multi-component multi- phase system	Yes	Yes
minerals and meta-minerals	Yes	Yes
high temperature	Yes	Little
high pressure	Yes	No

ChemApp provides a set of interface subroutine which permits its integration into an existing program code like GeoSys. We developed an interface module to perform the geochemical simulations using ChemApp, which handles the data transfer between GeoSys and ChemApp. This interface module has been implemented in a first version as a new object into GeoSys/RockFlow. The required steering parameters for the ChemApp simulations are specified via a text input setting file, while data transfer of e.g. species amounts and concentrations is code internal. The main function and options are shown in Figure 1.
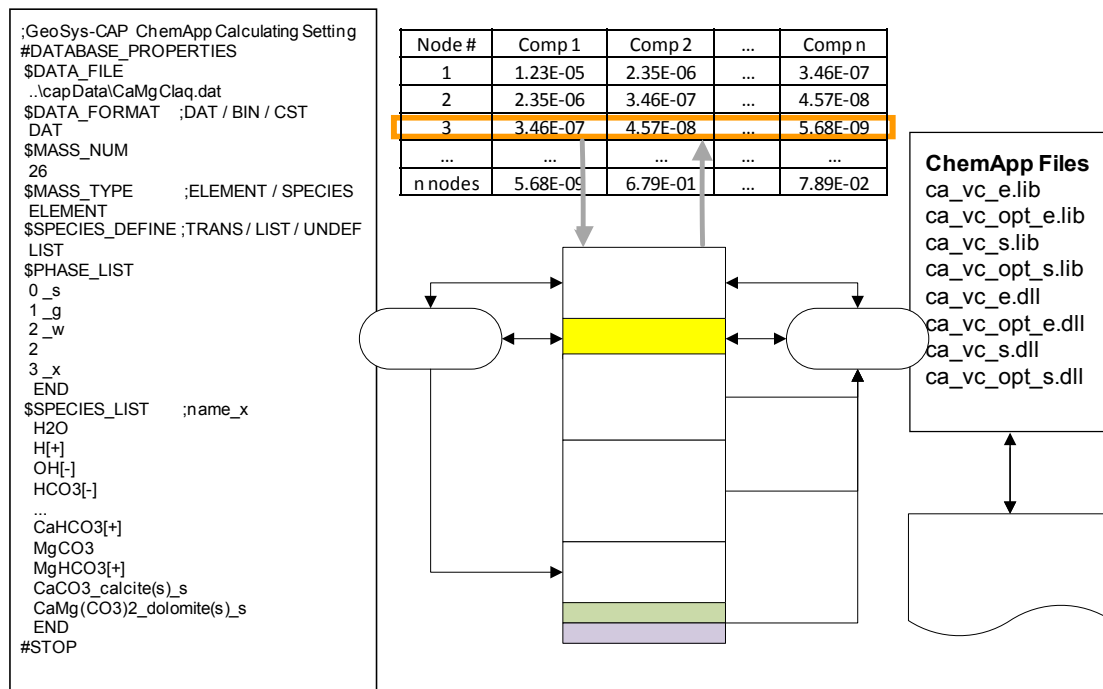
Fig. 1. Schematic diagram of the GeoSys – ChemApp interface.

The reactive transport equation is basically split into conservative transport and geochemical reactions. By this, we obtain one global conservative transport equation for each component and at each grid node the local reactions. Our reactive interface module will calculate the geochemical reaction equilibrium each time step and provide updated species concentrations. The interface sets up a close and flexible contact between GeoSys and ChemApp. It allows to choose the suitable databases and select the reactive species to be considered through a user-specified list. Therefore no change of the data base is necessary if certain species are to be included or excluded. Element or species input to ChemApp may be chosen. All data exchange between GeoSys and ChemApp is handled by the interface directly,

without any external files. The results of the geochemical simulation are directly written to the solution vectors of GeoSys.

In this section, a 1D transport and calcite dissolution case was adopted to verity our new coupling program. Here the employed 1 D reactive transport model is about a magnesium chloride solution flowing through a column containing calcite described by (Engesgaard and Kipp, 1992). This test example was proposed to verify MST1D code against the CHEMTRNS model by (Noorishad et al., 1987). In this study, both PHREEQC and ChemApp coupled to GeoSys/RockFlow were employed for the simulations. Using PHREEQC, the results from (Noorishad et al., 1987) are reproduced and thus compare well with MST1D, CHEMTRNS and PHT3D. Figure 2 shows the results of GeoSys-ChemApp and using PHREEQC. Comparison shows some deviation between the two results. The hypothesis is, that the different databases are the reason for this.
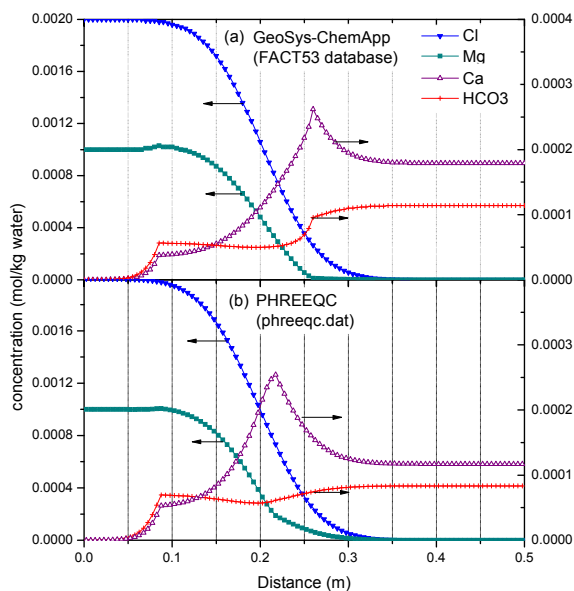
Fig. 2. Total aqueous elements (Cl, Mg and Ca) and species (HCO_3^-) concentration profiles at 21000 s for (a) GeoSys-ChemApp and (b) PHREEQC (using respective database).

In order to eliminate the differences stemming from the databases and test and compare both GeoSys-ChemApp and our previous coupled interface program, GeoSys-PHREEQC, one of the PHREEQC database files (phreeqc.dat) was converted to a ChemApp suitable database file. Basically speaking, the equilibrium constant method (PHREEQC) is the mathematical expression of the minimum Gibbs free energy method (ChemApp) for a chemical reaction. The two methods are conceptually equivalent. So we can get a new transformed database from phreeqc.dat. Using the transformed database for the same verification example as before, a very good correspondence of the two simulations is found (see Figure 3). Thus the differences observed before are due to differences in the databases. Therefore the new interface program, GeoSys-ChemApp, is correct and working correctly.

(a)

(b)
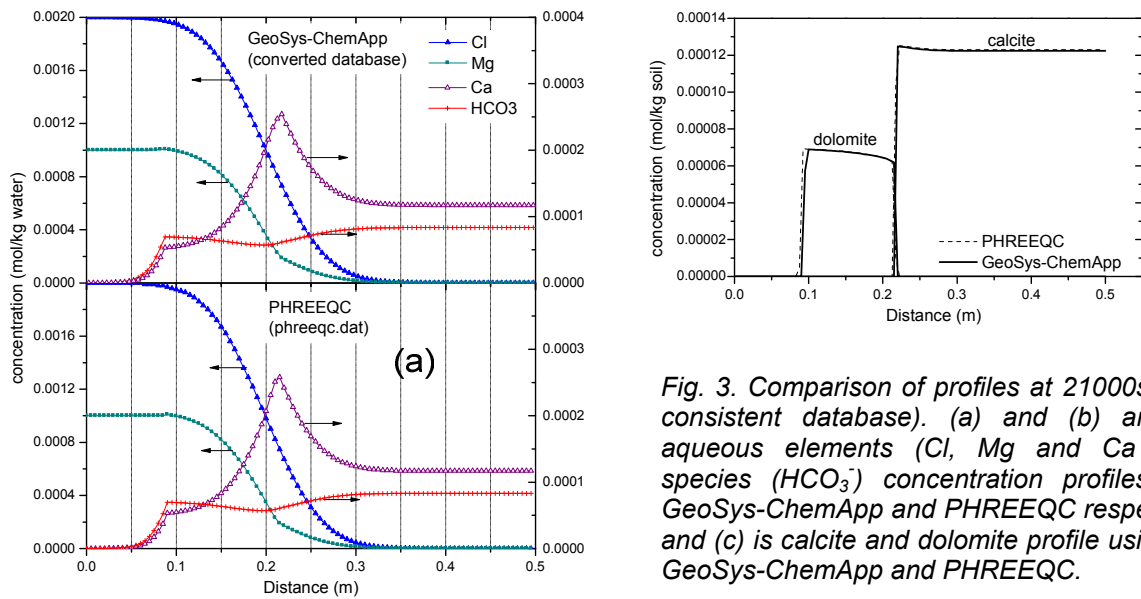
Fig. 3. Comparison of profiles at 21000s (using consistent database). (a) and (b) are total aqueous elements (Cl, Mg and Ca) and species (HCO_3^-) concentration profiles using GeoSys-ChemApp and PHREEQC respectively, and (c) is calcite and dolomite profile using both GeoSys-ChemApp and PHREEQC.

ChemApp allows to specify the input either as chemical species or by the total amount of the elements considered. The second option is the one also used in PHREEQC. In general, the SPECIES option should be more accurate, as the individual species are accounted for. However, the ELEMENT option allows for a faster code execution, as the number of elements is smaller than the number of geochemical mobile species. As the advection-dispersion equation has to be solved for either each species or each element, the element approach will become more efficient for high species numbers, as typically encountered during CO_2 sequestration. A comparison was performed using both the ELEMENT and the SPECIES transport option for ChemApp. As shown in Figure 4 (a) and (b), element transport reproduces the result of species transport closely, and may thus be an efficient way of simulating multi-species systems. After comparing the time required for the calculation (Figure 4 (c)), it is found that the species option needs more time for transport calculation because it includes more transport equations than the element option, while the reactive time becomes smaller than for the element option. The reason is that using species values as starting input for ChemApp leads to a faster solution of the equilibrium chemistry. In this case, the total nodes number is only 101, which is very small, so the transport time is far smaller than the reactive time. In practical applications, however, the node number will be much larger and we expect that element transport will save computation time.
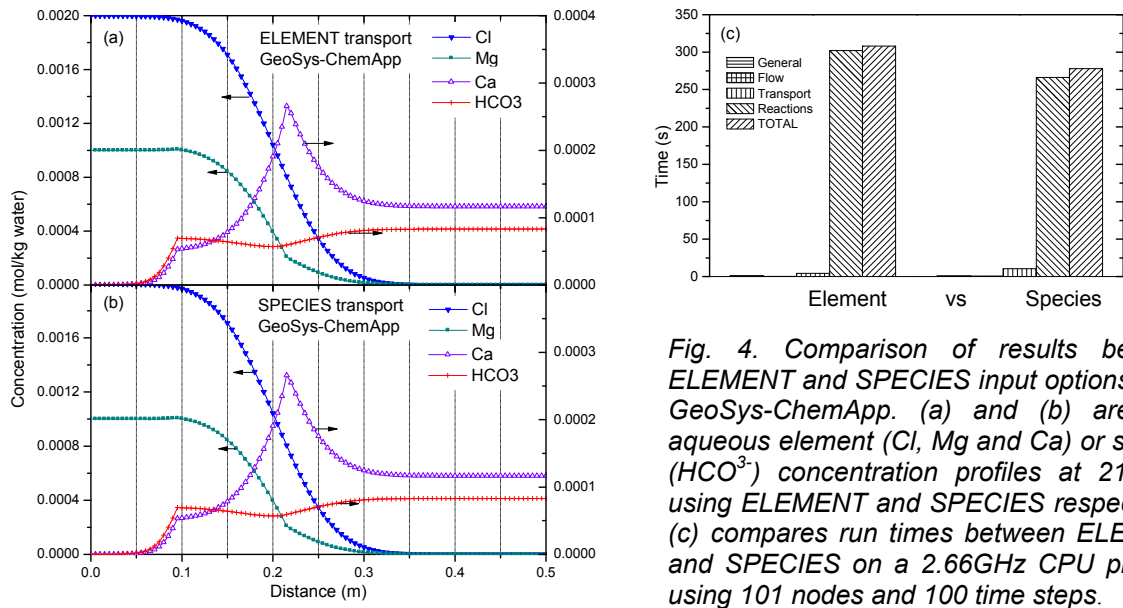
Fig. 4. Comparison of results between ELEMENT and SPECIES input options using GeoSys-ChemApp. (a) and (b) are total aqueous element (Cl, Mg and Ca) or species (HCO$_3^-$) concentration profiles at 21000 s using ELEMENT and SPECIES respectively. (c) compares run times between ELEMENT and SPECIES on a 2.66GHz CPU platform using 101 nodes and 100 time steps.
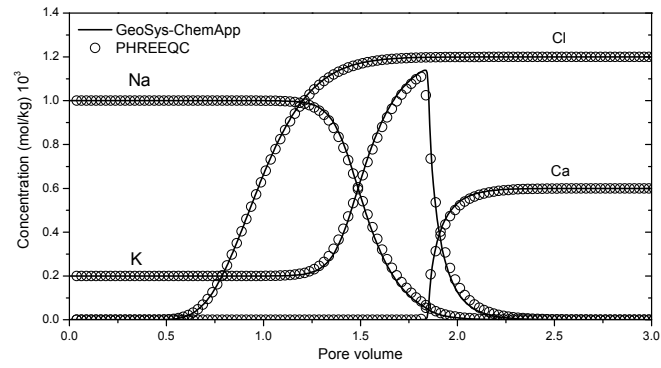
Fig. 5. Comparison of results obtained by GeoSys-ChemApp and PHREEQC on cation exchanger process

Using the converted database, it became also possible to simulate exchange processes using the ChemApp interface. Here the benchmark contains species transport and cation exchange and is employed to verify the new interface with PHREEQC. The details are described in the PHREEQC user's guide (PARKHURST and APPELO, 1999, p238). Figure 5 shows result of our simulation. The comparison shows a good correspondence of the two simulations. So GeoSys-ChemApp has the ability of exchange simulations using the converted database.

To test the geochemical codes for realistic conditions and settings, the Weyburn CO$_2$ inject site was chosen as a representative setting. For this site, the fundamental parameters and species compositions for the simulation of coupled geochemical reactions and fluid transport simulation are available (see Table 2)

Table 2: Physical-chemical features of the reservoir and composition of two selected wells

63

in Weyburn oil field (Emberley et al. 2005).

physical-chemical features			WEY 4	WEY 12
oil/water	0.3	T ºC	23.6	30.2
gas/oil	30	pH	6.34	6.57
oil gravity	29 api	pe	-6.13	-5.66
TDS brines	30-300 g/L	brine composition (unit mg/L)		
pressure	150 bar	HCO3	493.4	358.8
temperature	62°C	HS	125.4	125.4
porosity	25-14%	Na	40850	27730
Permeability	11-15 mD	K	558.7	337.3
Water/rock	0.48-0.28Gas	Ca	1319	1559
		Mg	687.9	157.2
gas phase partial pressure (atm)		Mn	0.56	0.08
CH4(g)	0.438	Li	24.3	10.54
CO2(g)	0.04	Fe	2.56	0.80
H2(g)	0.0001	Sr	44.38	84.07
H2O(g)	0.0059	Si	6.86	10.32
H2S(g)	0.013	Cl	60565	42315
N2(g)	0.221	SO4	3105	3595
		mineral composition (% vol)		
		calcite	14.25	94
		dolomite	80	3
		gypsum	3	-
		K-feldspar	1.25	0.25
		Kaolinite	0.25	-
		pyrite	0.5	0.5
		quartz	0.5	0.5
		anhydrite	-	2

From the above Table 2, it is expected that the difficulties during simulation will be the high pressure conditions (150 bar) and the complex composition of the fluids (multi-components and high concentration, especially of the brine). In order to check the ability of GeoSys-ChemApp for high pressure application, a higher pressure (1500 bar) was used for the simulations. Prior to simulation, CO_2 solubility was calculated employing the method of activity coefficient–equation of state to determine the CO_2 solubility accurately at the condition of Weyburn field site, temperature, brine composition and high pressure (1500 bar). The calculated CO_2 solubility is 1.6275 mol/kg, about twice the value when using a pressure of 150 bar (DUAN and SUN, 2003; DUAN et al., 2006). A 1 D column model was set up which contains CO_2 saturated formation water flowing through a 8.2 m column with a transport velocity of 1 m per year. The time step is 0.1 year, and total simulation time is 1000 years. A total of 15 chemical elements and about 67 chemical species are considered in the simulation. The fundamental conditions for the simulation are shown in Table 3.

Table 3: Fundamental conditions for simulation.

porosity	0.15	time step Δt	0.1 year
permeability	0.0013 D	total time	1000 year
dispersion	0.01 m	Δx	0.1 m
diffusion	1.0E-9 m2/s	total x	8.2 m
flow velocity	1.0 m/y	database	FACT53, PITZ
		mass transport	15 elements
		chemical reaction	67 species
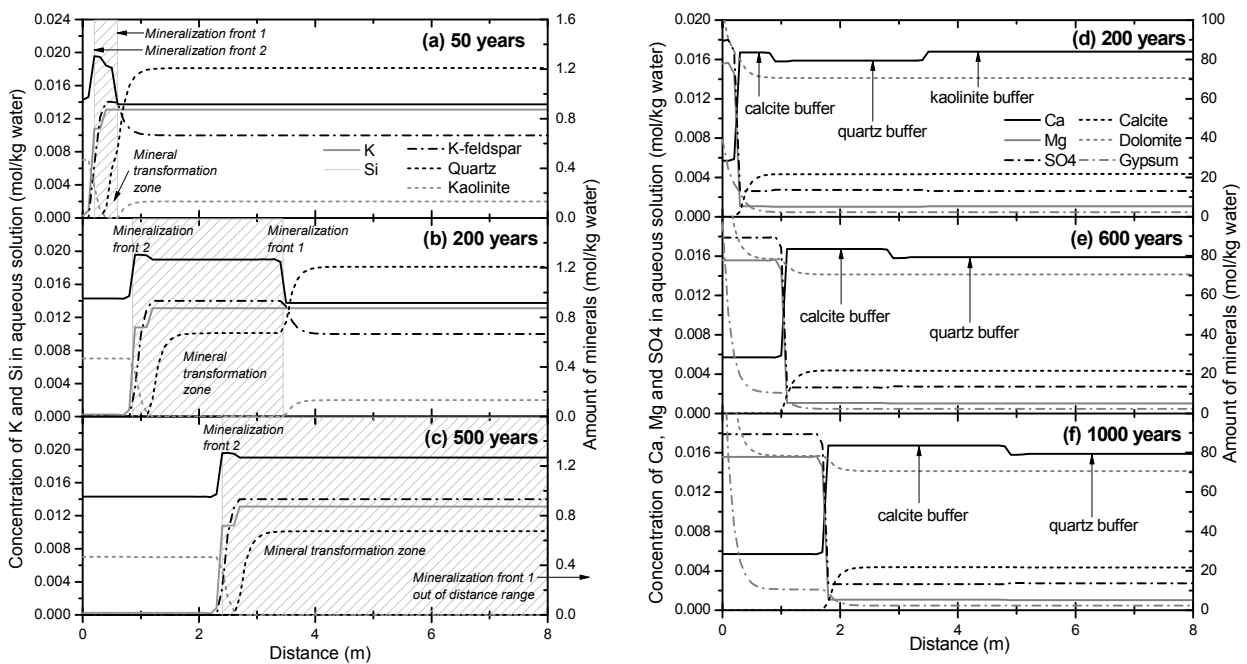
Fig. 6. Primary simulation result using GeoSys-ChemApp with Weyburn field data at high pressure.

The results are shown as concentration profiles versus distance for (a) 50, (b) 200 and (c) 500 years in Figure 6. Two mineralization steps are found. One is kaolinite+quartz→K-feldspar (mineralization front 1). Concentration of potassium increases during this reaction. The second mineralization front is K-feldspar+quartz→kaolinite. The concentration of potassium and silicon decreases, while quartz dissolves completely. Figure 6 also shows the relation between calcium, magnesium and their minerals versus distance after (d) 200, (e) 600 and (f) 1000 years. Due to the mineral assemblage, there are three buffers, which are kaolinite buffer, quartz buffer and calcite buffer. During calcite buffer, calcium and magnesium will form dolomite and gypsum while consuming CO_2 (compare dolomite and gypsum in Figure 6). So after the calcite dissolution, some CO_2 mineralization is found.

References

Eriksson G. and Petersen S. (2008). ChemApp - The Thermochemistry Library for your Software, Programmer's Manual Edition 3.12. GTT-Technologies, Herzogenrath, Germany, 1996-2008.

Kolditz O. and Bauer S. (2004). A process-oriented approach to computing multi-field problems in porous media. Journal of Hydroinformatics 6, 225-244.

Kolditz O. and Shao H. (2008). OpenTHMC Developer Benchmark Book based on GeoSys/RockFlow. 289pp.

Noorishad J., Carnahan C. L., and Benson L. V., (1987). Development of the nonequilibrium reactive chemical transport code CHEMTRNS, Rep. LBL-22361. Lawrence Berkeley Lab., Univ. of Calif., Berkeley.

Parkhurst D. L. and Appelo C. A. J. (1999). USER'S GUIDE TO PHREEQC (VERSION 2) —A COMPUTER PROGRAM FOR SPECIATION, BATCH-REACTION, ONE-DIMENSIONAL TRANSPORT, AND INVERSE GEOCHEMICAL CALCULATIONS. Water-Resources Investigations Report 99-4259. U. S. Geological Survey.

Petersen S. and Hack K. (2007). The thermochemistry library ChemApp and its applications. Int. J. Mater. Res. 98, 935-945.

Interaction of polyacrylic acid with dissolved Aluminium
- Preliminary modelling of polyacrylic acid titrations -

Johannes Lützenkirchen[1], John D. Wells[2], Jan van Maale[3], Frans Leermaakers[3] and Staffan Sjöberg[4]

[1] *Institut für Nukleare Entsorgung, Forschungszentrum Karlsruhe and Karlsruhe Institute of Technology, Postfach 3640, 76021 Karlsruhe, Germany*
[2] *Colloid and Environmental Chemistry laboratory, La Trobe University, Bendigo, P. O. Box 199, Bendigo, Victoria 3552, Australia*
[3] *Laboratory of Physical Chemistry and Colloid Science, Wageningen University, P.O. Box 9101 , 6700 HB Wageningen, The Netherlands*
[4] *Department of Chemistry, Umeå University, S-90187 Umeå, Sweden*

Interactions of natural organic matter with metal ions in the absence and presence of surfaces is an important issue in environmental sciences. Natural organic matter is a complexing agent for metal ions and can thus enhance contaminant concentrations and mobility. While the precise interaction of the metal ions with humic or fulvic substances is still not understood at the molecular level, it can be described and predicted rather well by approaches like the NICA-DONNAN model.

With a mineral like oxides, oxyhydroxides and hydroxides being present on the other hand, the interaction of metal ions with surfaces can be rather well understood, but the very detailed adsorption models are very difficult to transfer from well-defined laboratory systems to the real world environment.

The third sub-system considering the interaction of humic or fulvic substances with surfaces is complex because of various aspects:

- the adsorption of larger organic molecules bearing pH-dependent charges is affected by both the local charges on the surface and on the organic molecule, leading to charge regulated equilibria
- the interaction is further complicated by the ability of the molecules to complex metal ions from the mineral, thus enhancing the solubility of the mineral, and the possibility of adsorption of the resulting complex

Often, model organic substances are chosen to mimic the complex system, by attempting to decrease the complexity of the natural organic material. However, the use of polyacrylic acid obviously entails complications related to the size of the polyelectrolyte which can cause substantial conformational effects. We have used this polyelectrolyte to mimic natural organic matter as a secondary motivation. The primary motivation is the use of stabilising polyelectrolytes in the pulp and paper industry, where clays or aluminium minerals are frequently used. The intention of a model study is to achieve a better understanding of the concomitant interactions in the multi-component system.

The various sub-systems have been studied experimentally in a systematic way before studying the combined system. For the sub-systems we have tested various models to describe the respective interactions. This involves at present acid-base properties of the polyelectrolyte, dissolved aluminium and the surface. The hydrolysis of dissolved aluminium was not studied, since it well known for the conditions employed here.

We present experimental data on the interaction of polyacrylic acid (PAA) with dissolved aluminium in NaCl media. The solution study involves high precision potentiometric titrations of PAA in the presence and absence of dissolved aluminium. Complexation is evident from the shift of the titration curves with increasing concentrations of aluminium. Beyond a given Aluminium to carboxylate ratio, precipitation of a gel-like phase was observed.

The description of the acid base behaviour of polyelectrolytes is tested by different modelling approaches. Titration data obtained for polyacrylic acid at three different values of ionic strength as fixed by NaCl are used for the evaluation of the capabilities of the different models in terms of goodness of fit and realistic description of the underlying phenomena.

A simple surface complexation approach is found to be very successful: using the constant capacitance model only one pK_a value and a capacitance are required to obtain excellent fits to the data. Both parameters are ionic strength dependent, which is no surprise since the constant capacitance model cannot allow a self-consistent variation of parameters with ionic strength.

A second approach tests a Gouy-Chapman type of model using flat plate geometry, and approximate analytical solutions for spherical and cylindrical geometry. The ionic strength dependence of excluded volumes obtained with this model could not be brought into agreement with expected dependencies on ionic strength without including an additional constraint. The different geometries appear to be nearly indistinguishable from each other in terms of goodness of fit. This is explained by the high number of adjustable parameters involved in the models.

The third approach is the Non-Ideal Competitive Consistent Adsorption (NICCA) Donnan model. This model allows for a maximum of two distinct groups. However, even with only one functional group a very good description of the experimental data is possible.

The last model is based on the Self-Consistent-Field theory (SCF) and in the present case treats the polyelectrolyte solution as a sinlge molecule grafted in the centre of a spherical lattice. Since the concentration range of the PAA in the titrations is sufficiently low, no interaction between different molecules is expected. The model allows different states of the functional groups (protonated, deprotonated or complexed). With this approach one functional group cannot yield a satisfactory description of the data. With two segments (one being a monoprotic species, the other being a diprotic species) having dimensions that are in agreement with the chosen size of lattice discretization, a reasonable description of the data, including the ionic strength dependence is achieved. Moreover, the variation in size with pH can be obtained and corresponds to the expected tendency.

ORCHESTRA, a computational framework for combining geochemical, physical and biological process models

Johannes C.L. Meeussen
Energy research Centre of the Netherlands, P.O.Box 1, 1755 ZG, Petten, The Netherlands

Introduction

The ORCHESTRA framework is a software tool that was specifically designed to facilitate the implementation of complex geochemical equilibrium models, and to make it easier to use these models in combination with mass transport or biological impact models (Meeussen 2003).
To achieve this, a new chemical equilibrium module was designed that can calculate chemical equilibrium composition of a system for a given set of chemical reactions and mass balances constraints, but has an internal structure that is very different.

Key design features of geochemical module

External model definitions
In contrast with *de-facto* standard programs such as PHREEQC, MINTEQ, GWB or ECOSAT, in ORCHESTRA the equations that make up the geochemical models are not defined within the source code, but in an external file that is read at run-time. As this (text) file is readily accessible, users have the possibility to change or add the model definitions, without changing the ORCHESTRA source code.

Object oriented model structure
Apart from simply being accessible it is also important that the structure of the model definitions in this file is object oriented. This implies that that models do not have to be build from scratch but can be composed out of a set of basic building blocks (objects). This greatly helps to ensure that model definitions consistent, and also results in very compact model definitions.

Large set of available models
Because the structure of ORCHESTRA makes adding new models relatively simple, the current set of model implementations in the ORCHESTRA model database is quite extensive and contains state-of the art surface complexation model implementations such as; NICA-Donnan, CD-MUSIC Generalized two layer model, Basic Stern Constant Capacitance, solid solutions, minerals, gases ionic strength corrections etc.

Flexible input output variable definition
A further key design feature of the ORCHESTRA chemical equilibrium module is that any user defined geochemical model can be used as part of mass-transport or biological uptake or impact models (Vink and Meeussen, 2007). To make this possible, any variable that is used within the equilibrium module can be used in the communication with other modules. The set of variables that is used for input and output of the geochemical module are defined at run-time. In this process mass-transport or uptake modules define which "chemical" variables are required. This makes any variable available and at the same time prevents unnecessary passing of

large amounts of unused data. For example some mass transport modules only require total element concentrations in solution, while others require detailed information on distribution of elements over species, charges diffusion coefficients etc.

Graphical user interface for setting up equilibrium systems

The process of setting up complex chemical equilibrium systems is greatly facilitated by a graphical user interface. This user interface allows users to select a number of base components and then automatically selects all dependent (adsorption precipitation etc) reactions substances from the chosen database(s).

Design characteristics of mass transport module

The ORCHESTRA framework contains a mass transport module, that numerically solves finite differences scheme. Just as is the case for the chemical calculations also the transport model equations are defined outside the source code in an input file. In fact the same internal generic calculator is used for chemical and transport calculations. Transport equations are also defined in the external ORCHESTRA model database which contains model objects for (electro-neutral) diffusion and convection. Users can define specific transport equations if required. Most recent development is the implementation of unsaturated water flow (Richards equation module) that is being developed in collaboration with Wageningen University (S. van der Zee, A. van den Broek) that can be used in combination with reactive mass transport.

General

The ORCHESTRA program is written in Java and runs on any operating system for which a Java virtual machine is available (Windows, MacOSX, Linux). It is available free of charge from www.ecn.nl/orchestra.

Example applications

The use of ORCHESTRA for practical applications is illustrated by in a number of practical applications: chemical equilibrium system with large number of elements and processes (Dijkstra et al.), multi-component transport in system with diffusion and convection domain (Van Beinum et al 2004), radial diffusion large set of substances in of reactive (cementitious) systems (Van der Sloot et al 2006).

References

Meeussen J.C.L. (2003). ORCHESTRA: An object-oriented framework for implementing chemical equilibrium models, *Environmental Science & Technology*, 37 (6): 1175-1182.

Dijkstra J.J.; Meeussen J.C.L; Comans R.N.J. (2004). Leaching of heavy metals from contaminated soils: An experimental and modeling study, *Environmental Science & Technology*, 38 (16): 4390-4395.

Vink J.P.M., Meeussen J.C.L. (2007). BIOCHEM-ORCHESTRA: A tool for evaluating chemical speciation and ecotoxicological impacts of heavy metals on river flood plain systems. *Environmental Pollution*, 148 (3): 833-841.

Van Beinum W., Meeussen J.C.L, van Riemsdijk W.H. (2006). Competitive sorption and diffusion of chromate and sulphate in a flow system with goethite in gel beads, *Journal of Contaminant Hydrology*, 86:262-278.

Van der Sloot H.A., Meeussen J.C.L., van Zomeren A., Kosson D.S. (2006). Developments in the characterization of waste materials for environmental impact assessment purposes, *Journal of Geochemical Exploration*, 88:72-76.

Reactive transport modelling of cemented layer formation in sulfide-bearing mine tailings

Jeannet A. Meima, Torsten Graupner and Dieter Rammlmair
Federal Institute for Geosciences and Natural Resources (BGR)
Stilleweg 2, 30655 Hannover, Germany

Introduction

Sulfide-bearing mine tailings are known for their potential to form Acid Rock Drainage (ARD). The ARD-formation rate is strongly dependent on the amount and reactivity of the residual sulfide minerals and the accessibility of oxygen and water. The presence of buffering phases (e.g. carbonates, reactive mica's) has been shown to decrease the ARD-formation rate.

Natural attenuation processes may also result into the formation of hardpans or cemented layers, which are layers characterized by increased concentrations of secondary phases. Due to the amorphous or partially crystalline nature of these secondary phases, a substantial temporary attenuation of toxic compounds as well as a reduction in porosity and permeability may occur. Hardpans / cemented layers have predominantly been found in regions of increased stratification (Graupner et al., 2007).

In this study, possible effects of stratification on the potential of sulfide-bearing mine tailings to form protective cemented layers has been investigated by reactive transport modelling. The simulations were focussed on the presence or absence of biotite-rich layers and/or iron sulfide-rich heavy mineral layers. The presence of such layers usually contributes to the formation of geochemical interfaces, characterized by sudden changes in permeability and mineralogy.

Methods

Our reference site is the Muenzbachtal tailings impoundment from the poly-metallic sulfide mine district Freiberg, Saxony, Germany, which contains low sulfide low carbonate tailings (Graupner et al., 2007). Multiple cemented layers have been observed at the eastern rim of this site, which also shows a very complex stratification, revealing variations in particle size and mineralogy.

The reactive transport code FLOTRAN (Lichtner, 2007) was used for simulation of 1D reactive transport processes in the unsaturated tailings. The model was run in fully coupled mode, allowing changes in porosity due to mineral precipitation or dissolution to affect the hydraulic permeability. The upper boundary was defined by a constant temperature of 20 ^{o}C and a net rain water infiltration of 0.1 m.y^{-1}. The lower boundary was defined by a groundwater table at a depth of 5 meter, which is sufficient for not influencing the main zone of cemented layer formation (0 – 2 meter).

Three scenarios were defined to study the effect of the presence or absence of biotite-rich layers and/or iron sulfide-rich heavy mineral layers: HOM: a homogeneous distribution of reactive minerals (2 v/v-% iron sulfides, 5 v/v-% biotite, 10 v/v-% anorthite) in a loamy-sandy matrix (quartz). HET1: interbedded strata of biotite-rich (15 v/v-%) clay layers in a homogeneous loamy-sandy matrix containing iron sulfides (2 v/v-%), anorthite (10 v/v-%) and quartz. HET2: interbedded strata of biotite-rich (15

v/v-%) clay layers overlain by iron sulfide-rich (15 v/v-%) heavy mineral layers in a homogeneous loamy-sandy matrix containing anorthite (10 v/v-%) and quartz.

The initial concentrations of the primary phases were estimated on the basis of field data. Kinetically controlled reaction parameters were calibrated on the basis of column experiments (Meima et al., in prep.). Thermodynamic constants were taken from the minteq.v4 database (PHREEQC 2.13.05; Parkhurst and Appelo, 1999). Equilibrium constants for As(III) and As(V) aqueous species as well as solubility constants for crystalline and partly crystalline scorodite ($FeAsO_4.2H_2O$) and amorphous ferric arsenate ($FeAsO_4.2H_2O$) were taken from Langmuir et al. (2006). Hydraulic properties were based on average values for loamy sand and clay (HYDROUS1D).

Results and discussion

The simulated mineralogy and $O_2(g)$ levels after ~ 70 years for the cases HOM, HET1 and HET2 are presented in Figure 1. The following secondary phases were allowed to precipitate: jarosite, ferrihydrite (Fe-gel), silica gel, gypsum, gibbsite, alunite, and amorphous ferric arsenate (Fe-As-gel). These phases, except for gibbsite and alunite, are in accordance with the phases identified in cemented layer samples collected in the field (Graupner et al., 2007). The fate of Al is subject of ongoing research.

In the case of HOM, the simulated secondary phases were calculated to precipitate uniformly over the entire profile. The oxidation front was calculated to move downward continuously, as a result of the ongoing oxidation of sulfides. At the end of the simulation, the gas phase was calculated to be oxygen-saturated and the iron sulfides completely oxidized down to the assumed ground water table at 5 meter depth.

In the case of HET1, an accumulation of secondary phases was calculated in the biotite-rich layers. The oxidation front was calculated to remain at the third biotite-rich layer at 1.5 m depth. Consequently, the ongoing oxidation of sulfides at greater depths was largely prevented.

In the case of HET2, an accumulation of secondary phases was calculated in the biotite-rich layers as well. The oxidation front was calcuated to remain at the first biotite-rich layer at 0.3 m depth, and subsequently, the ongoing oxidation of sulfides at greater depths was largely prevented. In comparison with case HET1, the concentration of reactive minerals at the uppermost biotite-rich layer was much higher due to the presence of a heavy-mineral rich layer on top of the biotite-rich layer.
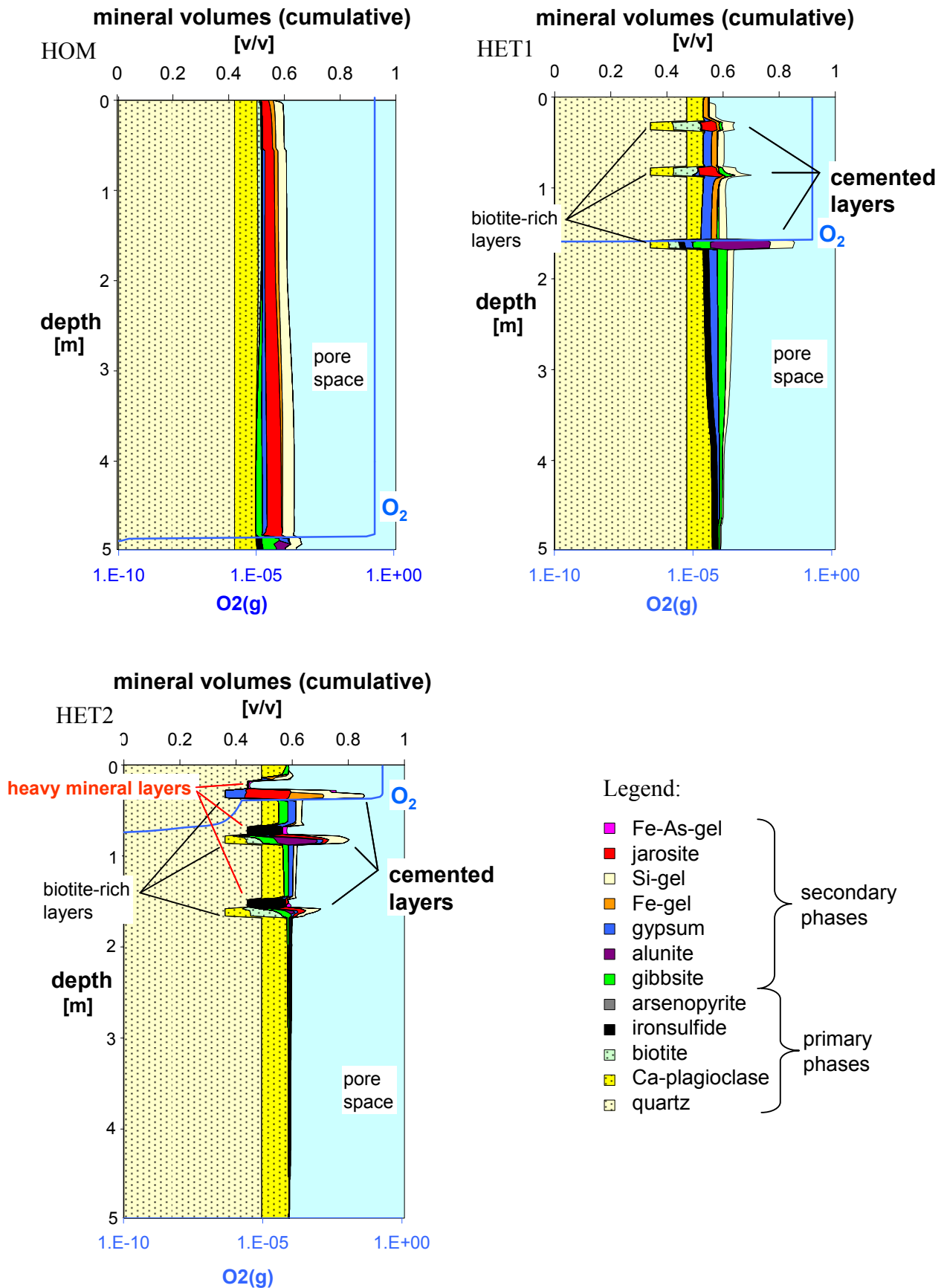
Fig. 1. Simulated effects of stratification on cemented layer formation after ~ 70 years for the cases HOM, HET1 and HET2.

The modelling results can be explained by the following processes: (a) diffusion of O_2 and oxidation of iron sulfides resulting in the generation of ARD; formation of an oxidation front, (b) downward transport of Fe^{2+}, SO_4^{2-}, and H^+, (c) buffering of the acid solution by dissolution of biotite, which causes the release of K^+ and results in the precipitation and accumulation of jarosite, Si-(Al) gels, and of Fe-hydroxides in biotite-rich layers, as well as (d) the dissolution of Ca-plagioclase from the sandy matrix, which causes the release of Ca^{2+} and contributes to the precipitation of gypsum and Si-(Al)-gels.

Conclusions

The presented modelling results, which are basically supported by field observations, have indicated that the formation of cemented layers consisting of oxyhydroxides (e.g. ferrihydrite) or hydroxysulfates (e.g. jarosite) is generally favoured at geochemical interfaces. In homogeneous systems without stratification, secondary phases do not accumulate in distinct horizons.

References

Graupner T., Kassahun A., Rammlmair D., Meima J.A., Kock D., Furche M., Fiege A., Schippers A., Melcher F. (2007). Formation of sequences of cemented layers and hardpans within sulfide-bearing mine tailings (mine district Freiberg, Germany). Applied Geochemistry 22, 2486-2508.

Langmuir D., Mahoney J., Rowson J. (2006). Solubility products of amorphous ferric arsenate and crystalline scorodite ($FeAsO_4.2H_2O$) and their application to arsenic behaviour in buried mine tailings. Geochim. Cosmochim. Acta 70, 2942-2956.

Lichtner P.C. (2007). FLOTRAN user's manual: two-phase nonisothermal coupled thermal-hydrologic-chemical (THC) reactive flow & transport code, Version 2.0: LA-CC 02-036, LANL Report LA-UR-01-2349, 26. Oktober 2007, Los Alamos, USA.

Parkhurst D.L. and Appelo C.A.J. (1999). User's guide to PHREEQC (version 2) – A computer program for speciation, batch-reaction, one-dimensional transport, and inverse geochemical calculations., Water-Resources Investigations Report 99-4259, U.S. Geological Survey.

Influence of Cl⁻ and CO₃²⁻ complexations on Eu³⁺ distribution at the mica–water interface: A Monte Carlo Study

Artur Meleshyn
Center for Radiation Protection and Radioecology, Leibniz Universität Hannover, Herrenhäuser Str. 2, 30419 Hannover, Germany

Muscovite mica is a clay mineral with a basal surface structure very similar to that of illite and montmorillonite, which are two other clay minerals of high importance in various environmental and industrial applications. In contrast to the latter two minerals, however, muscovite has cleavage properties, which allow to produce an atomically flat surface over a large area sufficient for use in X-ray reflectivity (Schlegel et al. 2006) or atomic force microscopy (Plaschke et al. 2000) measurements. The former method provides valuable information about the distribution of adsorbed species along the direction normal to the solid-liquid interface, whereas the latter method gives insight into the lateral structure of adsorbed aggregates, which can be strongly influenced by Eu^{3+} ions (Plaschke et al. 2000; Plaschke et al. 2002).Monte Carlo simulations of the interface between the cleaved surface of muscovite mica and aqueous solution containing Eu^{3+} as well as Cl^-, CO_3^{2-} or H_3O^+ ions at varying concentrations were carried out at ambient conditions. A detailed molecular-scale data on the structure of adsorbed water, equilibrium positions of the adsorbed ions as well as on the structure and type of their adsorption complexes at the muscovite-water interface were obtained. The simulated data were compared with results of X-ray reflectivity studies (Schlegel et al. 2006) and the preceding simulation studies (Meleshyn 2008a; Meleshyn 2008b) of muscovite-water interface as well as available literature data on hydration structure of Eu^{3+} and its adsorption on montmorillonite and illite (Rabung et al. 2005). The calculated equilibrium atomic density profiles were used to estimate electron density profiles and integrated electron densities. Since to the author's knowledge no X-ray reflectivity study of Eu^{3+} at the mica-water interface has been carried out yet, a comparison of the simulated and experimental distribution of Eu^{3+} were not possible. The simulated data can, however, be used as input for a best-fit of X-ray reflectivity data in a future experiment. In particular, simulation results reveal that distribution of Eu^{3+} depends on its surface concentration and the ligand type (Cl^- or CO_3^{2-}). The corresponding structural differences were predicted to be distinguishable with help of the X-ray reflectivity technique. This would also allow establishing a relation between surface and bulk solution concentrations of Eu^{3+} ions.

References

Schlegel M. L., Nagy K. L., Fenter P., Cheng L., Sturchio N. C., Jacobsen S. D. (2006). Cation sorption on the muscovite (100) surface in chloride solutions using high-resolution X-ray reflectivity. Geochim. Cosmochim. Acta, 70, 3549-3565.

Plaschke M., Römer J., Klenze R., Kim J. I. (2000). Influence of europium(III) on the adsorption of humic acid onto mica studied by AFM. Surf. Interface Anal., 30, 297-300.

Plaschke M., Rothe J., Schäfer T., Denecke M. A., Dardenne K., Pompe S., Heise K.-H. (2002). Combined AFM and STXM in situ study of the influence of europium(III) on the agglomeration of humic acid. Colloids Surf. A, 197, 245-256.

Fenter P., Park C., Nagy K. L., Sturchio N. C (2007). Resonant anomalous X-ray reflectivity as a probe of ion adsorption at solid-liquid interfaces, Thin Solid Films, 515, 5654-5659

Meleshyn A. (2008a). Two-dimensional ordering of water adsorbed on a mica surface at room temperature, J. Phys. Chem. C, 112, 14495-14500.

Meleshyn A. (2008b). Aqueous solution structure at the cleaved mica surface: Influence of K^+, H_3O^+, and Cs^+ adsorption, J. Phys. Chem. C, 112, 20018-20026.

Rabung Th., Poerret M. C., Bauer A., Geckeis H., Bradbury M. H., Baeyens B. (2005). Sorption of Eu(III)/Cm(III) on Ca-montmorillonite and Na-illite. Part 1: Batch sorption and time-resolved laser fluorescente spectroscopy experiments. Geochim. Cosmochim. Acta, 69, 5393-5402.

An alternative to permeability upscaling in reactive transport models

Jeremy Nos[1, 2], Vincent Lagneau[1] and V. Langlais[2]
[1]*Ecole des Mines de Paris – Centre de Géosciences, 35 rue St. Honoré, 77305 Fontainebleau Cedex, France*
[2]*AREVA NC – Business Unit Mines, Tour AREVA, 1 place Jean Millier, 92084 Paris La Défense Cedex, France*

Introduction

This work on the upscaling of reactive transport is part of the modelling effort of the *in situ* recovery (ISR) of uranium. ISR is a mining technique, which involves injecting a solution into the deposit to selectively dissolve uranium. The solution enriched in uranium is pumped out and processed. Once the uranium is removed, it is acidified and reinjected. AREVA NC takes an increasing interest in this mining technique and puts efforts to improve exploitation management tools.

The first step in modelling reactive transport is to define the spatial distribution of the required parameters: porosity, permeability and mineralogy. The discretization of these spatial distributions is often too fine to get reactive transport results within reasonable central processing unit (CPU) time, therefore upscaling can be utilized. In case of additive variables, upscaling only consists of calculating an arithmetic mean.

Permeability upscaling, which has long been studied in the petroleum field, is much more complex. In this presentation, we deal with two conventional methods of permeability upscaling in order to show their limitations in specific heterogeneous cases. Then, we propose an alternative method, which consists of uncoupling flow and transport. Conventional methods aim at upscaling all the simulation parameters, however another approach is possible: first calculating the flow on a fine grid, then calculating the transport on a coarse grid. From the permeability distribution and flow conditions on the fine grid, we calculate the flow rate field, which can be easily upscaled when defined on the borders of each mesh (that is typically the case when using reactive transport models with a finite volumes spatial discretization). Then, upscaling the other parameters (porosity, mineralogy) enables the calculation of the reactive transport on a coarse grid.

As a result of using the "uncoupling" approach to stationary flow, a gain in CPU time equivalent to permeability upscaling methods is achieved. It gives more accurate results and could turn out to be more flexible when modifying the flow conditions or the permeability field during the simulation. Indeed, the flow rates are not constant on site, and mineral precipitation and dissolution can result in a change in porosity and permeability.

Conventional upscaling techniques

Context

The primary benefit of upscaling is CPU time saving. In reactive transport models, the required CPU time can increase dramatically when dealing with more complex geochemistry. For example, a field with dimensions of 100 m x 100 m discretized into

a 50 x 50 mesh, with one injector and one producer well, the required CPU time for a 50 day simulation is roughly:

- 20 seconds for non-reactive transport
- 20 minutes for carbonate dissolution

Utilizing upscaling to a 25 x 25 mesh, the required CPU time reduces to:

- 5 seconds for non-reactive transport
- 5 minutes for carbonate dissolution

CPU time is proportional to the number of mesh. CPU time can be several hours or days when dealing with complex geochemistry, which is unacceptably long, therefore upscaling is a time-efficient tool.

Limits of permeability upscaling

Conventionally, upscaling in reactive transport equates to permeability upscaling since all other parameters are upscaled by calculating their arithmetic means. Two techniques have been studied in this work: the simplified renormalisation (Renard et al. 2000; King 1989) and the Output Least Squares (OLS) method (Holden and Nielsen, 2000). In general they work well, however, in some cases they yield poor results. Typically, they cannot capture a connectivity whose scale is small compared to the coarse mesh size. Here, we focus on such a case, illustrated by the fine permeability field in figure 1, the porosity is assumed to be constant (0.35). Figure 2 shows the coarse permeability field obtained by the OLS method. Figures 3 and 4 represent the spatial distribution of a non reactive tracer, injected by the injector well (I) and pumped by the producer well (P) for the same period of time in the fine case and the upscaled case.
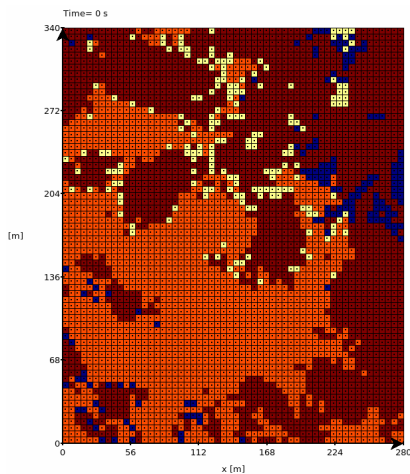
Fig. 1. Initial permeability field (in m/s.).
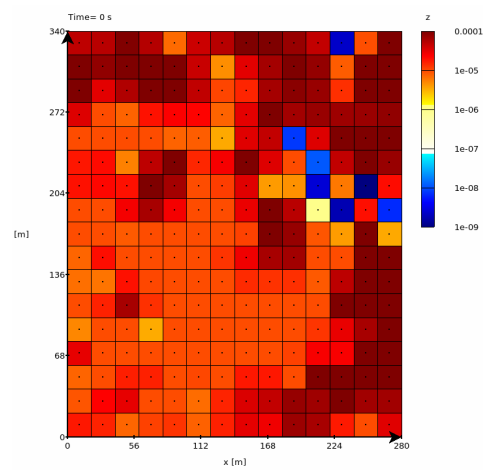
Fig.2. Upscaled permeability field (in m/s).
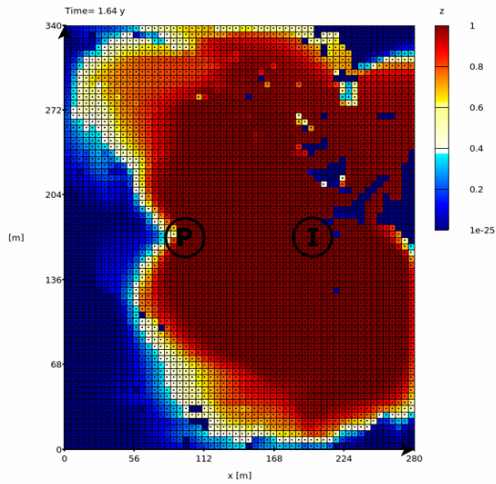
Fig. 3. Spatial distribution of a non-reactive
tracer in the initial case.
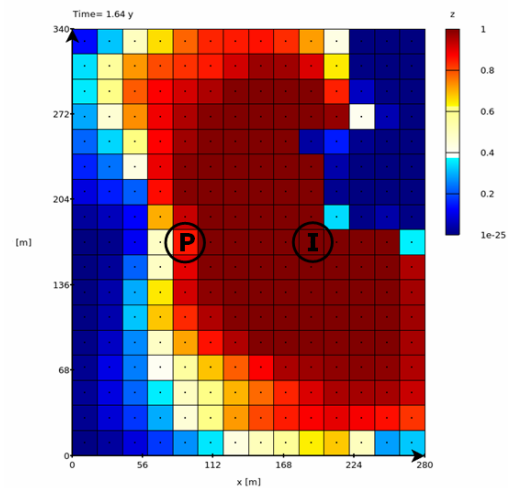
Fig.4. Spatial distribution of a non-reactive
tracer in the upscaled case.

On the eastern part of the fine permeability field, a clayey area can be observed (many meshes at a 10^{-9} m/s permeability), where the connectivity is very slight. The paths, through which the solution can reach the eastern part of the field, are very tight. On the coarse field, the OLS method has turned this slight connectivity into a strong permeability barrier, the solution is unable to go through this clayey area. The impact of upscaling is clearly misleading.

With simplified renormalisation (results not presented) the impact of upscaling is less significant because the permeability field is not scalar anymore. Thus, it gives a permeability barrier along the Y axis but not along the X. The trajectory of the injected tracer around this eastern part of the field is substantially different from what it is in the fine case. This method is unable to describe correctly what was observed on the fine scale.

Uncoupling flow and transport

The main objective of this method is to avoid permeability upscaling. As mentioned in before, the required CPU time for reactive transport simulation depends more on the geochemistry than on the flow calculation. Consequently, calculating the flow at the fine or coarse scale does not impact significantly on CPU time. Moreover, the permeability field is not necessary to calculate the transport, as seen in the general equation:

$$\phi \frac{\partial c}{\partial t} = div(D \cdot grad(c) - cU),$$

with:
ϕ the porosity,
c the tracer concentration,
D the dispersion (assumed to be constant),
U the flow rate.

Therefore, it is easier to calculate the flow at the fine scale and then upscale the flow rate field. To do it properly, the flow rate at the borders of each mesh must be known so that the fluxes through the mesh can be upscaled. On a regular grid, the

equivalent flow rate at the coarse scale is simply the arithmetic mean of the flow rates at the fine scale. Schematically, it comes down to:

$$\begin{array}{cc} \overrightarrow{q_{21}} & \overrightarrow{q_{22}} \\ \overrightarrow{q_{11}} & \overrightarrow{q_{41}} \\ & \\ \overrightarrow{q_{12}} & \overrightarrow{q_{42}} \\ \overrightarrow{q_{31}} & \overrightarrow{q_{32}} \end{array} \rightarrow \begin{array}{cc} & \overrightarrow{Q_2} \\ \overrightarrow{Q_1} & \overrightarrow{Q_4} \\ & \overrightarrow{Q_3} \end{array}$$
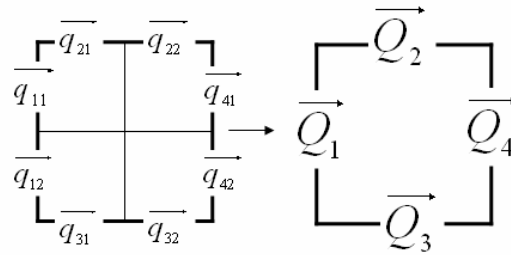
with $\overrightarrow{Q_1} = \overrightarrow{q_{11}} + \overrightarrow{q_{12}}$, etc.

Using this method, the spatial distribution of the tracer, represented in the figure 5, matches the fine case much better than the OLS method does. Take note that, in the fine case, almost no solution goes through the clayey mesh, which means that their effective porosity is almost zero. In realistic models, very low permeabilities are often linked to very low porosities. In our simplified model however, the porosity was assumed to be constant. To be more realistic, porosity values can be set to zero on the fine clayey mesh before upscaling. Fundamentally, as shown in figure 6, there are minor differences between both models.
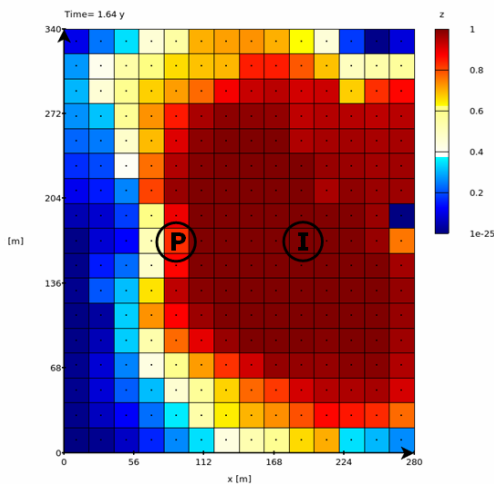
Fig. 5. Spatial distribution of the non-reactive tracer ("uncoupling" method, constant porosity).
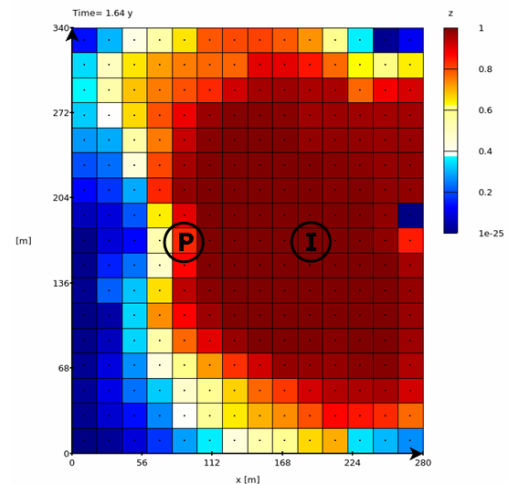
Fig6. Spatial distribution of the non-reactive tracer ("uncoupling" method, porosity = 0 at fine clayey meshes).

80

Conclusion

In conclusion, as long as the required CPU time depends more on the geochemistry than on the flow calculation, the "uncoupling" method results in the same CPU time as the conventional methods. It does however bring added advantages:
-   it is quite easy to compute and to integrate to a reactive transport model
-   it tends to give more accurate results than the conventional methods do

It seems to be a tool suited for our needs, even if the influence of the flow upscaling still needs to be analyzed. The next issue is the influence of the upscaling of the geochemical model.

Non-linearities in geochemistry must be dealt with, thus, upscaling a solubility product is a problem. Considering one mineral of solubility 1, composed of two constituents A and B (figure 7), this mineral is in equilibrium in 3 fine meshes (in grey), since the product of the concentrations of A and B is equal to 1. In the fourth mesh (in red), this product is lower than 1, resulting in dissolution of the mineral. When upscaling the geochemical model, which means calculating the arithmetic mean of the concentrations, the product of the upscaled concentration is higher than 1, which implies a precipitation of the mineral.
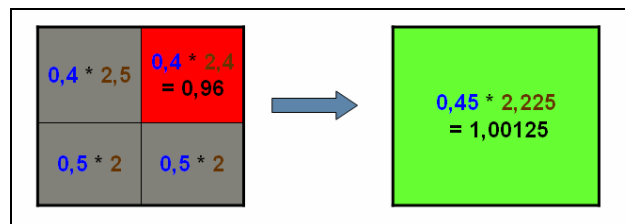
Fig.7. Impact of upscaling on a solubility product.

Another aspect of reactive transport is to deal with is the retroaction of the geochemistry on the transport. Mineral precipitation and dissolution result in changes in porosity, to which permeability is assumed to be linked. A downscaling is necessary. Assumptions need to be made about how the changes in porosity are distributed in the fine field and about the relationship between porosity and permeability.
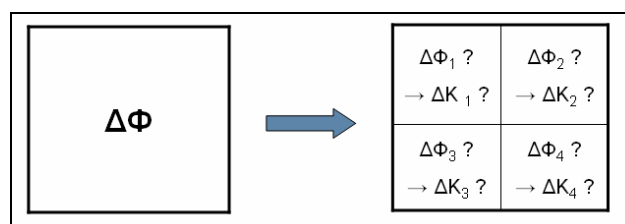
Fig. 8. Downscaling.

References

Renard P, Le Loc'h G, Ledoux E, de Marsily G, Mackay R. (2000). A fast algorithm for the Estimation of the Equivalent Hydraulic Conductivity of Heterogeneous Media. *Water Resources Research, 36*(12), 3567-3580.

King P. (1989). The Use of Renormalisation for Calculating Effective Permeability. *Transport in Porous Media*, 4, 37-58.

Holden L, Nielsen B.F (2000). Global Upscaling of Permeability in Heterogeneous Reservoirs; The Output Least Squares (OLS) Method. Transport in Porous Media, vol. 40, Number 2, August 2000.

Simulation of pulsed gas injections in respect to oxygen mass transfer and biogeochemical consumption

Sascha E. Oswald[1,*] and Gerd U. Balcke[2]
[1] *UFZ, Helmholtz Centre for Environmental Research – UFZ, Department of Hydrogeology, Permoserstr. 15, 04318 Leipzig, Germany*
[2] *metanomics GmbH, Tegeler Weg 33, 10589 Berlin, Germany*

One remediation technique is gas sparging that shall increase the levels of dissolved oxygen in an aquifer and by that enhance biodegradation processes for organic contaminants. However, gas sparging and its effects are difficult to assess, experimentally as well as numerically. We adapted and extended an existing numerical model called KBD, which is based on equations describing the mass transfer processes and gas phase development after injection in a kinetic framework. We used this approach to simulate a series of laboratory columns experiments with sandy aquifer material. The experiments included use of a partitioning tracer, measurement of breakthrough curves of dissolved gases and dissolved tracers for a number of oxygen gas pulses. The results showed that the oxygen transfer into the aqueous phase is slowing down with number of pulses of oxygen gas and strongly depends on the reverse transfer and accumulation of nitrogen. Further experiments established a chemical oxygen consuming reaction and proved that the degradation reaction, which depends on the transfer of oxygen into the aqueous phase, influences the fate of the gas phase noticeably. Simulations could provide the composition of the entrapped gas phase, the volumetric changes of the entrapped gas phase and the transport of oxygen through the columns. The numerical analysis then was extended to simulate a hypothetic field situation of gas sparging including a range of biological degradation rates. In this set-up also differences between injection of pure oxygen versus air were studied. The results give evidence that partitioning tracers and the naturally occurring nitrogen can contribute additional information and the gas dissolution process and thus the transfer of oxygen and the stimulation of biodegradation. Recently we started to extend the model to look into gas sparging in a large underground bioreactor discharged with local groundwater.

K_d and Competitive Sorption approach for the modelling of Ni Diffusion through Bentonite

Wilfried Pfingsten, Mike Bradbury and Bart Baeyens
Laboratory for Waste Management, Paul Scherrer Institut,CH-5232 Villigen PSI, Switzerland

In several international concepts for the deep geological disposal of high-level nuclear waste bentonite is the foreseen backfill material. Intensive research has been carried out on the long-term mechanical, thermal, hydraulic and geochemical properties of this material. Of special interest are, of course, the transport properties of safety relevant radionuclides. Most of the experiments focus on the determination of diffusion and sorption coefficients determined from laboratory experiments performed under a variety of boundary conditions (temperature, confining pressure, geochemical conditions,…). Diffusion tests are mostly carried out with samples on the centimetre scale. Since diffusion experiments with strongly sorbing radionuclides would require (very) long times, such sorption data is normally measured in so called batch sorption experiments at high liquid to solid ratios compared to low liquid to solid ratios present in diffusion experiments with compacted bentonite. In performance assessment calculations for radioactive waste repositories, the sorption of a radionuclide is described in terms of a single constant, the K_D value. Over the past years (quasi) mechanistic sorption models have been developed which are capable of describing uptake under different chemical conditions. Competitive sorption effects between a specific radionuclide and other dissolved metals in the groundwater and from the radioactive waste can be taken into account. These mechanistic sorption models can be included in reactive transport models which then allow the influence of factors such as varying groundwater compositions and mineral abundances to be taken into account in radionuclide transport calculation for different scenarios. The temporally varying conditions are directly included in the radionuclide transport calculations instead of trying to account for them by using a large range or uncertainty for a single K_D value.

At the moment reactive transport calculations are complex and require relatively long calculation times. Nevertheless, it is now possible to make judgements about calculations using the simplified K_D approach by comparing them to the more detailed reactive transport calculations and thereby reduce their uncertainty range. Further, for some radionuclides which compete with major ions in solution for the same sorption sites, such detailed calculations are necessary in order to be able to take important reactions into account when calculating radionuclide transport (Jakob et al.
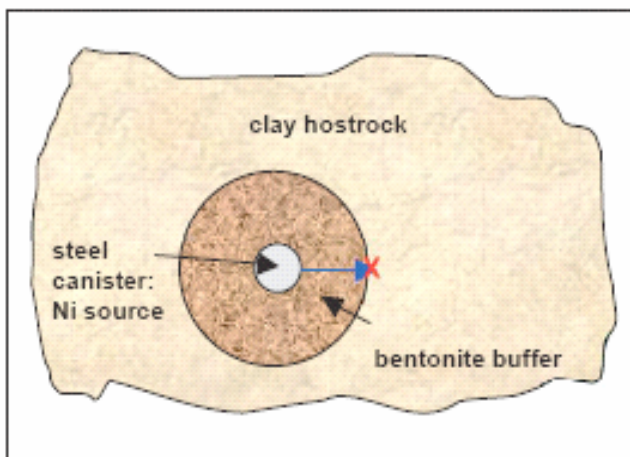
Fig. 1. Schematic cross-section through the near-field of a high-level nuclear waste repository. The migration path is indicated by the blue arrow; X indicates the interface at which the Ni arrival times are calculated.

2009). Fe(II), Mn(II), and Zn(II) for example are present at moderate concentrations in the bentonite porewater (values for Fe and Mn are given in Nagra 2002). These bi-valent metals will compete, for example, with [59]Ni(II) for the same sorption sites (Bradbury and Baeyens 2005a). In addition, Fe, Mn and Zn concentrations in the bentonite may vary with time due to canister corrosion processes and/or interaction with the host rock. As a consequence the number of accessible sorption sites for radionuclides may decrease, leading to additional desorption of radionuclides – additional radionuclides will dissolve back again in the porewater – which will in combination with an increased number of competing ions, may reduce the radionuclide retardation in the bentonite. Taking into account such processes is directly included when using multi-species reactive transport calculations and related sorption models at the same time with canister – bentonite – host rock interactions.In order to investigate Ni migration behaviour through compacted bentonite in detailed transport calculations, the 2SPNE SC/CE sorption model (Bradbury and Baeyens, 1997) was ported into the reactive transport code MCOTAC (Pfingsten 1996) and mechanistic sorption models were used for Ni, Fe, Mn and Zn. MX-80 bentonite consists of ~75 wt% Na-montmorillonite which is assumed to be the sorption relevant mineral phase in bentonite. Data from batch sorption experiments for Ni, Mn and Zn on Na-montmorillonite (Bradbury and Baeyens 1997) were used. For Fe(II), no experimental data were available and values for use in the sorption model were taken from the Linear-Free-Energy-Relationship (LFER) given in Bradbury and Baeyens (2005b).Transport, geochemical and Ni source term parameters for the modelling were taken from (Nagra 2002), i.e. an effective diffusion coefficient of $2 \cdot 10^{-10}$ m^2/s, the porewater composition as defined for MX-80 bentonite, and the initial Ni concentration was assumed to be constant and solubility limited at the steel canister - bentonite interface. Additional transport calculations using the K_D approach were performed with K_D values for Ni as used in Nagra (2002): Reference K_D value 0.2 m^3/kg, optimistic K_D value 5 m^3/kg, pessimistic K_D value 0.009 m^3/kg. The Ni arrival time or the Ni breakthrough at the bentonite – clay host rock interface was calculated for an assumed bentonite thickness of 0.46 m (see Figure 1).Figure 2 shows the Ni breakthrough in the compacted MX80-bentonite calculated for increasing sorption competition with respect to the number of major ions in the bentonite water taken into account. Starting from Ni sorption without competition, the competition is then increased in three steps from Ni with Fe, Ni with Fe and Mn and finally to Ni with Fe, Mn and Zn. The Fe and Mn concentration levels are assumed to be set by the solubility limits of siderite and rhodochrosite respectively. Both minerals are present in bentonite. Zn was assumed arbitrarily to be at a similar concentration as a further possible competing bi-valent ion. As can be seen, the Ni breakthrough occurs earlier and earlier with increasing sorption competition. Just taking into account competitive sorption with Fe(II), Ni(II) retardation is reduced by an order of magnitude, i.e. Ni(II) arrives an estimated 9000 years earlier at the bentonite - host rock interface predicted in the case where competitive sorption with Fe(II) is not taken into account. With increasing sorption competition, the breakthrough curves converge to the breakthrough curve calculated with the "reference case K_D value" with respect to the "initial breakthrough".
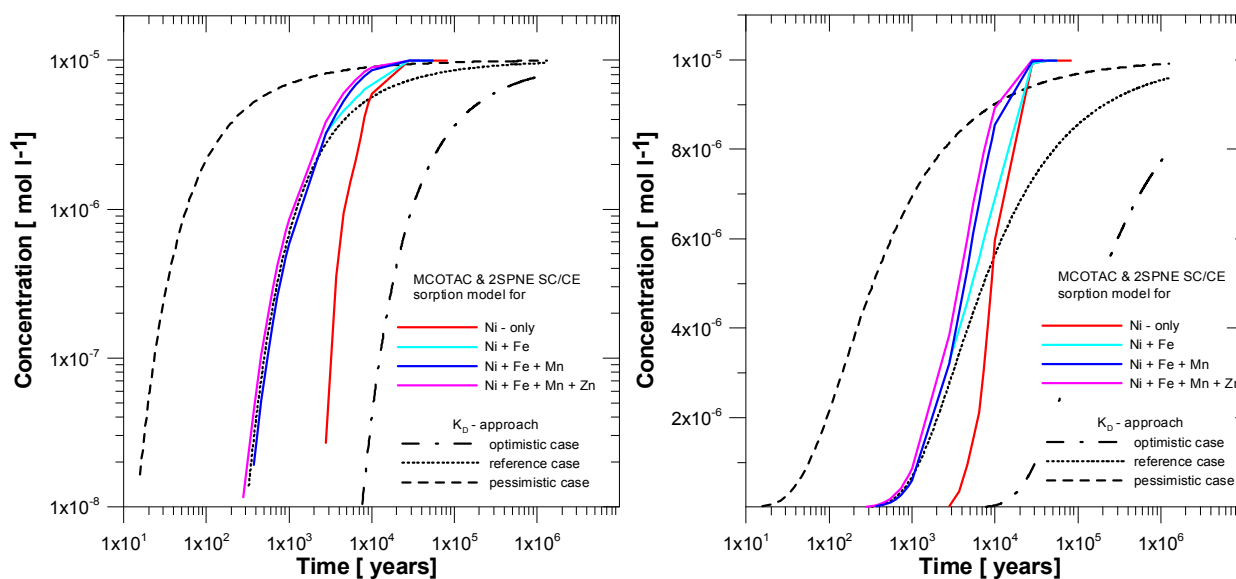
Fig. 2. Calculated Ni concentrations in the bentonite buffer 0.46 m away from the canister surface on a logarithmic-logarithmic scale (left) and a linear-logarithmic scale (right). The sorption of nickel is described in terms of the mechanistic sorption model by Bradbury and Baeyens (1997). A second set of calculations accounts for the effects of sorption competition between Ni and Fe; Ni, Fe and Mn; and Ni, Fe, Mn and Zn. For comparison, the results obtained from calculations based on the simple KD approach using bounding pessimistic and optimistic KD values for Ni (Nagra, 2002) are also shown.

However, when the linear-logarithmic plot of the breakthroughs (Figure 2) is examined, marked differences become apparent. The maxima in the breakthrough curves calculated with the sorption model are always earlier and higher than for the "reference" and "optimistic" K_D value cases. The maximums are even higher than in the "pessimistic K_D value case" after about 4000 years. To some extent these results show that sorption competition was "unknowingly" taken into account in batch sorption measurements, i.e. in the batch sorption tests dissolved Fe(II) , Mn(II) and Zn(II) were present at similar concentrations to those used in the calculations. It is important to realise that the batch sorption measurements are only valid for this one particular case. If the concentrations of Fe, Mn and Ni are higher or lower for whatever reason in the "real system" the K_D value chosen would be incorrect. Additional calculations showed that among all competition effects the sorption site capacity had the largest effect on the Ni breakthrough. Therefore, the temporal evolution of bentonite degradation and other precipitation and dissolution reactions at the canister-bentonite interface are important for the migration of Ni and will be investigated in more detail in the future. This work shows that the modelling of Ni diffusion experiments in bentonite requires analysis by reactive transport models which include complex sorption models. Incorrect transport parameter determinations may result from the analysis of laboratory diffusion experiments by more conventional methods e.g. a simple single-species K_D approach (see the example given in Jakob et al. 2009).

Acknowledgement

References

Bradbury M.H. and Baeyens B. (1997). A mechanistic description of Ni and Zn sorption on Na-montmorillonite Part II: modelling. Journal of Contaminant Hydrology, 27(3-4): 223-248.

Bradbury M.H. and Baeyens B. (2005a). Experimental measurements and modelling of sorption competition on montmorillonite. *Geochimica et Cosmochimica Acta* **69,** 4187-4197, and Erratum **69** 5863-5864.

Bradbury M.H. and Baeyens B. (2005b). Modelling the sorption of Mn(II), Co(II), Ni(II), Zn(II), Cd(II), Eu(III), Am(III), Sn(IV), Th(IV), Np(V) and U(VI) on montmorillonite: Linear free energy relationships and estimates of surface binding constants for some selected heavy metals and actinides. Geochimica et Cosmochimica Acta, 69(4): 875-892.

Jakob A., Pfingsten W., Van Loon L. (2009). Effects of sorption competition on caesium diffusion through compacted argillaceous rock. Geochem Cosmochem Acta (in press).

Pfingsten W. (1996). Efficient Modeling of Reactive Transport Phenomena by a Multispecies Random Walk Coupled to Chemical Equilibrium. Nuclear Technology, 116(2): 208-221.

Nagra (2003). Project Opalinus Clay: Safety Report. Demonstration for spent fuel, vitrified high-level waste and long-lived intermediate-level waste (Entsorgungsnachweis). NTB-02-05, Nagra, Wettingen, Switzerland.

Numerical modelling of tracer tests and estimation of hydro-geological properties of a shear zone at the Grimsel Test Site

Alexandra Pudewills, Florian Huber and Thorsten Schäfer
Forschungszentrum Karlsruhe GmbH, Institut für Nukleare Entsorgung, Karlsruhe, Germany

Crystalline rocks such as granite have been extensively investigated as a potential host rock for nuclear waste disposal. The crystalline rock matrix is nearly impermeable and the groundwater flows predominantly through discrete features as fractures or shear zones filled with porous material. Such features provide the primary pathway for the migration of radionuclides from an underground repository to the biosphere. In order to predict the movement of radionuclides, the processes involved must be understood and quantified. For this purpose, laboratory tests, field experiments and adequate numerical models are needed.

The Colloid Formation and Migration (CFM) project aims to investigate and quantify the impact of colloids on the transport of waste-derived radionuclides in a water-conducting fracture under near-natural hydrogeochemical conditions. The in situ experiment is located in the Grimsel Test Site (GTS) in Switzerland (Blechschmidt 2006). In the first phase of this project, different tracer tests with uranine as conservative tracer were performed. Prior to the tracer tests, the experimental tunnel was equipped with a 3m-diameter surface packer system. The scope of this packer was to avoid uncontrolled flow rates towards the tunnel wall, to reduce the hydraulic gradient in the shear zone and to achieve longer tracer travel times.

In this contribution the tracer tests performed in two different dipoles were analyzed numerically. The objectives of these numerical analyses are to calibrate the model and determine its parameters from a series of conservative tracer tests and to test the model with respect to its ability to simulate the migration of bentonite colloids. It was assumed that the groundwater flow and the solute transport take place in fractures filled with fault gouges, and the shear zone at the test location is plane which allows a two dimensional approach for the model geometry. The mathematical model is based on the Darcy's law for groundwater flow and the advection-dispersion equations for solute transport with a linear sorption in the fracture material. However, the model represents a planar confined porous media with a constant porosity and an anisotropic permeability. The analyses were performed with the ADINA-F finite element code (ADINA, Report ARD 01-9 2006). The calculation starts with the modelling of the steady-state groundwater flow field in each dipole experiment. After these conditions were established, the injection of the uranine solution was simulated. A comparison of the numerical results and test data is presented as breakthrough curves at the extraction holes where the uranine concentration is plotted versus time. The overall agreement of model results and experiment data is reasonable. Regarding the all hydraulic and transport properties obtained from this calibration work on tracer tests, it can be concluded that the area below the tunnel (dipole #2) is less permeable than the investigated region around the first dipole. However, these results confirm the earlier model proposed in Ref. (Meier et al., 2001).

References

Blechschmidt I. et al. (2006). GTS Phase VI - CFM Status Report on Field Work 2004-2005, Arbeitsbericht NAB 06-361, Nagra, Wettingen, Switzerland.

Adina R & D Inc. (2007). ADINA (Automatic Dynamic Incremental Nonlinear Analysis), Report ARD 01-9, Watertown, MA, USA.

Meier P. et al. (2001). Geostatistical inversion of cross-hole pumping tests for identifying preferential flow channels within a shear zone. Ground Water (39), 1: 10-17.

Experimental investigation and numerical modeling of diffusion/dispersion limited reactions in saturated porous media

Massimo Rolle, Christina Eberhardt, Gabriele Chiogna and Peter Grathwohl
Eberhard Karls University of Tübingen, Center for Applied Geosciences, Sigwartstrasse 10, D-72076 Tübingen, Germany

Diffusive and dispersive mixing in saturated porous media are fundamental processes that determine the extent of solute transport and reaction.

For groundwater contaminant plumes, hydrodynamic dispersive mixing is a significant mechanism controlling natural attenuation of the dissolved contaminants (Cirpka et al. 1999; Maier and Grathwohl 2006; Cirpka and Valocchi 2007). Typically, plumes of oxidizable organic pollutants (e.g. BTEX, PAHs etc.) contain a high load of electron donors whereas the background water is rich in dissolved electron acceptors. Biodegradation activity, which is the most important contaminant mass removal process, rely on mixing of organic contaminants and electron acceptors and is mainly confined to the fringe areas of the plume. The result of mixing and degradation activity is a succession of different redox zones often observed in contaminated aquifers (e.g. Baedecker et al. 1979; Chapelle et al. 1995; Anneser et al. 2008; Rolle et al. 2008).

The extent of mixing between dissolved reaction partners at the fringe of the plume determines the length of the plume and strongly depends on the groundwater flow field. In particular, transverse dispersion determined by cross-streamline diffusion is rather small in homogeneous sand and gravel aquifer sediments, with transverse dispersivities ranging from less than a millimeter to centimeters. A number of processes have been indicated to be responsible of mixing enhancement including transient flow fields and the physical heterogeneity of natural porous media containing high- and low-permeability zones.

In this study we investigated, under controlled laboratory conditions and with the support of numerical models, the influence of oscillating water table and flow focusing in high-permeability lenses on mixing enhancement of dissolved solutes. Although a number of laboratory experiments in similar settings were recently conducted with more complex microbially mediated reactions (Bauer et al., 2008a and b; Rolle et al., 2008) here we focus our attention on conservative tracers and on fast mixing-controlled abiotic reactions.

The experiments were carried out in a quasi-2D acrylic-glass flow-through tank with inner dimensions of 77.9 cm length, 15.0 cm height and 1.1 cm width (Fig. 1). The tank was equipped with 13 equally spaced ports (1.1 cm distance), for inlet and outlet on both sides and filled with glass beads. Two 12-channel high precision peristaltic pumps, one for the inlet ports and one for the outlet ports, were operated at identical pumping rates and an additional pump was connected at the tank inlet to generate transient flow conditions. In order to create a heterogeneous porous medium two inclusions of higher permeability made of glass beads of a grain size of 1-1.5 mm were embedded into finer glass beads (0.25-0.3 mm). Both high permeability lenses were placed directly in line with the plume's injection port and their thickness was equal to the injection height (1.1 cm). The most sensitive hydraulic properties and transport parameters such as hydraulic conductivity, porosity, longitudinal and transverse dispersivities were determined experimentally for the different grain sizes.
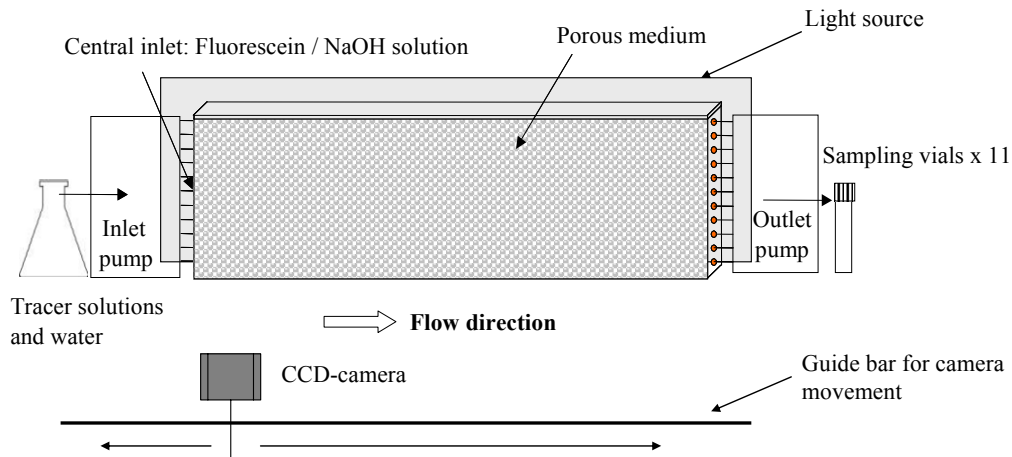
Fig. 1. Schematic of the experimental setup.

In the experiments with conservative color tracer, a sodium fluorescein solution with a concentration of 30 mg/L was injected through the middle inlet port, while clean water was injected through the other ports. Figure 2 shows the fluorescein plume under steady state and transient flow fields in the homogeneous setup (a and b) and in the heterogeneous system at steady state (c).
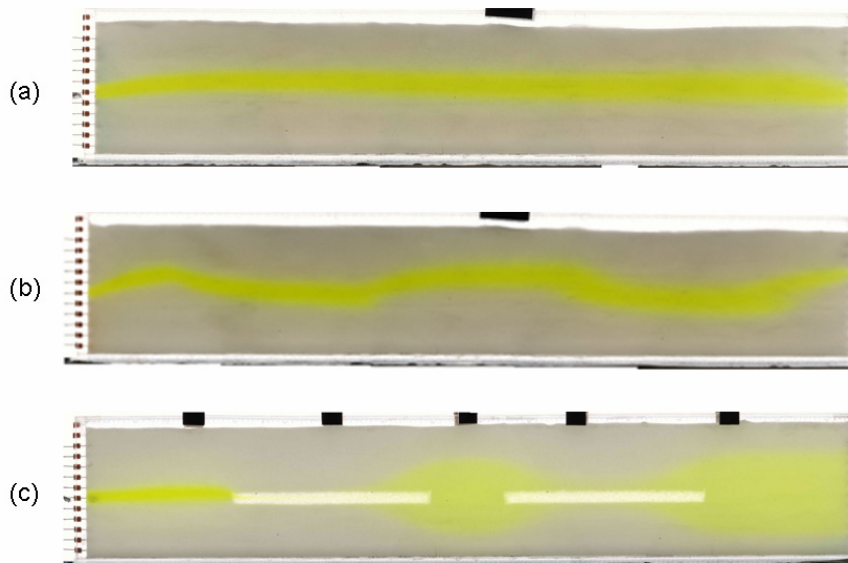
Fig. 2. Conservative tracer plumes.

In the reactive experiments, a solution of 0.004 mol/L NaOH (pH = 11.5) was injected through two middle inlet ports into an ambient solution of 0.01 mol/L HCl (pH = 2), which was injected through the surrounding ports. Both solutions contained the pH indicator bromophenol blue at a concentration of 5.92×10^{-6} mol/L. The indicator changed its color from yellow to blue in the pH interval 3 – 4.6.

Numerical modeling was performed to describe the flow and transport in the flow-through systems. Two-dimensional model grids were constructed with a discretization of $\Delta z = 7.5 \times 10^{-4}$ m in the direction perpendicular to flow and a varying discretization

(Δx_{min} = 1 x 10^{-3} m, Δx_{max} = 5 x 10^{-3} m) along the flow direction. The flow field was simulated using the numerical model MODFLOW (McDonald and Harbaugh, 1988) and particle tracking simulations were performed using MODPATH (Pollock, 1994). The flow-through systems were simulated as unconfined aquifers using the experimentally-determined hydraulic parameters. Neumann boundary conditions were applied and active cells, with interspace equivalent to the ports spacing in the experimental set-up, were used to simulate the inlet and outlet ports.

The non-reactive tracer experiments were simulated with the transport simulator MT3DMS (Zheng and Wang 1999) with the total variation diminishing (TVD) scheme in combination with an implicit finite difference method to solve the advection-dispersion problem.

Reactive transport simulations were carried out to model the reactive systems with the multi-component reactive transport code PHT3D (Prommer et al. 2003), which combines the transport simulator MT3DMS (Zheng and Wang 1999) with the geochemical model PHREEQC-2 (Parkhurst and Appelo 1999).

In the heterogeneous setup, the flowlines converge into the high-permeability inclusions and this flow focusing favors transverse displacement of the solute by diffusion and, therefore, mixing of reaction partners. This effect can be clearly observed in the reactive acid/base systems where the alkaline plume is considerably shorter in the heterogeneous than in the homogeneous tank, as shown by the snapshots (Fig. 3 a) and by the results of reactive simulations (Fig. 3b) reporting the contour at the titration end point (pH=4.6).
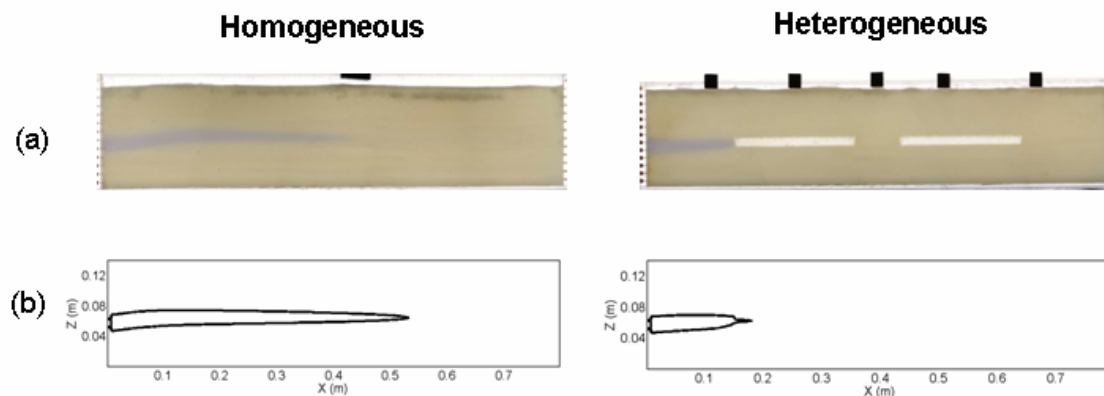
Fig. 3. Observed (a) and simulated (b) reactive plumes.

Based on the outcomes of the conservative and reactive numerical simulations, different parameters including second order spatial moments, dilution index (Kitanidis 1994), reaction enhancement factors (Werth et al. 2006) were calculated. These parameters allowed a quantification of mixing and mixing and reaction enhancements for the investigated experimental settings. Both the enhancement mechanisms investigated (i.e. transient flow fields and flow focusing) resulted in an increase of mixing and reaction compared to the equivalent homogeneous and steady state setup. The focusing of flow in the coarse grain inclusions resulted particularly effective with reaction enhancement factors up to three.

References

Anneser B., Einsiedl F., Meckenstock R.U., Richters L., Wisotzky F., Griebler C. (2008). High-resolution monitoring of biogeochemical gradients in a tar oil-contaminated aquifer. Appl. Geochem., 23, 1715-1730.

Baedecker MJ, Back W., 1979. Hydrogeological processes and chemical reactions at a landfill. Ground Water 17, 429–437.

Bauer R.D., Maloszewski P., Zhang Y., Meckenstock R.U., Griebler C. (2008a). Mixing-controlled aerobic and anaerobic biodegradation of toluene in porous media – results from two-dimensional laboratory experiments. J. Contam. Hydrol., 96, 150-168.

Bauer R., Rolle M., Eberhardt C., Grathwohl P., Bauer S., Kolditz O., Meckenstock R., Griebler C. (2008b). Enhanced biodegradation by hydraulic heterogeneities in petroleum hydrocarbon plumes. J. Contam. Hydrol., (in press).

Chapelle F.H., McMahon P.B., Dubrovsky N.M., Fuji R.F., Oaksford E.T., Vroblesky D.A. (1995). Deducing the distribution of terminal electron-accepting processes in hydrologically diverse groundwater systems. Water. Resour. Res. 31, 359-371.

Cirpka O.A., Frind E.O., Helmig R. (1999). Numerical simulation of biodegradation controlled by transverse mixing. J. Contam. Hydrol. 40, 159-182.

Cirpka O.A., Valocchi A.J. (2007). Two-dimensional concentration distribution for mixing-controlled bioreactive transport in steady state. Adv. Water Resour. 30, 1668-1679.

Kitanidis P.K. (1994). The concept of the dilution index. Water Resour. Res. 30, 2011-2026.

Maier U., Grathwohl P. (2006). Numerical experiments and field results on the size of steady state plumes. J. Contam. Hydrol. 85, 33-52.

McDonald M.G., Harbaugh A.W. (1988). A modular three-dimensional finite-difference ground-water flow model. Technical Report. U.S. Geological Survey Techniques of Water Resources Investigations.

Parkhurst D.L., Appelo C.A.J. (1999). User's guide to PHREEQC – A computer program for speciation, reaction-path, 1D-transport, and inverse geochemical calculations. Technical Report 99-4259, US Geol. Survey Water-Resources Investigations Report.

Pollock D.W. (1994). A particle tracking post-processing package for modflow: the U.S. Geological Survey finite-difference ground-water flow model. User's guide for modpath/modpath-plot, version 3. Of 94-464, U.S. Geol. Survey, Reston, VA.

Prommer H., Barry D.A., Zheng C. (2003). PHT3D - A MODFLOW/MT3DMS based reactive multi-component transport model. Ground Water 42, 247-257.

Rolle M., Bauer R., Griebler C., Meckenstock R., Bauer S., Kolditz O., Grathwohl P. (2008). Aerobic degradation of a toluene plume in homogeneous and heterogeneous porous media. IAHS Red Book Series, 324 (accepted for publication).

Rolle M., Clement T.P., Sethi R., Di Molfetta A. (2008). A Kinetic Approach for Simulating Redox-controlled Fringe and Core Biodegradation Processes in Groundwater: Model Development and Application to a Landfill Site in Piedmont, Italy. Hydrological Processes, 22, 4905-4921.

Werth C.J., Cirpka O.A., Grathwohl P. (2006). Enhanced mixing and reaction through flow focusing in heterogeneous porous media. Water Resour. Res. 42, W12414, doi:10.1029/2005WR004511

Zheng C., Wang P.P. (1999). MT3DMS: A modular three-dimensional multispecies model for simulation of advection, dispersion, and chemical reactions of contaminants in groundwater systems. Documentation and user's guide. Contract report SERDP-99-1. U.S. Army Engineer Research and Development Center, Vicksburg, MS.

Testing the K_d-approch with a multicomponent geochemical reactive transport model for a HLW repository in granite: The case of Ni

Javier Samper[1], Chuanhe Lu[1], José Luis Cormenzana[2], Hongyun Ma[1], Luis Montenegro[1] and Miguel Angel Cuñado[2]
[1] University of La Coruña, La Coruña, Spain
[2] ENRESA, C Emilio Vargas 7, Madrid, Spain

Motivation

Current PA models and tools such as Goldsim for radionuclide migration through the near field of a HLW repository usually rely on some simplifying assumptions such as: 1) The use of the "Kd approach" for nuclide sorption and "the limited solubility" for nuclide precipitation or coprecipitation. Testing the validity of these assumptions has been limited by: 1) the lack of nuclide surface complexation and cation exchange data; and 2) the availability of computer codes which could handle simultaneously the migration, sorption and precipitation of radionuclides together with the geochemical evolution of the near field.

Lab experiments performed in recent years, some of which have been carried out within the framework of EU projects such as FEBEX, NF-PRO, have provided substantial data and understanding on the mechanisms of nuclide sorption. On the other hand, sophisticated research-oriented process-based computer codes and models have been developed which allow for the simultaneous modelling of migration, sorption, nuclide precipitation and multicomponent geochemical evolution of the near field.

Objectives

The purpose of this paper is to test the validity of the "Kd approach" and "limited solubility" assumptions for nuclide sorption and precipitation. Such testing has been performed by benchmarking of a PA model (Goldsim) and a detailed process-model with the UDC code, CORE, for some selected radionuclides. Calculations have been performed for the compacted bentonite of the engineered barrier of a spent-fuel repository in granite according to the Spanish reference concept (ENRESA, 2005; 2006). Modelling of test cases using PA models were performed by ENRESA while UDC carried out the modelling with the reactive transport code CORE. Testing has been performed for some selected radionuclides for which detailed sorption data were available. The following nuclides have been analyzed: Ni, Cs, and U. Here we report the results for Ni.

Description of work

The following actives have been performed:

Adapting CORE to meet the needs of the benchmarking. Although CORE is a sophisticated code which allows for a full set of multicomponent chemical and isotopic species, it might be needed to account for the possibility of several types of sorption sites (weak and strong). It is also required to complete the verification of subroutines for radiochemical processes involved in nuclide dissolution and/or precipitation

Performing calculations for benchmark cases for the reference concept of SF in granite. The model will solve simultaneously for the long-term geochemical evolution of the near field and radionuclide migration, sorption (by cation exchange and/or

surface complexation) and dissolution/precipitation. The model will account for canister corrosion, the EDZ and the near field granite formation.
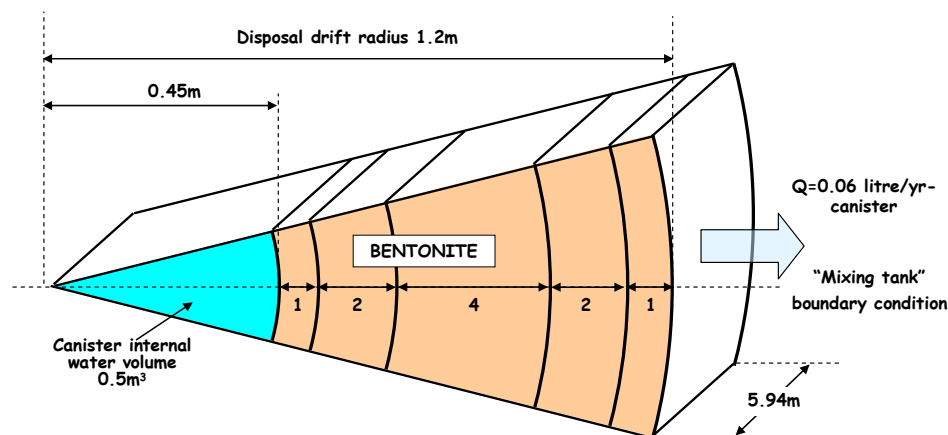
Fig. 1. Model for transport in the near field calculations.

A 1D axisymmetric flow model is used with a grid of 167 elements and 168 nodes to represent the length of disposal drift corresponding to a single canister. An extra element of 0.01mm thickness is added at the bentonite outer surface in order to be able to simulate the 'mixing tank' boundary condition. Solutes diffuse into this outermost element and the equivalent groundwater flow is injected and extracted from this element. An 'equivalent flow' of 0.06 litre/year(when canister length is 5.94 m) is used for the 'mixing tank' boundary condition at the bentonite outer surface (see Fig. 1 and 2). The first 16 finite elements represent the canister internal volume (up to a radius of 0.45m) and the next 151 elements represent the bentonite (up to a radius of 1.2m).
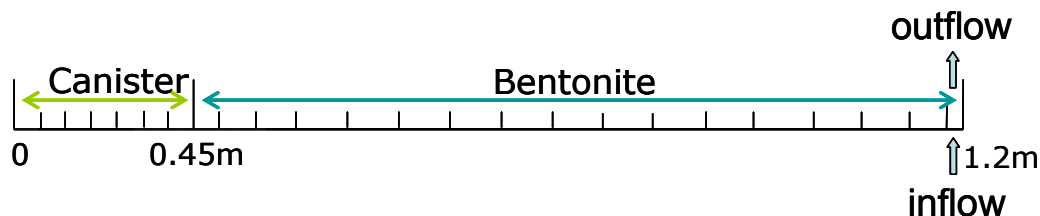
Fig. 2. Finite element mesh used in the 1-D axisymmetric model.

Relevant aqueous complexes were identified from speciation runs performed with EQ3/6 (Wolery, 1992). All these reactions are assumed at local chemical equilibrium. The Gaines-Thomas convention is used for cation exchange (Gaines and Thomas, 1953). The surface complexation is simulated as proposed by Bradbury and Baeyens (2005) without electrostatic contributions, considering one strong and two weak surface sites. Surface complexation reactions are not considered inside the canister. Chemical reactions and their equilibrium constants at 25 ºC for aqueous complexes and minerals (Wolery, 1992) are listed in Table 1, selectivity coefficients for exchangeable cations and protolysis constants for surface complexation (Bradbury and Baeyens, 2005; BENIPA, 2003; Fernández et al., 2004; Samper et al., 2007) are listed in
Table 2.
In UDC model the canister internal volume is treated as another porous medium. A very high porewater diffusion coefficient (3 orders of magnitude greater than that in bentonite) is used to ensure perfect mixing at any instant. A porosity of 0.132 is

defined for canister ensuring that internal water volume is 0.5 m3 (when canister length is 5.94 m) and consistent with GoldSim calculations.

Table 1: Equilibrium constants for aqueous complexes and minerals.

Aqueous complexes	Log K (25 °C)
$CaCl^+ \Leftrightarrow Ca^{2+} + Cl^-$	0.6956
$CaCl_2(aq) \Leftrightarrow Ca^{2+} + 2Cl^-$	0.6436
$CaCO_3(aq) + H^+ \Leftrightarrow Ca^{2+} + HCO_3^-$	7.0017
$CaHCO_3^+ \Leftrightarrow Ca^{2+} + HCO_3^-$	-1.0467
$CaH_3SiO_4^+ + H^+ \Leftrightarrow Ca^{2+} + 2H_2O + SiO_2(aq)$	8.7916
$CaSO_4(aq) \Leftrightarrow Ca^{2+} + SO_4^{2-}$	-2.1111
$CaOH^+ + H^+ \Leftrightarrow Ca^{2+} + H_2O$	12.850
$CO_2(aq) + H_2O \Leftrightarrow H^+ + HCO_3^-$	-6.3447
$CO_3^{2-} + H^+ \Leftrightarrow HCO_3^-$	10.329
$Fe^{3+} + 0.5H_2O \Leftrightarrow Fe^{2+} + H^+ + 0.25O_2(aq)$	-8.4900
$FeCl^+ \Leftrightarrow Fe^{2+} + Cl^-$	0.1605
$FeCO_3(aq) + H^+ \Leftrightarrow Fe^{2+} + HCO_3^-$	5.5988
$FeHCO_3^- \Leftrightarrow Fe^{2+} + HCO_3^-$	-2.0500
$FeSO_4(aq) \Leftrightarrow Fe^{2+} + SO_4^{2-}$	-2.2000
$HCl(aq) \Leftrightarrow H^+ + Cl^-$	0.6700
$HSO_4^- \Leftrightarrow H^+ + SO_4^{2-}$	-1.9791
$HSiO_3^- + H^+ \Leftrightarrow H_2O + SiO_2(aq)$	9.9525
$H_6(H_2SiO_4)_4^- + 2H^+ \Leftrightarrow 8H_2O + 4SiO_2(aq)$	13.446
$KCl(aq) \Leftrightarrow K^+ + Cl^-$	1.4946
$KSO_4^- \Leftrightarrow K^+ + SO_4^{2-}$	-0.8796
$MgCl^+ \Leftrightarrow Mg^{2+} + Cl^-$	0.1349
$MgCO_3(aq) + H^+ \Leftrightarrow Mg^{2+} + HCO_3^{-2}$	7.3499
$MgHCO_3^+ \Leftrightarrow CaMg^{2+} + HCO_3^-$	-1.0357
$MgH_2SiO_4(aq) + 2H^+ \Leftrightarrow Mg^{2+} + SiO_2(aq) + 2H_2O$	17.482
$MgH_3SiO_4^+ + H^+ \Leftrightarrow Mg^{2+} + SiO_2(aq) + 2H_2O$	8.5416
$MgSO_4(aq) \Leftrightarrow Mg^{2+} + SO_4^{2-}$	-2.4117
$NaCl (aq) \Leftrightarrow Na^+ + Cl^-$	0.7770
$NaCO_3^- + H^+ \Leftrightarrow Na^+ + HCO_3^-$	9.8144
$NaHCO_3(aq) \Leftrightarrow Na^+ + HCO_3^-$	-0.1541
$NaHSiO_3(aq) + H^+ \Leftrightarrow Na^+ + SiO_2(aq) + H_2O$	8.3040
$NaOH(aq) + H^+ \Leftrightarrow Na^+ + H_2O$	14.180
$NaSO_4^- \Leftrightarrow Na^+ + SO_4^{2-}$	-0.8200
$NiCl^+ \Leftrightarrow Ni^{2+} + Cl^-$	0.9962
$Ni(OH)^- + H^+ \Leftrightarrow Ni^{2+} + H_2O$	11.535
$Ni(OH)_2(aq) + 2H^+ \Leftrightarrow Ni^{2+} + 2H_2O$	19.990
$Ni(OH)_3^- + 3H^+ \Leftrightarrow Ni^{2+} + 3H_2O$	30.985
$Ni_2(OH)^{3+} + H^+ \Leftrightarrow 2Ni^{2+} + H_2O$	10.700
$Ni_4(OH)_4^{4+} + 4H^+ \Leftrightarrow 4Ni^{2+} + 4H_2O$	27.680
$NiSO_4(aq) \Leftrightarrow Ni^{2+} + SO_4^{2-}$	-2.1257
$OH^- + H^+ \Leftrightarrow H_2O$	13.995
Minerals	**Log K (25 °C)**
$CaCO_3(s) + H^+ \Leftrightarrow Ca^{2+} + HCO_3^-$	1.8487
$CaSO_4 \cdot 2H_2O(s) \Leftrightarrow Ca^{2+} + SO_4^{2-} + 2H_2O$	-4.4823
$SiO_2(s) \Leftrightarrow SiO_2(aq)$	-3.9993
$Fe_3O_4(s) + 6H^+ \Leftrightarrow 3Fe^{2+} + 0.5O_2(aq) + 3H_2O$	-6.5076
$FeOOH(s) + 2H^+ \Leftrightarrow Fe^{2+} + 0.25O_2(aq) + 1.5H_2O$	-7.9555
$FeCO_3(s) + H^+ \Leftrightarrow Fe^{2+} + HCO_3^-$	-0.1920

Table 2: Selectivity coefficients for cation exchange reactions and protolysis constants for surface complexation reactions.

Cation exchange	$K_{Na-cation}$
$Na^+ + K-X \Leftrightarrow K^+ + Na-X$	0.1380
$Na^+ + 0.5Ca-X_2 \Leftrightarrow 0.5Ca^{2+} + Na-X$	0.2924
$Na^+ + 0.5Mg-X_2 \Leftrightarrow 0.5Mg^{2+} + Na-X$	0.2881
$Na^+ + 0.5Fe-X_2 \Leftrightarrow 0.5Fe^{2+} + Na-X$	0.5000
$Na^+ + 0.5Ni-X_2 \Leftrightarrow 0.5Ni^{2+} + Na-X$	0.5188
Surface complexation	Log K_{int}
$\equiv SOH_2^+ \Leftrightarrow \equiv SOH + H^+$	-4.5
$\equiv SO^- + H^+ \Leftrightarrow \equiv SOH$	7.9
$\equiv SONi^+ + H^+ \Leftrightarrow \equiv SOH + Ni^{2+}$	0.6
$\equiv SONiOH + 2 H^+ \Leftrightarrow \equiv SOH + Ni^{2+} + H_2O$	10.0
$\equiv SONi(OH)_2^- + 3 H^+ \Leftrightarrow \equiv SOH + Ni^{2+} + 2H_2O$	20.0
$\equiv W^1OH2^+ \Leftrightarrow \equiv W^1OH + H^+$	-4.5
$\equiv W^1O^- + H^+ \Leftrightarrow \equiv W^1OH$	7.9
$\equiv W^1ONi^+ + H^+ \Leftrightarrow \equiv W^1OH + Ni^{2+}$	3.3
$\equiv W^2OH2^+ \Leftrightarrow \equiv W^2OH + H^+$	-6.0
$\equiv W^2O^- + H^+ \Leftrightarrow \equiv W^2OH$	10.5

Table 3: Flow and transport parameters.

Material	Hydraulic conductivity (m/s)	Initial porosity	Initial effective diffusion (m²/s)
Bentonite	$5.71 \cdot 10^{-14}$	$4.07 \cdot 10^{-1}$	$4.07 \cdot 10^{-11}$
Canister	$5.71 \cdot 10^{-15}$	$1.32 \cdot 10^{-1}$	$4.07 \cdot 10^{-08}$

The chemical composition of inflow water coincides with that of initial granite porewater. The porewater in canister and bentonite have the same initial water. The boundary inflow water concentration and initial concentrations of bentonite are listed in Table 4 (BENIPA, 2003; Samper et al., 2007). There are 20 Kg Ni put in canister; the solubility limit is 0.001 mol/L.

Table 4: Boundary and initial water concentration.

Primary species	Initial bentonite water(mol/L)	Boundary water(mol/L)
Ca^{2+}	$3.101 \cdot 10^{-2}$	$1.522 \cdot 10^{-4}$
Cl^-	$2.756 \cdot 10^{-1}$	$3.949 \cdot 10^{-4}$
Fe^{2+}	$6.583 \cdot 10^{-5}$	$1.791 \cdot 10^{-8}$
pH	6.435	7.825
HCO_3^-	$1.689 \cdot 10^{-3}$	$5.049 \cdot 10^{-3}$
K^+	$1.507 \cdot 10^{-3}$	$5.371 \cdot 10^{-5}$
Mg^{2+}	$3.473 \cdot 10^{-2}$	$1.604 \cdot 10^{-4}$
Na^+	$1.841 \cdot 10^{-1}$	$4.350 \cdot 10^{-3}$
Eh (V)	-0.059	-0.188
$SiO_2(aq)$	$3.761 \cdot 10^{-4}$	$3.761 \cdot 10^{-4}$
SO_4^{2-}	$2.049 \cdot 10^{-2}$	$1.561 \cdot 10^{-5}$

The composition of initial porewaters is controlled by mineral dissolution/precipitation at chemical equilibrium (calcite and quartz), proton surface complexation and cation exchange.

Initial volume fractions of calcite and quartz in bentonite are all 0.01 (BENIPA, 2003; Samper et al., 2007). Gypsum, magnetite, siderite and goethite are minerals which are not initially present in the system, but are allowed to precipitate.

Cation exchange capacity (CEC) in bentonite is 87 meq/100g. Surface complexation site densities in bentonite are listed in Table 5.

Table 5: Surface complexes site density of bentonite.

Site densities in mol/g dry bentonite	
S^S-OH	$2 \cdot 10^{-6}$
S^{W1}-OH	$4 \cdot 10^{-5}$
S^{W2}-OH	$4 \cdot 10^{-5}$

It is found that the Kd of Ni depends nonlinearly in the concentration of dissolved Ni (nonlinear isotherm), and depends also on the the pH. Ni sorbed by surface complexes is the major part of solid Ni in bentonite (see Figure 1).
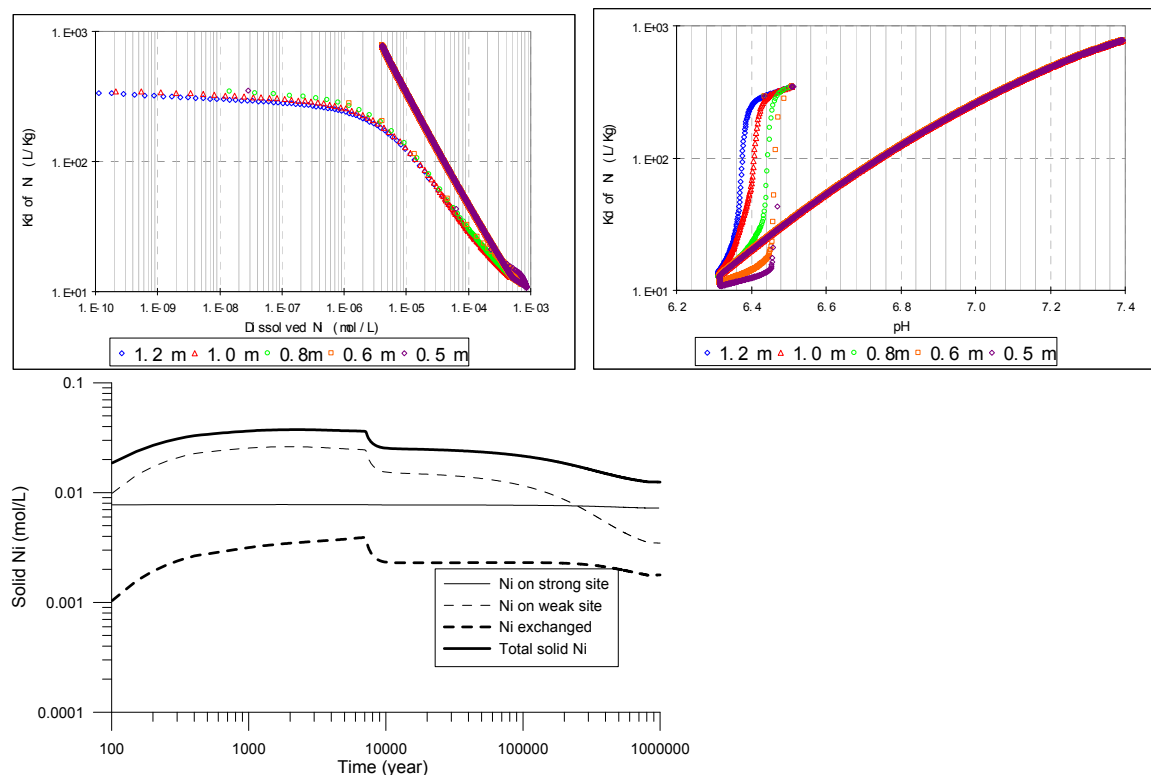
Fig. 1. K_d of Ni as a function of time (top left); K_d of Ni as a function of pH (top right); evolution of sorbed and exchanged Ni at r=0.5m (bottom left).

Sensitivity analyses have been performed to: 1) Diffusion coefficient of bentonite, 2) concentration of sorption sites.

Model results indicate that: 1) Kd is sensitivity to diffusion coefficient through dissolved and exchanged Ni concentrations; 2) Kd is sensitive to the concentration of weak sorption sites (see Figure 2).
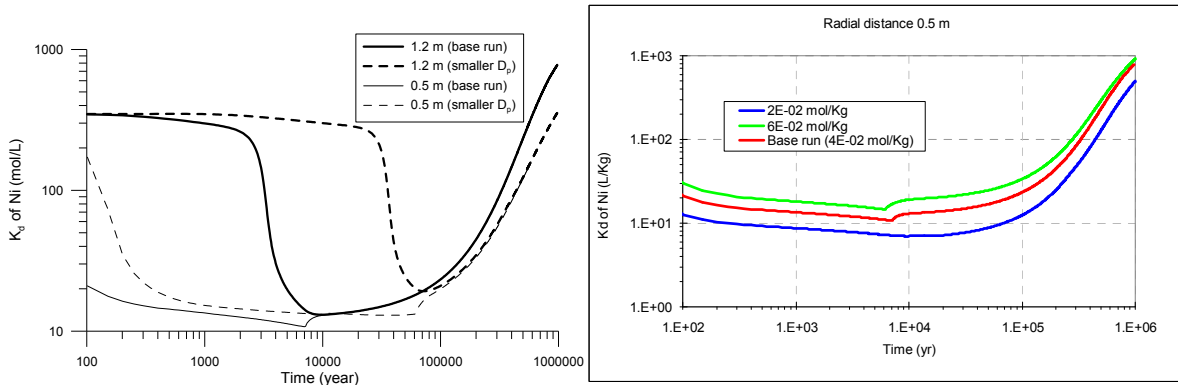
Fig. 2. Sensitivity of computed K_d to: 1) different diffusion coefficient of bentonite (left); 2) capacity of sorption sites (right).

To separate the dependence of Kd on the chemical variables from the variability on nuclide concentration, a run in which the chemistry is fixed and another run in which chemistry included pH is fixed are made. The concentration of granite water flux at the boundary equals to that of initial bentonite. The results show that Kd keeps almost constant when the chemistry except pH is fixed at the last part of simulation. When pH is fixed, Kd keeps constant at the last part of simulation (see figure 3), it means that Kd depend on both dissolved Ni and pH.
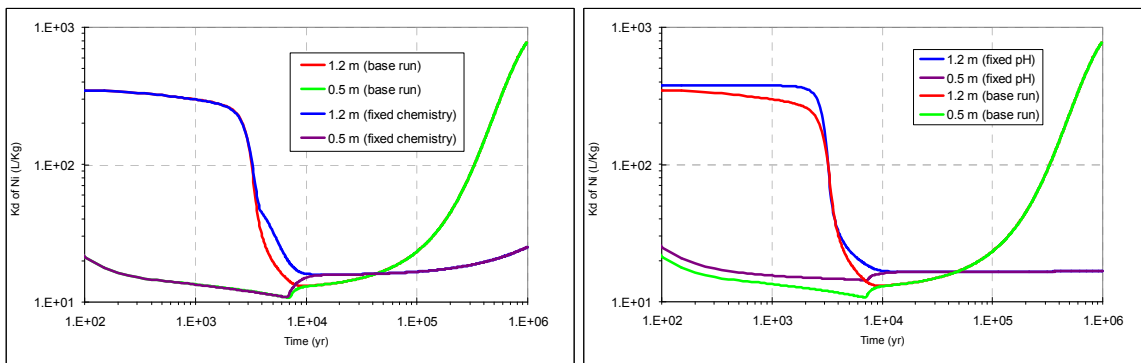
Fig. 3. K_d evolution with: 1) fixed chemistry except pH in bentonite (left); 2) chemistry including pH is fixed (right).

Several runs with different Kd (10, 20, 50 L/Kg respectively) are simulated, The dissolved Ni in models with Kd equals to 20 L/Kg gets a similar evolution trend to base sorption run at the increasing part. But when all the Ni in canister is dissolved out, the dissolved Ni in base run decreases fast than all the runs with Kd (see Figure 4).
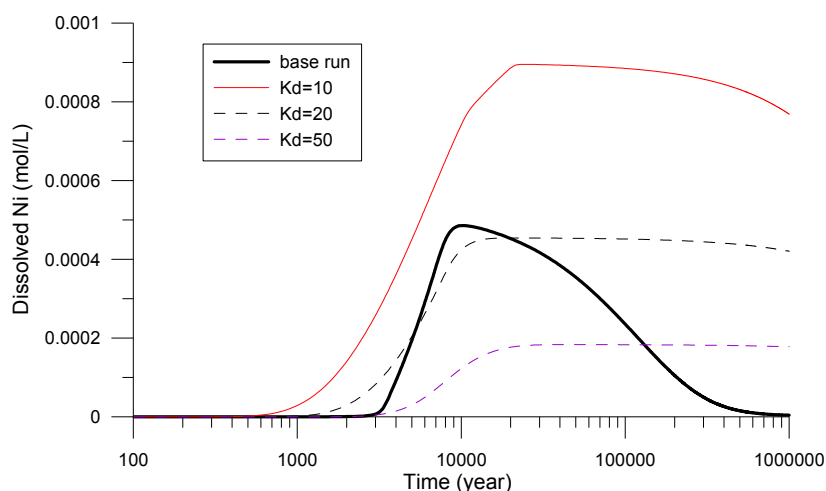
Fig. 4. Comparison of dissolved Ni evolution between constant Kd model and reactive transport model.

Acknowledgements

References

BENIPA (2003). Final Report of BENIPA Project: Bentonite Barriers in Integrated Performance Assessment. Report of the European Commission, EUR 21023.

Bradbury M.H. and Baeyens B. (2005). Modelling the sorption of Mn(II), Co(II), Ni(II), Zn(II), Cd(II), Eu(III), Am(III), Sn(IV), Th(IV), Np(V) and U(VI) on montmorillonite: Linear free energy relationships and estimates of surface binding constants for some selected heavy metals and actinides. Geochimica et Cosmochimica Acta 69 (4), 875–892.

ENRESA (2005). NF-PRO Project. Phenomenological description. Reference Concept (Spent Fuel-Carbon Steel Canister-Bentonite-Granite). Deliverable D5.1.1. Part 1. Final version.

Fernández A.M., Cuevas J., Rivas P. (2001). Pore water chemistry of the FEBEX bentonite. Mater. Res. Soc. Symp. Proc. 663, 573-588.

Gaines G.I., Thomas H.C. (1953). Adsorption studies on clay minerals. II. A formulation of the thermodynamics of exchange adsorption. Journal of Chemical Physics 21, 714-718.

Galíndez J.,M., Molinero J., Samper J., Yang C.B. (2006). Simulating concrete degradation processes by reactive transport models, J. Phys. IV France, Vol. 136, 177-188.

Samper J., Yang C., Montenegro L. (2003). CORE[2D] version 4: A code for non-isothermal water flow and reactive solute transport. Users Manual. University of La Coruña, Spain.

Samper J., Yang Ch., Montenegro L., Bonilla M., Lu C., Yang Q., Zheng L. (2007). Mass and energy balance and flux calculations for radionuclide release and geochemical evolution for SF carbon steel HLW repositories in clay and granite. NF-PRO project, Deliverable D5.1.13. University of A Coruña, Spain.

Samper J., C. Lu, Montenegro L. (2008a). Coupled hydrogeochemical calculations of the interactions of corrosion products and bentonite, Physics and Chemistry of the Earth, Vol. 33. Supplement 1, S306-S316. doi:10.1016/j.pce.2008.10.009.

Samper J., Zheng L., Montenegro L., Fernández A.M., Rivas P. (2008b). Testing coupled thermo-hydro-chemical models of compacted bentonite after dismantling the FEBEX in situ test, Appl Geochem, Vol 23/5: 1186-1201. doi:10.1016/j.apgeochem.2007.11.010.

Samper J., Zheng L., Fernández A.M., Montenegro L. (2008c). Inverse modeling of multicomponent reactive transport through single and dual porosity media, J Cont Hydrol, 10.1016/j.jconhyd.2008.03.008.

Samper J, Lu C., Cormenzana J.L., Ma H., Cuñado M.A. (2009). Testing the Kd-approch with a multicomponent geochemical reactive transport model for a HLW repository in granite: The case of Cs, in this volume of TREPRO 2009.

Yang C., Samper J., Molinero J., Bonilla M. (2007). Modelling geochemical and microbial consumption of dissolved oxygen after backfilling a high level radioactive waste repository, J Cont Hydrol, 93 130–148.

Yang, C., Samper J., Montenegro L. (2008). A coupled non-isothermal reactive transport model for long-term geochemical evolution of a HLW repository in clay, Environmental Geology, 53:1627–1638. DOI 10.1007/s00254-007-0770-2.

Testing the K_d-approch with a multicomponent geochemical reactive transport model for a HLW repository in granite: The case of Cs

Javier Samper[1], Chuanhe Lu[1], José Luis Cormenzana[2], Hongyun Ma[1], Luis Montenegro[1] and Miguel Angel Cuñado[2]

[1] *University of La Coruña, La Coruña, Spain*
[2] *ENRESA, C Emilio Vargas 7, Madrid, Spain*

Motivation

Current performance assessment (PA) models for radionuclide migration through the near field of a high-level radioactive waste (HLW) repository usually rely on simplifying assumptions such as the use of the "K_d approach" for nuclide sorption and "the limited solubility" for nuclide precipitation. Testing the validity of these assumptions has been limited by: 1) The lack of nuclide surface complexation and cation exchange data; and 2) Unavailability of computer codes which could handle simultaneously the migration, sorption and precipitation of radionuclides together with the geochemical evolution of the near field. Lab experiments performed in recent years have provided substantial data and understanding on the mechanisms of nuclide sorption. On the other hand, sophisticated research-oriented process-based computer codes and models have been developed which allow for the simultaneous modelling of migration, sorption, nuclide precipitation and multicomponent geochemical evolution of the near field. In this paper we test the validity of the "K_d approach" and "limited solubility" assumptions for nuclide sorption and precipitation for the 0.75 m thick compacted bentonite barrier of a spent-fuel repository in granite designed according to the Spanish reference concept (ENRESA, 2005). Such testing has been performed for some selected radionuclides by comparing the results of a PA model with those obtained with a reactive transport model performed with CORE (Samper et al., 2003). Testing has been performed for some selected radionuclides for which detailed sorption data were available. They include Ni, Cs, and U. Here we report the results for Cs, a chemical compound which sorbed by cation exchange on several different exchange sites.

Benchmarking of approaches was performed with CORE[2D], a 2-D finite element multicomponent reactive transport code which accounts for a wide range of chemical reactions and has been widely used in research projects dealing with HLW disposal at laboratory to model laboratory and in situ experiments (Samper *et al*., 2008a, b, c). To meet the needs of the benchmarking, CORE was updated to account for several types of exchange sites. Calculations were performed for the Spanish reference concept of repository in granite by simulating radionulide migration simultaneously to the long-term geochemical evolution of the near field. Canister corrosion is not considered at the present stage, although it is planned to account for it at a later stage.

Numerical model

The numerical model is similar to that used for Ni and U (described in Samper et al., 2009, in this volume). A 1D axisymmetric flow model is used. Selectivity coefficients

for exchangeable cations and protolysis constants for surface complexation were taken from Bradbury and Baeyens (2005), BENIPA (2003), Fernández et al. (2001) and Samper et al. (2007). Porewaters in the canister and bentonite are assumed to have initially the same chemical composition (BENIPA, 2003; Samper et al., 2007) which is controlled by mineral dissolution/precipitation at chemical equilibrium (calcite and quartz), proton surface complexation and cation exchange. Initial volume fractions of calcite and quartz in bentonite are both equal to 0.01 (BENIPA, 2003; Samper et al., 2007). Gypsum, magnetite, siderite and goethite are minerals which are not initially present in the system, but are allowed to precipitate. Cation exchange capacity (CEC) in bentonite is 87 meq/100g. The surface complexation site densities of strong site and two weak sites in bentonite are equal to $2 \cdot 10^{-6}$, $4 \cdot 10^{-5}$ and $4 \cdot 10^{-5}$ mol/g respectively. The chemical composition of inflow water coincides with that of initial granite porewater. The chemical compositions of bentonite and granite water are listed in Table 1. The instant release of Cs amounts to 0.202 Kg per canister. The mass flux of Cs in the canister is shown in Figure 1.

Model results

It is found that the Kd of Cs depends nonlinearly in the concentration of dissolved Cs. The nonlinear isotherm presents two parts: 1) A part during which Kd is constant (for t < 104 years) and 2) A second part in which Kd increases due to changes in dissolved concentrations of other cations (Figure 2).
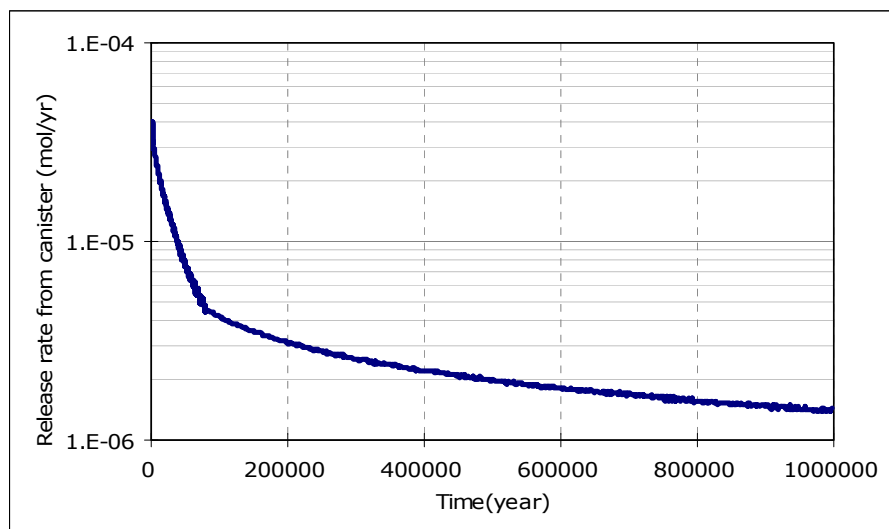
Fig. 1. Mass flux of Cs released in the canister.

Table 1. Chemical composition of boundary (granite) and initial (bentonite) waters.

Primary species	Bentonite (mol/L)	Boundary (mol/L)
Ca^{2+}	$3.101 \cdot 10^{-2}$	$1.522 \cdot 10^{-4}$
Cl^-	$2.756 \cdot 10^{-1}$	$3.949 \cdot 10^{-4}$
Fe^{2+}	$6.583 \cdot 10^{-5}$	$1.791 \cdot 10^{-8}$
pH	6.435	7.825
HCO_3^-	$1.689 \cdot 10^{-3}$	$5.049 \cdot 10^{-3}$

SO_4^{2-}	$2.049 \cdot 10^{-2}$	$1.561 \cdot 10^{-5}$
K^+	$1.507 \cdot 10^{-3}$	$5.371 \cdot 10^{-5}$
Mg^{2+}	$3.473 \cdot 10^{-2}$	$1.604 \cdot 10^{-4}$
Na^+	$1.841 \cdot 10^{-1}$	$4.350 \cdot 10^{-3}$
Eh (V)	-0.059	-0.188
$SiO_2(aq)$	$3.761 \cdot 10^{-4}$	$3.761 \cdot 10^{-4}$
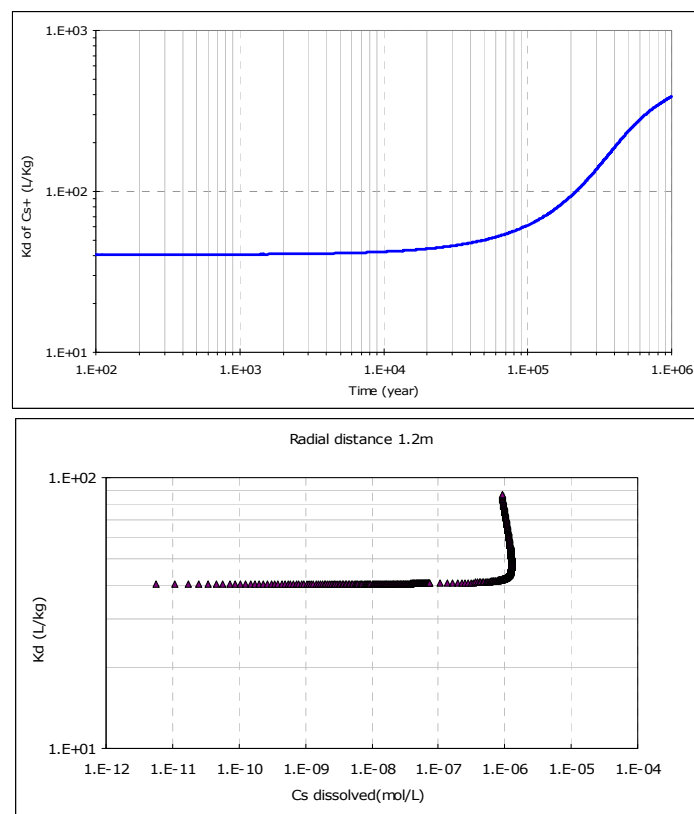
Fig. 2. Computed Kd of Cs at the outer surface of the bentonite (r = 1 2. m) as a function of time (left) and dissolved Cs concentration (right).

Sensitivity analyses have been performed to: 1) The diffusion coefficient of bentonite, 2) The CEC of bentonite, and 3) The water flux through granite, Q. Model results indicate that Kd is not very sensitive to the bentonite diffusion coefficient, slightly sensitive to CEC and very sensitivity to the flux through granite (Figure 3).

To separate the dependence of Kd on the water chemistry from the changes in Cs concentration, a run was made in which the water chemistry was fixed. The concentration of granite water is taken equal to that of the initial concentration in bentonite. Results are also shown in Figure 3. It can be seen that Kd remains constant when the chemistry is fixed. By fixing the chemistry, exchange of Cs is almost independent of the concentration of dissolved Cs because the concentration of Cs is much smaller than those of the rest of the dissolved cations. Cs behaves as tracer and therefore its Kd is almost constant when the chemical composition of the porewater does not change.

Several runs with values of Kd of 30, 50, and 70 mL/g were performed. Dissolved Cs at r = 1.2 m computed with a constant Kd has a trend similar to that of the base run at the rising part of the breakthrough curve. However, when all Cs in canister is

dissolved, the dissolved Cs in the base run decreases while computed Cs concentrations with the Kd model keeps increasing (Figure 4).

Work is in progress to derive expressions of Kd as a function of dissolved Cs concentration, pH and other geochemical variables that can be used in performance assessment models.
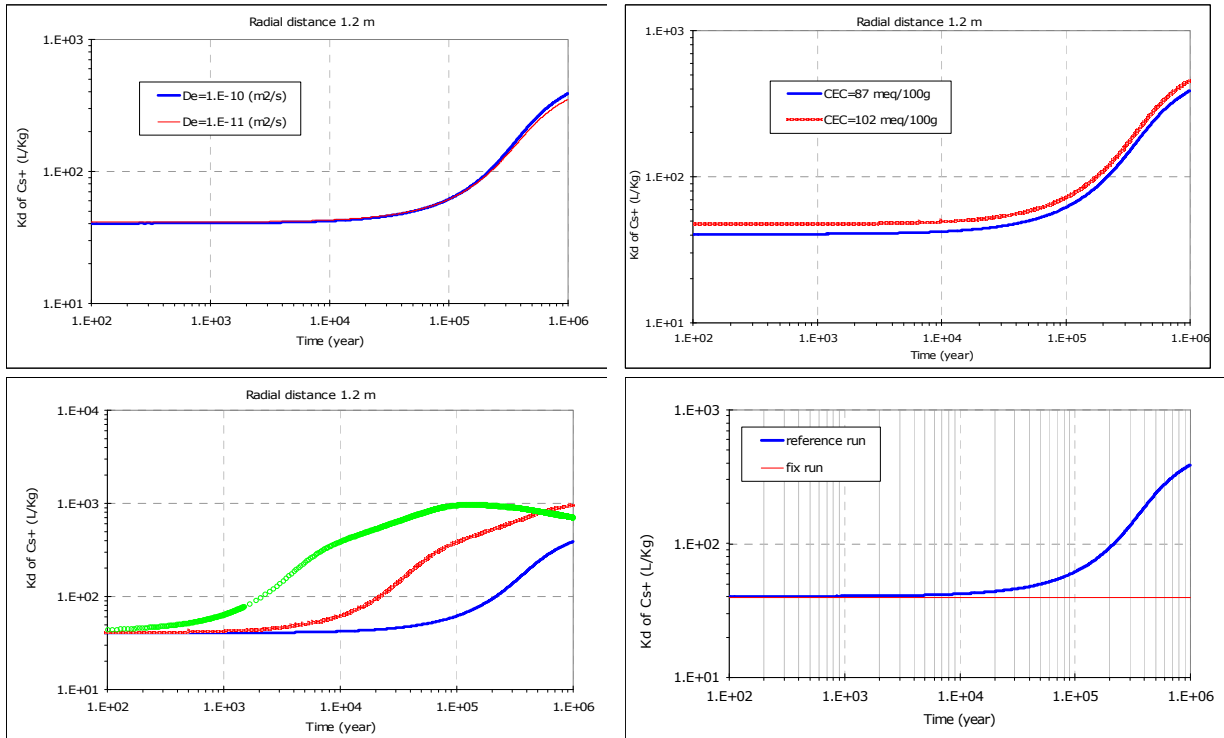
Fig. 3. Sensitivity of computed Kd to: 1) The diffusion coefficient of bentonite (top left); 2) Bentonite CEC (top right); 3) The water flux through granite (bottom left) and 4) Fixing the water chemistry (bottom right).
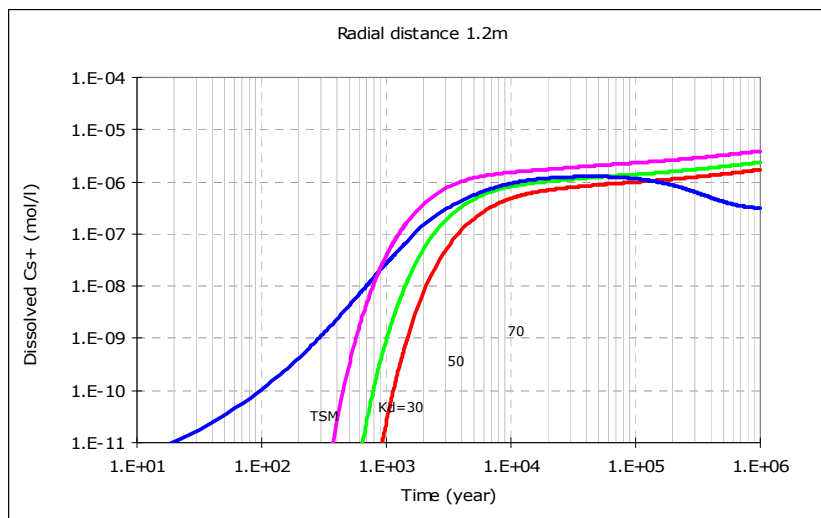
Fig. 4. Comparison of the Cs breakthrough curve at the outer surface of the bentonite (r = 1 2. m) computed with the reactive transport model and with a constant Kd model for different Kd values.

Conclusions

The results of the reactive transport calculations for Cs allow us to conclude that: 1) The Kd of Cs is not constant, but depends on the concentrations of other dissolved cations for t > 104 a; and 2) The release curve of Cs from the near field cannot be reproduced with a constant Kd model, even when Kd is varied from 30 to 70 mL/g. These results should be tested with experimental diffusion.
Future studies will account for canister corrosion and competitive sorption of Fe and other radionuclides.

Acknowledgements

References

BENIPA (2003). Final Report of BENIPA Project: Bentonite Barriers in Integrated Performance Assessment. Report of the European Commission, EUR 21023.

Bradbury M.H., Baeyens B. (2005). Modelling the sorption of Mn(II), Co(II), Ni(II), Zn(II), Cd(II), Eu(III), Am(III), Sn(IV), Th(IV), Np(V) and U(VI) on montmorillonite: Linear free energy relationships and estimates of surface binding constants for some selected heavy metals and actinides. Geochimica et Cosmochimica Acta 69 (4), 875–892.

ENRESA (2005). NF-PRO Project. Phenomenological description. Reference Concept (Spent Fuel-Carbon Steel Canister-Bentonite-Granite). Deliverable D5.1.1. Part 1. Final version.

Fernández A.M., Cuevas J., Rivas P. (2001). Pore water chemistry of the FEBEX bentonite. Mater. Res. Soc. Symp. Proc. 663, 573-588.

Pfingsten W., Baeyens B., Jakob A., Bradbury M.H. (2007). Mechanistic soprtion models included in reactive transport calculations- New insights with respect to Kd-sorption modeling and competitive sorption effects, Migration 2007, Munnich, Session C-2.

Samper J., Yang C., Montenegro L. (2003). CORE^{2D} version 4: A code for non-isothermal water flow and reactive solute transport. Users Manual. University of La Coruña, Spain.

Samper J., Yang Ch., Montenegro L., Bonilla M., Lu C., Yang Q., Zheng L. (2007). Mass and energy balance and flux calculations for radionuclide release and geochemical evolution for SF carbon steel HLW repositories in clay and granite. NF-PRO project, Deliverable D5.1.13. University of A Coruña, Spain.

Samper J., Lu C., Montenegro L. (2008a). Coupled hydrogeochemical calculations of the interactions of corrosion products and bentonite, Physics and Chemistry of the Earth, Vol. 33. Supplement 1, S306-S316. doi:10.1016/j.pce.2008.10.009.

Samper J., Zheng L., Montenegro L., Fernández A.M., Rivas P. (2008b). Testing coupled thermo-hydro-chemical models of compacted bentonite after dismantling the FEBEX in situ test, Appl Geochem, Vol 23/5: 1186-1201. doi:10.1016/j.apgeochem.2007.11.010.

Samper J., Zheng L., Fernández A.M., Montenegro L. (2008c). Inverse modeling of multicomponent reactive transport through single and dual porosity media, J Cont Hydrol, 10.1016/j.jconhyd.2008.03.008.

Samper J, Lu C, Cormenzana J.L., Ma H., Cuñado M.A. (2009). Testing the Kd-approch with a multicomponent geochemical reactive transport model for a HLW repository in granite: The case of Ni, in this volume of TREPRO 2009.

Testing the K_d approch with a multicomponent geochemical reactive transport model for a HLW repository in granite: The case of uranium

Javier Samper[1], Chuanhe Lu[1], José Luis Cormenzana[2], Hongyun Ma[1], Luis Montenegro[1] and Miguel Angel Cuñado[2]
[1] University of La Coruña, La Coruña, Spain
[2] ENRESA, C Emilio Vargas 7, Madrid, Spain

Motivation

Current PA models and tools such as Goldsim for radionuclide migration through the near field of a HLW repository usually rely on some simplifying assumptions such as: 1) The use of the "Kd approach" for nuclide sorption and "the limited solubility" for nuclide precipitation or coprecipitation. Testing the validity of these assumptions has been limited by: 1) the lack of nuclide surface complexation and cation exchange data; and 2) the availability of computer codes which could handle simultaneously the migration, sorption and precipitation of radionuclides together with the geochemical evolution of the near field.

Lab experiments performed in recent years, some of which have been carried out within the framework of EU projects such as FEBEX, NF-PRO, have provided substantial data and understanding on the mechanisms of nuclide sorption. On the other hand, sophisticated research-oriented process-based computer codes and models have been developed which allow for the simultaneous modelling of migration, sorption, nuclide precipitation and multicomponent geochemical evolution of the near field.

Objectives

The purpose of this paper is to test the validity of the "Kd approach" and "limited solubility" assumptions for nuclide sorption and precipitation. Such testing has been performed by benchmarking of a PA model (Goldsim) and a detailed process-model with the UDC code, COREV4 (Samper et al. 2003), for some selected radionuclides. Calculations have been performed for the compacted bentonite of the engineered barrier of a spent-fuel repository in granite according to the Spanish reference concept (ENRESA, 2005; 2006). Modelling of test cases using PA models were performed by ENRESA while UDC carried out the modelling with the reactive transport code COREV4 (Samper et al. 2003).

Testing has been performed for some selected radionuclides for which detailed sorption data were available. The following nuclides have been analyzed: Ni, Cs, and U. Here we report the results for U.

Description of work

The following activies have been performed:

1. Adapting COREV4 (Samper et al. 2003) to meet the needs of the benchmarking. Although COREV4 (Samper et al. 2003) is a sophisticated code which allows for a full set of multi-component chemical and isotopic species, it might be needed to account for the possibility of several types of

sorption sites (weak and strong). It is also required to complete the verification of subroutines for radiochemical processes involved in nuclide dissolution and/or precipitation

2. Performing calculations for benchmark cases for the reference concept of SF in granite. The model will solve simultaneously for the long-term geochemical evolution of the near field and radionuclide migration, sorption (by cation exchange and/or surface complexation) and dissolution/precipitation. The model will account for canister corrosion, the EDZ and the near field granite formation.

Table 1: Equilibrium constants for aqueous complexes and minerals.

Aqueous complexes	Log K (25 ºC)
$CaCl^+ \Leftrightarrow Ca^{2+} + Cl^-$	0.6956
$CaCl_2(aq) \Leftrightarrow Ca^{2+} + 2Cl^-$	0.6436
$CaCO_3(aq) + H^+ \Leftrightarrow Ca^{2+} + HCO_3^-$	7.0017
$CaHCO_3^+ \Leftrightarrow Ca^{2+} + HCO_3^-$	-1.0467
$CaH_3SiO_4^+ + H^+ \Leftrightarrow Ca^{2+} + 2H_2O + SiO_2(aq)$	8.7916
$CaSO_4(aq) \Leftrightarrow Ca^{2+} + SO_4^{2-}$	-2.1111
$CaOH^+ + H^+ \Leftrightarrow Ca^{2+} + H_2O$	12.850
$CO_2(aq) + H_2O \Leftrightarrow H^+ + HCO_3^-$	-6.3447
$CO_3^{2-} + H^+ \Leftrightarrow HCO_3^-$	10.329
$Fe^{3+} + 0.5H_2O \Leftrightarrow Fe^{2+} + H^+ + 0.25O_2(aq)$	-8.4900
$FeCl^+ \Leftrightarrow Fe^{2+} + Cl^-$	0.1605
$FeCO_3(aq) + H^+ \Leftrightarrow Fe^{2+} + HCO_3^-$	5.5988
$FeHCO_3^- \Leftrightarrow Fe^{2+} + HCO_3^-$	-2.0500
$FeSO_4(aq) \Leftrightarrow Fe^{2+} + SO_4^{2-}$	-2.2000
$HCl(aq) \Leftrightarrow H^+ + Cl^-$	0.6700
$HSO_4^- \Leftrightarrow H^+ + SO_4^{2-}$	-1.9791
$HSiO_3^- + H^+ \Leftrightarrow H_2O + SiO_2(aq)$	9.9525
$H_6(H_2SiO_4)_4^- + 2H^+ \Leftrightarrow 8H_2O + 4SiO_2(aq)$	13.446
$KCl(aq) \Leftrightarrow K^+ + Cl^-$	1.4946
$KSO_4^- \Leftrightarrow K^+ + SO_4^{2-}$	-0.8796
$MgCl^+ \Leftrightarrow Mg^{2+} + Cl^-$	0.1349
$MgCO_3(aq) + H^+ \Leftrightarrow Mg^{2+} + HCO_3^{-2}$	7.3499
$MgHCO_3^+ \Leftrightarrow CaMg^{2+} + HCO_3^-$	-1.0357
$MgH_2SiO_4(aq) + 2H^+ \Leftrightarrow Mg^{2+} + SiO_2(aq) + 2H_2O$	17.482
$MgH_3SiO_4^+ + H^+ \Leftrightarrow Mg^{2+} + SiO_2(aq) + 2H_2O$	8.5416
$MgSO_4(aq) \Leftrightarrow Mg^{2+} + SO_4^{2-}$	-2.4117
$NaCl(aq) \Leftrightarrow Na^+ + Cl^-$	0.7770
$NaCO_3^- + H^+ \Leftrightarrow Na^+ + HCO_3^-$	9.8144
$NaHCO_3(aq) \Leftrightarrow Na^+ + HCO_3^-$	-0.1541
$NaHSiO_3(aq) + H^+ \Leftrightarrow Na^+ + SiO_2(aq) + H_2O$	8.3040
$NaOH(aq) + H^+ \Leftrightarrow Na^+ + H_2O$	14.180
$NaSO_4^- \Leftrightarrow Na^+ + SO_4^{2-}$	-0.8200
$OH^- + H^+ \Leftrightarrow H_2O$	13.995
Minerals	**Log K (25 ºC)**
$CaCO_3(s) + H^+ \Leftrightarrow Ca^{2+} + HCO_3^-$	1.8487
$CaSO_4 \cdot 2H_2O(s) \Leftrightarrow Ca^{2+} + SO_4^{2-} + 2H_2O$	-4.4823
$SiO_2(s) \Leftrightarrow SiO_2(aq)$	-3.9993
$Fe_3O_4(s) + 6H^+ \Leftrightarrow 3Fe^{2+} + 0.5O_2(aq) + 3H_2O$	-6.5076
$FeOOH(s) + 2H^+ \Leftrightarrow Fe^{2+} + 0.25O_2(aq) + 1.5H_2O$	-7.9555
$FeCO_3(s) + H^+ \Leftrightarrow Fe^{2+} + HCO_3^-$	-0.1920

The numerical model is similar to that used for Ni (described in Samper et al., 2009, in this volume). A 1D axisymmetric flow model is used.

Relevant aqueous complexes were identified from speciation runs performed with EQ3/6 (Wolery, 1992). All these reactions are assumed at local chemical equilibrium. The Gaines-Thomas convention is used for cation exchange (Gaines and Thomas, 1953). The surface complexation is simulated as proposed by Bradbury and Baeyens (2005) without electrostatic contributions, considering one strong and two weak surface sites. Surface complexation reactions are not considered inside the canister.

Table 2: Equilibrium constants for aqueous uranium complexes.

Aqueous complexes	Log K (25 ºC)
$U^{3+} + 0.75O_2(aq) + 0.5 H_2O \Leftrightarrow UO_2^{2+} + H^+$	65.045
$U^{4+} + 0.5O_2(aq) + H_2O \Leftrightarrow UO_2^{2+} + 2 H^+$	33.945
$UOH^{3+} + 0.5O_2(aq) \Leftrightarrow UO_2^{2+} + H^+$	34.485
$U(OH)_2^{2+} + 0.5O_2(aq) \Leftrightarrow UO_2^{2+} + H_2O$	35.045
$U(OH)_3^+ + 0.5O_2(aq) + H^+ \Leftrightarrow UO_2^{2+} + 2H_2O$	38.645
$U(OH)_4(aq) + 0.5O_2(aq) + 2H^+ \Leftrightarrow UO_2^{2+} + 3H_2O$	43.945
$U_6(OH)_{15}^{9+} + 3O_2(aq) + 3H^+ \Leftrightarrow 6UO_2^{2+} + 9H_2O$	220.57
$U(CO_3)_4^{4-} + 0.5O_2(aq) + 2H^+ + H_2O \Leftrightarrow UO_2^{2+} + 4HCO_3^-$	40.140
$U(CO_3)_5^{6-} + 0.5O_2(aq) + 3H^+ + H_2O \Leftrightarrow UO_2^{2+} + 5HCO_3^-$	51.589
$USO_4^{2+} + 0.5O_2(aq) + H_2O \Leftrightarrow UO_2^{2+} + SO_4^{2-} + 2H^+$	27.365
$U(SO_4)_2(aq) + 0.5O_2(aq) + H_2O \Leftrightarrow UO_2^{2+} + 2SO_4^{2-} + 2H^+$	23.435
$UCl^{3+} + 0.5O_2(aq) + H_2O \Leftrightarrow UO_2^{2+} + Cl^- + 2H^+$	32.225
$UO_2^+ + 0.25O_2(aq) + H^+ \Leftrightarrow UO_2^{2+} + 0.5H_2O$	20.016
$UO_2 Cl_2(aq) \Leftrightarrow UO_2^{2+} + 2Cl^-$	1.1000
$UO_2 ClO_3^+ \Leftrightarrow UO_2^{2+} + 1.5 O_2(aq) + Cl^-$	16.770
$UO_2 CO_3(aq) + H^+ \Leftrightarrow UO_2^{2+} + HCO_3^-$	0.3888
$UO_2(CO_3)_2^{2-} + 2H^+ \Leftrightarrow UO_2^{2+} + 2HCO_3^-$	4.0476
$UO_2(CO_3)_3^{4-} + 3H^+ \Leftrightarrow UO_2^{2+} + 3HCO_3^-$	9.1464
$UO_2(CO_3)_3^{5-} + 0.25O_2(aq) + 4H^+ \Leftrightarrow UO_2^{2+} + 3HCO_3^- + 0.5H_2O$	44.053
$(UO_2)_3(CO_3)_6^{6-} + 6H^+ \Leftrightarrow 3UO_2^{2+} + 6HCO_3^-$	7.9728
$(UO_2)_2CO_3(OH)_3^- + 4H^+ \Leftrightarrow 2UO_2^{2+} + HCO_3^- + 3H_2O$	11.189
$(UO_2)_3CO_3(OH)_3^+ + 4H^+ \Leftrightarrow 3UO_2^{2+} + HCO_3^- + 3H_2O$	9.6688
$(UO_2)_{11}(CO_3)_6(OH)_{12}^{2-} + 18H^+ \Leftrightarrow 11UO_2^{2+} + 6HCO_3^- + 12H_2O$	25.543
$UO_2OH^+ + H^+ \Leftrightarrow UO_2^{2+} + H_2O$	5.2500
$UO_2(OH)_2(aq) + 2H^+ \Leftrightarrow UO_2^{2+} + 2H_2O$	12.150
$UO_2(OH)_3^- + 3H^+ \Leftrightarrow UO_2^{2+} + 3H_2O$	20.250
$UO_2(OH)_4^{2-} + 4H^+ \Leftrightarrow UO_2^{2+} + 4H_2O$	32.400
$(UO_2)_2OH^{3+} + H^+ \Leftrightarrow 2UO_2^{2+} + H_2O$	2.7000
$(UO_2)_2(OH)_2^{+2} + 2H^+ \Leftrightarrow 2UO_2^{2+} + 2H_2O$	5.6200
$(UO_2)_3(OH)_4^{+2} + 4H^+ \Leftrightarrow 3UO_2^{2+} + 4H_2O$	11.900
$(UO_2)_3(OH)_5^+ + 5H^+ \Leftrightarrow 3UO_2^{2+} + 5H_2O$	15.550
$(UO_2)_3(OH)_7^- + 7H^+ \Leftrightarrow 3UO_2^{2+} + 7H_2O$	32.200
$(UO_2)_4(OH)_7^+ + 7H^+ \Leftrightarrow 4UO_2^{2+} + 7H_2O$	21.900
$UO_2SO_3(aq) + 0.5O_2(aq) \Leftrightarrow UO_2^{2+} + SO_4^{2-}$	40.024
$UO_2SO_4(aq) \Leftrightarrow UO_2^{2+} + SO_4^{2-}$	-3.1500
$UO_2(SO_4)_2^{2-} \Leftrightarrow UO_2^{2+} + 2SO_4^{2-}$	-4.1400
$UO_2(SO_4)_3^{4-} \Leftrightarrow UO_2^{2+} + 3SO_4^{2-}$	-3.0200
$UO_2S_2O_3(aq) + 2O_2(aq) + H_2O \Leftrightarrow UO_2^{2+} + 2SO_4^{2-} + 2H^+$	130.74

Chemical reactions and their equilibrium constants at 25 ºC for aqueous complexes and minerals (Wolery, 1992) are listed in Table 1, chemical reactions and their equilibrium constants for aqueous uranium complexes are listed in Table 2, selectivity coefficients for exchangeable cations and protolysis constants for surface complexation (Bradbury and Baeyens, 2005; BENIPA, 2003; Fernández et al., 2004; Samper et al., 2007) are listed in Table 3.

Table 3: Selectivity coefficients for cation exchange reactions and protolysis constants for surface complexation reactions.

Cation exchange	$K_{Na-cation}$
$Na^+ + K\text{-}X \Leftrightarrow K^+ + Na\text{-}X$	0.1380
$Na^+ + 0.5Ca\text{-}X_2 \Leftrightarrow 0.5Ca^{2+} + Na\text{-}X$	0.2924
$Na^+ + 0.5Mg\text{-}X_2 \Leftrightarrow 0.5Mg^{2+} + Na\text{-}X$	0.2881
$Na^+ + 0.5Fe\text{-}X_2 \Leftrightarrow 0.5Fe^{2+} + Na\text{-}X$	0.5000
$Na^+ + 0.5UO_2\text{-}X_2 \Leftrightarrow 0.5\ UO_2^{2+} + Na\text{-}X$	0.8414
Surface complexation	**Log K_{int}**
$\equiv SOH_2^+ \Leftrightarrow \equiv SOH + H^+$	-4.5
$\equiv SO^- + H^+ \Leftrightarrow \equiv SOH$	7.9
$\equiv SOUO_2^+ + H^+ \Leftrightarrow \equiv SOH + UO_2^{2+}$	-3.1
$\equiv SOUO_2OH + 2\ H^+ \Leftrightarrow \equiv SOH + UO_2^{2+} + H_2O$	3.4
$\equiv SOUO_2(OH)_2^- + 3\ H^+ \Leftrightarrow \equiv SOH + UO_2^{2+} + 2\ H_2O$	11.0
$\equiv SOUO_2(OH)_3^{2-} + 4\ H^+ \Leftrightarrow \equiv SOH + UO_2^{2+} + 3\ H_2O$	20.5
$\equiv W^1OH2^+ \Leftrightarrow \equiv W^1OH + H^+$	-4.5
$\equiv W^1O^- + H^+ \Leftrightarrow \equiv W^1OH$	7.9
$\equiv W^1OUO_2^+ + H^+ \Leftrightarrow \equiv W^1OH + UO_2^{2+}$	-0.7
$\equiv W^1OUO_2OH + 2\ H^+ \Leftrightarrow \equiv W^1OH + UO_2^{2+} + H_2O$	5.7
$\equiv W^2OH2^+ \Leftrightarrow \equiv W^2OH + H^+$	-6.0
$\equiv W^2O^- + H^+ \Leftrightarrow \equiv W^2OH$	10.5

In UDC model the canister internal volume is treated as another porous medium. A very high porewater diffusion coefficient (3 orders of magnitude greater than that in bentonite) is used to ensure perfect mixing at any instant. A porosity of 0.132 is defined for canister ensuring that internal water volume is 0.5 m^3 (when canister length is 5.94 m) and consistent with GoldSim calculations.

Given the low hydraulic conductivity of bentonite, diffusion is the main solute transport mechanism in the engineered barrier. All dissolved chemical species are assumed to have the same effective diffusion coefficient which is equal to $4.07 \cdot 10^{-11}$ m^2/s. Dispersion does not play a major role. Therefore, a small longitudinal dispersivity of 0.003 m is used for all materials. Transverse dispersivity is assumed to be 3 times smaller than the longitudinal dispersivity. The model assumes that porosity is constant and all water is accessible for chemical reactions, that is, geochemical porosity coincides with total porosity. Flow and transport parameters are listed in Table (BENIPA, 2003; Samper et al., 2007).

Table 4. Flow and transport parameters.

Material	Hydraulic conductivity (m/s)	Initial porosity	Initial effective diffusion (m^2/s)
Bentonite	$5.71 \cdot 10^{-14}$	$4.07 \cdot 10^{-1}$	$4.07 \cdot 10^{-11}$
Canister	$5.71 \cdot 10^{-15}$	$1.32 \cdot 10^{-1}$	$4.07 \cdot 10^{-08}$

The chemical composition of inflow water coincides with that of initial granite porewater. The porewater in canister and bentonite have the same initial water. The boundary inflow water concentration and initial concentrations of bentonite are listed in Table 1. (BENIPA, 2003; Samper et al., 2007).

The composition of initial porewaters is controlled by mineral dissolution/precipitation at chemical equilibrium (calcite and quartz), proton surface complexation and cation exchange. Initial volume fractions of calcite and quartz in bentonite are all 0.01 (BENIPA, 2003; Samper et al., 2007). Gypsum, magnetite, siderite and goethite are minerals which are not initially present in the system, but are allowed to precipitate.

Table 5. Boundary and initial water concentration.

Primary species	Initial bentonite water(mol/L)	Boundary water(mol/L)
Ca^{2+}	$3.101 \cdot 10^{-2}$	$1.522 \cdot 10^{-4}$
Cl^-	$2.756 \cdot 10^{-1}$	$3.949 \cdot 10^{-4}$
Fe^{2+}	$6.583 \cdot 10^{-5}$	$1.791 \cdot 10^{-8}$
pH	6.435	7.825
HCO_3^-	$1.689 \cdot 10^{-3}$	$5.049 \cdot 10^{-3}$
K^+	$1.507 \cdot 10^{-3}$	$5.371 \cdot 10^{-5}$
Mg^{2+}	$3.473 \cdot 10^{-2}$	$1.604 \cdot 10^{-4}$
Na^+	$1.841 \cdot 10^{-1}$	$4.350 \cdot 10^{-3}$
Eh (V)	-0.059	-0.188
$SiO_2(aq)$	$3.761 \cdot 10^{-4}$	$3.761 \cdot 10^{-4}$
SO_4^{2-}	$2.049 \cdot 10^{-2}$	$1.561 \cdot 10^{-5}$

Cation exchange capacity (CEC) in bentonite is 87 meq/100g. Surface complexation site densities in bentonite are listed in Table 6.

Table 6. Surface complexes site density of bentonite.

Site densities in mol/g dry bentonite	
S-OH	$2 \cdot 10^{-6}$
W1-OH	$4 \cdot 10^{-5}$
W2-OH	$4 \cdot 10^{-5}$

Each disposal canister contains close to two tons of Uranium and by far the most abundant isotope is U^{238}. Due to its very long life (4.47 billion years) it can be treated as a stable isotope and its inventory per canister is the following:

Table 7. Uranium inventory per canister.

	Half-life (years)	Activity (Bq/canister)	Mass (kg/canister)	Mass (mol/canister)
U238	$4.47 \cdot 10^9$	$2.15 \cdot 10^{10}$	$1.73 \cdot 10^3$	7266

U^{238} is the main component of the UO_2 matrix and will be released slowly when the Uranium matrix oxidises due to alpha radiation.Because there is much uranium existing in canister in term of mineral, some uranium minerals are put in the canister, the initial amount is very large to make sure that there are enough uranium resources. Table 8 is the equilibrium constants for uranium minerals. A model is made in which just initial uranium mineral uranophane is put in canister; the initial volume fraction is 0.5 UO_2 (cr), $UO_2:2H_2O$ (am), $UO_3:2H_2O$, $UO_2(OH)_2$(b), UO_3(a), UO_3(b), $UO_3:0.9H_2O$, soddyite (syn) and soddyite (syn2) are considered to be precipitated. The results show that when uranophane is considered in canister, UO_2 (cr) is precipitated in canister and bentonite.

Table 8. Equilibrium constants for Uranium minerals.

Mineral	Reaction	logK
$UO_2(cr)$	$UO_2 + 2H^+ + 0.5O_2(aq) \rightleftharpoons UO_2^{2+} + H_2O$	29.1
$UO_2:2H_2O(am)$	$UO_2 : 2H_2O(am) + 2H^+ + 0.5O_2(aq) \rightleftharpoons UO_2^{2+} + 3H_2O$	35.4
$UO_3(a)$	$UO_3 + 2H^+ \rightleftharpoons UO_2^{2+} + H_2O$	9.52
$UO_3(b)$	$UO_3 + 2H^+ \rightleftharpoons UO_2^{2+} + H_2O$	8.3
$UO_3:0.9H_2O$	$UO_3 : 0.9H_2O + 2H^+ \rightleftharpoons UO_2^{2+} + 1.9H_2O$	5
$UO_3:2H_2O$	$UO_3 : 2H_2O + 2H^+ \rightleftharpoons UO_2^{2+} + 3H_2O$	5.96
$UO_2(OH)_2(b)$	$UO_2(OH)_2 + 2H^+ \rightleftharpoons UO_2^{2+} + 2H_2O$	4.93
Uranophane	$Ca(UO_2)_2(SiO_3OH)_2 : 5H_2O + 6H^+ \rightleftharpoons 2UO_2^{2+} + Ca^{2+} + 2SiO_2(aq) + 9H_2O$	9.42
Soddyite(syn)	$(UO_2)_2 SiO_4 : 2H_2O + 4H^+ \rightleftharpoons 2UO_2^{2+} + SiO_2(aq) + 4H_2O$	3.9
Soddyite(syn2)	$(UO_2)_2 SiO_4 : 2H_2O + 4H^+ \rightleftharpoons 2UO_2^{2+} + SiO_2(aq) + 4H_2O$	6.2

In this run the dissolved UO_2^{2+} concentration is increasing to a higher value 2.81 10^-4 mol/L, after 6.0 105 years, dissolved UO_2^{2+} concentration decreases, this caused by the dissolution rate of uranophane is changed and gets smaller. The total sorbed U in bentonite increases at the beginning, reaching a maximum in 2 105 years and decreases at the end according to the evolution of dissolved U. Total solid U increases faster than dissolved U, later the increase rate gets smaller, it's decreases is smaller than that of dissolved U at the end. So Kd of U increases at the beginning, then decreases and increases again at the end. Kd is constant for dissolved UO_2^{2+} less than 10^-6 mol/L. For larger concentrations, Kd decreases (see Figure 1). Uranophane dissolves in canister, and $UO_2(cr)$ precipitates in canister and the canister-bentonite interface. Most U sorbed on strong sorption sites.
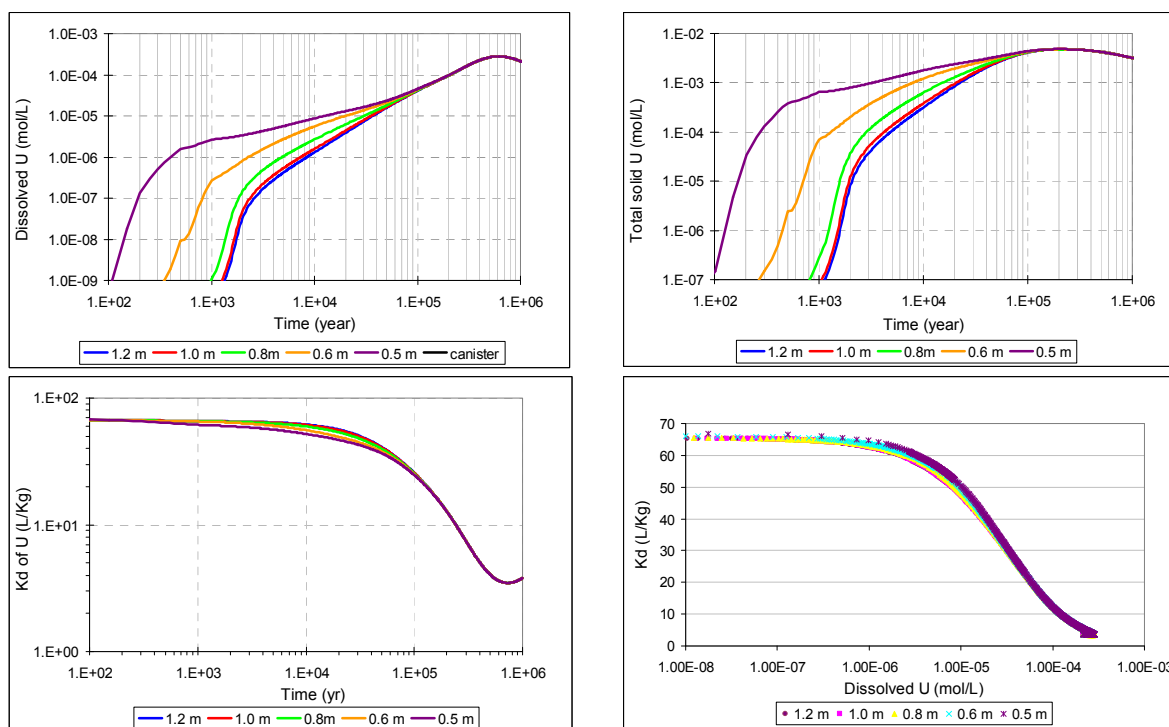
Figure 1- 1) Dissolved U evolution in canister (top left); 2) Solid U evolution in bentonite (top right); 3) Kd evolution as a function of time (bottom left) and 4) Kd as a function of dissolved U (bottom right).
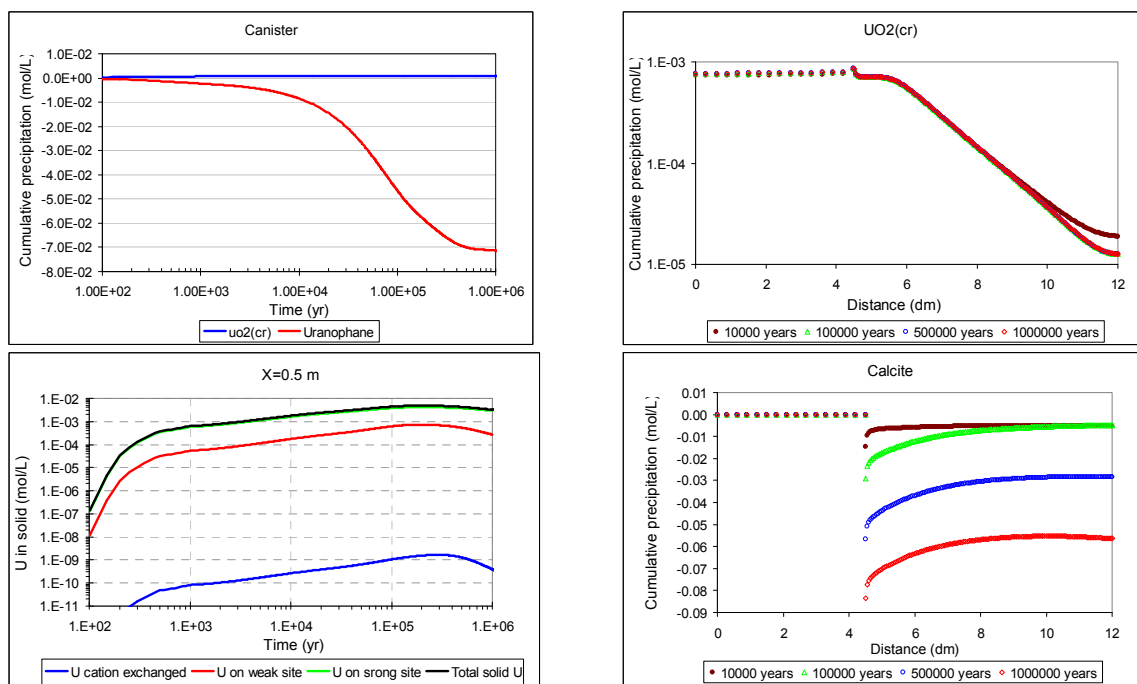
Figure 2- 1) Mineral evolution in canister (top left); 2) UO$_2$(cr) distribution (top right); 3) Sorbed U evolution in bentonite (bottom left) and 4) Calcite distribution with different time (bottom right).

Sorption on weak sites is 10 times smaller while U exchanged is much smaller. Calcite dissolves in bentonite partly due to the decrease of dissolved Ca^{2+} in bentonite by out-diffusion. Calcite dissolution is largest at the canister-bentonite interface. Goethite precipitation in bentonite is much smaller (see Figure 2).

The conclusion is that Kd of U depends on the dissolved U concentration and other variables such as pH through surface complexation. Uranophane dissolves in the canister and UO$_2$(cr) precipitates in the canister and the canister-bentonite interface. U sorbs mostly by surface complexation in strong surface sorption sites. The role of U mineral phases needs to be studied more in depth. Future models should account also for the effect of canister corrosion

Acknowledgements

References

BENIPA, 2003, Final Report of BENIPA Project: Bentonite Barriers in Integrated Performance Assessment. Report of the European Commission, EUR 21023.

Bradbury, M.H. and Baeyens, B., 2005, Modelling the sorption of Mn(II), Co(II), Ni(II), Zn(II), Cd(II), Eu(III), Am(III), Sn(IV), Th(IV), Np(V) and U(VI) on montmorillonite: Linear free energy relationships and estimates of surface binding constants for some selected heavy metals and actinides. Geochimica et Cosmochimica Acta 69 (4), 875–892.

ENRESA, 2005, NF-PRO Project. Phenomenological description. Reference Concept (Spent Fuel-Carbon Steel Canister-Bentonite-Granite). Deliverable D5.1.1. Part 1. Final version.

ENRESA, 2006, FEBEX: Updated final report. ENRESA Technical Publication PT 05-0/2006.

Fernández, A.M., Cuevas, J., Rivas, P., 2001. Pore water chemistry of the FEBEX bentonite. Mater. Res. Soc. Symp. Proc. 663, 573-588.

Fernández, A.M., Cuevas, J., Rivas, P., 2001, Pore water chemistry of the FEBEX bentonite. Mater. Res. Soc. Symp. Proc. 663, 573-588.

Gaines, G.I., Thomas, H.C., 1953, Adsorption studies on clay minerals. II. A formulation of the thermodynamics of exchange adsorption. Journal of Chemical Physics 21, 714-718.

Samper, J., Yang, C., Montenegro, L., 2003, CORE2D version 4: A code for non-isothermal water flow and reactive solute transport. Users Manual. University of La Coruña, Spain.

Samper, J., Yang, Ch., Montenegro, L., Bonilla, M., Lu, C., Yang, Q., Zheng, L., 2007. Mass and energy balance and flux calculations for radionuclide release and geochemical evolution for SF carbon steel HLW repositories in clay and granite. NF-PRO project, Deliverable D5.1.13. University of A Coruña, Spain.

Samper J, C Lu, JL Cormenzana, H Ma & MA Cuñado, 2009. Testing the Kd-approch with a multicomponent geochemical reactive transport model for a HLW repository in granite: The case of Ni, in this volume of TREPRO II 2009.

Wolery, T.J., 1992, EQ3/6, a software package for geochemical modeling of aqueous systems: Package overview and installation guide (version 7.0). Technical Report UCRL-MA-110662-Pt 1. Lawrence Livermore National Laboratory, CA, USA.

Dual continuum reactive transport with n-th order solute transfer term for structured unsaturated porous media

Liange Zheng[1] and Javier Samper[2*]
(1) Lawrence Berkeley National Lab, 1 Cyclotron Road, Berkeley, CA, 94720, USA
(2) E. T. S. Ingenieros de Caminos, Universidad de la Coruña, Campus de Elviña s/n, 15192 La Coruña, Spain

Introduction

Compacted bentonite is foreseen to be used as backfill and sealing material in high-level radioactive waste disposal. Experimental evidence indicates that bentonite exhibits two types of porosity: A macro-porous domain which is characterized by free water and a micro-porous domain mainly composed of double layer and interlayer water. Macro- and micro-domains have different hydrodynamic and geochemical properties, which calls for a fully coupled reactive transport Dual Continuum Model (DCM) to describe water flow, solute transport and hydrochemical reactions for compacted bentonite. Most DCMs assume a lumped first-order solute transfer term between both domains. However, it is well known that such a term is not correct over all time scales. A formulation for dual continuum flow and reactive transport conceptual model with an nth-order solute transfer term is presented here. The value of n is derived from an approximation of the analytical solution of diffusion through a thin slab. The formulation of DCM for flow can be found in Zheng and Samper (2005) and Zheng (2006).

Mass transfer term

The solute transfer term between macro- and micro-porous domains includes an advective Γ_s^a and a diffusive Γ_s^d term. Here we adopt an approach similar to that taken by Dykhuizen (1990) and Zimmerman (1993) to derive the diffusive solute transfer term which is based on the analogy between water flow and solute transport. Solute diffusion in the matrix block is governed by a differential equation:

$$\frac{\partial C}{\partial t} = D\nabla^2 C \qquad (1)$$

The mass flux can be found be integrating the flux out of the boundary of each matrix block by using Fick's law:

$$\Gamma_s = \frac{-1}{V_m}\int_{\partial V_m} D\frac{\partial C}{\partial n}dA \qquad (2)$$

The average concentration in the matrix block is given by:

$$\bar{C}_m = \frac{1}{V_m}\int_{V_m} C_m dV \qquad (3)$$

Integrating in space Equation (3) and using the divergence theorem one obtains the following expression for the time derivative of $\overline{C}_m$:

$$\frac{\partial \overline{C}_m}{\partial t} = \frac{1}{V_m} \int_{\partial V_m} D \frac{\partial C}{\partial n} dA$$

(4)

From (14) and (15) it follows that:

$$\frac{\partial \overline{C}_m}{\partial t} = -\Gamma_s$$

(5)

One of the most commonly used expressions for Γ_s is that of Warren and Root (1963):

$$\Gamma_s = D(C_f - C_m)$$

(6)

A more general exchange equation can be derived from the exact analytical solution of Equation (1). It is assumed that there is a thin slab block with thickness of l, C_0 is the concentration imposed at the outer boundary of the block at t = 0 and C_i is the initial concentration in the block. The analytical solution for this problem is given by (Crank 1975):

$$\frac{\overline{C}_m - C_i}{C_0 - C_i} = 1 - \frac{6}{\pi^2} \sum_{n=0}^{\infty} \frac{8}{(2n+1)^2 \pi^2} \exp\left\{-D(2n+1)^2 \pi^2 t / 4l^2\right\}$$

(7)

Vermeulen (1953) found that Equation (19) can be approximated by:

$$\frac{\overline{C}_m - C_i}{C_0 - C_i} = \left[1 - \exp\left(-D\pi^2 t / 4l^2\right)\right]^n$$

(8)

with an exponent n equal to 0.5. However, Vermeulen (1953) did not establish the conditions under which his approximation was valid. Vermeulen (1953) defined the dimensionless time $4\pi^2 Dt / l^2$ and illustrated the goodness of this approximation graphically. His approximation is poor when $4\pi^2 Dt / l^2$ is less than 0.6, i.e. for Dt/l² less than 23.66. In order to find a good approximation of the analytical solution for small values of Dt/l2, calculated average concentrations $\overline{C}_m$ with Equation (8) of different n are compared with that calculated with Equation (7). Zheng (2006) found that the analytical solution with an exponent equal to 0.72 provides an approximation which is better than that of n = 0.5. Differentiating Equation (8) with respect to t, and eliminating t from the result leads to:

$$\frac{d\overline{C}_m}{dt} = \frac{nD\pi^2}{4l^2} \frac{(C_0 - C_i)^{1/n} - (C_m - C_i)^{1/n}}{(C_m - C_i)^{1/n - 1}}$$

(9)

This expression can be generalized by assuming that C0 is equal to the concentration in the macro-porous domain and Ci is the initial concentration in the micro-porous domain:

$$\frac{d\overline{C}_m}{dt} = \frac{nD\pi^2}{4l^2} \frac{(C^{ma} - C^{ini})^{\frac{1}{n}} - (C^{mi} - C^{ini})^{\frac{1}{n}}}{(C^{mi} - C^{ini})^{\frac{1}{n}-1}} \qquad (10)$$

In order to ensure that $\frac{d\overline{C}_m}{dt}$ has the same sign as ($C_j^{ma} - C_j^{mi}$), an indicator variable δ is defined in such a way that δ = 1 when $C_j^{ma} > C_j^{mi}$ and δ = -1, otherwise. In addition, absolute values are used for exponential terms. The final expression of the diffusive flux, Γ_s^d, becomes:

$$\Gamma_s^d = \alpha_s^* \overline{D}_J \delta n \frac{\left| (C_j^{ma} - C_j^{ini})^{\frac{1}{n}} \right| - \left| (C_j^{mi} - C_j^{ini})^{\frac{1}{n}} \right|}{\left| (C_j^{mi} - C_j^{ini})^{\frac{1}{n}-1} \right|} \qquad (11)$$

where α_s^* is an empirical shape coefficient which is given by (Gerke and van Genuchten 1993a,b):

$$a_s^* = \frac{\beta}{\alpha^2} \gamma_s \qquad (12)$$

where β is a geometry-dependent coefficient and α is the radius for spheres (or cylinders) or the half width for cubes (m), and γs is a dimensionless scaling term. $\overline{D}_j$ in (16) is the weighted arithmetic average of effective diffusion coefficients of macro- and micro-pores, D_e^{ma} and D_e^{mi}, respectively:

$$\overline{D}_j = (D_e^{ma} + wD_e^{mi})/(w+1) \qquad (13)$$

The diffusive solute transfer term for n = 1 coincides with the first-order equation of Warren and Root (1963). For n = 0.5, one has a second-order term. A value of n = 0.72 will provide the best approximation in most cases (Zheng et al. 2005). The advective solute transfer Γ_s^a is given by:

$$\Gamma_s^a = \rho_l^* \Gamma_w^1 C_i^* \qquad (14)$$

where $\Gamma_w^1 = \frac{\alpha_w^* \overline{K}_{il} \overline{K}_{rl}}{\mu} \frac{(P_l^{ma} - P_l^{mi})\left[\left| P_l^{mi} - P_i^{mi} \right| + \left| P_l^{ma} - P_i^{ma} \right| \right]}{\left| P_l^{mi} - P_i^{mi} \right|}$, is the water transfer by a liquid pressure gradient. C_i^* is the concentration of solute depending on the direction of water transfer. The solute transfer term is finally given by:

$$\Gamma_s = \rho_l^* \Gamma_w^1 C_i^* + \alpha_s^* \bar{D}_J \delta n \frac{\left| (C_j^{ma} - C_j^{ini})^{1/n} \right| - \left| (C_j^{mi} - C_j^{ini})^{1/n} \right|}{\left| (C_j^{mi} - C_j^{ini})^{1/n-1} \right|}$$

(15)

The model has been implemented in a finite element code which solves for direct and inverse problems. The nth-order transfer term improves greatly the ability and accuracy of DCM to simulate reactive transport in bentonites.

Application to a permeation test

The reactive transport DCM has been tested with a long-term permeation test performed on a sample of compacted FEBEX bentonite. The experimental column used for the permeability test consists of a stainless steel cell in which a sample of compacted clay is subject to water flow (Fig. 1). The internal diameter of the cell is 5 cm and the length is 2.5 cm. A HPLC pump injects a solution at a pressure of $4.0 \cdot 10^3$ kPa through a porous stainless steel filter providing a flow rate of approximately $2.0 \cdot 10^{-3}$ L/month after stabilization. Outflowing water comes out through another stainless steel filter and it is recovered at the end of the compacted clay and sampled inside a syringe (Fernández et al., 2002). Porewater of the compacted clay began to be displaced on September 29th 1998 by means of the injection of a granitic water type. Hydrodynamic and chemical data were monitored during the duration of the experiment. Nearly $2 \cdot 10^{-3}$ L were needed for a complete chemical analysis; therefore samples could only be taken once the cell delivered the enough amount of water. The clay sample has a dry density of 1.65 g/cm^3, a porosity of 0.39. A total volume of $9.113 \cdot 10^{-2}$ L was collected after 1177 days. The quasi steady-state hydraulic conductivity of the clay is 2.7·10-14 m/s. The electrical conductivity of the effluent water decreased from 15536 in the first alliquot to 700 µS/cm in the last one. Most chemical species show clear dilution trends which are shown later. Chloride for instance decreases from 3500 to 64 g/m^3. DCM outperforms the Single Continuum Model (SCM) for pH and dissolved chloride, sodium and bicarbonate (Figures 2 and 3). These results indicate that the dual continuum behaviour is relevant for reactive transport in bentonite. Model results show also that solute transfer from micro- to macro-porous domains is responsible for the long tails of breakthrough curves of chloride and other chemical species.
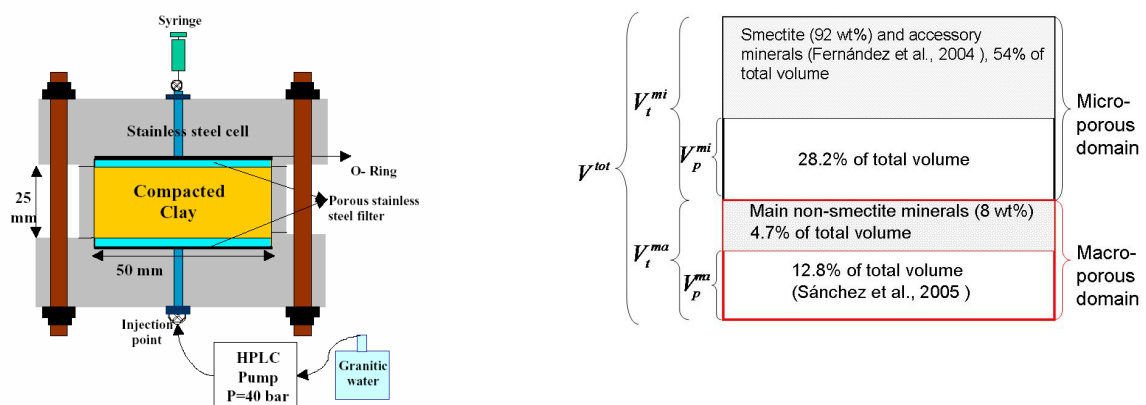
Fig. 1. Schematic design of the permeability test, left (Fernández et al. 2002) and schematic representation of macro- and micro-porous domains for the DCM (right).
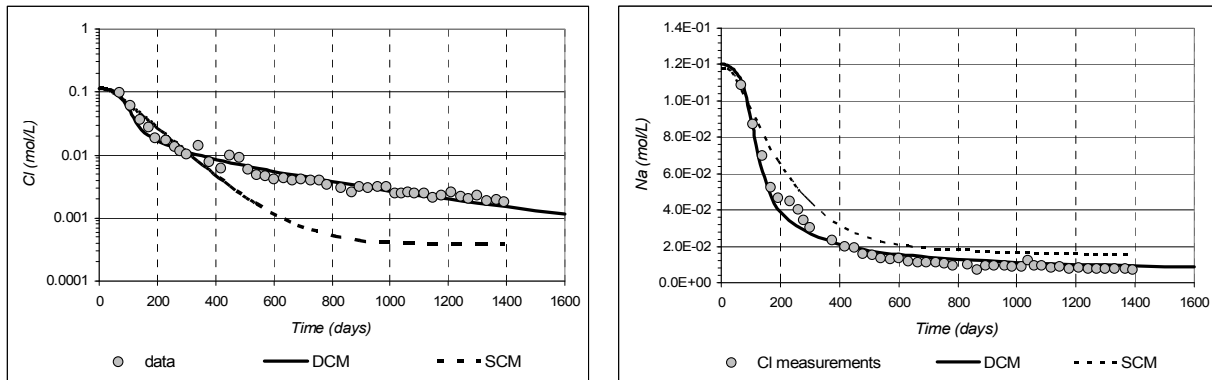
Fig. 2. Measured and computed (with DCM and SCM) time evolution of Cl^- (left) and SO_4^{2-} (right).
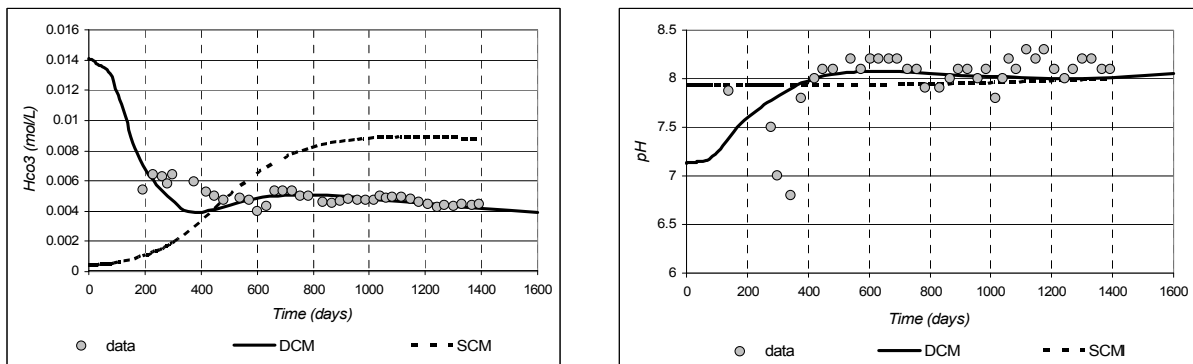
Fig. 3. Measured and computed (with DCM and SCM) time evolution of HCO_3^- (left) and pH (right).

Acknowledgements.

References

Crank J. (1975). The Mathematics of Diffusion. clarendon, Oxford.

Dykhuizen R.C. (1990). A new coupling term for dual-porosity models. Water Resour. Res., 26: 351-356.

Fernández A.M., Montenegro L., Rivas P. and Samper J., 2002. Pore water chemical compsition obtained in a permeability cell: infiltration flow test, CIEMAT, Madrid.

Gerke H.H. and van Genuchten M.T. (1993a). A dual porosity model for simulating the preferential movement of water and solutes in structured porous media. Water Resour. Res., 29: 305-319.

Gerke H.H. and van Genuchten M.T. (1993b). Evaluation of a first order water transfer term for variably saturated dual porosity flow models. Water Resour. Res., 29: 1225-1238.

Samper J., Zheng L., Fernández A.M., Montenegro L. (2008). Inverse modeling of multicomponent reactive transport through single and dual porosity media, J Cont Hydrol, Vol 98/3-4 pp 115-127. 10.1016/j.jconhyd.2008.03.008.

Vermeulen T. (1953). Theory of irreversible and constant-pattern solid diffusion. Ind. Eng. Chem., 45: 1664-1670.

Warren J.E. and Root P.J. (1963). The behavior of naturally fractured reservoirs. Soc.Petrol.Eng.J., 3: 245-255.

Zheng L. and Samper J. (2005). A dual continuum coupled multiphase flow model with mixed second order water transfer term for structured soil: I theory. In: J. Samper and A. Paz González (Editors), VII Jornadas de investigación en la Zona no Saturada de Suelo, La Coruña, Spain, pp. 295-301.

Zheng L., Samper J. and Montenegro L. (2005). A dual continuum coupled multiphase flow model with mixed second order water transfer term for structured soil: part II. Testing with synthetic cases and application to a real experiment. In: J. Samper and A. Paz González (Editors), VII Jornadas de investigación en la Zona no Saturada de Suelo, La Coruña, Spain, pp. 301-307.

Zimmerman R.W., Chen G., Hadgu T. and Bodvarsson G.S. (1993). A numerical dual-porosity model with semianalytical treatment of fracture/matrix flow. Water Resour. Res., 29: 2127-2137.

Application of Computational Chemistry to Investigate the Interactions of CSH-Gel and Alkyltriethoxysilanes

Julia Süßmuth[1] and Andreas Gerdes[2]
[1]*Institut für Funktionale Grenzflächen, Herrmann-von-Helmholtz-Platz 1, 76344 Eggenstein-Leopoldshafen, Germany*
[2]*Hochschule Karlsruhe-Technik und Wirtschaft, Moltkestraße 30, 76131 Karlsruhe, Germany*

A description of interactions of CSH as part of mineral based materials at the molecular level is still hardly possible. Morphology and composition are matter of research, but not fully understood. Because of the complexness of CSH, the chemical behaviour is still unavowed. The chemical behaviour of the hardened cement paste is e.g. determined through the number of the silanol groups and deprotonation sites. For the application of alkyltriethoxysilanes, which are used as water repellent agents, this is necessary, because they are influenced strongly through conditions like ph-value and temperature. Several kinds of alkyltriethoxysilanes with different alkylchains as well as with diverse solvents and variations of the released alcolhol are commercial available and utilised to protect infrastructure. So just empirical statements to penetration depths and concentration of the active ingredient can be done. Furthermore it is known, that the CSH-gel and the alkyltriethoxysilanes interact. To enlighten the interactions, semi-empirical calculations of the polycondenstaion of the alkyltriethoxysilanes and some calciumsilicates has been done. The macroscopic observed differences in the velocity of the ethanol release and the thermal release correspond with the ideas of the interactions at the molecular level.

Status of the COMEDIE-2D benchmark: a 3 code reactive transport inter-comparison of porosity reduction coupled to hydrodynamics

Laurent Trotignon[1], Benoit Cochepin[2], Carl Steefel[3], Vincent Lagneau[4], Nikos Leterrier[5] and Olivier Bildstein[1]

[1] *CEA, DEN, Service de Modélisation des Transferts et de Mesure Nucléaire, Laboratoire de Modélisation des Transferts dans l'Environnement, CE Cadarache, 13108 St Paul-lez-Durance, France*

[2] *Andra, Parc de la Croix Blanche, 1-7 rue Jean Monnet, 92 298 Châtenay-Malabry, France*

[3] *Earth Sciences Division, Lawrence Berkeley National Laboratory, 1 Cyclotron Road, Mail Stop 90-1116, Berkeley, CA 94720, USA*

[4] *Mines Paristech - Centre de Géosciences, Equipe Hydrodynamique et Réactions - Reactive Hydrodynamics Group, 77305 Fontainebleau, France*

[5] *CEA, DEN, Service Fluides Numériques, Modélisation et Etudes, Laboratoire de Modélisation des Transferts dans les Milieux Solides, CE Saclay, 91191 Saclay, France*

Introduction

COMEDIE-2D is a numerical clogging experiment that was designed in order to couple strongly, on a simple 2D reactor, porosity reduction and solution flow (Trotignon et al. 2005). Cochepin et al. (2008) presented a first benchmark run on this case with Hytec (Van der Lee et al. 2003) and Crunch (Steefel 2006). Leterrier et al. (2008) applied recently the Alliances platform, co-developed by Andra, CEA and Edf, (Bengaouer et al. 2005) to this case.

A summary of the benchmark principle is given and the major outcome of this code intercomparison work is presented.

Principle of the benchmark

The COMEDIE-2D reactor (Fig. 1) is a square flat box (0.14 m side) including three mineral zones (Q1 to Q3) and equipped with 2 fluid inlets and 1 fluid outlet. Q1 and Q3 zones are composed of quartz sand (initial porosity 0.3). The Q2 zone is initially composed of a mixture of quartz sand and portlandite (initial porosity 0.19).
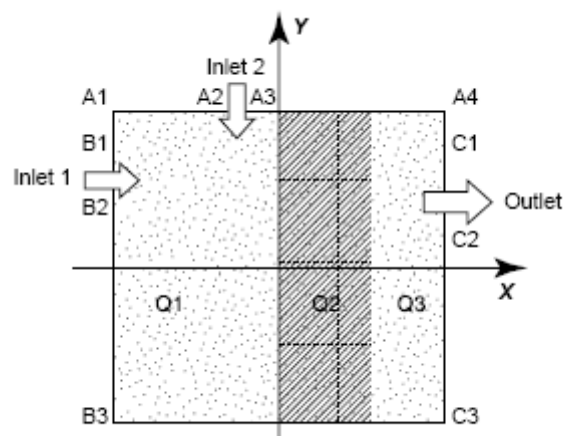
Fig. 1. Design of the COMEDIE-2D reactor.

Fluid injection (Inlet 1: NaCl, 0.02 M ; Inlet 2 : $Na_2C_2O_4$, 0.4 M) leads to the formation in the Q2 zone of a calcium oxalate precipitate at the expense of the initial

portlandite. The volume balance of this conversion is very positive, leading thus to the growth of a clogging obstacle that diverts the flow lines. Eventually, when portlandite is totally converted, redissolution of the oxalate precipitate starts and this leads to the perforation of the obstacle.

Reactive transport codes

The three reactive transport codes used for this benchmark adopt similar or specific approaches to describe the processes involved on the COMEDIE-2D benchmark. All of the codes use finite volume discretization. Heterogeneous chemical reactions may be represented at equilibrium (Hytec, Alliances) or using a kinetic approach (Crunch, Hytec, Alliances). Coupling between reaction and transport may approached either with the SIA approach (Hytec, Alliances), the SNIA approach (Crunch) or a global implicit method (Crunch). Permeability evolutions are updated explicitly at each time step.

Specific features of the different codes (e.g. reactive surface models, cementation models, etc) make the building of exactly matching test cases difficult (see Cochepin et al. 2008). In addition, the different simulation tools include or neglect different terms in the development of the flow equation:

$$-div\left(\rho \overset{\rho}{U}\right) = div(\overline{\overline{\rho K}}.\overset{\rho}{\nabla}h) = \frac{\partial \rho \omega}{\partial t}$$

In all three codes, permeability is computed through a Kozeny-Carman relationship. In Hytec, the transport module R2D2 is coupled to the chemical solver Chess. In Alliances, the transport module Cast3m is coupled to Allichess, a version of Chess plugged into the Alliances platform.

Major results and issues

All three codes predict evolutions in qualitative agreement: formation of the calcium oxalate wall that diverts the flow lines is followed by the subsequent perforation of this obstacle (Fig. 2 and 3). Detailed examination of the results reveals however interesting differences. The spatial distributions of precipitates are different, even for Hytec and Alliances results, in which chemistry is treated at local equilibrium with the same chemical module. In this case differences are thought to stem from both the treatment of the flow equation and the magnitude of numerical dispersion. The spatial distribution of calcium oxalate simulated by Crunch shows locally higher concentrations, leading thus to locally lower porosity and to a stronger coupling between flow and porosity reduction. This has for consequence the creation of portlandite islands, protected by oxalate precipitates. The origin of this discrepancy between Crunch and Hytec-Alliances simulations is found to be related to the surface area models used to describe the dissolution/precipitation of secondary minerals (Ca-oxalate in the present study) and more generally to the kinetic description of such secondary precipitation processes. This observation pinpoints the importance of properly describing and simulating the way the texture evolves in porous medium when porosity undergoes significant variations. In particular, the use of a chemical equilibrium assumption in modeling systems with strong cementation is questionable, since reactive surface areas markedly decrease and should thus limit reaction rates.

The construction of the actual experiment is now considered as the next step of this project. Main concerns deal with instrumentation (in vivo measurements or post mortem characterization of successive dissolution/precipitation events), tracer methods and coping with adverse 3D effects coming from density contrasts or heterogeneities.
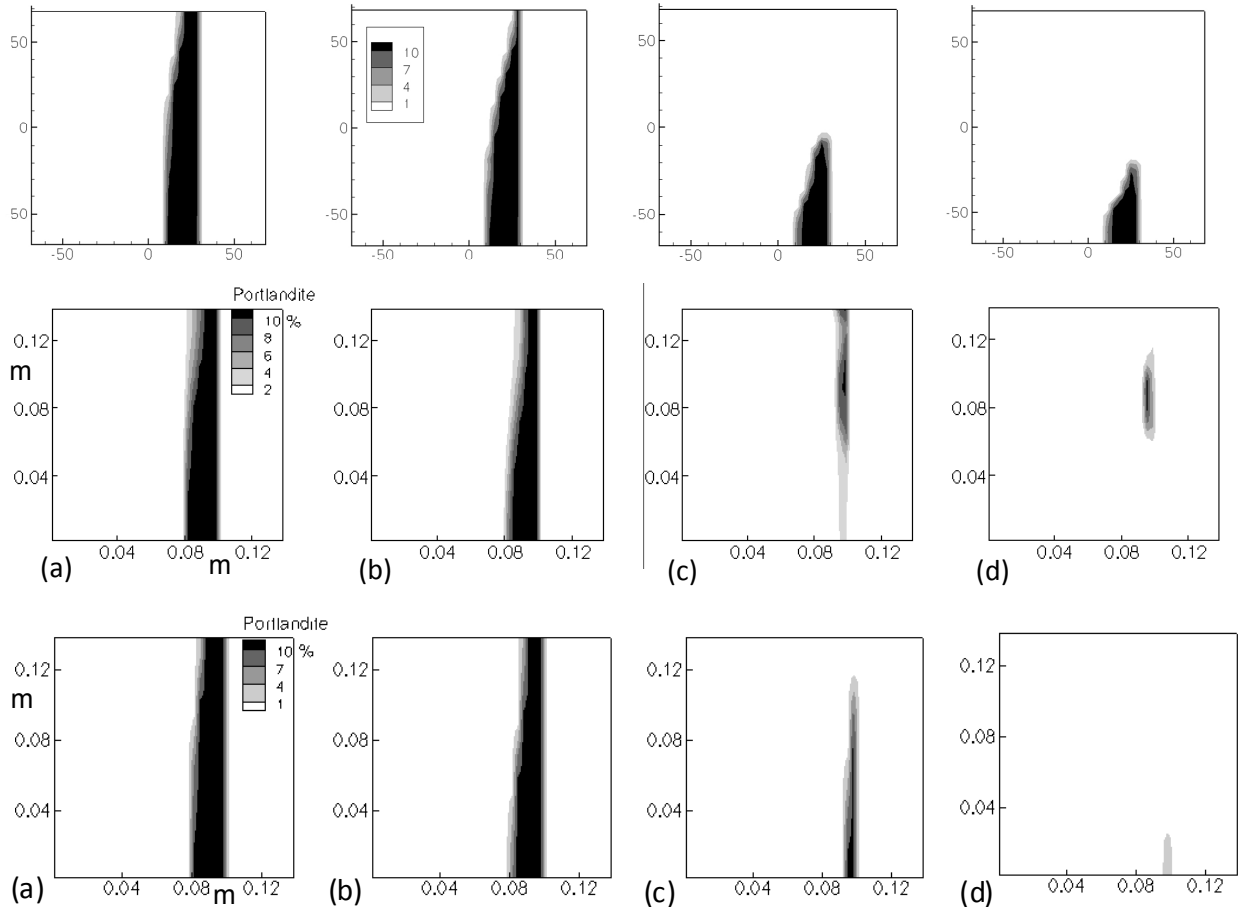
Fig. 2. Portlandite evolution at 5, 10, 30 and 40 days (top: Alliances, equilibrium ; middle : Crunch, kinetics ; bottom : Hytec, equilibrium).
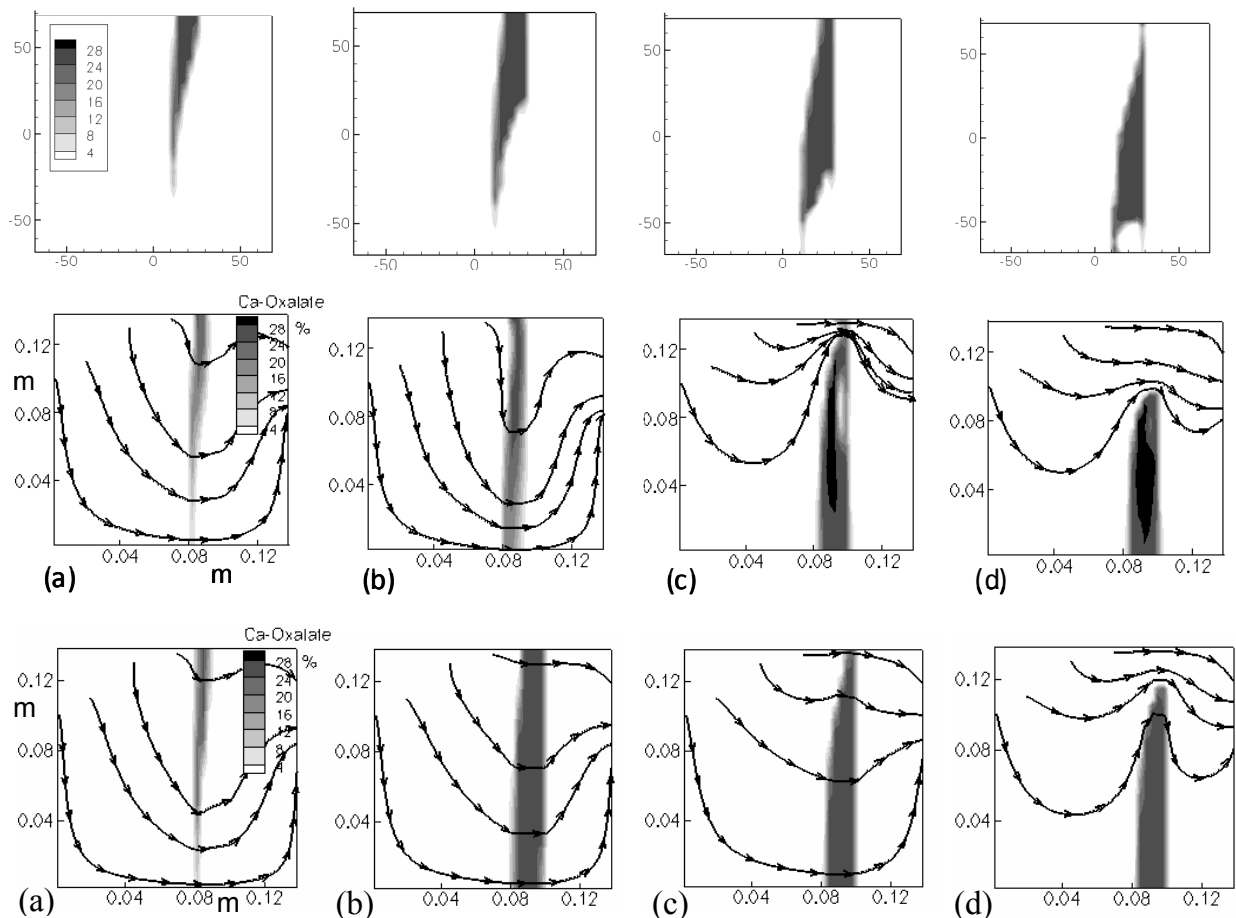
Fig. 3. Calcium oxalate evolution at 10, 20, 40 and 70 days (top: Alliances, equilibrium ; middle : Crunch, kinetics; bottom: Hytec, equilibrium). Flow lines are showed for Crunch and Hytec simulations.

References

Bengaouer A., et al., (2005). ALLIANCES: Simulation platform for radioactive waste disposal. Atw-International Journal for Nuclear Power 50(8-9): p. Xiii-Xiv.

Cochepin B. et al. (2008). Approaches to modelling coupled flow and reaction in a 2D cementation experiment, Advances in Water Resources 31,1540–1551.

Leterrier N. et al. (2008). Hydraulic Retroaction of Porosity change in Reactive Transport, CMWR XVII, July 2008.

Steefel C.I. (2006). Crunch - Users Guide., Lawrence Berkeley National Laboratory, USA.

Trotignon L., et al. (2005). Design of a 2-D cementation experiment in porous medium using numerical simulation. Oil & Gas Science and Technology-Revue De L Institut Francais Du Petrole, 60(2): p. 307-318

Van der Lee J. et al. (2003). Module-oriented modeling of reactive transport with HYTEC. Computers & Geosciences, 29(3): p. 265-275.

Study by near field microscopy by time resolved laser spectroscopy in to europium sorbed on alumina with and without humic acid

Khalil Abbas Ghaleb[1], Pascal Reiller[2] and François Viala[3]
[1]*DPC/SCP/LRSI*
[2]*DPC/ SECR/LRSM*
[3]*CEA/DEN/DANS/DPC/SCP/LRSI*

Introduction

The comprehension of the mechanisms of sorption of the radionuclide with long life is important for the evaluation of the long-term storage of the nuclear waste. The aim of the study is to evaluate the distribution on a nanometric scale and to determine the environment chemical of europium sorbed on a mineral surface: alumina Al_2O_3.By Time resolved laser induced fluorescence spectroscopy in scanning optical near field microscopy (TRLIF-SNOM), we were interested in sorption of europium on alumina-α in absence and in presence of humic acids. In this context, we seek to know the shape and the distribution of these humic acids sorbed on alumina.

Experimental procedure

Two types of solutions are prepared: either a europium perchlorate with an adjusted pH, or a solution of europium perchlorate and humic acid, starting from humic acid Aldricht. Alumina samples are immerged in these solutions then dried in the air.
We used an experimental construction. A pulsed laser OPO at 393 nm is focused on the sample. The fluorescence emitted by the europium of the sample is collected, in near field, by a sharpened optical fiber and is recorded on an spectrometer to acquire the wavelength spectrum or to determine the temporal decrease.

Results and discussion

The fluorescence spectrum of Eu^{3+} was measured on the two types of sample with changing the temporal delay between the excitation and fluorescence (Fig. 1). We recorded the temporal decrease of the fluorescence of the line at 592 nm and at 614 nm on the two types of sample (figure n°2). The decrease of europium without humic acids is simple exponential whereas that of complexed europium is bi-exponential. We have studied the values of the ratio of the intensities $R = I614/ I592$ of the lines at 614 nm and at 592 nm.

Conclusion

One can deduce from it that Eu3+ not complexed is sorbed on alumina-   in only one site with an environment which creates an important crystal field (R=4.3). Eu^{3+} complexed by the acids humic is sorbed on alumina in two types of site the first with an environment which creates a crystal field a little less important (R=3.8) and the second first with a crystal field extremely strong (R=6.7).
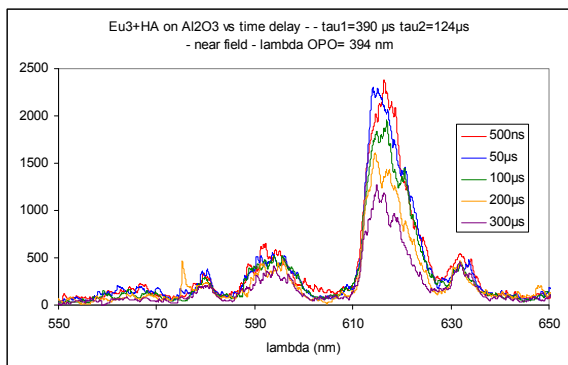
Fig. 1. The fluorescence spectrum of Eu^{3+} complexed by the acids humic at various temporal delay between the laser excitation and fluorescence.
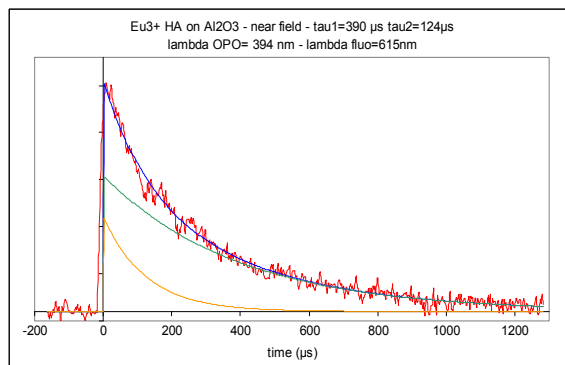
Fig. 2. Bi-exponential temporal decrease of the fluorescence of the line at 614 nm of Eu^{3+} complexed by the acids humic with many delay.

Modelling of through-diffusion experiments using PHREEQC2: influence of the characterization of uranyl sorption on mesoporous silica MCM-41 by a surface complexation model

Dušan Vopálka and Karel Štamberg
Department of Nuclear Chemistry, Czech Technical University in Prague, Břehová 7, 11519 Praha 1, Czech Republic

Introduction

The diffusion experiments in standard configurations (e.g., through-diffusion and in-diffusion) are used for the determination of parameters necessary for the modelling of diffusion transport in porous media. The ways of evaluation of such experiments are based on analytical solutions of diffusion equation for appropriate initial and boundary conditions (e.g. [1]). The Kd approach to description of interaction of dissolved species with the mineral surfaces based on the evaluation of batch experiments and/or diffusion experiments with the limited length of the specimen enables to simplify the modelling of contaminant transport for longer distances. As PHREEQC includes the possibility to model one-dimensional multicomponent transport, we have made an attempt to model the diffusion transport in the configuration of a standardized diffusion experiment with a non-trivial description of interaction. The aim of our study is to contribute to the discussion of the applicability of diffusion coefficients determined in laboratory for systems, for which the ion exchange and/or surface complexation control the interaction, also for modelling of diffusion transport in spacious layers. Our previous study of U(VI) interaction with highly sorbing mesoporous silica type of MCM-41 [2] lent us an instrument for such study.

MCM-41 falls into new family of molecular sieve and sorption materials the striking features of which, such as very large BET surface area, large pore volume and fast kinetics of sorption, attracted researchers to utilize them as sorbent and study its sorption behaviour towards chemical and radio toxic metal ions from various waste stream. For example, it was studied: (i) surface complexation modelling of uranyl ion sorption [2], (ii) sorption separation process for the purification of water [3] and (iii) the ability of MCM-41 to separate all types of analytes (basic, acidic, neutral) [4].

Table 1: MCM-41: results of the evaluation of the titration curve and U(VI) sorption in the absence and in the presence of carbonates.

Reaction	Symbols of constants	Values of constants, L/mol, for CEM (recalculated for $I = 0$)
$XO^- + H^+ = XOH^0$	K_{1p}	5.15×10^8
$XOH^0 + H^+ = XOH_2^+$	K_{2p}	1.03×10^{-1}
$UO_2^{2+} + XO^- = XOUO_2^+$	K_1	3.62×10^6
$UO_2OH^+ + XO^- = XOUO_2OH^0$	K_2	1.80×10^6
$(UO_2)_2(OH)_2^{2+} + XO^- = XO(UO_2)_2(OH)_2^+$	K_3	5.58×10^2
$(UO_2)_3(OH)_5^+ + XO^- = XO(UO_2)_3(OH)_5^0$	K_4	1.27×10^5
$(UO_2)_3(OH)_7^- + XO^- = XO(UO_2)_3(OH)_7^{2-}$	K_5	2.46×10^4
$UO_2CO_3^0 + XO^- = XOUO_2CO_3^-$	K_{1c}	1.50×10^6
$UO_2(CO_3)_2^{2-} + XO^- = XOUO_2(CO_3)_2^{3-}$	K_{2c}	1.55×10^4
$UO_2(CO_3)_3^{4-} + XO^- = XOUO_2(CO_3)_3^{5-}$	K_{3c}	1.14×10^3
$HCO_3^- + XOH_2^+ = XOH_2HCO_3^0$	K_{4c}	8.93×10^2
$CO_3^{2-} + XOH_2^+ = XOH_2CO_3^-$	K_{5c}	2.39×10^6

Total site density for CEM, mol/kg	ΣXOH	3.82

Evaluation of batch experiments

The method based on the classical batch technique [2] was used to the determination of the input data needed to the modelling of diffusion through the bed containing MCM-41. The surface acidity constants (K1p and K2p), the total site density (ΣXOH) and - in the case of CCM (Constant Capacitance Model) – the value of Helmholz capacitance (G) were obtained by fitting of acid-base titration data. The values of surface complexation constants were determined by fitting of sorption dependences on pH, namely, the constants K1-K5 in the absence of carbonates and K1c –K3c in the presence of carbonates; the values of constants K4c and K5c were taken from literature [5]. Three types of surface complexation models namely two electrostatic models (CCM and DLM – diffuse double layer model) and one chemical equilibrium non-electrostatic model (CEM) were employed to simulate the amphoteric and sorption properties of MCM-41. As the best one, the CEM was found. The results of evaluation of titration and sorption experiments are summarised in Table 1 and illustrated in Fig. 1. The specific surface area, SP, was determined by means of BET method (SP = 711 m^2g^{-1}).
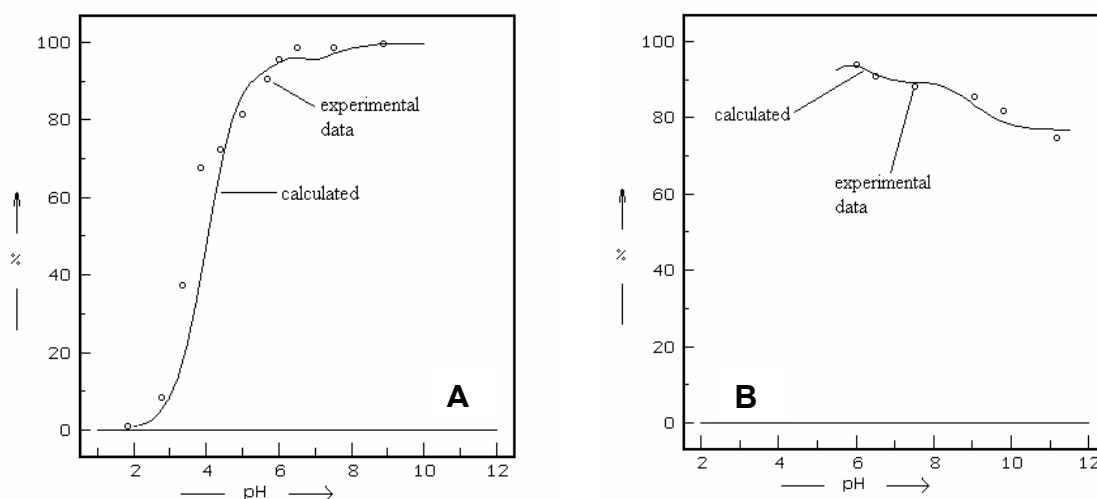
Fig. 1. Percentage sorption of U(VI) on MCM-41 in the absence of carbonates (A, I = 0.01) and in the presence of carbonates (B, I = 0.015).

From Fig.1A can be observed that, in the absence of carbonates, sorption of U(VI) - strong increases in the pH interval from 3 to 6 and then remains approx. on the same value. In the presence of carbonates, according to Fig. 1B, it is evident that sorption of U(VI) decreases with increase in pH, namely, due to the increase in the concentration of CO_3^{2-} (resulting in the conversion of HCO3- to CO_3^{2-}) displacing subsequently U(VI) from MCM-41.

Modelling of diffusion transport in PHREEQC2

The evaluation of diffusion experiments in the standard through-diffusion configuration enables to estimate both basic characteristics of diffusion, namely effective diffusion coefficient De and apparent diffusion coefficient Da. So we modelled such experiments for the porous layer containing sorbent MCM-41, interaction of which with uranium was described with the aim to discuss the influence

of interaction models (SCM) on the values of diffusion coefficients mentioned. For the description of reactions taking place in the liquid phase, the formation constants from database HATCHES distributed by NEA OECD was used. It is necessary to add, that the constants used for evaluation of batch experiments [2] were very close to the HATCHES values. The surface reactions of individual species were characterized using data collected in Table 1.
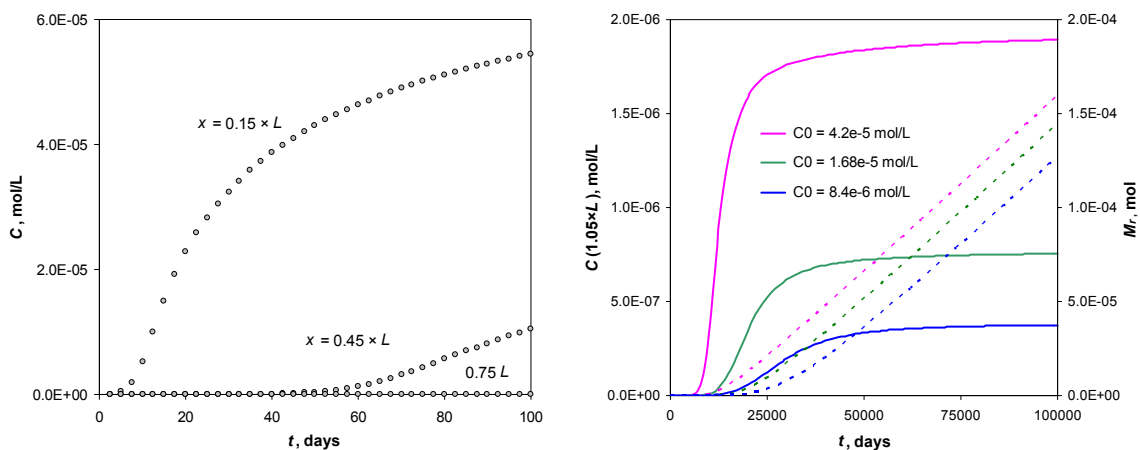
Fig. 2. Modelling of through-diffusion experiment for uranium without carbonates by pH 6 in the block of 10 cm length (L) containing sorbing MCM-41: left - concentration profiles in the three cuts of the diffuse layer, right - concentrations (full lines - C) in the output filter and total mass (dotted lines - Mr) diffused through the layer containing sorbing material. Numerical experiments were performed for three values of concentration in the input container.

To fulfil the boundary conditions that characterize the through-diffusion type of the experiment (constant concentration C_0 in the input container and zero concentration in the output container), the so-called Dirichlet type of boundary condition was chosen. All model computations were performed with the diffusion coefficient in pore water Dp equal to 3×10^{-10} m^2/s. The width of the porous inert material containing sorbent, amount of which was chosen to be 0.1 kg per 1 L of the liquid phase (= pore water), was divided into 10 small layers with the aim to enable the monitoring of the distribution of species in the porous body. In the eleventh small layer taken into account by computation (model of the boundary filter), the presence of the sorbent was not assumed. It deals with the layer used for the readout of the output concentration in the liquid phase. The numerical accuracy of the diffusion model realized in the PHREEQC2 environment was tested with success with regard to the width of the „small" layer (see results on Fig. 3) and to the elementary time step.

The results presented in Fig. 2 demonstrate the behaviour of the model. There are time dependences of the total U(VI) in the liquid phase for three cuts of the body, in the left part of this figure for elected conditions of the numerical experiment. These results could be used for the determination of apparent diffusion coefficient for both standard types of diffusion experiment, in-diffusion and through-diffusion, for systems being not in steady state. The integral value of all U(VI) species in liquid phase (Mr) in the boundary filter gives the total U(VI) diffused through the body. The derivation of this quantity enables to determine the value of effective diffusion coefficient De from the slope of the function Mr = f(t). The same slopes of tangent lines for different values of input concentrations, see the right part of Fig. 2, show that in our model De values are independent on the condition of experiments. This result corresponds with both real experimental findings and theory of diffusion of retarded species. That is to say that De describes diffusion in the steady state, in which the concentrations in

liquid and solid phase are in equilibrium for all species taken into account. The transformation of measured concentration in the boundary filter into quantity Mr enables further to determine the value of apparent diffusion coefficient Da, which globally describes the retardation of the transport caused by sorption. For the determination of Da from the results of experiment of the through-diffusion type, the so-called time-lag method (e.g. [1]) was used, by means of the relation Da = L2/6T. Here L is the width of the body of the porous material and T is time corresponding to the intersection of t-axis with the asymptote to total mass diffused (time dependent), in this work represented by quantity Mr. From the results presented in the right part of Fig. 2 it can be concluded that for the modelled system the Da value decreases with the fall of the input concentration, which means that the sorption isotherm is non-linear and the Kd values decrease with the increase of equilibrium concentration in the liquid phase.

Table 2. Results of the determination of Da×1012 values obtained by time-lag evaluation method of modelled through-diffusion experiments for two different chemical conditions. Modelled input concentration and length of the block were changed, C0 = 8.4×10^{-5} mol/L.

L, cm	Measured apparent diffusion coefficient $D_a \times 10^{12}$, m^2/s		
	2	5	10
A – pH 6, absence of carbonates			
C_0	1.92	1.81	2.09
$C_0/2$	1.40	1.32	1.23
$C_0/5$	1.02	0.87	0.82
$C_0/10$	0.58	0.60	0.60
B – pH 8, presence of carbonates			
C_0	3.26	3.07	3.13
$C_0/2$	3.33	3.06	3.13
$C_0/5$	3.32	3.06	3.12
$C_0/10$	3.27	3.05	3.02

Results of modelling

For both systems, which served for the construction of interaction model – without carbonates (A) and with carbonates (B), broader sets of numerical experiments for selected pH values were performed by means of the model constructed for the through-diffusion experiment. Results describing the influence of length of the diffusion body L and of value of concentration in the input container on computed Da values are presented in Table 2, for the system A data for pH 6 and for the system B data for pH 8. From results of batch experiments (Fig. 1) can be concluded that, for selected pH values, the retardation of diffuse transport in the system B should be lower than the retardation in the system A. The comparison of appropriate Da values testified this assumption: Da values of numerical experiments with system A is lower than comparable Da values of numerical experiments with system B, consequently the relation of retardation of the diffuse transport is inverse.

A marked influence of the input concentration on computed apparent diffusion coefficient Da was observed for the system A that could be explained by the non-linear character of equilibrium interaction isotherm. On the other hand, the system B did not show such dependence. So it could be for the modelled conditions characterized by the linear sorption isotherm. Another type of the quantification of the non-linear shape of interaction isotherm for the system A (pH 6) was demonstrated in Fig. 3, where concentration profiles of total uranium in both phases for different time values were compared. The concentration profiles in the liquid phase indicated for

higher time values the reaching of the steady state sooner than profiles in the solid phase. These results could be interpreted as the redistribution of uranium among various species on the surface along the diffusion path without significant change of the total concentration in the liquid phase. In the steady state the ratios between concentration on the surface (q) and in the liquid phase (C) in the profile of the studied body give the information about dependence of Kd on the equilibrium concentration. Also here could be concluded that this quantity decreased, for the conditions of the modelled system, with the increased equilibrium concentration in the liquid phase. The shape of concentration in the solid phase for the example, the results of which are presented in Fig. 3, implies further that when evaluating the results of the through-diffusion experiment by determination of profile of total concentration, the measured concentration at the end of the studied body could be unexpectedly high. The extent of this increase depends on the size of nonlinearity of the equilibrium isotherm and on the width of the output filter.
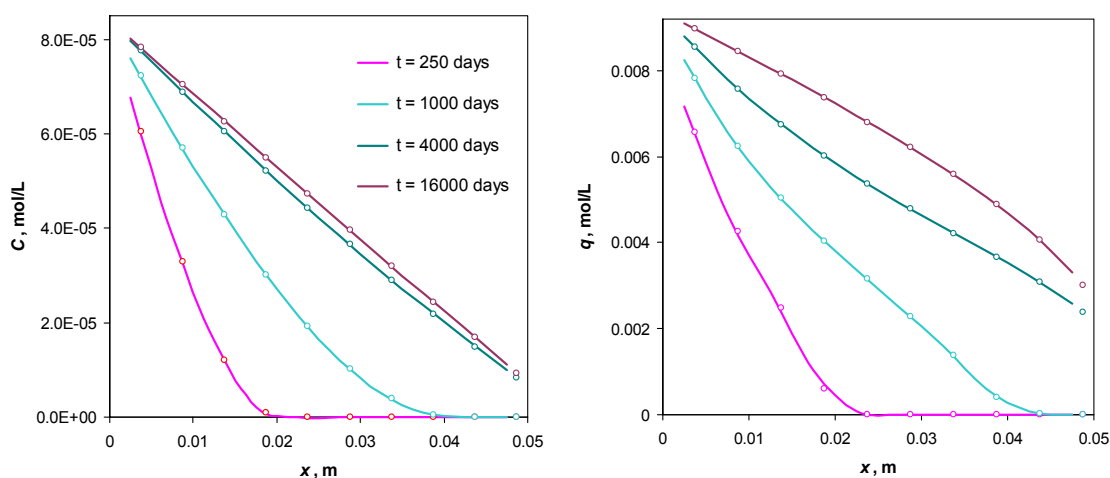
Fig. 3. Modelled concentration profiles in liquid (left) and solid (right) phases on the block of 5 cm length containing sorbing MCM-41 for input concentration 8.4×10^{-5} mol/L (pH 6, without carbonates). The block was mentioned to be divided on 10 (solid curves) or 20 (single points) layers.

Practically no influence of the body length on the value of Da was observed for the both studied systems (see Table 2). Here it should be mentioned that some experiments with the system A were influenced by a small systematically error connected with difficulties by determination of the steady state, knowledge of which is necessary for the accurate determination of time-lag T. From the previous fact can be concluded, surely for condition of our experiments, that also the sophisticated description of interaction of a set of species of some measurable contaminant form with the surface can induce a simple behaviour of this form as a whole. Namely, the ascertained constancy of Da with respect to length of the diffusion path allows to characterize the transport of the total U(VI) through the layer containing sorbent (for the constant uranium concentration in the input container), interaction of which with uranium is non-linear, by the model that was developed for the linear sorption isotherms.

References

Olin M. (1994). Diffusion in crushed rock and in bentonite clay. VTT Publications 175, Espoo, 98 p.

Štamberg K., Venkatesan K.A., Vasudeva Rao P.R. (2003). Colloids and Surfaces A: Physicochem. Eng. Aspects 221, 149-162.

Beck J.S., Calabro D.C., McCullen S.B., Pektine B.P., Schmitt K.D., Vartuli J.C. (1993). US Patent 5 220 101.

Grun M., Kurganov A.A., Schacht S., Unger K.K. (1996). J. Chromatogr. A 740 1-9.

Štamberg K., Vopálka D., Škrkal J., Beneš P., Chalupská K. (1998). Scientific Basis for Nuclear Waste Management XXI. Book Series: Materials Research Society Symposium Proceedings, 506, 485-493.

Dynamics and Reactivity at Mineral-Water Interfaces: Integrated X-ray, Neutron, Molecular Simulation and Hydrothermal Experimental Studies

D.J. Wesolowski[1], A.V. Bandura[2], P. Bénézeth[3], P.T. Cummings[4], M. Davis[5], P.A. Fenter[6], J.D. Kubicki[5], S.N. Lvov[5], M.L. Machesky[7], E. Mamontov[1], D.A. Palmer[1], M. Předota[8], M.K. Ridley[9], J. Rosenqvist[1], J.O. Sofo[5], L. Vlcek[4] and Z. Zhang[6]

[1]Oak Ridge National Laboratory, Oak Ridge, Tennessee, USA
[2]St. Petersburg State University, St. Petersburg, Russia
[3]Universite de Toulouse, III-CNRS-IRD-OMP, Toulouse, France
[4]Vanderbilt University, Nashville, Tennessee, USA
[5]Penn State University, University Park, Pennsylvania, USA
[6]Argonne National Laboratory, Argonne, Illinois, USA
[7]University of Illinois, Champaign, Illinois, USA
[8]Univ. South Bohemia, Ceske Budejovice, Czech Republic
[9]Texas Tech University, Lubbock, Texas, USA

The interface between minerals and aqueous solutions is the most significant reaction domain in the earth's upper crust, influencing elemental transport, colloid stability and migration, weathering and mineral transformation, water chemistry, biological processes and sequestration/remediation schemes. Fig. 1 is a snapshot from a classical molecular dynamics (CMD) simulation (Předota et al. 2004) of a 5-nanometer (nm) thick layer of liquid water containing dissolved $SrCl_2$ in contact with uncharged (110) surfaces of rutile (α-TiO_2) at 25°C. Such quantitative interfacial models and images are slowly beginning to replace conceptual cartoons in the scientific literature. If the simulation accurately reflected chemical reality, a wealth of information could be extracted regarding interfacial structure and dynamics, and such models are readily extrapolated to other temperatures, densities, chemical compositions and substrate bulk and surface structures. However, this simulation employs the nonreactive, rigid SPC/E water model (Berendsen et al. 1987), classical potentials estimated for two-body interactions only, and a relaxed surface structure and atom charges derived from a density functional theory (DFT) approximation. Such models must be compared against experimental evidence, and augmented or abandoned if necessary. The cutting edge of interfacial science lies in linking advanced molecular imaging and computational approaches with macroscopic observables to achieve a predictive capability.
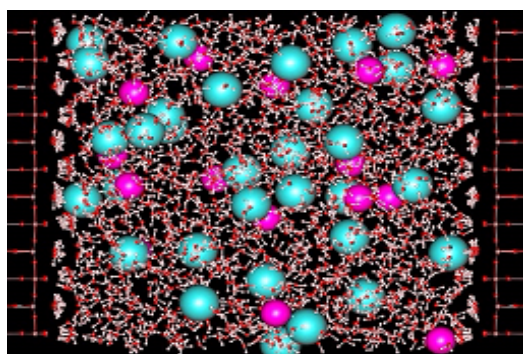
Fig. 1. MD simulation of 2 m $SrCl_2$ in contact with rutile (110) surfaces. Pink (Sr^{2+}), teal (Cl^-), white (H^+), red (O^{2-}), grey (Ti^{4+}). (Relative ionic radii altered for clarity).

Our recent efforts have focused on the (110) surfaces of rutile and isostructural cassiterite (α-SnO_2), because a.) they are among the most widely-studied surfaces in the scientific literature (Batzill and Diebold 2005; Diebold 2003); and b.) their surface

and bulk structures are very similar, but their bulk dielectric constants differ widely (εk = 120 for rutile, 9 for cassiterite), reflecting the lower polarizability of the valence electron orbitals in cassiterite. Sverjensky (2001) suggested that high-εk phases (with rutile as the archetypical example) promote 'inner sphere' adsorption of cations in contact with surface oxygens, and low-εk phases (εk = 4.6 for archetypical quartz, α-SiO_2) promote 'outer sphere' adsorption of fully-hydrated ions, and longer-range ordering of interfacial water. Many common rock-forming silicates have εk values close to that of cassiterite and quartz (Sahai and Sverjensky 1997). Quartz will be a primary target for future studies, both to test the hypothesis above, and because quartz is an ideal phase to attempt a quantitative link between the detailed structure and dynamics of the interface and mineral dissolution and precipitation mechanisms and rates.
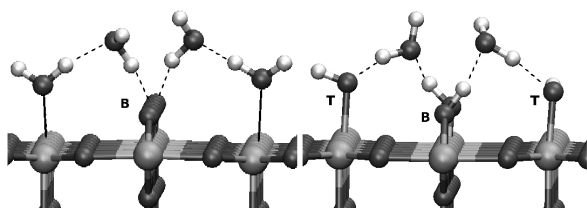
Fig. 2. Sorbed water configurations from CMD studies of rutile and cassiterite where first water layer is fully associated (left) or dissociated (right) (Vlcek et al. 2007).

We have conducted extensive pH titrations of surface charge densities (arising from pH-dependent protonation of surface oxygens) and multivalent cation adsorption on oxide powder suspensions to 290°C (50°C for cassiterite), and zeta potential (ZP) measurements to 260°C, using unique high temperature pH-cells at ORNL and electrophoretic mobility facilities at Penn State (Machesky et al. 2006, 2008a,b; Wesolowski et al. 2008). We found that the pH of zero charge (PZC) closely parallels the temperature dependence of the neutral pH of water (1/2pKw), and that the sorption affinities of multivalent cations increase strongly with increasing temperature and charge, and decreasing bare cation radius. Using synchrotron X-ray standing wave (XSW), crystal truncation rod (CTR) and absorption fine structure (EXAFS) methods (Zhang et al. 2006a,b, 2007; Vlcek et al. 2007) we determined the relaxation of rutile and cassiterite (110) single-crystal surfaces in contact with thick aqueous solution films, and the near-surface structure of water and sorbed ions (Rb^+, Sr^{2+}, Zn^{2+}, Y^{3+}, Cl^-, Br^-) at 25°C over a range of pH's and ionic strengths.
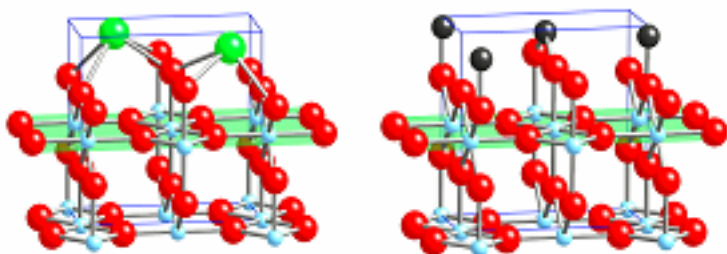
Fig. 3. Tetradentate sorption site (left) of Rb^+, Sr^{2+} and Y^{3+} on rutile (110), and the monodentate and bidentate Zn^{2+} sites (right identified by XSW and EXAFS methods (Zhang et al. 2006a,b).

Computational studies included calculation of relaxed surface configurations, atomic charges and force fields from DFT (Bandura et al. 2006, 2008) for input into large-scale CMD simulations (Předota et al. 2007a,b, Vlcek et al. 2007) of SPC/E water and ions optimized for SPC/E in contact with the DFT-optimized surfaces. These studies have revealed, at sub-angstrom resolution, the structure of sorbed water and ions at the rutile and cassiterite (110) surfaces, both of which are dominated by structural bridging (B) oxygens and terminal (T) chemisorbed water molecules (Fig.

2) bonded to metal atoms in the surface plane. On both surfaces, there is a tendency toward dissociation of the terminal water to produce a 'hydroxylated' or dissociated surface consisting of bridging and terminal hydroxyls. Static DFT and recent ab initio MD simulations indicate a stronger tendency toward dissociation on cassiterite, but our CMD simulations considered both end members as well as mixed surfaces, since the SPC/E model does not permit water dissociation. Two layers of highly-ordered water molecules were identified at both surfaces by CTR and CMD and the two approaches agree quantitatively. Negatively-charged surfaces were also studied by XSW and CTR in neutral-basic solutions and by manipulating the ratio of hydroxylated to nonhydroxylated surface oxygens in the CMD. Both approaches indicated inner sphere sorption of all cations studied (Fig. 3), and agreement among the experimental and computational approaches is remarkable (Fig. 4). The larger cations (Rb^+, Sr^{2+}, Y^{3+}, etc.) predominantly sorb at a 'tetradentate' site involving two bridging and two terminal oxygens (Fig. 3). Also shown in (Fig. 3) are the sorption sites found for Zn^{2+}, in approximately Ti-lattice-equivalent sites. DFT, XSW and EXAFS studies revealed that this ion undergoes a coordination change and hydrolysis upon adsorption. Recent CTR results indicate that Zn^{2+} sorption is similar on cassiterite, and we are now investigating the interactions of other ions with this surface by X-ray, computational and macroscopic experimental approaches.
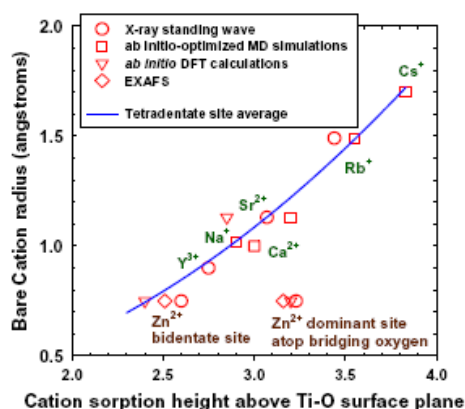
Fig. 4. Adsorption heights above rutile (110) surface versus bare cation radius (Wesolowski et al. 2008.
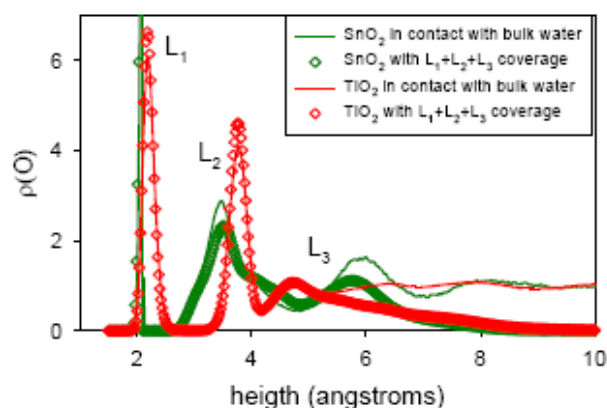
Fig. 5. CMD oxygen density profiles perpendicular to rutile (red) and cassiterite (green) (110) surfaces, showing three distinct layers (Mamontov et al. 2007), L1, L2, L3.

Using atomic charges, bond lengths and H-bonding of surface oxygens from our X-ray and computational studies, we have optimized the prediction of surface oxygen protonation equilibria within the revised and temperature-extrapolated MUSIC model (Hiemstra et al. 1996), accurately predicting the surface charging and PZC obtained from pH titrations of our rutile and cassiterite powders (Machesky et al. 2008b), consistent with second harmonic generation (SHG) measurements of the PZC on the rutile (110) single-crystal surface (Fitts et al. 2005). Combining these predicted surface protonation constants and crystallographically-determined site densities and ion adsorption stoichiometries obtained from the X-ray, CMD and DFT studies, we have developed Guoy-Chapman-Stern based models of Na^+, Rb^+, Ca^{2+}, Sr^{2+} and Nd^{3+} adsorption on rutile and cassiterite powder surfaces (Ridley et al. 2004, 2005; Machesky et al. 2006, 2008a) that contain a great deal of chemical reality. These studies reveal that 1:1 electrolytes are not 'indifferent' on such surfaces, but that the often-observed ionic strength dependence of weakly-sorbing ions like Ca^{2+} and Sr^{2+} is a result of direct competition with monovalent cations for inner sphere sorption at the same surface sites, whereas monovalent cations cannot compete with strong-

sorbers like Nd^{3+} and Zn^{2+}, due to their much weaker binding, regardless of their concentration. Also, the inner sphere sorption positions of both strong (Zn^{2+}) and weak (Sr^{2+}) sorbers were found to be independent of the background electrolyte concentration (Zhang et al. 2006a). While Gouy-Chapman-Stern models are shown to be conceptually consistent with our combined studies, application of such surface complexation models to our electrophoresis studies of rutile and cassiterite (Fedkin et al. 2003; Machesky et al. 2006) indicate a distance to the hypothetical 'shear plane' obtained from such models that is much larger than the decay lengths of water diffusivity at rutile and cassiterite surfaces extracted from our CMD studies (Předota et al. 2007a; Vlcek et al. 2007).

To begin testing and making use of the wealth of dynamic information in our simulations, we have initiated quasielastic neutron scattering (QENS) studies of the dynamics of sorbed water on rutile and cassiterite nanoparticle surfaces (with the (110) surface predominant) using the HFBS and DCS spectrometers at the U.S. National Institute of Standards and Technology (NIST) (Mamontov et al. 2007) and the BASIS spectrometer at ORNL's Spallation Neutron Source (SNS) (Mamontov et al. 2008; Ross et al. 2009). Measurements on hydrated nanoparticles, rather than single-crystal surfaces were necessary to eliminate the swamping signal from bulk water, while providing a large number of scattering centers due to the high surface area. Fig. 5 shows CMD-generated axial density profiles of the oxygen atoms of adsorbed water perpendicular to the (110) surfaces of dissociated cassiterite and associated rutile. The L1 peak is the terminal oxygen and L2 is the average position of the first water layer H-bonded to the terminal and bridging oxygens (Fig. 2). A third water layer (L3) is clearly defined in the simulations. Significant differences are observed in the water structures on the two surfaces, with a much thicker L2 layer on cassiterite. The open diamonds in Fig. 5 represent simulations at the same surfaces, but with only enough water in the simulation cells to make up L1+L2+L3 (no bulk water present), a hydration level equivalent to the hydrated nanoparticles in our QENS studies. Remarkably, the CMD axial (and lateral) distributions of sorbed water at these reduced coverages are virtually identical to the structure simulated for contact with bulk water. This gives us confidence that the water diffusional dynamics extracted from our QENS and CMD studies are useful in defining the dynamics of the bulk solution-solid interface.

Fig. 6 shows the characteristic times (τ) of water diffusional motions extracted from the QENS data as a function of inverse temperature. Three distinct motions can be detected in the picosecond (ps), tens of ps, and nanosecond (ns) time scales. Each spectrometer has a specific energy transfer range and resolution. The results for the slowest component are different for the BASIS and HFBS, because the latter instrument samples a much narrower energy transfer range. The CMD results indicate that the intermediate component is due to hindered rotations of H_2O molecules within localized cages of surrounding water molecules in all layers. The fastest component is due largely to translation-like diffusion of H_2O molecules in L3 facilitated by their undersaturated H-bonding environment (~3 H-bonds per oxygen). Fourier transformation of the CMD data into energy transfer space over the dynamic range of the DCS shows quantitative agreement with the QENS results for both phases (Fig. 6). The slowest component is due to translational jumps of L2 water molecules into L3, and this motion exhibits a non-Arrhenius temperature dependence with a dynamic transition at ~220K related to its fully H-bonded environment.
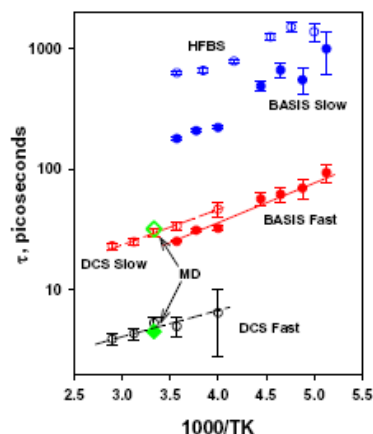
Fig. 6. QENS characteristic diffusion times (τ).
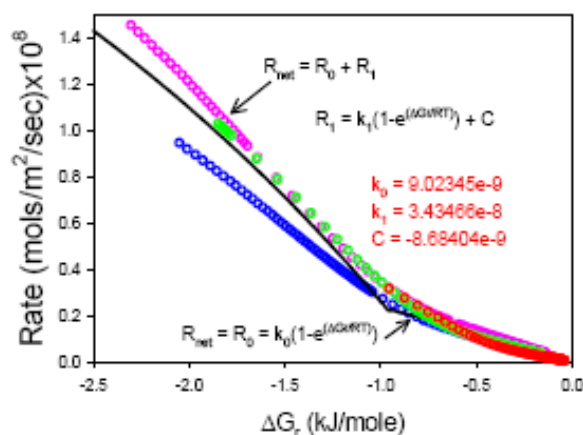
Fig. 7. Quartz dissolution rates in dilute NaC solutions (pH 8-9.5) at 125°C.

We have recently begun obtaining very-near-equilibrium quartz (α-SiO$_2$) dissolution and precipitation rates (Fig. 7) at temperatures to 200°C, using a new pH-perturbation approach (Bénézeth et al. 2008). The results obtained thus far are consistent with Dove's (2005) hypothesis that dissolution is controlled by step edge retreat very near equilibrium, and a faster rate further from equilibrium, related to the opening of etch pits. At far from equilibrium conditions, the rate law shown in Fig. 7 extrapolates to R_{far} = k0 + k1 + C and is in quantitative agreement with the new far-from equilibrium dissolution rate model of Bickmore et al. (2008). This new experimental approach will enable us to explore at unprecedented detail the effect of changes in bulk solution properties on reaction rates and mechanisms. A common geochemical dissolution-precipitation rate expression (Lasaga 1998) is R_{net} = k•Amin•exp(-Ea/RT)•a(H+)n•g(I)•$\prod$(am)i•f(ΔGr), where R_{net} is the overall reaction rate, k the rate constant, A_{min} the reactive surface area, Ea the activation energy, a(H+)n an explicit function of the activity of either H$^+$ or OH$^-$, g(I) a function of the solution ionic strength, $\prod$(am)i the product of activities of catalytic or inhibitory dissolved species, and f(ΔGr) a function of the free energy of reaction (ΔGr = 0 at equilibrium). Heretofore, these parameters have been evaluated empirically, much like the parameters in Guoy-Chapman-Stern models, which inevitably leads to ambiguities due to covariance. Numerous authors (Brantley 2004; Casey 2001; Ludwig and Casey 1996; Pokrovsky and Schott 2000a,b) have suggested that a more fundamental knowledge of the surface charge density and PZC will play a major role in interpreting heterogeneous kinetics over wide ranges of temperature and pH. Recent progress has been made in defining f(ΔGr) in relation to reaction rates and mechanisms (Dove et al. 2005; Beig and Lüttge 2006; Hellmann and Tisserand 2006) and a variety of computational studies have addressed the role of H$_3$O$^+$ and OH$^-$ in surface bond breaking (Xiao and Lasaga 1994; Sahai and Rosso 2006; Nangia et al. 2007; Mahadevan and Garofalini 2008). Ab initio calculations have also been employed to estimate activation energies (Pelmenschikov et al. 2000; Criscenti et al. 2006; Nangia and Garrison 2008). The influence of dissolved ions on the mechanisms and rates of dissolution and precipitation have been empirically assessed (Oelkers et al. 1994; Dove, 1999; Bickmore et al. 2006; Kowacz et al. 2007). Such studies strongly indicate that sorption of ions on the mineral surface, and/or the disruption of the hydrogen bonding network of water in the vicinity of the surface, play a major role in dissolution mechanisms, but a molecular-level understanding of these effects has not been established.

136

Acknowledgement:

References

Bandura A. V., Sofo, J. O., Kubicki J. D. (2006). Derivation of force field parameters for SnO2-H2O surface systems from plane-wave density functional theory. *Journal of Physical Chemistry B*, 110, 8386.

Bandura A. V., Kubicki J. D., Sofo J. O. (2008). Comparisons of multilayer H2O adsorption on the (110) surfaces of a-TiO2 as calculated with density functional theory. *Journal of Phys. Chem. B*, 112, 11616.

Batzill F., Diebold U. (2005). The surface and materials science of tin oxide. *Journal of Progressive Surface Science*, 79, 47.

Beig M. S., Luttge A. (2006). Albite dissolution kinetics as a function of distance from equilibrium: Implications for natural feldspar weathering. *Geochim. Cosmochim. Acta*, 70, 1402.

Bénezeth P., Palmer D. A., Wesolowski D. J. Dissolution/precipitation kinetics of boehmite and gibbsite: Application of a pH-relaxation technique to study near-equilibrium rates. *Geochim. Cosmochim. Acta*, 72, 4521.

Berendsen H. J. C., Grigera J. R., Straastma T. P. (1987). The missing term in effective pair potentials. *Journal of Physical Chemistry*, 91, 6269.

Bickmore B. R., Nagy K. L., Gray A. K., Brinkerhoff A. R. (2006). The effect of Al(OH)$_4^-$ on the dissolution rate of quartz. *Geochim. Cosmochim. Acta*, 70, 290.

Bickmore B. R., Wheeler J. C., Bates B., Nagy K. L., Eggett D. L. (2008). Reaction pathways for quartz dissolution determined by statistical and graphical analysis of macroscopic experimental data. *Geochim. Cosmochim. Acta*, 72, 4521.

Brantley S. L. (2004). Reaction kinetics of primary rock-forming minerals under ambient conditions. *Surface and Ground Water, Weathering and Soils: Treatise on Geochemistry*, 5, 73.

Casey W. H. (2001). A view of reactions at mineral surfaces from the aqueous phase. *Mineralogical Magazine*, 65, 323.

Criscenti L. J., Kubicki J. D., Brantley S. L. (2006). Silicate glass in mineral dissolution: Calculated reaction paths and activation energies for hydrolysis of a Q^3 Si by H$_3$O$^+$ using ab initio methods. *Journal of Physical Chemistry A*, 110, 198.

Diebold U. (2003). The Surface Science of Titanium Dioxide. *Surface Science Reviews*, 48, 53.

Dove P. M. (1999). The dissolution kinetics of quartz in aqueous mixed cation solutions. *Geochim. Cosmochim. Acta*, 63, 3715.

Dove P. M., Han N., De Yoreo J. J. (2005). Mechanisms of classical crystal growth theory explain quartz and silicate dissolution behavior. *Proc. National Acad. Sci. U.S.A.*, 102, 15357.

Fedkin M.V., Zhou X.Y., Kubicki J.D., Bandura A.V., Lvov S.N., Machesky M.L., Wesolowski D.J. (2003). High temperature microelectrophoresis studies of the rutile/aqueous solution interface. *Langmuir*, 19, 3797.

Fitts J. P., Machesky M. L., Wesolowski D. J., Shang X., Kubicki J.D., Flynn G.W., Heinz T.F., Eisenthal K.B., (2005). Second-harmonic generation and theoretical studies of protonation at the water/α-TiO$_2$(110) interface. *Chemical Physics Letters*, 411, 399.

Fragneto-Cusani G. (2001). Neutron reflectivity at the solid/liquid interface: Examples of applications in biophysics. *Journal of Physics: Condensed Matter*, 13, 4973.

Hellmann R., Tisserand D. (2006). Dissolution kinetics as a function of the Gibbs free energy of reaction: An experimental study based on albite feldspar. *Geochim. Cosmochim. Acta*, 70, 364.

Hiemstra T., Venema P., Van Riemsdijk W. H. (1996). Intrinsic proton affinity of reactive surface groups of metal (hydr)oxides: The bond valence principle. *J. Colloid Interface Sci.*, 184, 680.

Kowacz M., Putnis C. V., Putnis A. (2007). The effect of cation:anion ratio in solution on the mechanism of barite growth at constant supersaturation: Role of the desolvation process in the growth kinetics. *Geochim. Cosmochim. Acta*, 71, 5168.

Lasaga A. C. (1998). Kinetic Theory in the Earth Sciences. Princeton University Press, Princeton, 811p.

Ludwig C., Casey W. H. (1996). On the mechanisms of dissolution of bunsenite (NiO(s)) and other simple oxides. *J. Colloid Interface Sci.*, 178, 176.

Lvov S. N. (2007). Electrochemical techniques for studying high-temperature subcritical aqueous solutions. *Encyclopedia of Electrochemistry*, 5, 24

Machesky M. L., Wesolowski D. J., Palmer D. A., Ridley M. K., Benezeth P., Lvov S. N., Fedkin M. V. (2006). Ion adsorption into the hydrothermal regime: Experimental and modeling approaches. In: *Surface Complexation Modeling,* J. Lützenkirchen (ed.), Interface Science and Technolody, 11, 324.

Machesky M. L., Wesolowski D. J., Ridley M. K., Palmer D. A., Rosenqvist J., Lvov S. N., Fedkin M. V., Predota M., Vlcek L. (2008a). The protonation behavior of metal oxide surfaces to hydrothermal conditions. *ECS Trans*, 11, 151.

Machesky M. L., Predota M., Wesolowski D. J., Vlcek L., Cummings P. T., Rosenqvist J., Ridley M. K., Kubicki J. D., Bandura A. V., Kumar N., Sofo J. O. (2008b). Surface protonation at the rutile (110) interface: Explicit incorporation of solvation structure within the Refined MUSIC Model framework. *Langmuir*, 24, 12331.

Mamontov E., Vlcek L., Wesolowski D. J., Cummings P. T., Wang W., Anovitz L. M., Rosenqvist J., Brown C. M., Garcia-Sakai V. (2007). Dynamics and structure of hydration water on rutile and cassiterite nanopowders studied by quasielastic neutron scattering and molecular dynamics simulations. *J. Phys. Chem. C*, 111, 4328.

Mamontov E., Wesolowski D.J., Vlcek L., Cummings P.T., Rosenqvist J., Wang W., Cole D.R., (2008). Dynamics of hydration water on rutile studied by backscattering neutron spectroscopy and molecular dynamics simulation. *Journal of Physical Chemistry C*, 112, 12334.

Nangia S., Washton N. M., Mueller K. T., Kubicki J. D., Arrison B. J. (2007). Study of a family of 40 hydroxylated β-cristobalite surfaces using empirical potential energy functions. *Journal of Physical Chemistry C*, 111, 5169.

Nangia S. and Garrison B. J. (2008). Reaction rates and dissolution mechanisms of quartz as a function of pH. *Journal of Physical Chemistry A*, 112, 2027.

Oelkers E. H., Schott J., Devidal J. L. (1994). The effect of aluminum, pH and chemical affinity on the rates of aluminosilicate dissolution reactions. *Geochim. Cosmochim. Acta*, 58, 2011.

Pelmenschikov A., Strand J., Pettersson L. G. M., Leszczynski J. (2000). Lattice resistance to hydrolysis of Si-O-Si bonds of silicate minerals: Ab initio calculations of a single water attack on the (001) and (111) beta-cristobalite surfaces. *J. Phys. Chem. B*, 104, 5779.

Pokrovsky O. S., Schott J. (2000a). Forsterite surface composition in aqueous solutions: A combined potentiometric, electrokinetic, and spectroscopic approach. *Geochim. Cosmochim. Acta*, 64, 3299.

Pokrovsky O. S., Schott J. (2000b). Kinetics and mechanisms of forsterite dissolution at 25°C and from pH 1 to 12. *Geochim. Cosmochim. Acta*, 64, 3313.

Prédota M., Bandura A. V., Cummings P. T., Kubicki J. D., Wesolowski D. J., Chialvo A. A. Machesky M. L. (2004). Electrical double layer at the rutile (110) surface. 1. Structure of surfaces and interfacial water from molecular dynamics by use of ab initio potentials. *Journal of Phys. Chem. B*, 108, 12049.

Prédota M., Cummings P. T., Wesolowski D. J. (2007a). Electrical double layer at the rutile(110) surface. 3. Inhomogeneous viscosity measurements by computer simulations. *Journal of Physical Chemistry C*, 111, 3071.

Prédota M., Vlcek L. (2007b). Comment on parts 1 and 2 of the series: Electrical Double Layer at the Rutile (110) Surface. *Journal of Phys. Chem. B*, 111, 1245.

Ridley M.K., Machesky M.L., Wesolowski D.J., Palmer D.A., (2004). Modeling the surface complexation of calcium at the rutile-water interface to 250°C *Geochimica et Cosmochimica Acta*, 68, 239.

Ridley M.K., Machesky M.L., Wesolowski D.J., Palmer D.A., (2005). Surface complexation of neodymium at the rutile-water interface: A potentiometric and modeling study in NaCl media to 250°C *Geochimica et Cosmochimica Acta*, 69, 63.

Ross N.L., Spencer E.C., Levchenko A.A., Kolesnikov A.I., Wesolowski D.J., Cole D.R., Mamontov E., Vlcek L., (2009). Studies of Mineral-Water Surfaces. In (L. Liang, R. Rinaldi H. Schober, eds.), *Neutron Applications in Earth, Energy and Environmental Sciences*, Springer, New York, 235.

Sahai N., Rosso K. M. (2006). Computational molecular basis for improved silica surface complexation models. In: *Surface Complexations Models*, J. Lützenkirchen (ed.), Interface Science and Technology, 11: 37

Sahai N., Sverjensky D. A. (1997). Solvation and electrostatic model for specific electrolyte adsorption. *Geochim. Cosmochim. Acta*, 61, 2827.

Sverjensky D. A. (2001). Interpretation and prediction of triple-layer model capacitances and the structure of the oxide-electrolyte-water interface. *Geochim. Cosmochim. Acta*, 65, 3643

Vlcek L., Zhang Z., Machesky M. L., Fenter P. A., Rosenqvist J., Wesolowski D. J., Anovitz L., Predota M., Cummings P. T. (2007). Electrical double layer at metal oxide surfaces: Static properties of the cassiterite-water interface. *Langmuir*, 23, 4925.

Wesolowski D. J., Machesky M. L., Ridley M. K., Palmer D. A., Zhang Z., Fenter P. A., Predota M., Cummings P. T. (2008). Ion adsorption on metal oxide surfaces to hydrothermal conditions. *ECS Trans.*, 11, 167.

Xiao Y., Lasaga A. C. (1994). Ab initio quantum mechanical studies of the kinetics and mechanisms of silicate dissolution: H^{+}(H$_3$O^{+}) catalysis. *Geochim. Cosmochim. Acta*, 58, 5379.

Zhang Z., Fenter P. A., Cheng H. P., Sturchio N. C., Bedzyk M. J., Machesky M. L., Anovitz L. M., Wesolowski D. J. (2006a). Zn^{2+} and Sr^{2+} adsorption at the TiO$_2$ (110)-electrolyte interface: Influence of ionic strength, coverage, and anions. *J. Colloid Interface Sci.*, 295, 50.

Zhang Z., Fenter P. A., Kelly P., Catalano J. G., Bandura A. V., Kubicki J. D., Sofo J. O., Wesolowski D. J., Machesky M. L., Sturchio N. C., Bedzyk M. J. (2006b). Structure of hydrated Zn^{2+} at the rutile TiO$_2$ (110)-aqueous solution interface: Comparison of X-ray standing wave, X-ray absorption spectroscopy, and density functional theory results. *Geochim. Cosmochim. Acta*, 70, 4039.

Zhang Z., Fenter P. A., Sturchio N. C., Bedzyk M. J., Machesky M. L., Wesolowski D. J. (2007). Structure of rutile TiO$_2$ (110) in water and 1 molal Rb^{+} at pH 12: Inter-relationship among surface charge, interfacial hydration structure and substrate structural displacements. *Surface Science*, 601, 1129.

3D-Visualisation and Modelling of Transport Processes in Heterogeneous Structures

Martin Wolf[1], Johannes Kulenkampff[1], Johanna. Lippmann-Pipke[1], Marion Gründig[1], Frieder Enzmann[2] and Michael Richter[1]

[1]*Institute of interdisciplinary Isotope Research (IIF), Leipzig, Germany*
[2]*Institute of Geosciences, Johannes-Gutenberg University (JGU), Mainz, Germany*

Fluid flow processes in permeable structures play an essential role in many geological fields as hydrology, final repository research or raw material exploration. The transport parameters are determined by the prevailing heterogeneous inner structure of the material, so that heterogeneous behaviour has to be considered when choosing the examination method and modelling the processes. Classical flow-through experiments (Fig. 1 and 2) give only limited information about heterogeneously structured material but homogeneous structures are rather an exception in nature. Knowledge about the ongoing processes and transport mechanisms can be enlarged enormously when material transport within a rock sample can be displayed three-dimensionally, non-destructively and in situ. Therefore the positron-emission-tomography (PET) is suited notably as its data is quantifiable directly and highly sensible and provides sufficient spatial (almost 1 mm) and temporal resolution (1 minute) (Fig. 3) (Kulenkampff et al. 2008; Gründig et al. 2007). Within a BMBF - joint venture about mining damages of the potash- and salt mines of Stassfurt (Saxony-Anhalt) various hydrodynamic parameters as well as dissolution and diffusion processes are investigated at drilling cores of different lithologic units of the overburden and the salinar rock by means of the Geo-PET - method we developed for many years (Richter et al. 2000; Richter 2002).

Fig. 1. Sandstone drilling core consisting of heterogeneous material, pervaded by several material boundaries and fissures and prepared for column experiments.

Fig. 2. Layout of a conventional black box column experiment.

Quantification of hydrodynamic parameters is done by tagging a solution with a suited PET tracer and displaying the spatio-temporal distribution of that solution during an ongoing flow-through experiment (Richter 2002; Kulenkampff et al. 2008, Gründig et al. 2009). This distribution is afterwards aligned with the structure of the drilling core that is detected by means of computer-tomographic scanning (µXCT) up to the µm scale (Fig. 4). By combining PET with µXCT effective hydraulic pathways can be investigated, heterogeneity can be quantified as well as diverse hydrodynamic parameters in relation to structural conditions of a sample
Parameters as mass flow, dispersivity and flow velocity are investigated separately for single structural areas as fissures, matrix or material changes (Fig. 5) or whole cross sections (Fig. 6) and compared with parameters obtained from modelled general break-through curves. Within a new cooperation it is planned to align the attribution of different sets of parameters – measured and quantified with Geo-PET –

of distinct spatial zones in the sample that are assumed to be homogeneous with 3D simulations of the heterogeneous fluid flow in correspondingly zoned virtually samples.
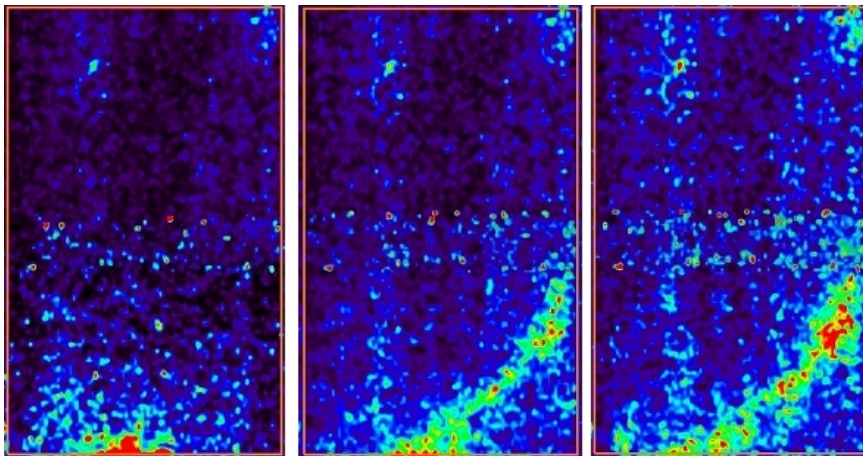
Fig. 3. Geo-PET image of a radiotracer experiment inside a sandstone drilling core. Core diameter is 10 cm, length is 15 cm. The drilling core consists of heterogeneous material, pervaded by several material boundaries and fissures. The tracer flows preferentially along a material boundary. Tracer is 124I in KI-solution. Left: 2h after injection. Middle: 11 h after injection. Right: 17 h after injection.
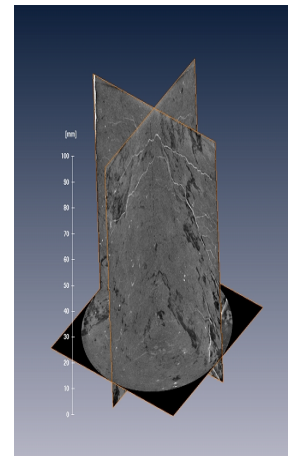
Fig. 4. High resolution 3-D computer tomographic image (µXCT) of the internal structures of a sample.
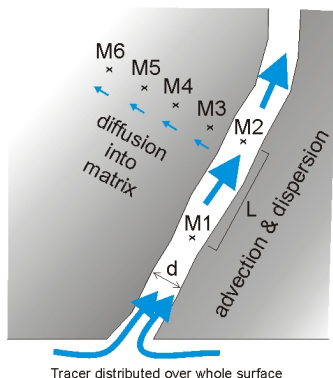
Fig. 5. Combined PET and µXCT data sets allow the investigation of effective hydraulic pathways, quantification of heterogeneity as well as city (e.g. in points M1 - M2) and diffusion rates (e.g. in points M3 - M6) of well-defined structures inside a sample can be measured directly.
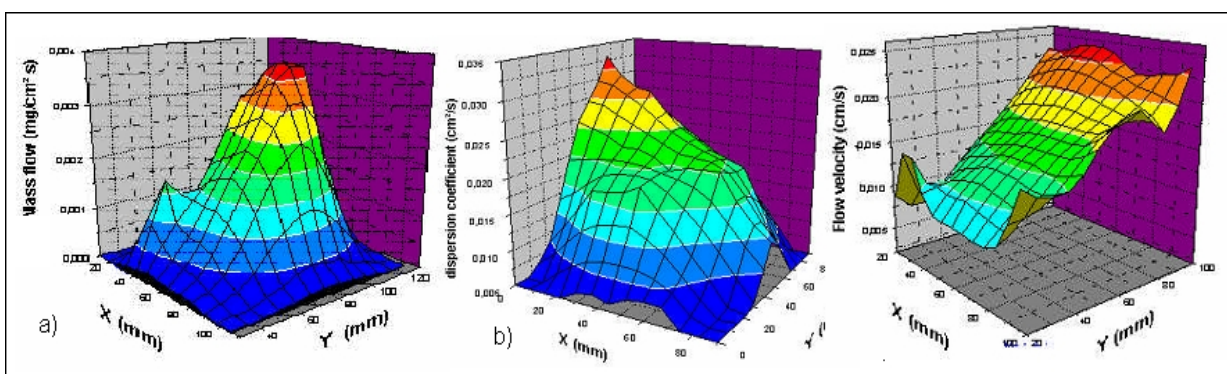
Fig. 6. Results of spatially resolved transport parameters over a cross section of a sample: a) mass flow, b) dispersion coefficient, c) flow velocity.

Studies concerning the quantification of solution-, dissolution- and diffusion processes are conducted at evaporite samples of different chemical composition and

different mechanical stress. The chemical composition of the used and partly highly salinar solutions is measured by means of ion chromatography before and after the experiments and additionally modelled with the geochemistry-reaction code PHRQPITZ (Plummer et al. 1988). First preliminary tests concerning solubility and diffusion velocities at a rock salt sample are conducted. The results substantiate the undisturbed character of the core used: within 10 days no noteworthy diffusion could be observed from a central drilling into the rock with the aid of the PET tracer 124I [KI].

It is planned to quantify diffusion processes by conducting diffusion experiments over 12 months within a rock salt sample with the long living PET tracer 22Na [NaCl] as well as to align PET measurements with modelling of dissolution processes at a rock salt drilling core flushed with demineralised water.

References

Kulenkampff J., Gründig M., Richter M., Wolf M., Dietzel O. (2008). First applications of a small-animal-PET scanner for process monitoring in rocks and soils.- Geophysical Research Abstracts, Vol. 10, EGU2008-A-03727.

Gründig M., Richter M., Seese A., Sabri, O. (2007). Tomographic radiotracer studies of the spatial distribution of heterogeneous geochemical transport processes.- Applied Geochemistry, 22, 2334-2343.

Richter M., Gründig M., Butz T. (2000). Tomographische Radiotracerverfahren zur Untersuchung von Transport- und Sorptionsprozessen in geologischen Schichten.- Zeitschrift für angewandte Geologie, 46, 101-109.

Richter M. (2002). Concepts for modelling of heterogeneous flow processes in soil columns on the basis of tomographic radiotracer experiments.- In: H.D. Schulz & G. Teutsch (Eds.), Geochemical Processes: Conceptual models for reactive transport in soil and groundwater - Research Report. Wiley-VCH, Weinheim, 20-38.

Kulenkampff J., Gründig M., Richter M., Enzmann F. (2008). Evaluation of Positron-Emission-Tomography for Visualisation of Migration Processes in Geomaterials. Physics and Chemistry of the Earth 33, 937-942.

Gründig M., Richter M. Enzmann F., Kulenkampff J., Seese A. (2009). Positron Emission Tomography for Modelling of Geochemical Transport Processes in Granite Fractures. Subm. to Applied Geochemistry

Plummer L.N.; Parkhurst D.L.; Fleming G.W., Dunkle S.A. (1988). A computer program incorporating Pitzer's equations for calculation of geochemical reactions in brines.- U.S. Geological Survey, Water Resources Investigations Report 88-4153.

<u>Codes</u>

Institution	Code used for reactive transport	Availability	Reason for using the code	Remarks
BGR, dep. "Energy Resources, Mineral Resources"	FLOTRAN	freeware	Modelling hardpan formation in mining residues	Two-Phase Nonisothermal Coupled Thermal-Hydrologic-Chemical (THC) Reactive Flow& Transport Code
Institut für Interdisziplinäre Isotopenforschung (IIF) Leipzig	PHRQPITZ	http://wwwbrr.cr.usgs.gov/projects/GWC_coupled/phrqpitz/	Pitzer equations are implemented, modelling of dissolution-precipitation reactions in brines	to date suficcient, but we want to change to PHREEQC
Institut für Interdisziplinäre Isotopenforschung (IIF) Leipzig	PHREEQC	http://wwwbrr.cr.usgs.gov/projects/GWC_coupled/phreeqc/index.html	includes Pitzer and 1-D transport	none
CEA/DTCD/SECM/LCLT	Hytec	consortium	Simulation of all chemical processes required by the problem (particularly kinetics)	none
	Alliances	consortium	Simulation of all chemical processes required by the problem (particularly kinetics)	not yet tested, but will be soon
CTU Prague	PHREEQC2	free	Convenient for the modelling of 1D reactive transport in simple bodies with a complex description of speciation in both liquid and solid phases	none
CTU Prague	GoldSim	free academic licence for education, paid licence for research (in cooperation with NRI Rez)	Possibility to build model of complex bodies with limited description of chemistry; recommended for the stochastic modelling necessary in PA	none

CTU Prague	MIVCYL	own development	The code was used for the modelling of transport of species for which the kinetic description of interaction with the surface had to be mentioned; the modelling of diffusion transport in the near-field region is comparable with the use of codes PAGODA and/or GoldSim	Numerical transport model using finite differences method for the solution of transport equation; up to 5 interacting species can be observed simultaneously; sophisticated description of sorption including kinetics is taken into account.
Paul Scherrer Institut - Labor fuer Endlagersicherheit	MCOTAC	free for non-commercial use	Flexible in-house developed code	1D, 2D advection/dispersion/diffusion, geochemical equilibrium, kinetics, different grain models, porosity permeability relationships included, 1D version coupled to a LMA and a GEM geochemical solver (further information: http://people.web.psi.ch/pfingsten/subdir3-publications/)
Paul Scherrer Institut - Labor fuer Endlagersicherheit	GeoSys/Rockflow	free for non-commercial use	Good relations to the code developer, long-term experience with the code	1D, 2D, 3dD FEM THMC code, various couplings to different geochemical modules (PHREEQC, GEMS-PSI, ChemApp….), parallel version.
Institute of Geosciences, University of Kiel	GeoSys-ChemApp	GeoSys free to developers joining the OpenTHMC developers group; ChemApp is company software	see paper Li and Bauer	none
UPC Technical University of Catalunya	CHEPROO (linked with various transport codes: proost, traconf, codebright)	Free	Flexible in-house developed code	Support SIA or DSA solving methods. Easy to link with transport codes. Object oriented designed (easy to expand functionality)

GRS mbH	d³f for density-driven flow simulations; r³t for transport simulations	Please contact GRS for further information about availability and licensing (d3f@grs.de).	Codes were developed lead-managed by GRS with regard to the transient, density-driven transport of salt and to the pollutant transport in very large model domains for long periods of time.	d³f regards the density driven flow. In r³t the retention is included in an phenomenological way. Reactive transport might be implemented in the future.
ZAG Uni Tübingen	PHT3D	free / contact developer	direct work with the developer (Dr. H. Prommer)	coupling of MT3DMS and PHREEQC-2
ZAG Uni Tübingen	MIN3P	free / contact developer	direct work with the developer (Dr. U. Mayer)	None
Loughborough University	ECOSAT	€250 + VAT	User friendliness and cost	Just starting to evaluate
Loughborough University	CORE	Free	User friendliness and cost	Just starting to evaluate
Loughborough University	JCHESS		Was free to us as we helped trial it	Speciation only, easier to use than PHREEQE
FZK-INE	ECOSAT	€250 + VAT	User friendliness and cost; allows for various surface complexation models, interaction with natural organic matter	flow part is restricted, very convenient for a fast first look
FZK-INE	GWB	expensive	user friendly, allows Pitzer calculations coupled to transport	flow part is restricted
FZK-INE	HBGC123D	freeware	advanced and very flexible chemistry options; equilibrium and kinetics	chemistry part is similar to codes we use for surface complexation

List of Posters

Intercomparison exercise on redox determination methods: A key activity within the EURATOM FP7 "ReCosy" project
M. Altmaier

Modeling the long term behaviour of glass in deep geological repositories: interactions between glass, steel and argilite
O. Bildstein, J.-E. Lartigue, L. Trotignon, E. Piault

EURATOM FP7 collaborative project "Redox phenomena controlling systems" (CP ReCosy)
G. Buckau, L. Duro, B. Kienzler

Modelling the influence of humic acid on the sorption of U(IV) to kaolin
N. Evans, N. Bryan

Study by near field microscopy by time resolved laser spectroscopy in to europium sorbed on alumina with and without humic acid
K. A. Ghaleb, P. Reiller, F. Viala

Modeling fluid–rock interaction and scale formation during geothermal heat extraction
F. Hingerl, G. Kosakowski, D. Kulik, S.V. Dmytrieva, T. Driesner, T. Wagner, K. Thomsen

Interaction of uranyl with quartz – experiments and modelling
F. Huber, J. Lützenkirchen

DIAMOND: Academic innovation in support of UK radioactive waste management
N. Hyatt, S. Biggs, F. Livens, J. Young, N. Evans

Modelling heterogeneity effects on radionuclide transport in the far field of a radioactive waste repository
S. Jain, N. Evans

Interaction of trivalent ions with various aluminium minerals
T. Kupcik, N. Huittinen, T. Rabung, J. Lützenkirchen, H. Geckeis, T. Fanghänel

Interaction of polyacrylic acid with dissolved aluminium - preliminary modelling of polyacrylic acid titrations
J. Lützenkirchen, J. D. Wells, J. van Maale, F. Leermaakers, S. Sjöberg

Reactive transport modelling of cemented layer formation in sulfide-bearing mine tailings
J.A. Meima, T. Graupner, D. Rammlmair

Kd and competitive sorption approach for the modelling of Ni diffusion through bentonite
W. Pfingsten, M. Bradbury, B. Baeyens

Numerical modelling of tracer tests and estimation of hydro-geological properties of a shear zone at the Grimsel Test Site
A. Pudewills, F. Huber, T. Schäfer

Testing the K_d-approch with a multicomponent geochemical reactive transport model for a HLW repository in granite: The case of Cs
J. Samper, C. Lu, J. L. Cormenzana, H. Ma, L. Montenegro, M.A. Cuñado

Testing the K_d approch with a multicomponent geochemical reactive transport model for a HLW repository in granite: The case of uranium
J. Samper, C. Lu, J. L. Cormenzana, H. Ma, L. Montenegro, M.A. Cuñado

Application of computational chemistry to investigate the interactions between mineral based materials and alkyltriethoxysilanes
J. Süßmuth, A. Gerdes

Modelling of through-diffusion experiments using PHREEQC2: influence of the characterization of uranyl sorption on mesoporous silica MCM-41 by a surface complexation model
D. Vopálka, K. Štamberg

3D-visualisation and modelling of transport processes in hterogeneous structures
M. Wolf, J. Kulenkampff, J. Lippmann-Pipke, M. Gründig, F. Enzmann, M. Richter